TAL TECH

DOCTORAL THESIS

Energetics and Calcium Handling in Hearts from Creatine-Deficient Mice

Jelena Branovets

TALLINNA TEHNIKAÜLIKOOL
TALLINN UNIVERSITY OF TECHNOLOGY
TALLINN 2022

TALLINN UNIVERSITY OF TECHNOLOGY
DOCTORAL THESIS
56/2022

Energetics and Calcium Handling in Hearts from Creatine-Deficient Mice

JELENA BRANOVETS

TAL TECH PRESS

TALLINN UNIVERSITY OF TECHNOLOGY
School of Science
Department of Cybernetics
This dissertation was accepted for the defence of the degree 12/08/2022

Supervisor: Rikke Birkedal Nielsen, PhD
Laboratory of Systems Biology
Department of Cybernetics
Tallinn University of Technology
Tallinn, Estonia

Opponents Coert J. Zuurbier, MEng PhD
Laboratory of Experimental Intensive Care and Anaesthesiology
Department of Anaesthesiology, Amsterdam UMC - AMC
University of Amsterdam
Amsterdam, The Netherlands

Iman Momken, PhD
Laboratory of Signalling and Cardiovascular Pathophysiology
INSERM UMR-S 1180
University of Paris-Saclay-University of Evry Val d'Essonne
Évry-Courcouronnes, Île-de-France, France

Defence of the thesis: 29/09/2022, Tallinn

Declaration:
Hereby I declare that this doctoral thesis, my original investigation and achievement, submitted for the doctoral degree at Tallinn University of Technology has not been submitted for doctoral or equivalent academic degree.

Jelena Branovets

---
signature

European Union
European Regional
Development Fund

Investing
in your future

Copyright: Jelena Branovets, 2022
ISSN 2585-6898 (publication)
ISBN 978-9949-83-900-1 (publication)
ISSN 2585-6901 (PDF)
ISBN 978-9949-83-901-8 (PDF)
Printed by Koopia Niini & Rauam

TALLINNA TEHNIKAÜLIKOOL
DOKTORITÖÖ
56/2022

Energeetika ja kaltsiumi käitlemine kreatiini puudulike hiirte südametes

JELENA BRANOVETS

TAL TECH
KIRJASTUS

Contents

List of publications 7

Author's contribution to the publications 8

Introduction 9

Abbreviations 11

1 Cardiac function and creatine kinase system 13

1.1 Cardiac function and energy metabolism 13

1.2 Creatine kinase system 16

1.3 The role of intracellular compartmentation in energy transfer 19

2 The role of creatine kinase and other phosphotransfer systems in the heart 20

2.1 Animal models with altered creatine kinase system 20

2.1.1 Pharmacological inhibition 20

2.1.2 Genetically modified animal models 20

2.1.3 Creatine-deficient mouse models 21

2.1.4 Limitations associated with use of AGAT KO mice 23

2.2 The impact of creatine kinase system impairment on cardiac function under stress conditions 23

2.3 Ultrastructural organization and mitochondrial respiration in creatine kinase and GAMT KO mice 24

2.4 Role of alternative phosphotransfer systems in energy transfer 25

2.5 Changes in alternative phosphotransfer systems in AGAT and GAMT mouse cardiomyocytes 26

3 Creatine kinase and adenylate kinase activities in heart homogenates and permeabilized cardiomyocytes from mice and rats 28

4 Calcium handling in mouse models with altered creatine kinase system 31

4.1 The interplay between creatine kinase and excitation-contraction coupling systems 31

4.2 Calcium handling in patch clamped AGAT KO cardiomyocytes 31

4.3 Calcium handling and excitation-contraction coupling in creatine-deficient mouse cardiomyocytes under physiological conditions 33

4.3.1 Calcium-induced calcium release 33

4.3.2 Calcium removal and cardiomyocyte relaxation 35

4.3.3 Adaptive changes in excitation-contraction coupling in AGAT KO cardiomyocytes 36

5 Conclusions 39

References 40

Acknowledgements 52
Abstract 53
Lühikokkuvõte 54
Appendix 1 55
Appendix 2 73
Appendix 3 93
Appendix 4 95
Appendix 5 119
Curriculum vitae 120
Elulookirjeldus 122

List of publications

The list of author's publications, on the basis of which the thesis has been prepared:

I **Branovets J**, Sepp M, Kotlyarova S, Jepihhina N, Sokolova N, Aksentijevic D, Lygate CA, Neubauer S, Vendelin M, Birkedal R

Unchanged mitochondrial organization and compartmentation of high-energy phosphates in creatine-deficient GAMT-/- mouse hearts.

Am J Physiol Heart Circ Physiol. 2013 Aug 15;305(4):H506-20. doi: 10.1152/ajpheart.00919.2012.

II **Branovets J**, Karro N, Barsunova K, Laasmaa M, Lygate CA, Vendelin M, Birkedal R

Cardiac expression and location of hexokinase changes in a mouse model of pure creatine deficiency.

Am J Physiol Heart Circ Physiol. 2021 Feb 1;320(2):H613-H629. doi: 10.1152/ajpheart.00188.2020.

III **Branovets J**, Vendelin M, Birkedal R

Intracellular compartmentalization shapes energy transfer – differences between adenylate kinase activities in homogenate and permeabilized cardiomyocytes.

(manuscript)

IV Laasmaa M, **Branovets J***, Barsunova K*, Karro N, Lygate CA, Birkedal R, Vendelin M

Altered calcium handling in cardiomyocytes from arginine-glycine amidinotransferase-knockout mice is rescued by creatine.

Am J Physiol Heart Circ Physiol. 2021 Feb 1;320(2):H805-H825. doi: 10.1152/ajpheart.00300.2020

V **Branovets J**, Kalda M, Laasmaa M, Stolova J, Shen X, Balodis MJ, Grahv C, Hendrikson E, Louch WE, Birkedal R, Vendelin M

Compromised creatine kinase energy transfer leads to adaptations in cardiac excitation-contraction coupling that are distinct from changes associated with heart failure.

(manuscript)

* Equal contribution

Author's contribution to the publications

I In Publication I, the author isolated cardiomyocytes, performed respiration and spectrophotometric measurements with isolated cells, analysis of the data, prepared some of the figures and dealt with mouse colony handling and genotyping

II In Publication II, the author isolated cardiomyocytes, performed respiration and spectrophotometric measurements with isolated cells, Western blot experiments, analysed the data, prepared some of the figures and dealt with mouse colony handling and genotyping

III In Publication III, the author performed all the experiments and data analysis, prepared some of the figures and wrote the draft of the manuscript

IV In Publication IV, the author performed the isolations of cardiomyocytes and dealt with mouse colony handling and genotyping

V In Publication V, the author isolated cardiomyocytes, performed part of the experiments (Ca^{2+} transients, sparks, and t-tubular network measurements), analysed the data from Ca^{2+} transient and Ca^{2+} spark measurements and dealt with mouse colony handling and genotyping

Introduction

The blood pumped by the heart supplies all the organs with nutrients and oxygen and eliminates waste products. Adequate energy production in mitochondria and efficient energetic communication between energy-producing and energy-utilizing sites are of vital importance for the normal functioning of the heart. The creatine kinase (CK) system is considered to play a crucial role in buffering and transporting high-energy phosphates in tissues with high and fluctuating energy needs. Almost 40 years ago, Bittl and Ingwall suggested that phosphoryl transfer by CK is ten times faster than ATP synthesis by mitochondrial respiration (Bittl and Ingwall, 1985). Since then, multiple studies have been performed to assess the relation of CK-flux to ATP synthesis by oxidative phosphorylation, presenting noticeably diverse data. Thus, over the years, the CK system has been considered one of the most important players in myocardial metabolism (Bessman and Carpenter, 1985; Wallimann et al., 1992; Saks et al., 1994; Joubert et al., 2002; Dzeja and Terzic, 2003).

The CK system changes in heart failure when the heart cannot pump blood efficiently around the body. The progression of heart failure is associated with impairments in energy metabolism, characterized by the inability of the heart to produce a sufficient amount of energy needed to match its functional demands. In 1939 the reduction of total creatine levels in failing myocardium was first described by Herrmann and Decherd (Hermann and Decherd, 1939), followed by the detection of elevated serum CK levels after myocardial infarction (MI) in the early 1960s (Duma and Siegel, 1965). After MI, due to the tissue damage, CK is released from the myofibrils. The elevated serum CK levels correlate with the infarct size, so that larger infarct sizes evoke larger CK release into the blood flow. Since then, extensive research has been carried out to understand what causes heart failure development. After MI, total CK enzymatic activity and creatine levels are reduced (Ingwall and Weiss, 2004; Lygate et al., 2007; Neubauer, 2007), leading to compromised energy metabolism in the failing heart. Moreover, the infarct severity depends on its duration, so more PCr is consumed during a longer infarct, causing more severe consequences. Thus, the PCr/ATP ratio is a well-known indicator of the myocardial energy state and is widely used as a prognostic marker of patient mortality after heart failure (Neubauer et al., 1997; ten Hove and Neubauer, 2007).

Cardiac energetics and the contribution of the functional CK system to energy transfer in healthy and failing hearts were studied in several models, where the CK system was altered (Lygate and Neubauer, 2014). However, the outcomes of these studies were equivocal and even contradictory. On the one hand, the basic cardiac function of creatine-deficient and CK KO animals was normal (Hove et al., 2005; Nahrendorf et al., 2006; Faller et al., 2018; Aksentijević et al., 2020), and compromised CK function did not worsen heart failure (Nahrendorf et al., 2005; Lygate et al., 2013). On the other hand, several other studies reported the improvement of postischemic cardiac dysfunction and protection against heart failure due to the overexpression of CK (Akki et al., 2012; Gupta et al., 2012; Whittington et al., 2018). Therefore, further investigations are needed to get a clearer insight into the CK system's role in regulating cardiac metabolism. Of particular interest is the importance of CK as an energy transfer system, which, for a long time, was thought to be crucial in a healthy heart and compromised in heart failure.

Ca^{2+} plays an essential role in cardiac contraction and regulation of energy metabolism, participating in the regulation of ATP utilization by ATPases and ATP generation by mitochondria. Changes in the Ca^{2+} handling were demonstrated in CK KO

mouse hearts (Crozatier et al., 2002; Spindler et al., 2004). Although these animals exhibited unchanged myocardial Ca^{2+} homeostasis at baseline, impaired Ca^{2+} handling and excitation-contraction (EC) coupling were observed under acute stress conditions. Therefore, revealing the aspects of tight interaction of Ca^{2+} dynamics and regulation of cardiac energetics is of great importance in understanding the underlying causes of the heart's inability to meet the body's fluctuating needs under pathophysiological conditions.

In the current dissertation, the energetic communication between cellular compartments, ultrastructural organization, and Ca^{2+} handling in cardiomyocytes from mouse models with altered CK system was studied. Two mouse models of creatine-deficiency were used. Both are creatine free due to the lack of one of the enzymes that synthesise creatine, either L-arginine:glycine amidinotransferase (AGAT) or guanidinoacetate *N*-methyltranferase (GAMT). In addition, data from different experimental measurements were used as input for various mathematical models of heart cells to estimate intracellular compartmentation and how communication between cellular compartments and Ca^{2+} handling is modified in creatine-deficient hearts. The results of this work broaden the understanding of the CK system's role in regulating energy metabolism and Ca^{2+} dynamics in the heart.

The thesis is organized as follows. The first chapter of this thesis briefly overviews cardiac function and metabolism. In the next chapter, studies on creatine-deficient animal models are described with the results from **Publications I and II**. As mouse was used in these studies, in contrast to the use of rats in earlier works studying intracellular energy transfer, the relevant bioenergetics parameters from rat and mouse cardiac preparations were compared in **Publication III** and summarized in Chapter 3. Finally, results linking creatine-deficiency to EC coupling (**Publications IV and V**) are described in Chapter 4 and followed by the overall conclusions.

Abbreviations

ADP	adenosine diphosphate
AGAT	arginine:glycine amidinotransferase
AGAT KO	mouse lacking arginine:glycine amidinotransferase
AK	adenylate kinase
AMP	adenosine monophosphate
AMPK	AMP-activated protein kinase
ANT	adenine nucleotide translocase
ATP	adenosine triphosphate
ATPase	adenosine triphosphatase
CICR	Ca^{2+} induced Ca^{2+} release
CK	creatine kinase
CK KO	mouse lacking muscle and mitochondrial creatine kinase
Cr	creatine
CrT	creatine transporter
CrT KO	mouse lacking creatine transporter
CrTOE	mouse overexpressing creatine transporter
EC	excitation-contraction
ETC	electron-transport chain
GAMT	guanidinoacetate methyltransferase
GAMT KO	mouse lacking guanidinoacetate methyltransferase
GAPDH	glyceraldehyde 3-phosphate dehydrogenase
hArg	homoarginine
HK	hexokinase
IA	iodoacetamide
I-R	ischemia-reperfusion
ISO	isoprenaline
KO	knockout
LTCC	L-type calcium channel
M-CK	muscle creatine kinase
M-CK KO	mouse lacking muscle creatine kinase
MCU	mitochondrial Ca^{2+} uniporter
MI	myocardial infarction
MOM	mitochondrial outer membrane
mtCK	sarcomeric mitochondrial creatine kinase
mtCK KO	mouse lacking sarcomeric mitochondrial creatine kinase
NADH	reduced nicotinamide adenine nucleotide
NCX	Na^{+}/ Ca^{2+} exchanger
NCXrev	Na^{+}/ Ca^{2+} exchanger operating in the reverse mode
PCr	phosphocreatine
PEP	phosphoenolpyruvate

PK	pyruvate kinase
PLB	phospholamban
ROS	reactive oxygen species
RyR	ryanodine receptor
SL	sarcomere length
SERCA	sarcoplasmic reticulum Ca^{2+} -ATPase
SR	sarcoplasmic reticulum
TnC	troponin C
VDAC	voltage dependent anion carrier
β-GPA	beta-guanidinopropionic acid

1 Cardiac function and creatine kinase system

1.1 Cardiac function and energy metabolism

The heart beats and pumps the blood around the body throughout life, constantly and without rest. Cardiac output is around 5 litres per minute in a human. Thus, the heart has the highest energy demand compared to any other organ in the body. Consequently, mitochondrial content, occupying one-third of the cell volume, is the highest in the heart, while myofilaments take up half of the cardiomyocyte volume (Barth et al., 1992; Katz, 2011).

The heart's contraction is initiated by the action potential (AP), a transient change in membrane potential generated by the pacemaker cells in the sinoatrial node (SA) node of the heart. The electrical excitation and contraction of the myofibrils are linked by the EC coupling (Figure 1). With this, the propagation of an action potential leads to voltage change across the sarcolemma and subsequent opening of voltage-dependent L-type Ca^{2+} channels (LTCC), causing Ca^{2+} influx into the cell. That, in turn, triggers a more prominent Ca^{2+}-induced Ca^{2+} release (CICR) from the sarcoplasmic reticulum (SR) through Ca^{2+} release channels, the ryanodine receptors (RyRs). When intracellular Ca^{2+} increases, Ca^{2+} binds to troponin C (TnC), the Ca^{2+} - binding subunit of the troponin complex (Tn), located on the actin filaments, and allows myosin binding to actin. This causes sliding of the actin filaments over the myosin filaments, and thus the myofilament contraction, driven by adenosine triphosphate (ATP) hydrolysis by myosin-ATPases. For relaxation, Ca^{2+} is pumped back to the SR by SR Ca^{2+}-ATPase (SERCA) or exported out of the cell by the Na^{+}-Ca^{2+} exchanger (NCX) and the sarcolemmal Ca^{2+}-ATPase (Bers, 2002).

Ca^{2+} also plays a role in the regulation of ATP generation. Ca^{2+} enters the mitochondria through the mitochondrial Ca^{2+} uniporter (MCU), stimulates dehydrogenases in the citric acid cycle (Krebs cycle) to produce NADH, and participates in the activation of F_1F_O-ATPase (Franzini-Armstrong, 2007). Although mitochondria take up and release Ca^{2+} under physiological conditions, they are not involved in EC coupling. They thus do not liberate Ca^{2+} in response to stimulation or when required by the cell (Williams et al., 2013). Nevertheless, the mitochondrial Ca^{2+} transients could play an essential role in regulating ATP regeneration and mitochondrial energetics (Glancy and Balaban, 2012). Thus, Ca^{2+} plays a critical role in regulating muscle contraction in parallel with mitochondrial energy production, termed "parallel activation" (Balaban, 2002).

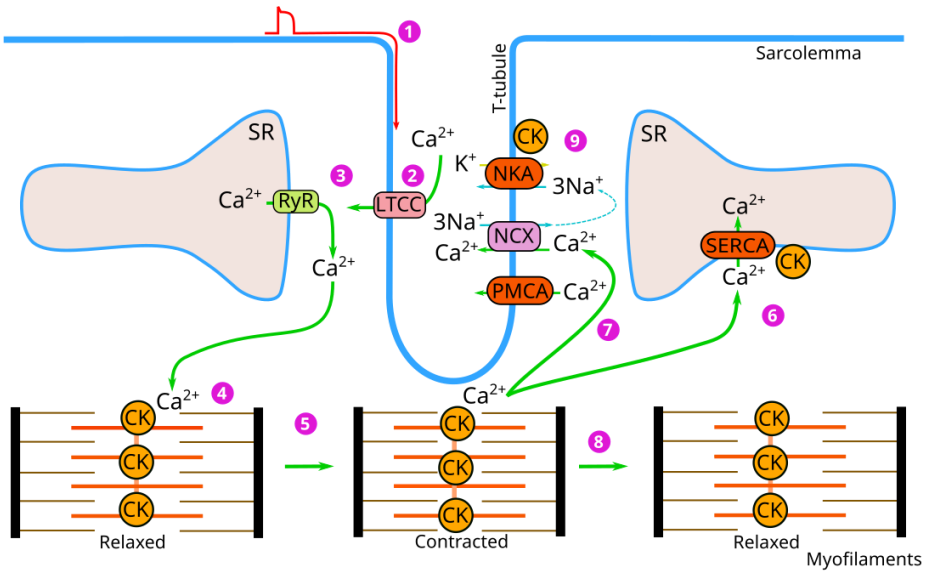

Figure 1. Cardiac muscle excitation, contraction and relaxation. 1. The cardiac action potential (AP) spreads through the heart, causing depolarization along the sarcolemma and t-tubular system; 2. Voltage-gated Ca^{2+} channels (LTCC) open and let Ca^{2+} ions to enter the cell; 3. Ca^{2+} ions cause Ca^{2+} release from intracellular Ca^{2+} stores in sarcoplasmic reticulum (SR), through ryanodine receptors (RyRs); 4. The free intracellular Ca^{2+} concentration increase allows Ca^{2+} binding to myofilaments; 5. Ca^{2+} binding to myofilaments enables the interaction between thin and thick filaments and leads to a muscle contraction; 6. After the contraction, Ca^{2+} is taken up into the SR by sarcoplasmic reticulum Ca^{2+} -ATPase (SERCA); or 7. transported out of the cell by sodium-calcium exchanger (NCX); 8. The decline in cytosolic Ca^{2+} concentration allows the relaxation of the myofilament to occur; 9. Na^+/K^+-ATPase (NKA) restores Na^+ and K^+ gradients and maintains resting potential across the plasma membrane. The contribution of sarcolemmal Ca^{2+}-ATPase (PMCA) to Ca^{2+} extrusion is negligible and constitutes only 1%. In the heart, cytosolic creatine kinase (CK) is bound to the M-band of myofibrils and coupled to myosin ATPases. Also, it is located near and coupled to SERCA and NKA.

The contraction of the heart is fueled by ATP, most of which is obtained from the oxidation of carbohydrates and fats employing glycolysis and oxidative phosphorylation. Cardiac energy metabolism involves both anabolic and catabolic reactions, synthesizing building blocks for cellular structure and ATP, respectively. Catabolism consists of three main components: cellular uptake and subsequent breakdown of the substrates received with the food; the ATP production by oxidative phosphorylation in mitochondria; and, finally, the transfer of energy-rich phosphate bonds to the cytosolic sites of ATP-consumption and their subsequent utilization (Neubauer, 2007) (Figure 2).

After substrates are taken up by the cell, they are metabolised by beta-oxidation and glycolysis, leading to acetyl coenzyme A (Acetyl-CoA) formation. Next, Acetyl-CoA is oxidized in the Krebs cycle within mitochondria to form CO_2 and reducing agents (NADH, $FADH_2$), which pass their electrons further to the respiratory chain or electron-transport chain (ETC). Since ATP produced by glycolysis is not enough to fuel heart beating, oxidative phosphorylation is the primary energy source in the heart, responsible for producing over 95% of ATP in the heart (Ingwall, 2002). ETC consists of four protein complexes that pass electrons from electron donors (NADH, $FADH_2$) to electron acceptors

and transfer the protons across the mitochondrial inner membrane to the intermembrane space, creating a proton gradient. Then, adenosine diphosphate (ADP) is converted to ATP by ATP-synthase, powered by this gradient (Figure 2).

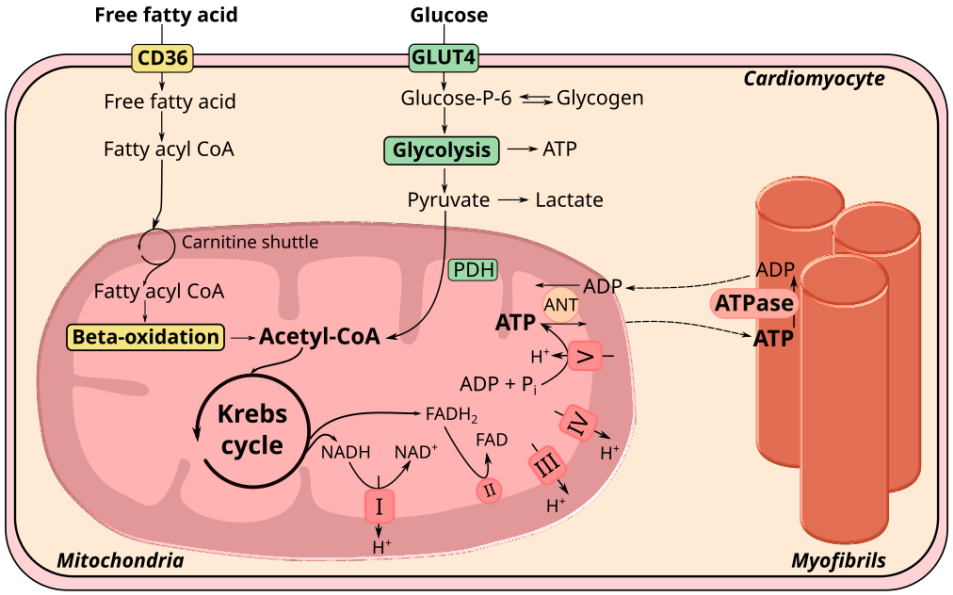

Figure 2. Cardiac energy metabolism. Fatty acids and glucose are the main substrates of myocardial metabolism. They are transported from the bloodstream into the cell via fatty acid transporter (mainly CD36) and glucose transporter (GLUT4). In the cell, glucose is metabolized in the glycolysis pathway, forming pyruvate, which enters mitochondria, where pyruvate dehydrogenase (PDH) catalyses the formation of acetyl-CoA. Free fatty acids are converted to fatty acyl CoA, which enters mitochondria through a carnitine-mediated exchange. Fatty acyl CoA is oxidized in the beta-oxidation pathway in the mitochondria, forming acetyl-CoA. Acetyl-CoA from both pyruvate and fatty acids is further oxidized in the citric acid cycle (Krebs cycle), producing reduced nicotinamide adenine nucleotide (NADH) and flavin adenine dinucleotide ($FADH_2$). The respiratory chain uses these reducing agents to build up a proton gradient, used further by ATP synthase to generate ATP by ADP phosphorylation. Finally, ATP is transported to the sites of utilization in the cytosol. ANT—adenine nucleotide translocase.

During cardiac development, due to an increase in workload, the growth of the heart is first enhanced by hyperplasia followed by hypertrophy. In parallel, cardiac energy production relying initially on the utilization of carbohydrates, switches to fatty acid oxidation, allowing the heart to adapt both its energy generation and contractile capacity to new needs of the organism to ensure proper cardiac function (Piquereau and Ventura-Clapier, 2018). The heart is very flexible in swapping the metabolic orientation in response to changes in different factors, such as the energy demand, oxygen consumption, the availability of the substrates, the activity of enzymes implicated in energy transfer etc. In addition to the metabolic maturation, the heart undergoes significant development and rearrangement of the intracellular organization, leading to a more organized and compartmentalized architecture in adult cardiomyocytes. Namely, during the maturation of cardiomyocytes, there is a significant increase in the volume of intracellular structures like myofilaments, SR and mitochondria, and a decrease in the

cytosolic compartment (Piquereau et al., 2010). Further development of the specialized structures engaged in EC coupling, such as SR and transverse tubules (t-tubules), cause the formation of a compartmented Ca^{2+} handling system. At the same time, as a result of the growth and remodelling of the mitochondrial network, the mitochondria become densely packed and organized in a crystal-like pattern together with the multiple parallel rows of myofilaments leading to the formation of the energetic microdomains (Vendelin et al., 2005; Birkedal et al., 2006, 2014).

The efficient and fast energy transfer between ATP-producing mitochondria and ATP-consuming ATPases plays a crucial role in cardiac energetics. Energy transfer can take place through a direct diffusion of ATP and ADP, diffusion facilitated by phosphotransfer systems, or both (Figure 3). The speed of the diffusion depends on the distance and obstacles that adenine nucleotides must overcome. The close association of mitochondria with SR or myofilaments, leading to a direct adenine nucleotide channelling, improves the communication between the mitochondria and ATPases (Kaasik et al., 2001). The heart is known for its high metabolic stability, keeping ADP levels unaltered even during significant changes in workload (Katz et al., 1989; Balaban, 2002). However, although ADP concentration in the cell, varying in the micromolar range (10–35 μM), is much lower than millimolar concentrations of ATP (3–5 mM) and P_i (1.5–2 mM), it plays a crucial role in energetics (Wallimann et al., 1992). Near ATPases, when ATP is hydrolysed (ATP + H_2O → ADP + P_i), ADP has to be removed as fast as possible. This will ensure sufficient phosphorylation potential and hence, free energy available from ATP hydrolysis ($\Delta G = \Delta G^{0\prime} + RTln\frac{[ADP][P_i]}{[ATP]}$), needed to drive ATP-dependent reactions. One could calculate using this equation and assuming that standard free energy of ATP hydrolysis $\Delta G^{0'}$ = -30 kJ/mol, universal gas constant R = 8.314 kJ/mol, temperature T = 310.15 K the influence of varying concentrations of ATP, ADP and P_i on ΔG. Consequently, even small increases (in the micromolar range) in ADP concentration result in a much more significant impact on free energy released from ATP hydrolysis than comparable changes in ATP concentration. Therefore, it was assumed that specialized energy transfer systems are essential to maintain the phosphorylation potential near ATPases. The family of CK isoenzymes is traditionally considered the main phosphotransfer system.

1.2 Creatine kinase system

CK catalyzes the reversible phosphoryl transfer between ATP/creatine (Cr) and ADP/phosphocreatine (PCr) (ATP + Cr ↔ ADP + PCr), facilitating energy transfer between mitochondria and ATPases (Wyss and Kaddurah-Daouk, 2000). Although PCr (Eggleton and Eggleton, 1928) and ATP (Fiske and Subbarow, 1929) were discovered almost at the same time in the late 1920s, for more than thirty years, PCr was thought to be the primary energy source in the body. Lohmann first recognized the CK reaction in 1934 during his studies of muscle contraction (Bessman and Carpenter, 1985). Subsequently, CK was purified and crystallized from a rabbit muscle by Kuby et al. (Kuby et al., 1954). In 1962, Cain and Davies showed that the energy released during ATP hydrolysis is used for muscle contraction, but ATP levels decline if CK is inhibited (Cain and Davies, 1962). This suggested that PCr used by CK can buffer ATP levels.

The substrate for CK reaction, Cr, is a naturally occurring compound obtained from the diet or synthesized in the body, mainly in the kidney and liver, from arginine, glycine, and methionine (Figure 3). Cr is synthesized by two enzymatic reactions involving

L-arginine:glycine amidinotransferase (AGAT; EC 2.1.4.1), catalysing the transfer of an amidino group from arginine to glycine, yielding guanidinoacetate (GA) and ornithine, and guanidinoacetate methyltransferase (GAMT; EC 2.1.1.2), methylating GA to form Cr (Wyss and Kaddurah-Daouk, 2000). Further, Cr is distributed by the bloodstream to the various tissues, where it is imported across the cell membrane through a specific Cr transporter (CrT or SLC6A8). PCr and Cr concentrations vary with muscle type, but they are typically found in the range of 20—35 mM and 5—10 mM, respectively (Wallimann et al., 1992). Finally, Cr is converted nonenzymatically to creatinine and excreted by the kidneys.

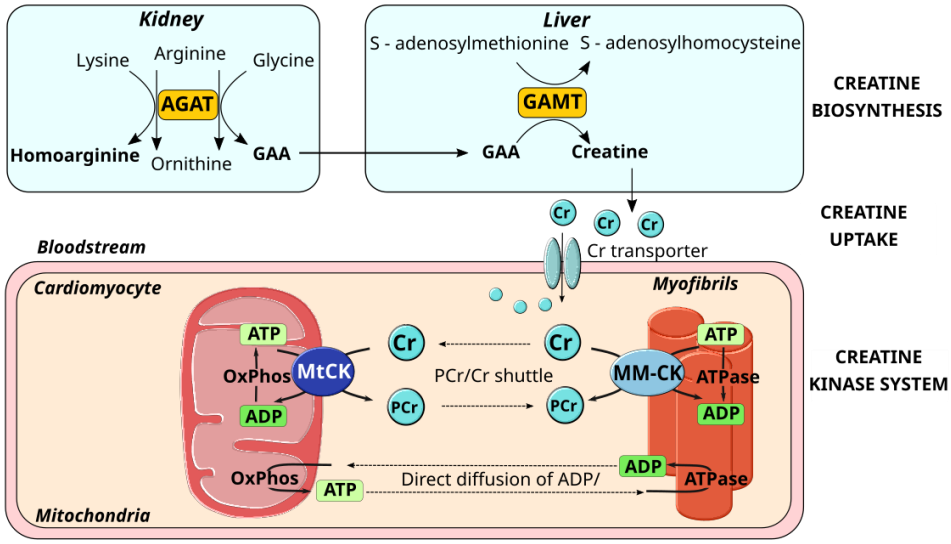

Figure 3. Creatine (Cr) synthesis and creatine kinase (CK) system. Cr is synthesised mainly in the kidney and liver or obtained via food. The first reaction catalysed by AGAT in the kidney yields either homoarginine (hArg) or creatine precursor guanidinoacetate (GAA), which is transported through the bloodstream to the liver and pancreas, where it is further converted to Cr by GAMT. Next, Cr is released into the bloodstream and transported to the organs of utilization, where the Cr transporter takes it up. In the cell, mitochondrial CK (mtCK), localized in the intermembrane space of mitochondria, catalyses the transfer of phosphoryl group from ATP produced by oxidative phosphorylation (OXPhos) to Cr, forming ADP and PCr. PCr diffuses to sites of energy utilization, where it is used by cytosolic CK (MM-CK) to regenerate ATP from ADP, liberated from ATP hydrolysis by ATPases. Released Cr diffuses back to the mitochondria. PCr/Cr shuttle is conducted in parallel with a direct diffusional exchange of ADP and ATP.

CK is mainly expressed at prominent levels in cells with high and fluctuating energy demands, such as skeletal, cardiac and brain cells. Furthermore, it is expressed at significant levels in smooth muscle, kidney, retina photoreceptor cells, spermatozoa and sensory hair cells of the inner ear (Wallimann et al. 1992; Saks et al. 2007). There are four genes for CK found in vertebrate tissues, which are named according to the tissue in which they were first identified: two cytosolic forms, muscle-type CK (M-CK) and brain-type CK (B-CK), and two mitochondrial forms (mtCK), sarcomeric mtCK (smtCK) expressed mainly in striated muscle tissue (skeletal and heart) and ubiquitous mtCK (umtCK) expressed in the rest of the tissues (Wallimann et al., 1992; Wyss et al., 1992).

In vivo, cytosolic M-CK and B-CK subunits combine into homo- or hetero-dimers, forming MM-CK, BB-CK and MB-CK isoenzymes. Whereas MM-CK is rather specific in differentiated skeletal muscles, BB-CK is widely distributed in the brain and many other tissues, and MM-, MB-, and BB-CK are found in the heart (Wallimann et al., 2011). Both mtCK isoforms form homodimers and homooctamers but usually exist as octamers. MM-CK is either free in the cytoplasm, or exists as a structural protein of the myofilaments functionally coupled to myosin-ATPases (Wallimann et al., 1984; Hornemann et al., 2000), or is firmly bound near and functionally coupled to Na^+-K^+-ATPase (NKA) (Grosse et al., 1980), Ca^{2+}-ATPase SERCA (Rossi et al., 1990; Minajeva et al., 1996; Ventura-Clapier et al., 1998), and ATP-sensitive K^+ channel (Crawford et al., 2002) (Figure 1). The functional coupling of CK with ATPases maintains a high local ATP/ADP ratio near the sites of energy consumption. Thus, CK acts as a temporal energy buffer, regenerating ATP from PCr and ADP and providing an efficient energy supply for contraction and Ca^{2+} uptake (Veksler et al., 1997; De Sousa E. et al., 1999). Moreover, CK maintains phosphorylation potential at a sufficient level, preventing an increase in ADP level near ATPases. MtCK is localised in the intermembrane space of mitochondria and interacts with voltage dependent anion carrier (VDAC) in the mitochondrial outer membrane (MOM) and adenine nucleotide translocase (ANT) in the mitochondrial inner membrane. The functional coupling of mtCK and ANT helps to maintain a low ATP/ADP level near the sites of energy production, where it catalyses the transfer of phosphate from ATP to Cr, and regenerated ADP is used to stimulate mitochondrial oxidative phosphorylation (Wallimann et al., 1992; Vendelin et al., 2004).

In addition to temporal buffering function, CK was suggested to function as a spatial buffering system providing energy transfer through PCr/Cr shuttle, where no net consumption of high-energy phosphoryls occurs (Bessman and Geiger, 1981). In this shuttle, the CK system facilitates the diffusion of ATP and ADP between ATPases and mitochondria, forming a parallel energy circuit with PCr and Cr (Figure 3). The speed of diffusion of metabolites in solution depends on the absolute difference in their concentrations and diffusion coefficient. Since PCr and Cr are smaller molecules than ADP and ATP, they diffuse faster (Meyer et al., 1984). Moreover, due to the fast CK reaction rate and high equilibrium constant $K_{CK} = \frac{[Cr][ATP]}{[PCr][ADP]} = 166$ (Lawson and Veech, 1979), even a small change in ADP concentration leads to a greater change in Cr concentration, amplifying the ADP signal. In this way, due to the larger diffusion coefficient and concentration gradient, Cr diffuses faster than ADP from ATPases to mitochondria.

Since the discovery of the PCr/Cr shuttle, the importance of CK system as an energy transfer system, especially in the heart, has been the subject of discussion (Bessman and Carpenter, 1985; Wallimann et al., 1992; Saks et al., 1994; Joubert et al., 2002; Dzeja and Terzic, 2003). For instance, Meyer et al. proposed that energy transfer catalysed by CK is just a consequence of the CK reaction and that it is not vital in cardiac muscle, where diffusion distances are small. That means that CK is mainly important in the heart as a temporal energy buffer, regenerating ATP when energy consumption exceeds energy production. Furthermore, the temporal and spatial buffering functions of the CK system are actually very closely connected and cannot be considered separately (Meyer et al., 1984). In addition, the modelling results of NMR measurements on perfused rat hearts proposed that, under normal conditions, both ATP/ADP and PCr/Cr diffusion could contribute to energy transfer between energy production and utilization sites. However, at increased workloads, CK-mediated transfer could be bypassed by direct ATP transport (Vendelin et al., 2010).

1.3 The role of intracellular compartmentation in energy transfer

In the heart, where the fast energy transfer is of great importance in matching energy demand with supply, the diffusion of ADP and ATP is restricted by diffusion barriers, localised mainly at the level of MOM or in the cytosol, and composed of physical membrane structures and protein-dense domains in myofilaments (Birkedal et al., 2014). Although these barriers' exact location and identity are still uncertain, the primary candidates are SR and MOM. The membrane structures within the cell, represented by SR, mitochondria, and t-tubules, together with myofibrils, form intracellular compartments, known as modules or intracellular energetic units (Saks et al., 2001) with local concentration of ATP, ADP and P_i. Thereby, the location of diffusion barriers plays a role in defining whether they promote or restrict diffusion. In comparison to the slower overall diffusion across numerous compartments, the shorter diffusion distances within the modules lead to faster diffusion of the molecules and hence faster energy transfer. It was suggested that the CK system plays a pivotal role in overcoming diffusion obstacles at the level of MOM within each separate module by facilitating energy transfer between mitochondria and ATPases (Saks et al., 1993). Therefore, the CK system as a spatial energy buffer could be important in the tissues, where diffusion of ATP/ADP is restricted, or, in the cells with longer diffusion distances, as in polar cells such as spermatozoa, retina photoreceptor cells, etc. (Wallimann et al., 2011). Knowing precisely which intracellular structures represent diffusion barriers and where they are located will improve our understanding of the functional role of the CK system in regulating energy metabolism.

In this thesis, the overall aim was to study how the absence of a functional CK system affects cardiomyocyte function and, from that, to learn more about the role of CK in the heart.

2 The role of creatine kinase and other phosphotransfer systems in the heart

2.1 Animal models with altered creatine kinase system

To gain a deeper insight into the role of CK-catalysed reactions in regulating cardiac energy homeostasis, pharmacological and genetic techniques have been employed to modify the CK system functioning in various research models.

2.1.1 Pharmacological inhibition

One of the pharmacological inhibition studies includes the usage of iodoacetamide (IA), an alkylating agent that precludes the formation of disulphide bonds, causing a fast and irreversible inhibition of the CK enzyme activity (Hamman et al., 1995; Tian and Ingwall, 1996). IA is highly toxic and could be used only for acute *ex vivo* experiments (Lygate and Neubauer, 2014). In addition, IA has been shown to inhibit glyceraldehyde-3-phosphate dehydrogenase (GAPDH) (Fossel and Hoefeler, 1987). Thus, its limiting effect on glycolysis cannot be entirely excluded, although, in one paper, an unchanged myocardial glycolytic rate was reported in the presence of IA (Tian et al., 1997). Moreover, as IA inhibits equally all CK isoforms, it gives limited insight into the characteristic impact of different CK isoforms colocalised with various intracellular structures. The effect of acute inhibition of CK activity was minimal under basal conditions, showing normal cardiac performance, and the suppression of cardiac contractile reserve was only observed under stress conditions (high workload) (Hamman et al., 1995; Tian and Ingwall, 1996; Ren et al., 2009).

Another approach to chemical inhibition involves the usage of beta-guanidinopropionic acid (β-GPA), a creatine analogue that competes with Cr for cellular uptake by CrT (Oudman et al., 2013), leading to a reduction in Cr. Although CK can phosphorylate β-GPA, it is a poor substrate for mitochondrial CK. The effect of β-GPA is prolonged and becomes discernible only over time, resulting in variable and incomplete Cr depletion, leading to the reduction of the body weight and inducing various metabolic adaptations [reviewed in (Wyss and Kaddurah-Daouk, 2000; Oudman et al., 2013)]. In skeletal muscle, β-GPA treatment leads to increased aerobic capacity and diminished glycolytic potential. In contrast, in the hearts of Cr-depleted rats, the changes in metabolic regulation and the reduction of myocardial contractility were minimal. However, rat hearts exhibit significant hypertrophy as a complication of chronic β-GPA treatment (Mekhfi et al., 1990; Clark et al., 1994). Therefore, due to the limitations and side effects of this technique, the corresponding studies reported variable results. In all studies, the apparent impact of CK deficiency came into view mainly at higher workloads.

2.1.2 Genetically modified animal models

The development in the field of genetically manipulated animal models led to the generation of mouse models lacking various components of the CK system. First, mice deficient in different CK isoforms such as muscle isoform or M-CK KO (van Deursen et al., 1993), sarcomeric mitochondrial isoform or mtCK KO (Steeghs et al., 1997b), and both muscle and mitochondrial CK isoforms or CK KO (Steeghs et al., 1997a), were generated. Later, creatine-deficient mouse models lacking either one of the Cr synthesis enzymes, GAMT KO (Schmidt et al., 2004) and AGAT KO (Choe et al., 2013b), or Cr transporter, CrT KO (Skelton et al., 2011; Stockebrand et al., 2018), were created. Compared to

pharmacologically inhibited models, transgenic mouse models were expected to render a greater specificity and a more thorough CK system obstruction.

The mouse knockout models for all muscle CK isoforms have been created and extensively investigated during the last 30 years (starting from the early 90s). Surprisingly, given the assumed pivotal significance of the CK system in regulating energy homeostasis, the CK KO mice were viable and normal in appearance. The findings of the studies on their cardiac phenotype were quite variable between different groups, some demonstrating the prevalence of functional alterations and adaptations in CK KO mice (Boehm et al., 2000; Kaasik et al., 2001; Nahrendorf et al., 2005), others showing more prominent changes in cardiac energetics (Saupe et al., 1998, 2000). Nevertheless, the energetics of CK KO mice was significantly altered, revealing the increase in ADP concentration and decrease in free energy released from ATP hydrolysis during high workload (Saupe et al., 1998), as well as lower PCr levels and ATP synthesis rate (Saupe et al., 2000). The basal cardiac performance of these animals was normal, showing minor impairments caused by the absence of a functional CK system (Nahrendorf et al., 2006).

Some previously published works using CK KO or mtCK KO mice reported rather contradictory results, showing either the presence (Kaasik et al., 2001; Gustafson and van Beek, 2002; Spindler et al., 2002; Nahrendorf et al., 2005, 2006) or the absence (Saupe et al., 1998; Bonz et al., 2002; Spindler et al., 2004) of cardiac hypertrophy in mice on a mixed genetic background (C57BL/6 and 129/Sv). In the study using mtCK KO mice on a pure C57BL/6 background, no LV hypertrophy was detected (Lygate et al., 2009). Moreover, compensatory adaptations that were not observed previously, such as increased MM-CK activity and mitochondrial content, were presented. Therefore, the disparity between the earlier studies could be explained in part by using the mice on a mixed genetic background and unrelated C57BL/6 as controls (non-littermate controls). Later, the same group showed that appropriate genetic background and concomitant genetic drift, together with gender and age, are crucial in developing congestive heart failure in CK KO, as only ageing males on mixed background developed LV hypertrophy contractile dysfunction (Lygate et al., 2012b).

2.1.3 Creatine-deficient mouse models

Alternative mouse models with a modified CK system are Cr-deficient mice (AGAT KO, GAMT KO, CrT KO). In the current PhD thesis, two of them were used, both lacking one of the enzymes that participate in Cr synthesis, either L-arginine:glycine amidinotransferase (AGAT) or guanidinoacetate *N*-methyltranferase (GAMT), that results in their whole-body Cr and PCr deficiency (Schmidt et al., 2004; Choe et al., 2013b). These animal models are remarkable since intracellular CK expression stays intact and CK reaction is inactive through the absence of Cr.

The basal cardiac function and structure of GAMT KO were minimally disturbed under baseline conditions and stayed normal up to 1 year of age (Hove et al., 2005; Schneider et al., 2008). For instance, cardiac hypertrophy was absent, the ejection fraction was normal, and only LV systolic pressure was slightly lower. However, in the recent research conducted by Lygate group, when cardiac function and metabolic profile were studied in over 1-year-old GAMT KO mice, the development of GAMT KO phenotype with age was demonstrated (Aksentijević et al., 2020). It was the first study to show adaptational changes, such as a decline in cardiac function and mitochondrial volume, caused by prolonged creatine-deficiency and GAA accumulation in GAMT KO hearts. As hemodynamic modifications, such as lower heart rate and left ventricular (LV) systolic pressure, and

slower pressure generation and relaxation were not related to heart failure, it was proposed that compensatory adaptations are adjusted in response to reduced energy demand in ageing GAMT KO mice.

Although GAMT mice lack Cr, they accumulate the creatine precursor guanidinoacetate (GAA), which can be phosphorylated by CK to phospho-guanidinoacetate (P-GAA) and used instead of PCr. It was established that P-GAA could compensate to some extent for the lack of PCr in skeletal muscle during acute ischaemia (Kan et al., 2004; Hove et al., 2005), but it was not enough to support the recovery after reperfusion (Hove et al. 2005). The participation of GAA in phosphotransfer via CK was previously thought to be negligible, as CK reaction rate was 100-fold lower with P-GAA than with Cr when measured *in vitro* (Boehm et al., 1996). Moreover, as mtCK does not react with GAA, it cannot be used instead of Cr in energy transfer across MOM. These results were complemented with *in vivo* measurements of CK reaction velocity, where ATP synthesis from P-GAA was undetectable (Lygate et al., 2013). Furthermore, there could be some adverse effects caused by GAA accumulation associated with ageing (Aksentijević et al., 2020) or similar to those observed in rat brain, leading to Na^+/K^+ pump inhibition or reduction of glutamate uptake and antioxidant capacity (Zugno et al., 2003, 2007, 2008). Although seizures have not been reported in the GAMT KO mice (Rossi et al., 2021), Schulze et al. demonstrated abnormal electrical rhythms in the brain of young GAMT KO compared to WT, pointing to an electrical seizure activity that was reduced in response to GAA lowering (Schulze et al., 2016). GAMT KO animals from the mouse colony kept in our animal facility experience seizures, usually starting from around one year of age (personal observations; unpublished). Therefore, when studying cardiac function in ageing GAMT KO mice, the effect of epileptic seizures on whole body metabolism cannot be excluded.

AGAT is the first enzyme in Cr biosynthesis pathway that catalyses GAA formation. Therefore AGAT KO, considered a pure creatine-deficiency mouse model, does not accumulate GAA (Choe et al., 2013b). However, AGAT KO have low levels of homoarginine (hArg) (Figure 3)(Choe et al., 2013a), another AGAT product and an indicator for cardiac disease and stroke outcome (März et al., 2010; Pilz et al., 2011). Due to creatine-deficiency, AGAT KO mice exhibited reduced ATP and elevated P_i levels, leading to chronic activation of adenosine monophosphate (AMP)-activated protein kinase (AMPK) in skeletal muscle, liver and adipose tissue, but not in cardiac muscles (Choe et al., 2013b; Faller et al., 2018). AMPK is a metabolic energy sensor associated with cardioprotection and stress adaptation, which is activated by AMP under low energy conditions (energetic stress) (Pucar et al., 2004; Dolinsky and Dyck, 2006). In addition, enhanced glucose tolerance, reduced lipid accumulation, and protection from metabolic syndrome were demonstrated in AGAT KO mice (Choe et al., 2013b). The activation of AMPK leads to a shift in the overall metabolism of AGAT KO mice to a catabolic state, inducing upregulation of ATP-generating pathways and inhibition of ATP-consuming processes (Choe et al., 2013b). That was also confirmed by different alterations in metabolic gene expression found in skeletal muscles of AGAT KO (Stockebrand et al., 2016).

Knockout of the creatine transporter (CrT) results in a third model of creatine-deficiency. The outcomes of studies using different CrT KO mouse models were sometimes contradictory, showing, for instance, variable residual Cr levels in the heart, and were focused mainly on brain function (Skelton et al., 2011; Baroncelli et al., 2014; Wawro et al., 2021). Moreover, cardiac phenotype has not been reported for any CrT KO mouse models. Detailed characterization of Cr loss effect on skeletal muscle by Stockebrand

et al. revealed that the muscular phenotype of CrT KO resembled that of AGAT KO (Nabuurs et al., 2013). They detected lower muscle strength, severe muscle atrophy and similar metabolic changes, such as reduced PCr and ATP levels and increased glucose tolerance, leading to AMPK activation (Stockebrand et al., 2018).

Both CK KO and creatine-deficient mouse models exhibit a similar shift of the skeletal muscles towards a more aerobic metabolism. That is expressed in elevated mitochondrial volume and increased activity of citrate synthase and cytochrome oxidase, markers of mitochondrial volume density and aerobic capacity, respectively (van Deursen et al., 1993; Steeghs et al., 1997a; Schmidt et al., 2004; Nabuurs et al., 2013; Barsunova et al., 2020). In contrast to CK KO models having normal body weight (Momken et al., 2005), creatine-deficient mouse models (GAMT, AGAT KO), with their muscle atrophy and lower body weight, show a more severe phenotype. Although both GAMT and AGAT KO are deprived of Cr, GAMT KO phenotype (Schmidt et al., 2004) is generally milder than the AGAT KO phenotype (Nabuurs et al., 2013). For instance, muscle atrophy and changes in the activities of marker enzymes of muscle phenotype were more prominent in AGAT than in GAMT KO mice (Barsunova et al., 2020). The muscle phenotype differences between AGAT and GAMT KO could be explained, as noted above, by the fact that P-GAA can partially substitute for PCr in GAMT KO mice, albeit with lower efficiency (Boehm et al., 1996; Kan et al., 2004; Hove et al., 2005; Balestrino and Adriano, 2020; Sasani et al., 2020).

2.1.4 Limitations associated with use of AGAT KO mice

When studying the cardiac function of AGAT KO mice, it should be considered that since Cr is synthesized in the liver and transported to the organs for utilization by the circulatory system, it is absent in the whole body of creatine-deficient mice. Therefore, the effect of systemic changes and adaptations in whole body signalling on phenotype occurring during the development due to creatine-deficiency cannot be excluded. These modifications activate and maintain the subsequent structural and functional reorganization of the heart (Taegtmeyer et al., 2005). Functional remodelling includes alterations in the expression of various metabolic genes detected in skeletal muscle, brain and heart of AGAT KO mice (Stockebrand et al., 2016; Jensen et al., 2020b, 2020a). In the skeletal muscles of AGAT KO mice, chronic activation of AMPK leads to the shift in metabolic signalling by downregulation of anabolic or energy-requiring pathways and stimulation of catabolic or energy-saving and -producing pathways (Choe et al., 2013b). In addition to the skeletal muscle, fat and liver, decreased Cr levels in the brain of AGAT KO mice lead to elevated phosphorylation of AMPK (Choe et al., 2013b), and hence, its upregulation in the hypothalamus, which is known for its essential regulatory role on the whole-body metabolism (Liu et al., 2021). Therefore, it remains unclear whether the absence of a functional CK system is directly responsible for adaptational changes revealed in AGAT KO mice or other internal systemic stimuli could have caused these modifications.

2.2 The impact of creatine kinase system impairment on cardiac function under stress conditions

Under acute myocardial stress conditions, either due to ischemia or an increase in cardiac work, the cardiac function of CK, as well as GAMT KO, was compromised, showing limited contractile reserve and reduced functional recovery from ischemia-reperfusion (I-R) injury (Crozatier et al., 2002; Spindler et al., 2004). However, the response to chronic

myocardial infarction (MI) represented by survival, *in vivo* cardiac function, and LV structural remodelling, were unchanged in both GAMT KO (Lygate et al., 2013) and CK KO (Nahrendorf et al., 2005, 2006), when compared to corresponding WT controls. Besides, the maximal exercise capacity of GAMT KO mice was similar to their wild-type littermates (Lygate et al., 2013). Thereby, it was suggested that deprivation of both CK and Cr do not aggravate contractile dysfunction in heart failure. In contrast, experiments using rats deprived of Cr with β-GPA before MI demonstrated 93-100% (Horn et al., 2001; Lorentzon et al., 2007) of animal mortality within 24-hours. Species differences could partly explain this discrepancy since rats were predisposed to increased ventricular arrhythmia after MI (Lygate, 2006; Lorentzon et al., 2007). The authors of the mouse studies tried to exclude off-target effects of β-GPA, showing unchanged animal mortality between control and KO groups when they received β-GPA instantly before and after MI (Lygate et al., 2013). However, since the effect of β-GPA depends on the duration of the treatment, these results are unconvincing due to the short duration of β-GPA administration. Therefore, the potential side effects of β-GPA treatment should be still taken into consideration. However, since β-GPA has multiple targets in the living organism and is not specific only to the CK system, sometimes it could be difficult to distinguish between confounding side effects and effects associated only with energy starvation induced by β-GPA treatment (Wyss and Kaddurah-Daouk, 2000). On the other hand, when rats were fed with β-GPA after MI, decreased levels of ATP and Cr, but unchanged mortality was detected (Horn et al., 2001), suggesting in agreement with GAMT KO (Lygate et al., 2013), that prolonged creatine-deficiency is not crucial in the progression of heart failure.

Overall, despite the previously acknowledged determinative role of the CK system in the regulation of myocardial metabolism and progression of heart failure, CK KO and creatine-deficient models, as well as β-GPA treated animals, demonstrated that impairment of the CK system is, for the most part, not detrimental, as there are no changes in basal cardiac function or the progression of heart failure. In contrast, augmentation of the CK system due to overexpression of M-CK or mtCK was shown to have protective effects, such as improved cardiac contractile function and viability, against induced heart failure (Akki et al., 2012; Gupta et al., 2012; Whittington et al., 2018). However, studies using other models of CK system augmentation, Cr transporter overexpression (CrTOE), exhibited discrepant results (Wallis et al., 2005). Surprisingly, very high levels of Cr were demonstrated to be disadvantageous and lead to progressive cardiac dysfunction (Wallis et al., 2005; Phillips et al., 2010), while a moderate increase in creatine level, although not beneficial in chronic heart failure, protected CrTOE mice from acute myocardial infarction by reducing their susceptibility to cardiac I-R injury (Lygate et al., 2012a).

2.3 Ultrastructural organization and mitochondrial respiration in creatine kinase and GAMT KO mice

Previous studies on mice lacking both cytosolic and mitochondrial CK isoforms revealed cytoarchitectural modifications and changes in the regulation of mitochondrial respiration in the heart (Kaasik et al., 2001). Namely, disorganization of mitochondrial and myofilament structures and higher apparent ADP affinity of respiration were detected in CK KO compared to WT. The changes in ultrastructure led to a reduction of the diffusion distances and promoted direct adenine nucleotide channelling between mitochondria and ATPases. This could at least partially explain the minimal changes in

cardiac performance revealed in CK KO mice (Nahrendorf et al., 2006). Thereby, in our study, **we aimed to determine whether similar compensatory changes could be detected in GAMT KO (Publication I**) (Schmidt et al., 2004).

In GAMT KO, no adaptations neither in the mitochondrial organization nor in the regulation of mitochondrial respiration and intracellular compartmentation were detected in this study (**Publication I**). Besides, unchanged diffusion across MOM, suggested by mathematical modelling, points to a minor role of mtCK in promoting energy transfer across mitochondrial membranes. The findings from Lygate's group complemented these results, showing unchanged adenylate kinase activity and mitochondrial respiration in GAMT KO in comparison to WT (Lygate et al., 2013), as well as unchanged regulation of mitochondrial respiration in ageing GAMT KO (Aksentijević et al., 2020). The discrepancy between our findings and results from CK KO mice could be again explained by differences in genetic background, the same way as it was previously reported for CK KO and mtCK KO. In addition, it is still unclear how much GAA is involved in CK-catalysed reactions, so its compensatory role as an energy source cannot be excluded, even though the flux of CK reaction is much lower when GAA is used instead of Cr (Boehm et al., 1996).

2.4 Role of alternative phosphotransfer systems in energy transfer

Apart from the CK system, the major phosphotransfer system, cardiomyocytes have other energy transfer systems implicated in the regulation of cellular bioenergetics, such as adenylate kinase (AK) and glycolytic enzymes (Dzeja and Terzic, 2003). These systems can at least partially compensate for each other by facilitating the diffusion of ATP and ADP between energy generation and utilization sites. This is possible due to close intracellular localization and interaction of CK, AK, and glycolytic systems. The involvement and contribution of each phosphotransfer enzyme vary between species, tissues, developmental levels, and physiological conditions (Dzeja et al., 1998; Neumann et al., 2003; Dzeja and Terzic, 2007). CK, AK and glycolytic enzymes also play a role in the regulation of ATP-sensitive K^+ channel activity, one of the membrane metabolic sensors that couples cellular metabolism to membrane potential and regulates cardioprotection, ensuring the proper functioning of cardiomyocytes and contributing to the maintenance of cellular homeostasis (Dzeja and Terzic, 1998; Abraham et al., 2002). Moreover, the potential compensatory role for AK and glycolytic enzymes was demonstrated by their upregulation in the hearts (Dzeja et al., 2011) of CK KO mice. In line with these findings, the increasing role of glycolytic enzymes as an alternative phosphotransfer system was also shown in CK and AK double KO mice (Janssen et al., 2003).

AK is known as the second most important system after CK, that promotes high-energy phosphoryl flux by catalysing the reversible transfer of P_i between ATP, ADP and AMP (Dzeja et al., 1998; Dzeja and Terzic, 2009; Aksentijević et al., 2010), as well as takes part in the compartmentalization of adenine nucleotides (Gellerich, 1992; Laterveer et al., 1997). Although phosphotransfer catalysed by AK accounts only for ~ 1/10 of the total ATP turnover (Dzeja et al., 1999b), its significance increases in response to metabolic stress (Dzeja et al., 2007). For example, despite declined AK activity (Dzeja et al., 1999a), the contribution of AK to overall phosphotransfer flux was elevated in dog hearts with induced heart failure (Dzeja et al., 1999b). Although unchanged AK activity was reported in another study using two different mouse models of chronic heart failure, it was suggested that AK contribution to the overall phosphotransfer was still increased in response to depressed CK function (Aksentijević et al., 2010). Considering the assumed

importance of AK in the regulation of energy homeostasis in response to metabolic stress, it was surprising that AK-overexpressing mice exhibited a decline in baseline cardiac function and changes in metabolic profile and absence of anticipated cardioprotective effect (Zervou et al., 2021). Thus, it was proposed that AK's role in the regulation of basic myocardial homeostasis is more specific than just a response to stress.

The glycolytic enzymes, such as hexokinase (HK) and pyruvate kinase (PK), as well as GAPDH and phosphoglycerate kinase, represent another system that facilitates energy transfer and distribution of high-energy phosphates between mitochondria and ATPases (Dzeja and Terzic, 2003; Dzeja et al., 2007; Chung et al., 2010). For instance, in rabbit cardiac and skeletal muscles, the glycolytic enzymes were colocalized with SR and functionally coupled to SERCA-ATPase, providing it with the energy needed for Ca^{2+} loading (Xu et al., 1995; Xu and Becker, 1998). In addition, in CK KO mice, impaired SR Ca^{2+} uptake was rescued by the glycolytic system, ensuring SERCA with energy in the absence of CK, albeit only under baseline conditions (Boehm et al., 2000).

HK catalyses the first step of the glycolytic pathway by phosphorylating glucose to glucose-6-phosphate using ATP as a phosphoryl source. The intracellular localisation of the two main cardiac HK isoforms (HKI and HKII) is associated with the regulation of glucose metabolism (John et al., 2011). Mitochondrially bound HKI directs glucose to the glycolytic pathway, and HKII, due to its dynamic location, is related to glycogen synthesis when detached from mitochondria and located in the cytoplasm. HK associated with mitochondria is bound to the external part of the MOM through the VDAC-ANT complex (Beutner et al., 1996; Brdiczka et al., 2006). As already mentioned, mitochondrial CK also forms complexes with VDAC and ANT in the intermembrane space of mitochondria, but HK and CK cannot bind to the same contact site (Brdiczka et al., 2006). Therefore, HK competes with CK for VDAC-ANT interaction from the cytosolic side of the mitochondria. The formation of these mitochondrial contact sites between inner and outer mitochondrial membranes with CK or HK enables the direct channelling of ADP, formed in CK and HK-catalysed reactions, to the oxidative phosphorylation in the mitochondrial matrix (Gellerich et al., 1987). Thus, mitochondrial contact sites play a significant role in regulating mitochondrial energetics. Moreover, mitochondrially associated HK is involved in reactive oxygen species (ROS) production (da-Silva et al., 2004; Santiago et al., 2008) and inhibition of mitochondrial permeability transition pore (Beutner et al., 1996; Brdiczka et al., 2006), and hence regulation of cell death and apoptosis. All this points to a significant contribution of mitochondrial HK to cardioprotection (Zuurbier et al., 2009; Calmettes et al., 2015; Halestrap et al., 2015). Therefore, HK was chosen among other glycolytic enzymes for further investigation in the following study.

2.5 Changes in alternative phosphotransfer systems in AGAT and GAMT mouse cardiomyocytes

As we did not detect any adaptational changes due to inactivation of the CK system by GAMT deficiency in **Publication I**, **our second study, reported in Publication II, was undertaken to determine whether the expression, activity and mitochondrial association of AK and HK could be altered or upregulated in GAMT and AGAT KO mouse hearts.** Respective redistribution of energy fluxes via alternative phosphotransfer routes in the absence of an active CK system could rescue cardiac energetics by overcoming energetic shortage in mouse models deprived of Cr as was shown in CK KO mice. However, in contrast to CK KO (Dzeja et al., 2011), in GAMT mice, the activity,

expression and distribution of alternative phosphotransfer enzymes, presented by AK and HK, were similar in KO and WT (**Publication II**). In the same way, AK activity, expression and mitochondrial association were unchanged in AGAT KO (Figure 4).

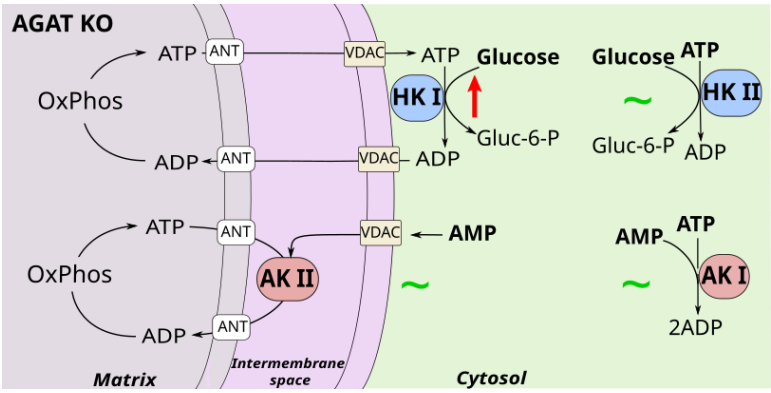

Figure 4. Alternative phosphotransfer pathways in AGAT KO mice. The alterations in the activity or subcellular localization of hexokinase (HK) or adenylate kinase (AK) as alternative phosphotransfer systems compensating for the lack of functioning CK system, studied in creatine-deficient mouse hearts. No change in the activities of cytosolic hexokinase (HK II) and both mitochondrial (AK II) and cytosolic (AK I) adenylate kinase isoforms is indicated by the green waves. Increased activity of mitochondrial hexokinase isoform (HK I) is indicated by the red arrow.

These results are consistent with the previous findings showing unchanged total AK activity in GAMT and AGAT KO (Lygate et al., 2013; Faller et al., 2018). Nevertheless, the elevation of AK activity during ageing was demonstrated in GAMT KO (Aksentijević et al., 2020). The only difference that was detected in **Publication II**, was the increased activity of HK in the mitochondrial fraction and accordingly elevated protein expression of mitochondrial HK isoform (HKI) in AGAT KO hearts (Figure 4). However, as the respiration rate stimulated by HK was lower in AGAT KO, it was proposed that this upregulation of HKI is unlikely to compensate for the lack of the active CK system as a spatial transfer buffer but rather could be important in mitochondrial regulation and ROS production.

The absence of adaptive upregulation of AK- and HK-catalysed phosphotransfer in creatine-deficient AGAT and GAMT hearts denotes that a substantial part of intracellular phosphoryl transfer is conducted by direct diffusion of adenine nucleotides. In line with this, measurements on the whole heart indicate that, under certain conditions, the energy transfer is more likely carried out through direct ATP/ADP diffusion than PCr/Cr (Vendelin et al., 2010). Furthermore, unchanged intracellular compartmentation, and hence, a conserved modular organization in GAMT KO mice (**Publication I**), speaks in favor of undisturbed energy transfer within the modules. Therefore, along with the absence of upregulation of alternative phosphotransfer systems in both GAMT and AGAT mice (**Publication II**), it is tempting to speculate that phosphotransfer systems are not crucial for energy transfer between ATP-generating and ATP-utilizing sites across the mitochondrial membrane in the mouse hearts at baseline. Together with high mitochondrial content, and thus high oxidative capacity of the heart muscle this could explain the relatively mild cardiac phenotype of AGAT and GAMT KO mice (Branovets et al., 2013; Lygate et al., 2013; Faller et al., 2018).

3 Creatine kinase and adenylate kinase activities in heart homogenates and permeabilized cardiomyocytes from mice and rats

For many years it has been believed that the ADP flux through CK exceeds the ADP flux through mitochondrial respiration by an order of magnitude. This consensus has emerged on the basis of studies on rat hearts. Furthermore, in previous works on rat cardiomyocytes, it was shown that the ADP flux through mitochondrially associated CK alone was sufficient to stimulate the mitochondrial respiration to its maximum (Gellerich and Saks, 1982; Guzun et al., 2009; Timohhina et al., 2009; Tepp et al., 2011). The mitochondrially associated CK is recorded by first stimulating respiration with ATP and creatine, so CK generates ADP that stimulates respiration. Then, a competitive ADP-trapping system consisting of phosphoenolpyruvate (PEP) and pyruvate kinase (PK) in excess is added. PK competes with mitochondrial respiration for ADP in solution so that respiration is stimulated only by ADP that is directly channelled from CK to mitochondria. In previous works on rat hearts (Guzun et al., 2009; Timohhina et al., 2009; Tepp et al., 2011), CK stimulated respiration to its maximal levels even in the presence of PEP and PK. Our results from **Publication II**, in which we studied mouse hearts, contradicted this consensus. When all CK was activated, the mitochondrial respiration was stimulated only to ~80% of its maximum. Thus, this was far from the finding that ADP generation by CK is 10 times faster than ADP consumption by mitochondria (Bittl and Ingwall, 1985; Ingwall, 2002). In addition, our results revealed that in the presence of PEP and PK, only ~25% of maximal respiration was supported by CK through direct ADP channelling to mitochondria (**Publication II**). Although the literature reported relatively similar CK activities in rat and mouse homogenates (Ventura-Clapier et al., 1998), this led to the speculation whether there might be a species difference between mice and rats in terms of CK capacity relative to the respiration and the fraction of mitochondrially associated CK.

Another interesting finding in **Publication II** was that AK activity seemed to be exclusively in the cytosol. This was in agreement with previous findings demonstrating a minimal AK activity in both rat and mouse heart mitochondria (Jacobus and Lehninger, 1973; Pucar et al., 2002; Noma, 2005). On the contrary, in another study, a strong functional coupling between AK and mitochondrial respiration was shown in rat hearts (Gellerich, 1992).

The study, summarized in Publication III, had two main aims. First, we wanted to find out whether there are any species-dependent differences between rat and mouse hearts concerning their total CK or AK activity and the capacity of CK or AK to stimulate mitochondrial respiration, either relative to the maximal respiration or through ADP channelling. Second, we wanted to understand how our previous results, showing the inability of CK to stimulate respiration to its maximal levels (Publication II), **could be compared with the findings in whole heart homogenates and in intact hearts.** In both mouse and rat hearts, the total enzyme activities of CK and AK were assessed in whole heart homogenates, and CK- or AK-stimulated respiration measurements were performed in permeabilized cardiomyocytes.

In **Publication III**, we found that ADP flux through CK was insufficient to maintain mitochondrial respiration at the maximum level in both rat and mouse hearts, although CK-stimulated respiration rate in relation to the maximal respiration rate (V_{CK}/V_{max}) was lower in mice than in rats (~75% and ~89%, respectively). This was consistent with our

previous results in mouse hearts in **Publication II**. In addition, we could not repeat the findings from other studies on rat hearts (Guzun et al., 2009; Timohhina et al., 2009; Tepp et al., 2011), showing unchanged CK-stimulated respiration rate in the presence of PEP and PK. On the contrary, and consistent with our recent findings in mouse hearts (**Publication II**), the respiration rates were decreased after the addition of PEP and PK in both rats and mice, with a smaller fraction of CK being inhibited in mouse compared to rat hearts.

An unexpected outcome of this study was that the CK and AK activities in homogenates and permeabilized cardiomyocytes were not the same. In both mouse and rat hearts, the CK and AK activities were 2 and 9 times higher, respectively, in homogenates than in permeabilized cardiomyocytes (Figure 5). This could be explained by the different localized compartments in the intact intracellular milieu of cardiomyocytes, where the concentration of substrates and products is different from the rest of the cell and surrounding solution. Due to this compartmentation, the enzyme reaction is expected to be slowed down by the diffusion of substrates and products to and from the compartment.

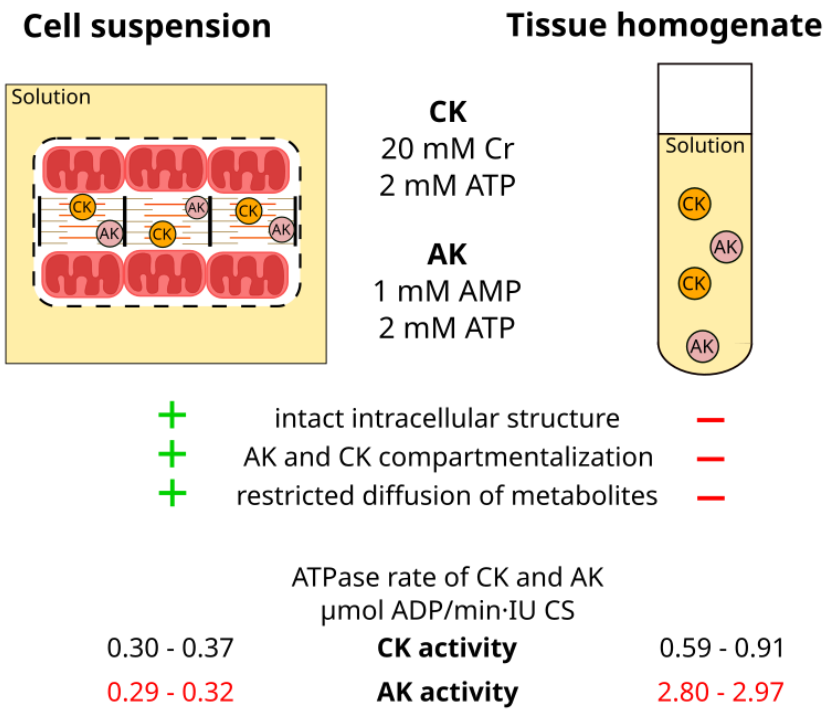

Figure 5. In cardiac preparations from both rats and mice, the activities of creatine kinase (CK) and, in particular, adenylate kinase (AK) are several times higher in homogenates compared to permeabilized cardiomyocytes. CK and AK activities were assessed by stimulating their ATPase rate with 2 mM ATP and 20 mM Cr, 2 mM ATP and 1 mM AMP, respectively. The presence or absence of intact intracellular structure, compartmentalization of the enzymes and restricted diffusion of metabolites is marked for each preparation, with green pluses and red minuses, respectively.

Intracellular compartmentation has been noticed in cardiomyocytes while studying different processes. Cytosolic Ca^{2+} environments, visualized with Ca^{2+} -sensitive fluorescent dyes (Wang et al., 2004), are of great importance in regulating EC coupling (Rios and Stern, 1997). Besides, mitochondrial Ca^{2+}-uptake through MCU is also facilitated by local areas with elevated Ca^{2+} concentrations (local Ca^{2+} microdomains) due to a close association of mitochondria and SR Ca^{2+} release sites (Franzini-Armstrong, 2007; Williams et al., 2013). Recent findings suggest an increasing role for the VDAC in the coordination of SR Ca^{2+} release and mitochondrial Ca^{2+}-uptake (Rosencrans et al., 2021; Sander et al., 2021). Furthermore, the modulation of cyclic AMP (cAMP) signalling by local compartments is another example of the role of local microenvironments in cardiomyocytes (Kritzer et al., 2012; Mika et al., 2012). For instance, the membrane barriers such as the t-tubular network or caveolae (smaller invagination of plasma membrane) ensure closer physical proximity of cAMP with its diverse subcellular targets. Therefore, caution should be taken while extrapolating the results received from different processed preparations to the situation *in vivo*, as intracellular integrity and structural and metabolic compartmentalization are of great importance in maintaining the metabolic homeostasis of the heart.

In summary, in **Publication III,** we were unable to reproduce data from other groups, and we showed that the ADP flux through CK does not exceed the ADP flux through mitochondrial respiration neither in rat nor mouse hearts. Thus, these results challenge the consensus that the CK flux capacity is 10 times higher than the respiration flux capacity. This may also explain why we observed relatively few adaptations in the ATP-generating mitochondria in creatine-deficient mice (**Publications I and II**). In contrast, more changes were detected at the ATP-consuming sites, i.e. the ATPases responsible for Ca^{2+} handling and contraction of the heart. These changes will be described in the following chapter.

4 Calcium handling in mouse models with altered creatine kinase system

4.1 The interplay between creatine kinase and excitation-contraction coupling systems

The ATPases involved in EC coupling, such as myosin-ATPase, SERCA and Na^+/K^+-ATPase are the main energy consumers in the heart. After ATP is generated in the mitochondria, it diffuses to the sites of ATP utilization, where it is hydrolysed and released energy is used by these ATPases to drive the EC coupling machinery (contraction, Ca^{2+} reuptake to SR, ion homeostasis) (Figure 1).

As described above (section 1.1), Ca^{2+} is an important regulator of different cellular functions. Since Ca^{2+} regulates ATP production by mitochondria as well as muscle contraction and thus ATP consumption by ATPases, a close interplay between Ca^{2+} dynamics and mitochondrial bioenergetics is essential for proper cardiac functioning. Moreover, CK is coupled with the main ATP-utilizing ATPases involved in the EC coupling mechanism and is structurally associated with the corresponding cellular structures (Wallimann et al., 1992; Ventura-Clapier et al., 1998). Together with CK's role in regulating ATP-sensitive K-channel activity (Abraham et al., 2002), it points to a close interconnection between CK and EC coupling systems. To better understand this mutual relationship, the influence of an altered CK system on Ca^{2+} homeostasis and EC coupling was studied in hearts of CK KO mouse models (Bonz et al., 2002; Crozatier et al., 2002; Spindler et al., 2004). In one of the studies, the absence of CK-catalysed energy transfer was proposed to be compensated by glycolytic pathways and tight interaction between mitochondria and SR, allowing normal ventricular function at a basal level. However, impaired contractile response to beta-adrenergic stimulation emerged both *in vivo* and *in vitro* in skinned fibres and isolated cardiomyocytes (Crozatier et al., 2002). These results were complemented by Spindler et al., showing the association of disturbed Ca^{2+} homeostasis with impaired recovery from I-R injury under acute energy demand conditions in CK KO mice (Spindler et al., 2004). In creatine-deficient GAMT KO mice, cardiac phenotype seems to be similar to CK KO, showing normal cardiac performance at baseline, but blunted response to beta-adrenergic stimulation (Hove et al., 2005). However, AGAT KO mice, considered a pure creatine-deficiency mouse model, lacking both Cr and hArg, exhibit slower contractility already at baseline (Faller et al., 2018).

While there is a possible interaction between creatine-deficiency and EC coupling, EC coupling and Ca^{2+} handling, in particular, have not been previously systematically studied in the creatine-deficient heart. The research performed in this thesis addresses this gap.

4.2 Calcium handling in patch clamped AGAT KO cardiomyocytes

Our next study, presented in **Publication IV**, **was conducted to assess whether alterations in Ca^{2+} handling could explain the impaired contractility of AGAT KO hearts** (Faller et al., 2018). In this study, experimental results from electrophysiological measurements on isolated cardiomyocytes from AGAT KO and WT mice were complemented with analysis using mathematical modelling to assess whether Ca^{2+} handling is modified (**Publication IV**). As a result, an overall decrease in Ca^{2+} dynamics, such as diminished Ca^{2+} influx through LTTC, decreased LTCC inactivation, and slower Ca^{2+} transient decay, was reported. In addition, diminished Ca^{2+} transfer between subspace

and cytosol was predicted by mathematical modelling (Figure 6). The protein expression of LTCC and SERCA was unchanged in AGAT KO compared to WT. Finally, impaired Ca^{2+} handling was fully recovered by lifelong dietary Cr supplementation.

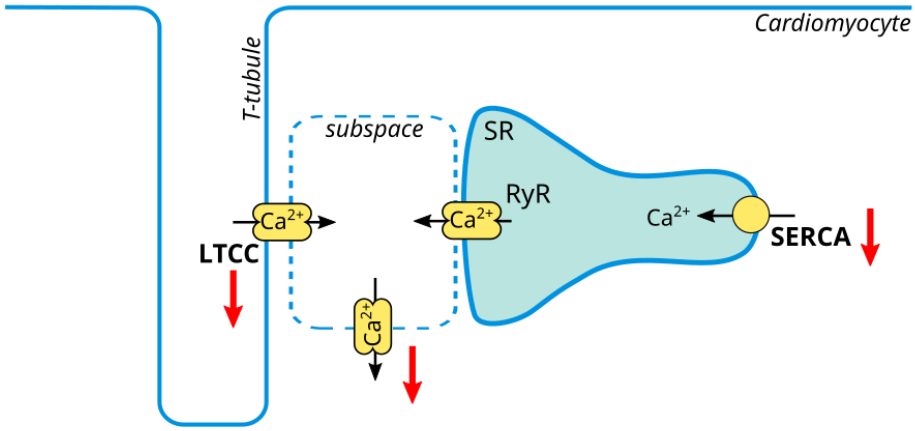

Figure 6. Altered Ca^{2+} handling in patch clamped cardiomyocytes of AGAT KO. Reduced Ca^{2+} influx through LTCC, Ca^{2+} transfer between dyadic space and cytosol, and Ca^{2+} efflux through SERCA are marked with red arrows.

In this work, the whole cell patch clamp technique was used. After attachment of the pipette to and rupture of the cell membrane, the pipette solution was equilibrated with the intracellular environment of the cell. Therefore, due to the presence of PCr in the patch pipette solution for all experimental groups (control, KO, and KO+Cr) and essentially unchanged CK activity reported previously in AGAT KO hearts (Faller et al., 2018), long-term modifications in Ca^{2+} handling independent of CK-catalysed phosphotransfer were studied. That means that the activity, expression and regulation of proteins related to EC coupling were mainly accountable for corresponding changes in Ca^{2+} cycling.

In **Publication IV**, the slower LTCC inactivation in AGAT KO was fully rescued by adrenergic stimulation, which could have increased Ca^{2+} release via RyR. In addition, Ca^{2+} transient decay time was also rescued, although only partially, by adrenergic stimulation. Therefore, together with the unchanged SERCA and LTCC total protein expression, the implication of regulatory modifications, such as phosphorylation level of Ca^{2+} handling proteins, was proposed to be involved in altered Ca^{2+} handling in AGAT KO. Phosphorylation of the proteins is a mechanism playing a key role in the regulation of multiple cellular processes. It could modify the activity, stability and intracellular localization of proteins associated with various signalling pathways in the cell. SR has a major role in managing Ca^{2+} cycling in cardiomyocytes, and precise regulation and interaction of RyR and SERCA functioning ensures a proper balance between Ca^{2+} release and uptake by SR. Thus, the protein expression and phosphorylation of RyR and SERCA regulatory protein PLB, the most studied so far, were the object of investigation in the following study.

To further study Ca^{2+} handling and EC coupling in creatine-deficient hearts, we performed experiments under conditions closer to physiological conditions using isolated cardiomyocytes from AGAT and GAMT KO mice. The results of this work are discussed in the following section.

4.3 Calcium handling and excitation-contraction coupling in creatine-deficient mouse cardiomyocytes under physiological conditions

Due to the changes in Ca^{2+} dynamics revealed in AGAT KO (**Publication IV**), in the following study, summarised from **Publication V**, additional experiments were performed on creatine-deficient mouse cardiomyocytes. **In this work, the impact of creatine-deficiency on EC coupling and Ca^{2+} handling proteins was assessed under conditions closer to those occurring *in vivo*.** Intact cells were field-stimulated, leading to an action potential generation, while in **Publication IV**, cell stimulation was performed via a patch pipette. In addition, in **Publication V**, Cr was absent in the AGAT and GAMT KO cardiomyocytes, as *in vivo* for these animal models. The main results from **Publication V** are summarized in Table 1 and discussed below.

4.3.1 Calcium-induced calcium release

Although smaller LTCC current was reported previously in AGAT KO (**Publication IV**), larger amplitude and longer duration of Ca^{2+} transients were detected in AGAT KO in comparison to WT. In the experimental setup used in **Publication IV**, the contribution of NCX operating in reverse mode (NCXrev) to Ca^{2+} cycling was minimal, which could explain similar amplitudes of Ca^{2+} transients in AGAT KO and WT. In contrast, in intact cell preparation used in **Publication V**, NCXrev could have had a more significant role in Ca^{2+} dynamics. An increase in Ca^{2+} influx via the reverse mode of NCX could be one of the reasons for the higher amplitude of Ca^{2+} transients in AGAT KO. However, it is still unclear whether it is only due to an adaptational increase in Ca^{2+} influx via the reverse mode of NCX or increased CICR triggered via NCX and LTCC. Therefore, different Ca^{2+} fluxes should be investigated further to elucidate their contribution to increased Ca^{2+} transient amplitude in AGAT KO compared to WT.

In addition to Ca^{2+} release via RyRs induced during EC coupling, local elementary Ca^{2+} events, Ca^{2+} sparks, could be spontaneously released from SR under unstimulated conditions (Cheng et al., 1993; Cheng and Lederer, 2008). In the same experimental setup as for Ca^{2+} transients, we recorded Ca^{2+} sparks at rest to check whether the frequency and temporal and spatial characteristics of individual Ca^{2+} events differed in creatine-deficient mouse cardiomyocytes and could explain changes in CICR proposed from patch clamp experiments. As a result, in **Publication V**, we found that the Ca^{2+} sparks were more frequent, longer, and wider in AGAT KO compared to WT (Table 1). Moreover, females exhibited more frequent sparks in all studied groups.

The supplementary measurements of RyR positioning that can affect Ca^{2+} release synchronicity and characteristics of the sparks showed unchanged RyR density in all groups and alterations in RyR arrangement due to creatine-deficiency only in AGAT KO females and not males when compared to corresponding WT. Thus, a higher number of RyR clusters, but smaller in size, were demonstrated in AGAT KO females (Table 1). In addition, the expression of the total protein and phosphorylated state of RyR were unchanged between AGAT KO and WT.

On the one hand, the modelling results from Sobie et al. study suggested that at lower local cytosolic Ca^{2+} concentrations, RyR clusters, depending on the regulation via coupled gating (Marx et al., 2001), have a lower opening probability than uncoupled individual RyRs (Sobie et al., 2006). The mutual regulation of RyR gating is associated with their highly packed organization in the clusters. Since cooperative gating was recognized *in vitro* in planar lipid bilayer experiments, it is still uncertain how it is actually regulated in intact cells (Cheng and Lederer, 2008). Nevertheless, it could be assumed that smaller RyR clusters, where coupling between RyRs is lower, are more likely to be activated. Thus, they could have a theoretically higher probability of Ca^{2+} release than bigger RyR clusters. This could have been one of the possibilities for the higher Ca^{2+} spark frequency, but only in AGAT KO females compared to WT. However, this assumption is inconsistent with the Ca^{2+} spark measurements in males, showing unchanged RyR cluster size but higher Ca^{2+} spark frequency in KO versus WT. Moreover, in another study, the dependency of higher spark frequency on bigger RyR cluster size was demonstrated (Galice et al., 2018). Again, part of the results from **Publication V** is in line with this finding, such as female WT, having larger RyR clusters, showed increased spark frequency than male WT. However, it cannot explain the differences arising due to creatine-deficiency. This inconsistency and lack of distinct correlation between changes in Ca^{2+} spark measurements and RyR arrangement point to the fact that other mechanisms could be involved.

One of the possible mechanisms would be that AGAT females are more sensitive to Ca^{2+} and tend to release Ca^{2+} more easily, explaining both higher Ca^{2+} release and higher Ca^{2+} spark frequency. Alternatively, on the basis of electrophysiological measurements and mathematical modelling, it was suggested that Ca^{2+} transfer between subsarcolemmal space (dyadic space) and cytosol is reduced (**Publication IV**). In **Publication IV**, LTCC current inactivation time was longer under control conditions and rescued by beta-adrenergic stimulation with isoprenaline (ISO) in AGAT KO compared to WT. Thus, the beta-adrenergic stimulation had a significantly larger effect in AGAT KO than in WT. In line with this finding, ISO treatment had a more significant effect on Ca^{2+} transient amplitude than under control conditions in both intact (**Publication V**) and patch clamped AGAT KO cardiomyocytes (**Publication IV**), as well as Ca^{2+} sparks were detected only in the presence of ISO (**Publication V**). Therefore, it was proposed that ISO treatment restrict Ca^{2+} diffusion from the dyadic space, leading to a higher Ca^{2+} concentration in dyadic space in AGAT KO and hence, to a larger Ca^{2+} transient amplitude. Similarly, the longer duration of Ca^{2+} sparks is not necessarily caused only by higher Ca^{2+} release via RyR, but also diffusion of Ca^{2+} matters. In this sense, longer and wider sparks could also be explained by the restricted diffusion of Ca^{2+} from dyadic space to cytosol.

Ca^{2+} release from SR via RyR is not regulated directly by ATPases, suggesting that adaptive changes to creatine-deficiency in the properties of Ca^{2+} sparks are not directly connected to the absence of energy transfer catalyzed by CK. However, intracellular Ca^{2+} signalling is implemented in a circuit, and all processes involved are still coupled to each other to a greater or lesser extent. Overall Ca^{2+} fluxes in the cell must be balanced on a beat-to-beat basis to avoid Ca^{2+} mishandling leading to contractile dysfunction (Eisner et al., 2017). Thus, the proposed increase in Ca^{2+} entering the cell in AGAT KO should be followed by a corresponding rise in Ca^{2+} removal.

To study further the regulation of Ca^{2+} release and explain the changes in properties of Ca^{2+} sparks and transients, we assessed the expression and phosphorylation of RyR. In line with unchanged overall RyR density, protein expression levels of total and phosphorylated forms of RyR were unaltered in AGAT KO and WT. The phosphorylation

of the RyR, mainly by PKA or CaMKII, is directly linked with its activity regulation. However, despite extensive research, the functional consequences of RyR phosphorylation remain highly debatable (George, 2008; Eschenhagen, 2010; Dobrev and Wehrens, 2014). Regardless of this controversy between different studies, the importance of RyR in the regulation of cardiac function under normal and pathophysiological conditions is undoubtable (Santulli and Marks, 2015; Santulli et al., 2017). Although we showed unaltered phosphorylation of RyR in AGAT KO, only one phosphorylation site, Ser2808, phosphorylated by PKA, was checked. Therefore, as RyR could be phosphorylated at multiple sites by different kinases, other targets for regulatory modifications in RyR activity are of interest for future studies.

Several sex-dependent changes in Ca^{2+} handling were revealed in AGAT KO cardiomyocytes. Using Ca^{2+} transient recordings, Ca^{2+} release synchronicity was assessed, showing higher systolic dyssynchrony of Ca^{2+} transients only in AGAT KO females and higher diastolic dyssynchrony in both females and males. During heart failure, the heterogeneity of Ca^{2+} release was previously associated with alterations in the t-tubular network (Louch et al., 2010; Frisk et al., 2016; Kolstad et al., 2018). We also looked at the t-tubular organization of cardiomyocytes from AGAT KO and WT. As a result, the t-tubular network was less branched and shorter in total length only in AGAT KO males (compared to WT littermates). In contrast to the reduction in transversal t-tubules in failing hearts, in AGAT KO, a decrease only in longitudinal t-tubules was detected. This could be the reason why changes in the t-tubular organization were not reflected in systolic dyssynchrony of Ca^{2+} transients in males.

In failing cardiomyocytes, dispersed RyR clusters were previously associated with increased dyssynchrony of Ca^{2+} transients (Kolstad et al., 2018). However, it was not the case in AGAT KO cardiomyocytes in **Publication V**. On the one hand, smaller RyR clusters in AGAT KO females were in line with higher systolic dyssynchrony of Ca^{2+} transients. On the other hand, the distribution of RyR clusters was similar in AGAT KO females and WT males. Therefore, in **Publication V**, neither changes in t-tubular nor RyR cluster organization could explain the increased dyssynchrony of Ca^{2+} transients in female AGAT KO mice.

In line with our previous findings in GAMT KO mice, where we did not detect any potential adaptive modification in the regulation of mitochondrial energetics (**Publication I and II**), Ca^{2+} handling was also minimally affected in GAMT KO cardiomyocytes. In particular, unchanged Ca^{2+} transients, Ca^{2+} release synchronicity, and Ca^{2+} sparks frequency were demonstrated in GAMT KO compared to WT.

4.3.2 Calcium removal and cardiomyocyte relaxation

For relaxation of the heart, Ca^{2+} has to be removed from the cytosol mainly by energy-requiring uptake into SR by SERCA (around 90% of Ca^{2+} reuptake in mouse cardiomyocytes) and to a minor degree by the sarcolemmal Na^{+}-Ca^{2+} exchange via NCX (Li et al., 1998; Bers, 2002). According to our previous findings showing slower SR Ca^{2+} reuptake and thus decreased SERCA activity even in the presence of PCr (**Publication IV**), we expected Ca^{2+} transient decay to be slower in the absence of the functioning CK system. However, in contrast to our expectations, when the rate of Ca^{2+} reuptake was assessed from Ca^{2+} transient recordings, no change between AGAT KO and WT was detected (**Publication V**). According to our data, the Ca^{2+} transient amplitude was larger, meaning that more time was needed to eliminate Ca^{2+} from the cytosol. Thus, the Ca^{2+} transient duration was longer, but the Ca^{2+} reuptake rates were similar in AGAT KO and

WT. In patch clamped experiments, although only partially, Ca^{2+} transient decay time was rescued by adrenergic stimulation (**Publication IV**). Therefore, together with unchanged SERCA total protein expression (**Publication IV**)(Laasmaa et al., 2020), the implication of regulatory modifications, such as phosphorylation level of phospholamban (PLB), SERCA regulatory protein, was proposed to be involved in altered Ca^{2+} handling in AGAT KO. Unphosphorylated PLB bound to SERCA lowers its affinity to Ca^{2+}. At the same time, phosphorylation of PLB in response to sympathetic stimulation leads to activation of the SERCA pump and elevation of SR Ca^{2+} loading (Periasamy et al., 2008). In the current work, PLB expression and phosphorylation level were assessed. As a result, in line with unchanged Ca^{2+} uptake rates in AGAT KO, our data showed unaltered PLB protein expression and extent of phosphorylation for both Ser16 and Thr17 phosphorylation sites.

Two hypotheses could explain the unchanged Ca^{2+} decay rate in isolated cardiomyocytes from AGAT KO. One of the explanations is that SERCA was probably not energetically limited in intact cardiomyocytes and could be fueled with sufficient energy for its functioning through direct ATP transfer from mitochondria. This point of view agrees with the unchanged mitochondrial respiration and activities of alternative phosphotransfer systems reported previously in creatine-deficient mouse cardiomyocytes (**Publication I and II**). Together, these results suggest that the functional CK system in AGAT KO is not crucial in facilitating energy buffering and transfer between mitochondria and ATPases under given conditions. Another hypothesis implies an elevation of Ca^{2+} efflux through NCX. Since an increased contribution of Ca^{2+} influx through NCX was suggested to influence higher Ca^{2+} transient amplitudes in AGAT KO, Ca^{2+} efflux via NCX should also be increased to keep transsarcolemmal Ca^{2+} fluxes balanced. The implied increase in the contribution of NCX in Ca^{2+} handling in AGAT KO is in line with the situation in heart failure, where NCX is upregulated (Bers and Despa, 2006). In neonatal cardiomyocytes, which are more tolerant to an energy deficit, the majority of Ca^{2+} cycling is across the sarcolemma by NCX, which, together with a higher degree of colocalization of NCX with RyR, plays a more prominent role in the regulation of EC coupling that CICR from SR (Huang et al., 2008). These two hypotheses are not mutually exclusive and cannot be distinguished based on the current data. Thus, further studies are required in creatine-deficient mouse hearts to clarify the actual contribution of SERCA and NCX to Ca^{2+} reuptake and the relative organization of Ca^{2+} handling proteins.

Although the main adaptive modifications in Ca^{2+} handling were detected in a pure model of creatine-deficiency, AGAT KO, there were changes in diastolic Ca^{2+} levels in GAMT and AGAT KO. In particular, diastolic Ca^{2+} levels were increased in both GAMT and AGAT KO compared with corresponding WT. This result suggests that Ca^{2+} elimination from the cytosol was compromised in these mouse models.

4.3.3 Adaptive changes in excitation-contraction coupling in AGAT KO cardiomyocytes

As significant alterations in Ca^{2+} transients were found in **Publication V**, we studied whether the contractility of isolated cardiomyocytes at different stimulation frequencies was also affected. Although in AGAT KO cardiomyocytes, adrenergic stimulation with ISO led to increased Ca^{2+} transient amplitude and shortened Ca^{2+} transient duration, the response to changes in frequencies was blunted. Surprisingly, the decreased Ca^{2+} transient duration was not reflected in sarcomere length (SL) shortening duration, which

was not affected by ISO treatment. In addition, SL shortening amplitude was similar between AGAT KO and WT under the control condition or with ISO treatment (Table 1). Thus, in AGAT KO cardiomyocytes, the contraction measured under unloaded conditions did not match the alterations in Ca^{2+} handling. These results suggest the development of adaptive modifications in the contractility of AGAT KO cardiomyocytes in response to elevated Ca^{2+} levels and longer Ca^{2+} transient duration.

One of the reasons for such compensatory response in AGAT KO could be the changes in Ca^{2+} sensitivity at the myofibrillar level. The phosphorylation of TnI, the inhibitory subunit of Tn complex, following beta-adrenergic stimulation, leads to the lowering of Ca^{2+} sensitivity of Tn complex and faster dissociation of Ca^{2+} from the myofilaments (Davis and Tikunova, 2008), and, consequently, to faster relaxation of cardiac muscle. This was demonstrated in **Publication V** by diminished SL shortening duration in the presence of ISO in all studied groups except AGAT KO. Thus, the absence of a similar response in AGAT KO cardiomyocytes could be explained by potential alterations in myofibrillar Ca^{2+} sensitivity, like reduced Ca^{2+} - binding affinity of Tn complex, which could compensate for longer than in WT Ca^{2+} transients. Moreover, the adaptations in sarcomere dynamics may point towards a partial decrease in ATP consumption in AGAT KO mice. However, such complicated processes as EC coupling and relaxation of cardiac muscle cannot be regulated only by one protein. Other factors, such as intracellular Ca^{2+} concentration, specific features of myosin isoenzymes and the interaction of contractile proteins with each other (cross-bridge formation) also play a role in this regulation.

While several adaptive modifications in Ca^{2+} handling and EC coupling were revealed in AGAT KO due to creatine-deficiency, some issues remained unresolved. Namely, the influence of RyR sensitivity and activity and transsarcolemmal Ca^{2+} influx via NCX on increased Ca^{2+} levels require further clarification and investigation. Moreover, it is still uncertain whether these alterations are associated with the absence of a functional CK system in AGAT KO (**Publication IV and V**). For instance, two other papers showed normal myocardial baseline contractility in CK KO (Bonz et al., 2002) and GAMT KO mice (Lygate et al., 2013). Herewith, unchanged Ca^{2+} handling in CK KO mice (Bonz et al., 2002) could be explained in part by intracellular structural reorganization (Kaasik et al., 2001), leading to a closer association of mitochondria with SR and myofibrils or by glycolysis providing SERCA with energy in the absence of functional CK system (Boehm et al., 2000). However, that is not the case in creatine-deficient mouse models, where neither compensatory upregulation of alternative phosphotransfer pathways (**Publication II**) nor structural adaptations in the mitochondrial organization were detected (**Publication I**). Therefore, as with the regulation of mitochondrial energetics, normal cardiac contractility could be due to P-GAA being used instead of PCr in GAMT KO hearts. As for AGAT KO, several aspects should be taken into consideration. Although altered Ca^{2+} handling could be associated with complete inhibition of the CK system, unchanged baseline contractility of CK KO mice argues against it (Bonz et al., 2002). Another factor is the near absence of hArg alone or together with Cr. Finally, systemic changes associated with the metabolic changes in the whole body should also be considered.

Table 1. The main outcomes from the Ca^{2+} handling experiments in intact AGAT cardiomyocytes.

	AGAT KO Female	AGAT KO Male	Notes
Calcium transients 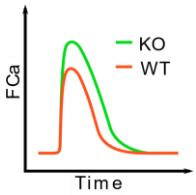	- Longer duration - Larger amplitude - Unchanged Ca^{2+} decay rate		- adrenergic stimulation resulted in a shorter duration, larger amplitude and faster decay rates
	- Increased systolic and diastolic dyssynchrony	- Increased diastolic dyssynchrony	- adrenergic stimulation resulted in more synchronous Ca^{2+} transients in males
Calcium sparks 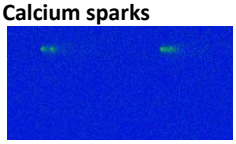	- Increased frequency - Wider width - Longer duration		- females had higher spark frequency than males
RyR organization 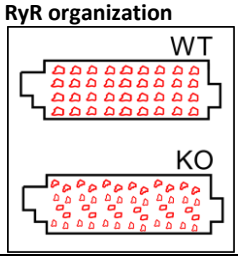	- Unchanged RyR density		
	- Smaller RyR clusters - Increased RyR cluster and CRU density	- Increased CRU density	
T-tubular network 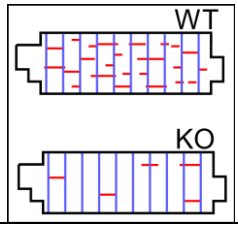		- Reduced network due to fewer longitudinal t-tubules	
Calcium handling proteins 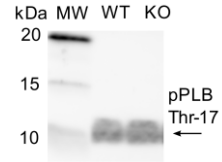	- Unchanged RyR total expression and phosphorylation - Unchanged PLB total expression and phosphorylation		
Sarcomere dynamics 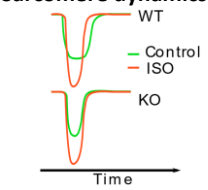	- ISO did not change SL shortening duration		- SL duration exhibited blunted frequency response

SL - sarcomere length; CRU - calcium release unit

5 Conclusions

The findings of this dissertation help to expand our understanding of how an inactive CK system affects cardiac metabolism, Ca^{2+} handling and EC coupling. Although the CK system is assumed to be important for energy transfer in the heart, no change in the regulation of mitochondrial bioenergetics and ultrastructural organization was found in GAMT KO mouse cardiomyocytes (**Publication I**). Therefore, we assessed whether there were any adaptational changes in alternative phosphotransfer systems, such as HK and AK. However, no upregulation of alternative phosphotransfer enzymes was observed in GAMT KO mice, and only a slight upregulation of mitochondrial HK was detected in AGAT KO (**Publication II**). These results may relate to the fact that CK phosphotransfer capacity does not exceed the respiratory capacity of mitochondria (**Publication III**), together suggesting that CK is not as important as previously thought. Moreover, the complexity of the regulation of cardiac energetics was underscored by experiments on mouse and rat hearts, showing a significant difference in enzymatic activities depending on the intactness of ultrastructural organization and compartmentalization (**Publication III**). However, more changes and adaptations in response to creatine-deficiency were demonstrated in Ca^{2+} handling and EC coupling, but mainly in AGAT KO cardiomyocytes. The results from patch clamped cardiomyocytes suggested a slowing of Ca^{2+} cycling in AGAT KO mice (**Publication IV**). The subsequent experiments with intact AGAT KO cardiomyocytes revealed changes in Ca^{2+} transients and inconsistent adaptations in sarcomere dynamics in both females and males, and sex-dependent alteration in Ca^{2+} transient dyssynchrony, Ca^{2+} sparks, t-tubular and RyR organization (**Publication V**). Whether these modifications are due to the absence of the functional CK system in cardiomyocytes or systemic changes in the whole organism is uncertain. Altogether, the outcomes of these studies suggest that in the heart, while the absence of a functional CK system has minor effects on energy metabolism and transfer, it may lead to adaptive modifications in Ca^{2+} dynamics and contractility.

References

Abraham, M.R., Selivanov, V.A., Hodgson, D.M., Pucar, D., Zingman, L.V., Wieringa, B., et al. (2002). Coupling of Cell Energetics with Membrane Metabolic Sensing. Journal of Biological Chemistry *277*: 24427–24434.

Akki, A., Su, J., Yano, T., Gupta, A., Wang, Y., Leppo, M.K., et al. (2012). Creatine kinase overexpression improves ATP kinetics and contractile function in postischemic myocardium. American Journal of Physiology - Heart and Circulatory Physiology *303*: H844–H852.

Aksentijević, D., Lygate, C.A., Makinen, K., Zervou, S., Sebag-Montefiore, L., Medway, D., et al. (2010). High-energy phosphotransfer in the failing mouse heart: role of adenylate kinase and glycolytic enzymes. Eur. J. Heart Fail *12*: 1282–1289.

Aksentijević, D., Zervou, S., Eykyn, T.R., McAndrew, D.J., Wallis, J., Schneider, J.E., et al. (2020). Age-Dependent Decline in Cardiac Function in Guanidinoacetate-N-Methyltransferase Knockout Mice. Front Physiol *10*:.

Balaban, R.S. (2002). Cardiac energy metabolism homeostasis: role of cytosolic calcium. J.Mol.Cell Cardiol. *34*: 1259–1271.

Balestrino, M., and Adriano, E. (2020). Presence of guanidinoacetate may compensate creatine absence and account for less statin-induced muscle damage in GAMT-deficient compared to AGAT-deficient mice. Amino Acids *52*: 667–669.

Baroncelli, L., Alessandrì, M.G., Tola, J., Putignano, E., Migliore, M., Amendola, E., et al. (2014). A novel mouse model of creatine transporter deficiency. F1000Res *3*:.

Barsunova, K., Vendelin, M., and Birkedal, R. (2020). Marker enzyme activities in hindleg from creatine-deficient AGAT and GAMT KO mice - differences between models, muscles, and sexes. Sci Rep *10*: 7956.

Barth, E., Stammler, G., Speiser, B., and Schaper, J. (1992). Ultrastructural quantitation of mitochondria and myofilaments in cardiac muscle from 10 different animal species including man. J Mol Cell Cardiol *24*: 669–681.

Bers, D.M. (2002). Cardiac excitation-contraction coupling. Nature *415*: 198–205.

Bers, D.M., and Despa, S. (2006). Cardiac myocytes Ca2+ and Na+ regulation in normal and failing hearts. J.Pharmacol.Sci. *100*: 315–322.

Bessman, S.P., and Carpenter, C.L. (1985). The creatine-creatine phosphate energy shuttle. Annu.Rev.Biochem. *54*: 831–862.

Bessman, S.P., and Geiger, P.J. (1981). Transport of energy in muscle: the phosphorylcreatine shuttle. Science *211*: 448–452.

Beutner, G., Rück, A., Riede, B., Welte, W., and Brdiczka, D. (1996). Complexes between kinases, mitochondrial porin and adenylate translocator in rat brain resemble the permeability transition pore. FEBS Letters *396*: 189–195.

Birkedal, R., Laasmaa, M., and Vendelin, M. (2014). The location of energetic compartments affects energetic communication in cardiomyocytes. Front Physiol *5*: 376.

Birkedal, R., Shiels, H.A., and Vendelin, M. (2006). Three-dimensional mitochondrial arrangement in ventricular myocytes: from chaos to order. Am J Physiol Cell Physiol *291*: C1148-1158.

Bittl, J.A., and Ingwall, J.S. (1985). Reaction rates of creatine kinase and ATP synthesis in the isolated rat heart. A 31P NMR magnetization transfer study. J. Biol. Chem. *260*: 3512–3517.

Boehm, E., Ventura-Clapier, R., Mateo, P., Lechene, P., and Veksler, V. (2000). Glycolysis supports calcium uptake by the sarcoplasmic reticulum in skinned ventricular fibres of mice deficient in mitochondrial and cytosolic creatine kinase. J.Mol.Cell Cardiol. *32*: 891–902.

Boehm, E.A., Radda, G.K., Tomlin, H., and Clark, J.F. (1996). The utilisation of creatine and its analogues by cytosolic and mitochondrial creatine kinase. Biochim. Biophys. Acta *1274*: 119–128.

Bonz, A.W., Kniesch, S., Hofmann, U., Küllmer, S., Bauer, L., Wagner, H., et al. (2002). Functional properties and [Ca2+]i metabolism of creatine kinase--KO mice myocardium. Biochem. Biophys. Res. Commun. *298*: 163–168.

Branovets, J., Sepp, M., Kotlyarova, S., Jepihhina, N., Sokolova, N., Aksentijevic, D., et al. (2013). Unchanged mitochondrial organization and compartmentation of high-energy phosphates in creatine-deficient GAMT-/- mouse hearts. Am. J. Physiol. Heart Circ. Physiol. *305*: H506-520.

Brdiczka, D.G., Zorov, D.B., and Sheu, S.-S. (2006). Mitochondrial contact sites: their role in energy metabolism and apoptosis. Biochim Biophys Acta *1762*: 148–163.

Cain, D.F., and Davies, R.E. (1962). Breakdown of adenosine triphosphate during a single contraction of working muscle. Biochem. Biophys. Res. Commun. *8*: 361–366.

Calmettes, G., Ribalet, B., John, S., Korge, P., Ping, P., and Weiss, J.N. (2015). Hexokinases and Cardioprotection. J Mol Cell Cardiol *0*: 107–115.

Cheng, H., Lederer, W., and Cannell, M. (1993). Calcium sparks: elementary events underlying excitation-contraction coupling in heart muscle. Science *262*: 740–744.

Cheng, H., and Lederer, W.J. (2008). Calcium Sparks. Physiological Reviews *88*: 1491–1545.

Choe, C., Atzler, D., Wild, P.S., Carter, A.M., Böger, R.H., Ojeda, F., et al. (2013a). Homoarginine Levels Are Regulated by l-Arginine:Glycine Amidinotransferase and Affect Stroke Outcome Results From Human and Murine Studies. Circulation *128*: 1451–1461.

Choe, C., Nabuurs, C., Stockebrand, M.C., Neu, A., Nunes, P., Morellini, F., et al. (2013b). l-arginine:glycine amidinotransferase deficiency protects from metabolic syndrome. Human Molecular Genetics *22*: 110–123.

Chung, S., Arrell, D.K., Faustino, R.S., Terzic, A., and Dzeja, P.P. (2010). Glycolytic network restructuring integral to the energetics of embryonic stem cell cardiac differentiation. J Mol Cell Cardiol *48*: 725–734.

Clark, J.F., Khuchua, Z., Kuznetsov, A.V., Vassil'eva, E., Boehm, E., Radda, G.K., et al. (1994). Actions of the creatine analogue beta-guanidinopropionic acid on rat heart mitochondria. Biochem. J. *300 (Pt 1)*: 211–216.

Crawford, R.M., Ranki, H.J., Botting, C.H., Budas, G.R., and Jovanovic, A. (2002). Creatine kinase is physically associated with the cardiac ATP-sensitive K+ channel in vivo. FASEB J. *16*: 102–104.

Crozatier, B., Badoual, T., Boehm, E., Ennezat, P.V., Guenoun, T., Su, J., et al. (2002). Role of creatine kinase in cardiac excitation-contraction coupling: studies in creatine kinase-deficient mice. FASEB J. *16*: 653–660.

Davis, J.P., and Tikunova, S.B. (2008). Ca2+ exchange with troponin C and cardiac muscle dynamics. Cardiovasc Res *77*: 619–626.

De Sousa E., Veksler V., Minajeva A., Kaasik A., Mateo P., Mayoux E., et al. (1999). Subcellular Creatine Kinase Alterations. Circulation Research *85*: 68–76.

Deursen, J. van, Heerschap, A., Oerlemans, F., Ruitenbeek, W., Jap, P., Laak, H. ter, et al. (1993). Skeletal muscles of mice deficient in muscle creatine kinase lack burst activity. Cell *74*: 621–631.

Dobrev, D., and Wehrens, X.H.T. (2014). Role of RyR2 Phosphorylation in Heart Failure and Arrhythmias. Circulation Research *114*: 1311–1319.

Dolinsky, V.W., and Dyck, J.R.B. (2006). Role of AMP-activated protein kinase in healthy and diseased hearts. AJP: Heart and Circulatory Physiology *291*: H2557–H2569.

Duma, R.J., and Siegel, A.L. (1965). Serum Creatinine Phosphokinase In Acute Myocardial Infarction: Diagnostic Value. Archives of Internal Medicine *115*: 443–451.

Dzeja, P., and Terzic, A. (2009). Adenylate Kinase and AMP Signaling Networks: Metabolic Monitoring, Signal Communication and Body Energy Sensing. Int J Mol Sci *10*: 1729–1772.

Dzeja, P.P., Chung, S., and Terzic, A. (2007). Integration of Adenylate Kinase and Glycolytic and Glycogenolytic Circuits in Cellular Energetics. In Molecular System Bioenergetics, (John Wiley & Sons, Ltd), pp 265–301.

Dzeja, P.P., Hoyer, K., Tian, R., Zhang, S., Nemutlu, E., Spindler, M., et al. (2011). Rearrangement of energetic and substrate utilization networks compensate for chronic myocardial creatine kinase deficiency. The Journal of Physiology.

Dzeja, P.P., Pucar, D., Redfield, M.M., Burnett, J.C., and Terzic, A. (1999a). Reduced activity of enzymes coupling {ATP}-generating with {ATP}-consuming processes in the failing myocardium. Mol. Cell. Biochem *201*: 33–40.

Dzeja, P.P., and Terzic, A. (1998). Phosphotransfer reactions in the regulation of ATP-sensitive K+ channels. FASEB J *12*: 523–529.

Dzeja, P.P., and Terzic, A. (2003). Phosphotransfer networks and cellular energetics. J Exp Biol *206*: 2039–2047.

Dzeja, P.P., and Terzic, A. (2007). 6.3 Mitochondria-Nucleus Energetic Communication: Role for Phosphotransfer Networks in Processing Cellular Information. In Handbook of Neurochemistry and Molecular Neurobiology: Brain Energetics. Integration of Molecular and Cellular Processes, A. Lajtha, G.E. Gibson, and G.A. Dienel, eds. (Boston, MA: Springer US), pp 641–666.

Dzeja, P.P., Terzic, A., and Wieringa, B. (2004). Phosphotransfer dynamics in skeletal muscle from creatine kinase gene-deleted mice. Mol. Cell. Biochem *256–257*: 13–27.

Dzeja, P.P., Vitkevicius, K.T., Redfield, M.M., Burnett, J.C., and Terzic, A. (1999b). Adenylate kinase-catalyzed phosphotransfer in the myocardium: {I}ncreased contribution in heart failure. Circ. Res *84*: 1137–1143.

Dzeja, P.P., Zeleznikar, R.J., and Goldberg, N.D. (1998). Adenylate kinase: kinetic behavior in intact cells indicates it is integral to multiple cellular processes. Mol. Cell. Biochem *184*: 169–182.

Eggleton, P., and Eggleton, G.P. (1928). Further observations on phosphagen. J. Physiol. (Lond.) *65*: 15–24.

Eisner, D.A., Caldwell, J.L., Kistamás, K., and Trafford, A.W. (2017). Calcium and Excitation-Contraction Coupling in the Heart. Circ Res *121*: 181–195.

Eschenhagen, T. (2010). Is ryanodine receptor phosphorylation key to the fight or flight response and heart failure? J Clin Invest *120*: 4197–4203.

Faller, K.M.E., Atzler, D., McAndrew, D.J., Zervou, S., Whittington, H.J., Simon, J.N., et al. (2018). Impaired cardiac contractile function in arginine:glycine amidinotransferase knockout mice devoid of creatine is rescued by homoarginine but not creatine. Cardiovasc Res *114*: 417–430.

Fiske, C.H., and Subbarow, Y. (1929). PHOSPHORUS COMPOUNDS OF MUSCLE AND LIVER. Science *70*: 381–382.

Fossel, E.T., and Hoefeler, H. (1987). Complete inhibition of creatine kinase in isolated perfused rat hearts. Am.J.Physiol *252*: E124–E129.

Franzini-Armstrong, C. (2007). ER-mitochondria communication. How privileged? Physiology (Bethesda) *22*: 261–268.

Frisk, M., Ruud, M., Espe, E.K.S., Aronsen, J.M., Røe, Å.T., Zhang, L., et al. (2016). Elevated ventricular wall stress disrupts cardiomyocyte t-tubule structure and calcium homeostasis. Cardiovasc Res *112*: 443–451.

Galice, S., Xie, Y., Yang, Y., Sato, D., and Bers, D.M. (2018). Size Matters: Ryanodine Receptor Cluster Size Affects Arrhythmogenic Sarcoplasmic Reticulum Calcium Release. J Am Heart Assoc *7*: e008724.

Gellerich, F., and Saks, V.A. (1982). Control of heart mitochondrial oxygen consumption by creatine kinase: the importance of enzyme localization. Biochem Biophys Res Commun *105*: 1473–1481.

Gellerich, F.N. (1992). The role of adenylate kinase in dynamic compartmentation of adenine nucleotides in the mitochondrial intermembrane space. FEBS Lett. *297*: 55–58.

Gellerich, F.N., Schlame, M., Bohnensack, R., and Kunz, W. (1987). Dynamic compartmentation of adenine nucleotides in the mitochondrial intermembrane space of rat-heart mitochondria. Biochim Biophys Acta *890*: 117–126.

George, C.H. (2008). Sarcoplasmic reticulum Ca2+ leak in heart failure: mere observation or functional relevance? Cardiovasc Res *77*: 302–314.

Glancy, B., and Balaban, R.S. (2012). Role of Mitochondrial Ca2+ in the Regulation of Cellular Energetics. Biochemistry *51*: 2959–2973.

Groof, A.J.C. de, Oerlemans, F.T.J.J., Jost, C.R., and Wieringa, B. (2001). Changes in glycolytic network and mitochondrial design in creatine kinase–deficient muscles. Muscle & Nerve *24*: 1188–1196.

Grosse, R., Spitzer, E., Kupriyanov, V.V., Saks, V.A., and Repke, K.R. (1980). Coordinate interplay between (Na+ + K+)-ATPase and creatine phosphokinase optimizes (Na+/K+)-antiport across the membrane of vesicles formed from the plasma membrane of cardiac muscle cell. Biochim.Biophys.Acta *603*: 142–156.

Gupta, A., Akki, A., Wang, Y., Leppo, M.K., Chacko, V.P., Foster, D.B., et al. (2012). Creatine kinase–mediated improvement of function in failing mouse hearts provides causal evidence the failing heart is energy starved. J. Clin. Invest. *122*: 291–302.

Gustafson, L.A., and Beek, J.H. van (2002). Activation time of myocardial oxidative phosphorylation in creatine kinase and adenylate kinase knockout mice. Am.J.Physiol Heart Circ.Physiol *282*: H2259–H2264.

Guzun, R., Timohhina, N., Tepp, K., Monge, C., Kaambre, T., Sikk, P., et al. (2009). Regulation of respiration controlled by mitochondrial creatine kinase in permeabilized cardiac cells in situ: Importance of system level properties. Biochimica et Biophysica Acta (BBA) - Bioenergetics *1787*: 1089–1105.

Halestrap, A.P., Pereira, G.C., and Pasdois, P. (2015). The role of hexokinase in cardioprotection – mechanism and potential for translation. Br J Pharmacol *172*: 2085–2100.

Hamman, B.L., Bittl, J.A., Jacobus, W.E., Allen, P.D., Spencer, R.S., Tian, R., et al. (1995). Inhibition of the creatine kinase reaction decreases the contractile reserve of isolated rat hearts. Am.J.Physiol *269*: H1030–H1036.

Hermann, G., and Decherd, G.M. (1939). THE CHEMICAL NATURE OF HEART FAILURE*. Annals of Internal Medicine.

Hoang-Trong, T.M., Ullah, A., and Jafri, M.S. (2015). Calcium Sparks in the Heart: Dynamics and Regulation. Res Rep Biol *6*: 203–214.

Horn, M., Remkes, H., Strömer, H., Dienesch, C., and Neubauer, S. (2001). Chronic phosphocreatine depletion by the creatine analogue beta-guanidinopropionate is associated with increased mortality and loss of ATP in rats after myocardial infarction. Circulation *104*: 1844–1849.

Hornemann, T., Stolz, M., and Wallimann, T. (2000). Isoenzyme-specific interaction of muscle-type creatine kinase with the sarcomeric M-line is mediated by NH(2)-terminal lysine charge-clamps. J.Cell Biol. *149*: 1225–1234.

Hove, M. ten, Lygate, C.A., Fischer, A., Schneider, J.E., Sang, A.E., Hulbert, K., et al. (2005). Reduced inotropic reserve and increased susceptibility to cardiac ischemia/reperfusion injury in phosphocreatine-deficient guanidinoacetate-N-methyltransferase-knockout mice. Circulation *111*: 2477–2485.

Hove, M. ten, and Neubauer, S. (2007). MR spectroscopy in heart failure—clinical and experimental findings. Heart Fail. Rev. *12*: 48–57.

Huang, J., Hove-Madsen, L., and Tibbits, G.F. (2008). Ontogeny of Ca2+-induced Ca2+ release in rabbit ventricular myocytes. Am.J.Physiol Cell Physiol *294*: C516–C525.

Ingwall, J.S. (2002). ATP and the Heart: An Overview. In ATP and the Heart, J.S. Ingwall, ed. (Boston, MA: Springer US), pp 3–6.

Ingwall, J.S., and Weiss, R.G. (2004). Is the Failing Heart Energy Starved? On Using Chemical Energy to Support Cardiac Function. Circ Res *95*: 135–145.

Jacobus, W.E., and Lehninger, A.L. (1973). Creatine kinase of rat heart mitochondria. Coupling of creatine phosphorylation to electron transport. J Biol Chem *248*: 4803–4810.

Janssen, E., Terzic, A., Wieringa, B., and Dzeja, P.P. (2003). Impaired intracellular energetic communication in muscles from creatine kinase and adenylate kinase (M-CK/AK1) double knock-out mice. J Biol Chem *278*: 30441–30449.

Jensen, M., Müller, C., Choe, C., Schwedhelm, E., and Zeller, T. (2020a). Analysis of L-arginine:glycine amidinotransferase-, creatine- and homoarginine-dependent gene regulation in the murine heart. Scientific Reports *10*: 4821.

Jensen, M., Müller, C., Schwedhelm, E., Arunachalam, P., Gelderblom, M., Magnus, T., et al. (2020b). Homoarginine- and Creatine-Dependent Gene Regulation in Murine Brains with l-Arginine:Glycine Amidinotransferase Deficiency. International Journal of Molecular Sciences *21*: 1865.

John, S., Weiss, J.N., and Ribalet, B. (2011). Subcellular Localization of Hexokinases I and II Directs the Metabolic Fate of Glucose. PLoS ONE *6*: e17674.

Joubert, F., Mazet, J.-L., Mateo, P., and Hoerter, J.A. (2002). 31P {NMR} detection of subcellular creatine kinase fluxes in the perfused rat heart: contractility modifies energy transfer pathways. J. Biol. Chem. *277*: 18469–18476.

Kaasik, A., Veksler, V., Boehm, E., Novotova, M., Minajeva, A., and Ventura-Clapier, R. (2001). Energetic crosstalk between organelles: architectural integration of energy production and utilization. Circ Res *89*: 153–159.

Kan, H.E., Renema, W.K.J., Isbrandt, D., and Heerschap, A. (2004). Phosphorylated Guanidinoacetate Partly Compensates for the Lack of Phosphocreatine in Skeletal Muscle of Mice Lacking Guanidinoacetate Methyltransferase. J. Physiol. (Lond.) *560*: 219–229.

Katz, A.M. (2011). Physiology of the Heart (Philadelphia, USA: Lippincott Williams & Wilkins).

Katz, L.A., Swain, J.A., Portman, M.A., and Balaban, R.S. (1989). Relation between phosphate metabolites and oxygen consumption of heart in vivo. Am J Physiol *256*: H265–H274.

Kolstad, T.R., Brink, J. van den, MacQuaide, N., Lunde, P.K., Frisk, M., Aronsen, J.M., et al. (2018). Ryanodine receptor dispersion disrupts Ca2+ release in failing cardiac myocytes. Elife *7*: e39427.

Kritzer, M.D., Li, J., Dodge-Kafka, K., and Kapiloff, M.S. (2012). AKAPs: The architectural underpinnings of local cAMP signaling. Journal of Molecular and Cellular Cardiology *52*: 351–358.

Kuby, S.A., Noda, L., and Lardy, H.A. (1954). Adenosinetriphosphate-creatine transphosphorylase. I. Isolation of the crystalline enzyme from rabbit muscle. J. Biol. Chem. *209*: 191–201.

Laasmaa, M., Branovets, J., Barsunova, K., Karro, N., Lygate, C.A., Birkedal, R., et al. (2020). Altered calcium handling in cardiomyocytes from arginine-glycine amidinotransferase-knockout mice is rescued by creatine. American Journal of Physiology-Heart and Circulatory Physiology *320*: H805–H825.

Laterveer, F.D., Nicolay, K., and Gellerich, F.N. (1997). Experimental evidence for dynamic compartmentation of ADP at the mitochondrial periphery: coupling of mitochondrial adenylate kinase and mitochondrial hexokinase with oxidative phosphorylation under conditions mimicking the intracellular colloid osmotic pressure. Mol. Cell. Biochem. *174*: 43–51.

Lawson, J.W., and Veech, R.L. (1979). Effects of pH and free Mg2+ on the Keq of the creatine kinase reaction and other phosphate hydrolyses and phosphate transfer reactions. J.Biol.Chem. *254*: 6528–6537.

Li, L., Chu, G., Kranias, E.G., and Bers, D.M. (1998). Cardiac myocyte calcium transport in phospholamban knockout mouse: relaxation and endogenous CaMKII effects. Am J Physiol *274*: H1335-1347.

Liu, T., Xu, Y., Yi, C.-X., Tong, Q., and Cai, D. (2021). The hypothalamus for whole-body physiology: from metabolism to aging. Protein Cell.

Lorentzon, M., Råmunddal, T., Bollano, E., Soussi, B., Waagstein, F., and Omerovic, E. (2007). In Vivo Effects of Myocardial Creatine Depletion on Left Ventricular Function, Morphology, and Energy Metabolism—Consequences in Acute Myocardial Infarction. Journal of Cardiac Failure *13*: 230–237.

Louch, W.E., Sejersted, O.M., and Swift, F. (2010). There Goes the Neighborhood: Pathological Alterations in T-Tubule Morphology and Consequences for Cardiomyocyte Ca2+ Handling. Journal of Biomedicine and Biotechnology *2010*: 1–18.

Lygate, C. (2006). Surgical models of hypertrophy and heart failure: Myocardial infarction and transverse aortic constriction. Drug Discovery Today: Disease Models *3*: 283–290.

Lygate, C.A., Aksentijevic, D., Dawson, D., Hove, M. ten, Phillips, D., Bono, J.P. de, et al. (2013). Living without creatine: unchanged exercise capacity and response to chronic myocardial infarction in creatine-deficient mice. Circ. Res. *112*: 945–955.

Lygate, C.A., Bohl, S., Hove, M. ten, Faller, K.M.E., Ostrowski, P.J., Zervou, S., et al. (2012a). Moderate elevation of intracellular creatine by targeting the creatine transporter protects mice from acute myocardial infarction. Cardiovasc Res *96*: 466–475.

Lygate, C.A., Fischer, A., Sebag-Montefiore, L., Wallis, J., Hove, M. ten, and Neubauer, S. (2007). The creatine kinase energy transport system in the failing mouse heart. J.Mol.Cell Cardiol. *42*: 1129–1136.

Lygate, C.A., Hunyor, I., Medway, D., Bono, J.P. de, Dawson, D., Wallis, J., et al. (2009). Cardiac phenotype of mitochondrial creatine kinase knockout mice is modified on a pure C57BL/6 genetic background. J. Mol. Cell Cardiol. *46*: 93–99.

Lygate, C.A., Medway, D.J., Ostrowski, P.J., Aksentijevic, D., Sebag-Montefiore, L., Hunyor, I., et al. (2012b). Chronic creatine kinase deficiency eventually leads to congestive heart failure, but severity is dependent on genetic background, gender and age. Basic Res Cardiol *107*: 276–286.

Lygate, C.A., and Neubauer, S. (2014). The Myocardial Creatine Kinase System in the Normal, Ischaemic and Failing Heart. In Cardiac Energy Metabolism in Health and Disease, G.D. Lopaschuk, and N.S. Dhalla, eds. (New York, NY: Springer), pp 155–168.

Marx, S.O., Gaburjakova, J., Gaburjakova, M., Henrikson, C., Ondrias, K., and Marks, A.R. (2001). Coupled Gating Between Cardiac Calcium Release Channels (Ryanodine Receptors). Circulation Research *88*: 1151–1158.

März, W., Meinitzer, A., Drechsler, C., Pilz, S., Krane, V., Kleber, M.E., et al. (2010). Homoarginine, Cardiovascular Risk, and Mortality. Circulation *122*: 967–975.

Mekhfi, H., Hoerter, J., Lauer, C., Wisnewsky, C., Schwartz, K., and Ventura-Clapier, R. (1990). Myocardial adaptation to creatine deficiency in rats fed with beta-guanidinopropionic acid, a creatine analogue. Am. J. Physiol *258*: H1151–H1158.

Meyer, R.A., Sweeney, H.L., and Kushmerick, M.J. (1984). A simple analysis of the 'phosphocreatine shuttle'. Am. J. Physiol. *246*: C365–C377.

Mika, D., Leroy, J., Vandecasteele, G., and Fischmeister, R. (2012). PDEs create local domains of cAMP signaling. Journal of Molecular and Cellular Cardiology *52*: 323–329.

Minajeva, A., Ventura-Clapier, R., and Veksler, V. (1996). Ca2+ uptake by cardiac sarcoplasmic reticulum ATPase in situ strongly depends on bound creatine kinase. Pflugers Arch. *432*: 904–912.

Momken, I., Lechêne, P., Koulmann, N., Fortin, D., Mateo, P., Doan, B.T., et al. (2005). Impaired voluntary running capacity of creatine kinase-deficient mice. J. Physiol. (Lond.) *565*: 951–964.

Nabuurs, C.I., Choe, C.U., Veltien, A., Kan, H.E., Loon, L.J.C. van, Rodenburg, R.J.T., et al. (2013). Disturbed energy metabolism and muscular dystrophy caused by pure creatine deficiency are reversible by creatine intake. J Physiol *591*: 571–592.

Nahrendorf, M., Spindler, M., Hu, K., Bauer, L., Ritter, O., Nordbeck, P., et al. (2005). Creatine kinase knockout mice show left ventricular hypertrophy and dilatation, but unaltered remodeling post-myocardial infarction. Cardiovascular Research *65*: 419–427.

Nahrendorf, M., Streif, J.U., Hiller, K.-H., Hu, K., Nordbeck, P., Ritter, O., et al. (2006). Multimodal functional cardiac MRI in creatine kinase-deficient mice reveals subtle abnormalities in myocardial perfusion and mechanics. Am. J. Physiol. Heart Circ. Physiol. *290*: H2516–H2521.

Neubauer, S. (2007). The failing heart–an engine out of fuel. N Engl J Med *356*: 1140–1151.

Neubauer, S., Horn, M., Cramer, M., Harre, K., Newell, J.B., Peters, W., et al. (1997). Myocardial phosphocreatine-to-ATP ratio is a predictor of mortality in patients with dilated cardiomyopathy. Circulation *96*: 2190–2196.

Neumann, D., Schlattner, U., and Wallimann, T. (2003). A molecular approach to the concerted action of kinases involved in energy homoeostasis. Biochemical Society Transactions *31*: 169–174.

Noma, T. (2005). Dynamics of nucleotide metabolism as a supporter of life phenomena. The Journal of Medical Investigation *52*: 127–136.

Oudman, I., Clark, J.F., and Brewster, L.M. (2013). The Effect of the Creatine Analogue Beta-guanidinopropionic Acid on Energy Metabolism: A Systematic Review. PLoS One *8*:.

Periasamy, M., Bhupathy, P., and Babu, G.J. (2008). Regulation of sarcoplasmic reticulum Ca2+ ATPase pump expression and its relevance to cardiac muscle physiology and pathology. Cardiovasc Res *77*: 265–273.

Phillips, D., Ten Hove, M., Schneider, J.E., Wu, C.O., Sebag-Montefiore, L., Aponte, A.M., et al. (2010). Mice over-expressing the myocardial creatine transporter develop progressive heart failure and show decreased glycolytic capacity. J Mol Cell Cardiol *48*: 582–590.

Pilz, S., Meinitzer, A., Tomaschitz, A., Drechsler, C., Ritz, E., Krane, V., et al. (2011). Low homoarginine concentration is a novel risk factor for heart disease. Heart *97*: 1222–1227.

Piquereau, J., Novotova, M., Fortin, D., Garnier, A., Ventura-Clapier, R., Veksler, V., et al. (2010). Postnatal development of mouse heart: formation of energetic microdomains. J. Physiol. (Lond.) *588*: 2443–2454.

Piquereau, J., and Ventura-Clapier, R. (2018). Maturation of Cardiac Energy Metabolism During Perinatal Development. Front Physiol *9*:.

Pucar, D., Bast, P., Gumina, R.J., Lim, L., Drahl, C., Juranic, N., et al. (2002). Adenylate kinase AK1 knockout heart: energetics and functional performance under ischemia-reperfusion. Am J Physiol Heart Circ Physiol *283*: H776-782.

Pucar, D., Dzeja, P.P., Bast, P., Gumina, R.J., Drahl, C., Lim, L., et al. (2004). Mapping hypoxia-induced bioenergetic rearrangements and metabolic signaling by 18O-assisted 31P {NMR} and 1H {NMR} spectroscopy. Mol. Cell. Biochem *256–257*: 281–289.

Ren, J., Davidoff, A.J., and Ingwall, J.S. (2009). Creatine kinase inhibitor iodoacetamide antagonizes calcium-stimulated inotropy in cardiomyocytes. Clin Exp Pharmacol Physiol *36*: 141–145.

Rios, E., and Stern, M.D. (1997). Calcium in close quarters: microdomain feedback in excitation-contraction coupling and other cell biological phenomena. Annu Rev Biophys Biomol Struct *26*: 47–82.

Rosencrans, W.M., Rajendran, M., Bezrukov, S.M., and Rostovtseva, T.K. (2021). VDAC regulation of mitochondrial calcium flux: From channel biophysics to disease. Cell Calcium *94*: 102356.

Rossi, A.M., Eppenberger, H.M., Volpe, P., Cotrufo, R., and Wallimann, T. (1990). Muscle-type MM creatine kinase is specifically bound to sarcoplasmic reticulum and can support Ca2+ uptake and regulate local ATP/ADP ratios. J. Biol. Chem. *265*: 5258–5266.

Rossi, L., Nardecchia, F., Pierigè, F., Ventura, R., Carducci, C., Leuzzi, V., et al. (2021). Intellectual Disability and Brain Creatine Deficit: Phenotyping of the Genetic Mouse Model for GAMT Deficiency. Genes (Basel) *12*: 1201.

Saks, V., Kaambre, T., Guzun, R., Anmann, T., Sikk, P., Schlattner, U., et al. (2007). The creatine kinase phosphotransfer network: thermodynamic and kinetic considerations, the impact of the mitochondrial outer membrane and modelling approaches. Subcell. Biochem. *46*: 27–65.

Saks, V.A., Kaambre, T., Sikk, P., Eimre, M., Orlova, E., Paju, K., et al. (2001). Intracellular energetic units in red muscle cells. Biochem.J. *356*: 643–657.

Saks, V.A., Khuchua, Z.A., Vasilyeva, E.V., Belikova, O.Y., and Kuznetsov, A.V. (1994). Metabolic compartmentation and substrate channelling in muscle cells. Role of coupled creatine kinases in in vivo regulation of cellular respiration–a synthesis. Mol.Cell Biochem. *133–134*: 155–192.

Saks, V.A., Vasil'eva, E., Belikova, Y.O., Kuznetsov, A.V., Lyapina, S., Petrova, L., et al. (1993). Retarded diffusion of ADP in cardiomyocytes: possible role of mitochondrial outer membrane and creatine kinase in cellular regulation of oxidative phosphorylation. Biochim Biophys Acta *1144*: 134–148.

Sander, P., Gudermann, T., and Schredelseker, J. (2021). A Calcium Guard in the Outer Membrane: Is VDAC a Regulated Gatekeeper of Mitochondrial Calcium Uptake? International Journal of Molecular Sciences *22*: 946.

Santiago, A.P.S.A., Chaves, E.A., Oliveira, M.F., and Galina, A. (2008). Reactive oxygen species generation is modulated by mitochondrial kinases: Correlation with mitochondrial antioxidant peroxidases in rat tissues. Biochimie *90*: 1566–1577.

Santulli, G., and Marks, A.R. (2015). Essential Roles of Intracellular Calcium Release Channels in Muscle, Brain, Metabolism, and Aging. Curr Mol Pharmacol *8*: 206–222.

Santulli, G., Nakashima, R., Yuan, Q., and Marks, A.R. (2017). Intracellular calcium release channels: an update. The Journal of Physiology *595*: 3041–3051.

Sasani, A., Hornig, S., Grzybowski, R., Cordts, K., Hanff, E., Tsikas, D., et al. (2020). Muscle phenotype of AGAT- and GAMT-deficient mice after simvastatin exposure. Amino Acids *52*: 73–85.

Saupe, K.W., Spindler, M., Hopkins, J.C., Shen, W., and Ingwall, J.S. (2000). Kinetic, thermodynamic, and developmental consequences of deleting creatine kinase isoenzymes from the heart. Reaction kinetics of the creatine kinase isoenzymes in the intact heart. J.Biol.Chem. *275*: 19742–19746.

Saupe, K.W., Spindler, M., Tian, R., and Ingwall, J.S. (1998). Impaired cardiac energetics in mice lacking muscle-specific isoenzymes of creatine kinase. Circ.Res. *82*: 898–907.

Schmidt, A., Marescau, B., Boehm, E.A., Renema, W.K., Peco, R., Das, A., et al. (2004). Severely altered guanidino compound levels, disturbed body weight homeostasis and impaired fertility in a mouse model of guanidinoacetate N-methyltransferase (GAMT) deficiency. Hum. Mol. Genet. *13*: 905–921.

Schneider, J.E., Stork, L.-A., Bell, J.T., Hove, M. ten, Isbrandt, D., Clarke, K., et al. (2008). Cardiac structure and function during ageing in energetically compromised Guanidinoacetate N-methyltransferase (GAMT)-knockout mice – a one year longitudinal MRI study. J. Cardiovasc. Magn. Reson. *10*: 9.

Schulze, A., Tran, C., Levandovskiy, V., Patel, V., and Cortez, M.A. (2016). Systemic availability of guanidinoacetate affects GABAA receptor function and seizure threshold in GAMT deficient mice. Amino Acids *48*: 2041–2047.

Silva, W.S. da-, Gómez-Puyou, A., Gómez-Puyou, M.T. de, Moreno-Sanchez, R., Felice, F.G.D., Meis, L. de, et al. (2004). Mitochondrial Bound Hexokinase Activity as a Preventive Antioxidant Defense: steady-state ADP formation as a regulatory mechanism of membrane potential and reactive oxygen species generation in mitochondria. J. Biol. Chem. *279*: 39846–39855.

Skelton, M.R., Schaefer, T.L., Graham, D.L., deGrauw, T.J., Clark, J.F., Williams, M.T., et al. (2011). Creatine Transporter (CrT; Slc6a8) Knockout Mice as a Model of Human CrT Deficiency. PLOS ONE *6*: e16187.

Sobie, E.A., Guatimosim, S., Gómez-Viquez, L., Song, L.-S., Hartmann, H., Saleet Jafri, M., et al. (2006). The Ca2+ leak paradox and 'rogue ryanodine receptors': SR Ca2+ efflux theory and practice. Progress in Biophysics and Molecular Biology *90*: 172–185.

Spindler, M., Meyer, K., Strömer, H., Leupold, A., Boehm, E., Wagner, H., et al. (2004). Creatine kinase-deficient hearts exhibit increased susceptibility to ischemia-reperfusion injury and impaired calcium homeostasis. Am. J. Physiol. Heart Circ. Physiol. *287*: H1039–H1045.

Spindler, M., Niebler, R., Remkes, H., Horn, M., Lanz, T., and Neubauer, S. (2002). Mitochondrial creatine kinase is critically necessary for normal myocardial high-energy phosphate metabolism. Am.J.Physiol Heart Circ.Physiol *283*: H680–H687.

Steeghs, K., Benders, A., Oerlemans, F., Haan, A. de, Heerschap, A., Ruitenbeek, W., et al. (1997a). Altered Ca2+ responses in muscles with combined mitochondrial and cytosolic creatine kinase deficiencies. Cell *89*: 93–103.

Steeghs, K., Heerschap, A., Haan, A. de, Ruitenbeek, W., Oerlemans, F., Deursen, J. van, et al. (1997b). Use of gene targeting for compromising energy homeostasis in neuro- muscular tissues: the role of sarcomeric mitochondrial creatine kinase. J.Neurosci.Methods *71*: 29–41.

Stockebrand, M., Nejad, A.S., Neu, A., Kharbanda, K.K., Sauter, K., Schillemeit, S., et al. (2016). Transcriptomic and metabolic analyses reveal salvage pathways in creatine-deficient AGAT-/- mice. Amino Acids *48*: 2025–2039.

Stockebrand, M., Sasani, A., Das, D., Hornig, S., Hermans-Borgmeyer, I., Lake, H.A., et al. (2018). A Mouse Model of Creatine Transporter Deficiency Reveals Impaired Motor Function and Muscle Energy Metabolism. Front Physiol *9*: 773.

Taegtmeyer, H., Wilson, C.R., Razeghi, P., and Sharma, S. (2005). Metabolic energetics and genetics in the heart. Ann. N. Y. Acad. Sci. *1047*: 208–218.

Tepp, K., Shevchuk, I., Chekulayev, V., Timohhina, N., Kuznetsov, A.V., Guzun, R., et al. (2011). High efficiency of energy flux controls within mitochondrial interactosome in cardiac intracellular energetic units. Biochimica et Biophysica Acta (BBA) - Bioenergetics *1807*: 1549–1561.

Tian, R., Christe, M.E., Spindler, M., Hopkins, J.C., Halow, J.M., Camacho, S.A., et al. (1997). Role of MgADP in the development of diastolic dysfunction in the intact beating rat heart. J Clin Invest *99*: 745–751.

Tian, R., and Ingwall, J.S. (1996). Energetic basis for reduced contractile reserve in isolated rat hearts. Am.J.Physiol *270*: H1207–H1216.

Timohhina, N., Guzun, R., Tepp, K., Monge, C., Varikmaa, M., Vija, H., et al. (2009). Direct measurement of energy fluxes from mitochondria into cytoplasm in permeabilized cardiac cells in situ: some evidence for Mitochondrial Interactosome. J. Bioenerg. Biomembr *41*: 259–275.

Veksler, V.I., Lechene, P., Matrougui, K., and Ventura-Clapier, R. (1997). Rigor tension in single skinned rat cardiac cell: role of myofibrillar creatine kinase. Cardiovascular Research *36*: 354–362.

Vendelin, M., Beraud, N., Guerrero, K., Andrienko, T., Kuznetsov, A.V., Olivares, J., et al. (2005). Mitochondrial regular arrangement in muscle cells: a 'crystal-like' pattern. Am J Physiol Cell Physiol *288*: C757-767.

Vendelin, M., Hoerter, J.A., Mateo, P., Soboll, S., Gillet, B., and Mazet, J.-L. (2010). Modulation of energy transfer pathways between mitochondria and myofibrils by changes in performance of perfused heart. J. Biol. Chem *285*: 37240–37250.

Vendelin, M., Lemba, M., and Saks, V.A. (2004). Analysis of Functional Coupling: Mitochondrial Creatine Kinase and Adenine Nucleotide Translocase. Biophys J *87*: 696–713.

Ventura-Clapier, R., Kuznetsov, A., Veksler, V., Boehm, E., and Anflous, K. (1998). Functional coupling of creatine kinases in muscles: species and tissue specificity. Mol.Cell Biochem. *184*: 231–247.

Wallimann, T., Schlosser, T., and Eppenberger, H.M. (1984). Function of M-line-bound creatine kinase as intramyofibrillar ATP regenerator at the receiving end of the phosphorylcreatine shuttle in muscle. J. Biol. Chem. *259*: 5238–5246.

Wallimann, T., Tokarska-Schlattner, M., and Schlattner, U. (2011). The creatine kinase system and pleiotropic effects of creatine. Amino Acids *40*: 1271–1296.

Wallimann, T., Wyss, M., Brdiczka, D., Nicolay, K., and Eppenberger, H.M. (1992). Intracellular compartmentation, structure and function of creatine kinase isoenzymes in tissues with high and fluctuating energy demands: the 'phosphocreatine circuit' for cellular energy homeostasis. Biochem. J. *281*: 21–40.

Wallis, J., Lygate, C.A., Fischer, A., Hove, M. ten, Schneider, J.E., Sebag-Montefiore, L., et al. (2005). Supranormal myocardial creatine and phosphocreatine concentrations lead to cardiac hypertrophy and heart failure: insights from creatine transporter-overexpressing transgenic mice. Circulation *112*: 3131–3139.

Wang, S.-Q., Wei, C., Zhao, G., Brochet, D.X.P., Shen, J., Song, L.-S., et al. (2004). Imaging Microdomain Ca2+ in Muscle Cells. Circulation Research *94*: 1011–1022.

Wawro, A.M., Gajera, C.R., Baker, S.A., Nirschl, J.J., Vogel, H., and Montine, T.J. (2021). Creatine transport and pathological changes in creatine transporter deficient mice. Journal of Inherited Metabolic Disease *44*: 939–948.

Whittington, H.J., Ostrowski, P.J., McAndrew, D.J., Cao, F., Shaw, A., Eykyn, T.R., et al. (2018). Over-expression of mitochondrial creatine kinase in the murine heart improves functional recovery and protects against injury following ischaemia-reperfusion. Cardiovasc. Res. *114*: 858–869.

Williams, G.S.B., Boyman, L., Chikando, A.C., Khairallah, R.J., and Lederer, W.J. (2013). Mitochondrial calcium uptake. PNAS *110*: 10479–10486.

Wyss, M., and Kaddurah-Daouk, R. (2000). Creatine and creatinine metabolism. Physiol Rev. *80*: 1107–1213.

Wyss, M., Smeitink, J., Wevers, R.A., and Wallimann, T. (1992). Mitochondrial creatine kinase: a key enzyme of aerobic energy metabolism. Biochimica et Biophysica Acta (BBA) - Protein Structure and Molecular Enzymology *1102*: 119–166.

Xu, K.Y., and Becker, L.C. (1998). Ultrastructural localization of glycolytic enzymes on sarcoplasmic reticulum vesticles. J Histochem Cytochem *46*: 419–427.

Xu, K.Y., Zweier, J.L., and Becker, L.C. (1995). Functional coupling between glycolysis and sarcoplasmic reticulum Ca2+ transport. Circ.Res. *77*: 88–97.

Zervou, S., McAndrew, D.J., Whittington, H.J., Lake, H.A., Park, K.C., Cha, K.M., et al. (2021). Subtle Role for Adenylate Kinase 1 in Maintaining Normal Basal Contractile Function and Metabolism in the Murine Heart. Front. Physiol. *12*:.

Zugno, A.I., Oliveira, D.L., Scherer, E.B.S., Wajner, M., Wofchuk, S., and Wyse, A.T.S. (2007). Guanidinoacetate inhibits glutamate uptake in rat striatum of rats at different ages. Neurochem Res *32*: 959–964.

Zugno, A.I., Stefanello, F.M., Scherer, E.B.S., Mattos, C., Pederzolli, C.D., Andrade, V.M., et al. (2008). Guanidinoacetate decreases antioxidant defenses and total protein sulfhydryl content in striatum of rats. Neurochem Res *33*: 1804–1810.

Zugno, A.I., Stefanello, F.M., Streck, E.L., Calcagnotto, T., Wannmacher, C.M.D., Wajner, M., et al. (2003). Inhibition of Na+, K+-ATPase activity in rat striatum by guanidinoacetate. Int J Dev Neurosci *21*: 183–189.

Zuurbier, C.J., Smeele, K.M.A., and Eerbeek, O. (2009). Mitochondrial hexokinase and cardioprotection of the intact heart. Journal of Bioenergetics and Biomembranes *41*: 181–185.

Acknowledgements

This work was performed in the Laboratory of System Biology, the Institute of Cybernetics at Tallinn University of Technology. Foremost, I would like to thank my supervisor Dr. Rikke Birkedal for guidance and support throughout my studies. I am grateful for her encouragement, patience and helpful advice during the preparation of this dissertation. I am also thankful to the head of the laboratory Dr. Marko Vendelin, for giving me the opportunity to work in his research group, learn new things, and get a fascinating experience in the field of heart physiology. I would also like to thank all my colleagues who worked with me for their help, valuable discussions, and for sharing their knowledge and experience with me.

I would like to express my sincere gratitude to my family for their support and love. Thank you for believing in me during all these years.

This work was financed by Wellcome Trust (081755), European Regional Development Fund (CENS), Estonian Science Foundation (ETF8041), Estonian Research Council (IUT33-7, PRG-1127), Archimedes Foundation (Kristjan Jaak scholarship).

Abstract

Energetics and calcium handling in creatine-deficient mouse hearts

The creatine kinase (CK) system is considered to play a crucial role in maintaining cardiac energy homeostasis, ensuring a precise balance between energy production and utilisation. Heart failure is associated with impairments in the CK system, correlating with disease progression. However, studies using various mouse models with a modified CK system have shown contradictory outcomes, especially in the heart. Under baseline conditions, CK knockout (KO) mice showed mainly normal cardiac performance that was affected only at high workloads or under stress conditions. In the current thesis, the cardiomyocytes from two alternative mouse models with an inhibited CK system were studied. Creatine-deficient mice lack one of the enzymes of the creatine synthesis pathway, either guanidinoacetate methyltransferase (GAMT) or arginine:glycine amidinotransferase (AGAT). In both GAMT and AGAT KO mice, creatine is absent in the whole body, and CK function is compromised.

Despite the assumed importance of CK as an energy transfer system in the heart, according to our results, the regulation of mitochondrial energetics and ultrastructural organisation was unaltered in the GAMT mouse heart. Therefore, the potential adaptations in hexokinase (HK) and adenylate kinase (AK), which form alternative energy transfer systems, were assessed in GAMT and AGAT KO mice. Whereas there were no alterations in GAMT KO, there was a slight upregulation of mitochondrial HK in AGAT KO. This minor change in energetics, together with the lower CK phosphotransfer capacity compared to the mitochondrial respiratory capacity, suggests that CK is not as crucial as it was believed. Moreover, the complexity of the regulation of cardiac energetics was underscored by experiments on mouse and rat hearts, showing the significance of intact ultrastructural organization and compartmentalization for enzymatic activities. However, more noticeable changes were demonstrated in Ca^{2+} dynamics and contractility in AGAT KO cardiomyocytes. The experiments with patch clamped cells revealed slower Ca^{2+} handling in AGAT KO. Further, complex changes in SR Ca^{2+} handling, t-tubular and RyR organization, and sarcomere dynamics were shown in intact cells. However, it remains an open question whether adaptational changes develop due to the lack of an active CK system in cardiomyocytes or the changes in whole body composition or metabolism.

Taken together, our results suggest that in the heart, creatine-deficiency has only a minor effect on metabolism and energy transfer but may lead to adaptations in Ca^{2+} dynamics and contractility.

Lühikokkuvõte

Energeetika ja kaltsiumi käitlemine kreatiini puudulike hiirte südametes

Kreatiinkinaasi (CK) süsteemi peetakse üliolulisеks südame energia homöostaasi säilitamisel, mis tagab täpse tasakaalu energia tootmise ja kasutamise vahel. Südamepuudulikkust seostatakse CK-süsteemi häiritustega, mis on korrelatsioonis haiguse progresseerumisega. Eelnevad uuringud modifitseeritud CK-süsteemiga hiirte mudelitega on aga näidanud vastuolulisi tulemusi, eriti südames. Nimelt on varasemalt näidatud, et normaaltingimustes on CK nokaut (KO) hiirte südametegevus võrreldav metsiktüüpi hiirte omaga, mis aga seevastu oli mõjutatud ainult suure töökoormuse või stressitingimuste korral. Käesolevas väitekirjas uuriti kahe alternatiivse inhibeeritud CK-süsteemiga hiiremudeli kardiomüotsüüte. Nendes kreatiini puudulikkusega hiirte mudelites puudub üks kreatiini sünteesi raja ensüümidest, kas guanidinoatsetaat metüültransferaas (GAMT) või arginiini-glütsiini amidinotransferaas (AGAT). Nii GAMT kui ka AGAT KO hiirtel puudub kreatiin kogu kehas ja CK funktsioon on seetõttu inhibeeritud.

Vaatamata CK kui energia ülekandesüsteemi oletatavale tähtsusele südames, ei muutunud antud töö tulemuste kohaselt mitokondriaalse energia metabolismi regulatsioon ja ultrastruktuur GAMT hiire südames. Seetõttu hinnati GAMT ja AGAT KO hiirtel potentsiaalseid kohastumusi alternatiivsetes energia ülekandesüsteemides nagu heksokinaas (HK) ja adenülaatkinaas (AK). Kui GAMT KO-s muutusi ei täheldatud, siis AGAT KO-s esines mitokondriaalse HK kerge ülesreguleerimine. Need tulemused võivad olla seotud asjaoluga, et CK fosfaadi ülekandevõime ei ületa mitokondrite hingamisvõimet, mis viitab omakorda sellele, et CK ei ole nii oluline, kui varem on arvatud. Lisaks, katsed hiirte ja rottide südametega näitasid, et ultrastruktuur ja kompartmentatsioon on olulised ensüümide aktiivsuse jaoks. See omakorda rõhutab südame energeetika regulatsiooni keerukust ja sõltuvust erinevatest teguritest. AGAT KO kardiomüotsüütides ilmnesid aga märkimisväärsed muutused kaltsiumi dünaamikas ja kontraktiilsuses. Membraanilapikese kinnitamise meetodi katsed AGAT KO hiirte kardiomüotsüütides näitasid aeglasemat kaltsiumi käitlemist. Järgnevate katsetega intaktsetes kardiomüotsüütides näidati aga keerulisi muutusi sarkoplasmaatilise retiikulumi kaltsiumi käitlemises, t-torukeste ja rüanodiinretseptorite organisatsioonis ning sarkomeeride dünaamikas. Siiski jääb lahtiseks küsimus, kas kohastumused on tingitud aktiivse CK-süsteemi puudumisest kardiomüotsüütides või süsteemsetest muutustest kogu organismis.

Kokkuvõtteks, antud töö tulemuste põhjal saab öelda, et südames on kreatiini puudulikkusel vaid väike mõju ainevahetusele ja energia ülekandele, kuid see toob kaasa kohastumuslikke muutusi kaltsiumi dünaamikas ja kontraktiilsuses.

Appendix 1

Publication I

Branovets J, Sepp M, Kotlyarova S, Jepihhina N, Sokolova N, Aksentijevic D, Lygate CA, Neubauer S, Vendelin M, Birkedal R

Unchanged mitochondrial organization and compartmentation of high-energy phosphates in creatine-deficient GAMT-/- mouse hearts.

Am J Physiol Heart Circ Physiol. 2013 Aug 15;305(4):H506-20. doi: 10.1152/ajpheart.00919.2012.

Am J Physiol Heart Circ Physiol 305: H506–H520, 2013.
First published June 21, 2013; doi:10.1152/ajpheart.00919.2012.

Unchanged mitochondrial organization and compartmentation of high-energy phosphates in creatine-deficient GAMT$^{-/-}$ mouse hearts

Jelena Branovets,[1] Mervi Sepp,[1] Svetlana Kotlyarova,[1] Natalja Jepihhina,[1] Niina Sokolova,[1] Dunja Aksentijevic,[2] Craig A. Lygate,[2] Stefan Neubauer,[2] Marko Vendelin,[1] and Rikke Birkedal[1]

[1]*Laboratory of Systems Biology, Institute of Cybernetics, Tallinn University of Technology, Tallinn, Estonia; and* [2]*Department of Cardiovascular Medicine, Wellcome Trust Centre for Human Genetics, University of Oxford, Oxford, United Kingdom*

Submitted 12 December 2012; accepted in final form 6 June 2013

Branovets J, Sepp M, Kotlyarova S, Jepihhina N, Sokolova N, Aksentijevic D, Lygate CA, Neubauer S, Vendelin M, Birkedal R. Unchanged mitochondrial organization and compartmentation of high-energy phosphates in creatine-deficient GAMT$^{-/-}$ mouse hearts. *Am J Physiol Heart Circ Physiol* 305: H506–H520, 2013. First published June 21, 2013; doi:10.1152/ajpheart.00919.2012.—Disruption of the creatine kinase (CK) system in hearts of CK-deficient mice leads to changes in the ultrastructure and regulation of mitochondrial respiration. We expected to see similar changes in creatine-deficient mice, which lack the enzyme guanidinoacetate methyltransferase (GAMT) to produce creatine. The aim of this study was to characterize the changes in cardiomyocyte mitochondrial organization, regulation of respiration, and intracellular compartmentation associated with GAMT deficiency. Three-dimensional mitochondrial organization was assessed by confocal microscopy. On populations of permeabilized cardiomyocytes, we recorded ADP and ATP kinetics of respiration, competition between mitochondria and pyruvate kinase for ADP produced by ATPases, ADP kinetics of endogenous pyruvate kinase, and ATP kinetics of ATPases. These data were analyzed by mathematical models to estimate intracellular compartmentation. Quantitative analysis of morphological and kinetic data as well as derived model fits showed no difference between GAMT-deficient and wild-type mice. We conclude that inactivation of the CK system by GAMT deficiency does not alter mitochondrial organization and intracellular compartmentation in relaxed cardiomyocytes. Thus, our results suggest that the healthy heart is able to preserve cardiac function at a basal level in the absence of CK-facilitated energy transfer without compromising intracellular organization and the regulation of mitochondrial energy homeostasis. This raises questions on the importance of the CK system as a spatial energy buffer in unstressed cardiomyocytes.

creatine kinase shuttle; mitochondrial positioning; confocal imaging; intracellular diffusion barriers; respiration and ATPase kinetics; guanidinoacetate methyltransferase

CREATINE KINASE (CK) plays an important role as an energy buffer in several cell types, including heart, skeletal muscle, and brain. It catalyzes the phosphotransfer between creatine (Cr) and ATP. The importance of CK is highlighted by its strong regulation of local ATP concentration as shown by studies of sarcolemmal ATP-sensitive K^+ channels (1) and rigor formation in permeabilized fibers (55, 57). After induction of ischemia, contraction correlates with the phosphocreatine (PCr) level (14), and, after heart failure, the PCr-to-ATP ratio in the heart is a strong predictor of patient mortality (20). Additionally, a recent study (15) has shown that overexpression of cytosolic CK improves cardiac contractile function and viability after induced heart failure.

Cr deficiency inhibits the CK system. It may occur due to deficiency of the enzymes that synthesize Cr [L-arginine:glycine amidinotransferase (AGAT) and guanidinoacetate methyltransferase (GAMT)] or the Cr transporter (CrT or SLC6A8), which imports Cr across the sarcolemma. All three cases of Cr deficiency have been found in humans (8, 43), and all have been reproduced in mouse models (AGAT$^{-/-}$, GAMT$^{-/-}$, and CrT$^{-/-}$ mice). The GAMT$^{-/-}$ model is the most studied to date.

Considering the presumed importance of CK in the heart, it is remarkable that the baseline cardiac function of GAMT$^{-/-}$ mice is so little affected by the lack of a functional CK system. For example, ejection fraction is normal and only LV systolic pressure is slightly lower in GAMT$^{-/-}$ mice (19, 42). Furthermore, when the maximal exercise capacity and response to chronic myocardial infarction was compared in GAMT$^{-/-}$ and wild-type (WT) mice, no significant difference was observed (30). It is only under acute stress conditions that functional deficits are observed in both GAMT$^{-/-}$ and CK$^{-/-}$ hearts, e.g., reduced inotropic reserve and impaired recovery from ischemia-reperfusion injury (10, 19, 47). The near-normal basal cardiac performance in GAMT$^{-/-}$ mice could be due to extensive compensatory changes not identified in Ref. 30, similar to those described in the hearts of CK$^{-/-}$ mice, where the CK system is disabled by the lack of both cytosolic and mitochondrial muscle-specific CK isoforms. CK$^{-/-}$ hearts show only minor changes in performance (35), explained in part by cytoarchitectural changes that facilitate direct cross-talk between mitochondria and ATPases (23). Direct cross-talk between organelles is possible due to intracellular diffusion restrictions (60), as evidenced by a low apparent ADP affinity of mitochondrial respiration in permeabilized cardiomyocytes (27), which leads to the coupling of endogenous ATPases to mitochondria or glycolysis (44, 45) as well as anisotropy in diffusion (21, 51). In CK$^{-/-}$ mice, in the absence of Cr, the apparent ADP affinity of mitochondrial respiration was higher than in control experiments with WT mice (23). This suggests a reduction of the overall diffusion restriction between mitochondria and the surrounding solution (36). However, diffusion was sufficiently restricted for sarco(endo)plasmic reticulum Ca^{2+}-ATPase (SERCA) and myosin ATPase to preferentially use ATP generated in mitochondria as efficiently as in WT mice (23).

The aim of this study was to determine whether the hearts of GAMT$^{-/-}$ mice exhibit similar compensatory changes as those observed in the hearts of CK$^{-/-}$ mice. We used three approaches that we have previously applied to rat cardiomyo-

Address for reprint requests and other correspondence: M. Vendelin, Laboratory of Systems Biology, Institute of Cybernetics, Tallinn Univ. of Technology, Akadeemia 21, Tallinn 12618, Estonia (e-mail: markov@ioc.ee).

 Licensed under Creative Commons Attribution CC-BY 3.0: the American Physiological Society. ISSN 0363-6135.

Downloaded from journals.physiology.org/journal/ajpheart (193.040.253.082) on June 1, 2022.

cytes. Using confocal microscopy, we quantified the three-dimensional (3-D) relative position of mitochondrial centers (as in Ref. 4). This allowed us to detect whether mitochondrial positioning is different in GAMT$^{-/-}$ mice. On permeabilized cardiomyocytes, we recorded a full set of kinetic data to analyze the intracellular compartmentation of ADP/ATP using mathematical models. In rat cardiomyocytes, we discovered a strong functional coupling between pyruvate kinase (PK) and a fraction of ATPases (45). Because the activity of other phosphotransfer systems increases in CK$^{-/-}$ mice (34) and because failing hearts experiencing a loss of CK (2), we speculated whether the coupling between PK and ATPases is upregulated in GAMT$^{-/-}$ mice. Finally, we used fluorescence microscopy to record changes in NADH and flavoprotein (Fp) autofluorescence when permeabilized cardiomyocytes were exposed to increasing doses of ADP (as in Ref. 22). This would test whether the ADP kinetics of respiration, as recorded on a population level, also occurred on the single cell level.

MATERIALS AND METHODS

Animal procedures were approved by the Estonian National Committee for Ethics in Animal Experimentation (Estonian Ministry of Agriculture).

Animals. We received GAMT$^{-/-}$ mice and WT littermates, which had been bred at The Wellcome Trust Centre for Human Genetics (Oxford, UK). Mice had been backcrossed on to a C57Bl/6J background for at least eight generations. Animals were kept in our local animal facility in cages with free access to water and food (vegetable-based, Cr-free chow, R70 from Lactamin). Mice of different genotypes were housed separately to prevent GAMT$^{-/-}$ mice from taking up Cr via coprophagia of feces from WT littermates (41).

Cardiomyocytes were successfully isolated from eight GAMT$^{-/-}$ mice (4 females and 4 males) and nine WT mice (5 females and 4 males) of similar age (female WT: 46.9 ± 4.9 wk and female GAMT$^{-/-}$: 45 ± 4.3 wk; male WT: 45.6 ± 1.5 wk and male GAMT$^{-/-}$: 45.9 ± 1.4 wk).

Genotyping. Knockout and WT mice were genotyped by PCR. Briefly, genomic DNA was extracted from tissue samples by SDS/proteinase K digestion followed by isopropanol precipitation. PCR amplification of the DNA fragments was performed using the following specific primers: 5′-CAGGCTCCCACCCACTTGA-3′, 5′-AGGCCTACCCGCTTCCATTG-3′, 5′-CCTCAGGCTCCCACCCACTTG-3′, and 5′-GGTCTCCCAACGCTCCATCACT-3′. PCRs were carried out in a 25-μl volume containing 1× PCR buffer (Bioline Immobuffer), 0.5 mM dNTP mixture (Fermentas), 2 mM $MgCl_2$ (Bioline), 0.5–0.7 pmol of each primer (TAG Copenhagen), 5% DMSO (Sigma), 0.6 M betaine (Sigma), 0.06 U/μl IMMOLASE DNA polymerase (Bioline), and 5 μl template DNA. After the initial denaturation step at 94°C for 5 min, nine cycles of PCR were carried out as follows: denaturation at 94°C for 60 s, annealing at 60°C for 60 s, and extension at 72°C for 30 s. In each cycle, the temperature was decreased by 0.5°C in each consequent annealing step. This was followed by 34 cycles of the following PCR: denaturation at 94°C for 60 s, annealing at 55°C for 60 s, and extension at 72°C for 30 s. This was done in a thermal cycler (Bio-Rad DNA Engine Peltier Thermal Cycler). PCR products were electrophoresed on a 1% agarose gel with ethidium bromide in 1× Tris-borate-EDTA. Amplification of a single 265-bp product or a 427-bp PCR product corresponded to WT GAMT (GAMT$^{+/+}$) or homozygous GAMT knockout (GAMT$^{-/-}$) genotype, respectively. Simultaneous amplification of a 265- and 427-bp fragments corresponded to a heterozygous GAMT (GAMT$^{+/-}$) genotype.

Total Cr content. The total Cr content was measured enzymatically from mouse hindlimb skeletal muscle. The metabolite extraction from tissue samples was done as follows. A 50- to 100-mg piece of tissue was homogenized in 2 ml of 0.6 M perchloric acid with 2 mM EDTA. Water was added to provide a total volume of 10 ml, and the suspension was centrifuged at 10,000 *g* for 10 min at 4°C. The supernatant was neutralized with KOH, the precipitated salt was removed by centrifugation, and total Cr levels were assayed immediately from the resulting extract (pH 7.0–7.2) via coupled enzymatic reactions using a spectrofluorophotometer. The enzymatic reaction was performed in 500 μl of 100 mmol/l potassium phosphate buffer (pH 7.5) containing 5 mmol/l $MgCl_2$, 16 kU/l CK, 8 mmol/l ADP, 16 kU/l hexokinase, 4 mM glucose, 40 kU/l creatinase, 20 kU/l sarcosine oxidase, 4 kU/l horseradish peroxidase, 10 μmol/l Amplex red, and 6–40 μl tissue extract. This mixture ensured that Cr and PCr were degraded by creatinase, which led to the production of H_2O_2 (which was later determined fluorescently using Amplex red conversion to resorufin). The blank mixture was identical except for the omission of creatinase. The reaction mixture was incubated for 30 min at room temperature. H_2O_2 was determined spectrofluorometrically in 2 ml of 100 mmol/l phosphate buffer containing 5 mmol/l $MgCl_2$. Fluorescence measurements were performed using 4-ml plastic cuvettes (four-faced transparent cuvettes, Deltalab, Rubí, Spain) in an RF-5301 PC spectrofluorometer (Shimadzu Scientific Instruments, Kyoto, Japan). The temperature was maintained at 25°C (Julabo F12-ED, JULABO Labortechnik). First, background fluorescence of the buffer without enzymes was measured, and 1 μl of 5 mM Amplex red and 5 μl of 100 U/ml horseradish peroxidase were then added to measure the contribution of Amplex red to fluorescence intensity. Finally, the fluorescence of the diluted reaction mixture was measured. At the end of each experiment, a calibration signal was generated with five additions of 1 μl of 0.1 mM H_2O_2, each leading to a concentration increase of 50 nM. Measured fluorescence intensities (emission/excitation = 585/570 nm) were fitted assuming a linear relationship between fluorescence and the resorufin concentration in the cuvette, with the offset determined by the background fluorescence of the buffer. The fit was performed by minimizing the least-square difference between calculated and measured fluorescence through variation of the gain (fluorescence-to-resorufin concentration ratio), total Cr content, and resorufin contamination of Amplex red solution (proportional to the Amplex red concentration). Cr concentrations were expressed as nanomoles per milligram wet weight tissue. All measurements were repeated with three different dilutions, and a paired *t*-test between recordings with and without creatinase (sample vs. blank) was used to determine whether the total Cr content was identifiable by the method (a significance level of $P < 0.05$ was used).

Isolation of cardiomyocytes. Isolation of cardiomyocytes was carried out as previously described (45). Briefly, the heart was excised and immediately transferred to ice-cold wash solution (see composition below). It was cannulated via the aorta on a Langendorff perfusion system, which was thermostatted to 38.5°C (Julabo ED, JULABO Labortechnik). The heart was first perfused with wash solution at a constant pressure of 80 cmH_2O for at least 5 min. The flow rate under these conditions was 3.68 ± 1.68 ml/min ($n = 17$). After the heart was washed free of blood, the perfusion was switched to a digestion solution containing an additional 0.25 mg/ml collagenase P (Roche) and 3 mg/ml BSA. Perfusion was also switched to a constant flow of 1 ml/min until the pressure had decreased to 10–15% of the initial pressure at 80 cmH_2O and the heart was soft. After perfusion, the ventricles were isolated. They were cut into four pieces, which were incubated further in the digestion solution at 38.5°C with gentle shaking until the tissue started falling apart. Cells were further dissociated with a 5-ml pipette. Sedimentation solution (5 ml) was added before the cells were filtered into a glass tube. As a result, the cell suspension was a mix of isolated cardiomyocytes from the left and right ventricles. Cells were washed by sedimentation. First, extracellular Ca^{2+} was gradually increased to 1 mM to ensure Ca^{2+} tolerance of the cells (Ca^{2+} from a stock of 1 M $CaCl_2$ was added to the sedimentation solution). After this, extracellular Ca^{2+} was washed out again by washing the cells three times with 10 ml sedimentation solution.

Downloaded from journals.physiology.org/journal/ajpheart (193.040.253.082) on June 1, 2022.

Mitochondrial imaging. Freshly isolated cells kept in sedimentation solution were loaded with 1 μM TMRE (T-669, Molecular Probes, Life Technologies) for at least 15 min. A small fraction of the cells was added to 200 μl sedimentation solution in the chamber of a flexiPERM micro 12 reusable silicone cell culture chamber (Greiner Bio-One) attached to a coverslip. Confocal images were acquired on a Zeiss LSM 510 Duo built around an inverted Axio Observer Z1 microscope (Carl Zeiss) with a ×63/1.2 numerical aperture (NA) water-immersion objective. The signal was acquired via a high-voltage single photomultiplier tube using 8-bit mode; the pinhole was set to one Airy disk. TMRE was excited with a 543-nm laser, and emission was recorded through a 575-nm long-pass filter. These experiments were carried out at room temperature.

Estimating the relative positioning of mitochondrial centers. Mitochondrial positioning was quantified by statistical analysis of the relative distances between neighboring mitochondrial centers, as in Ref. 4. In short, the following procedure was used. Each stack of confocal images was blurred by a 3-D Gaussian blur with a SD of 0.3 μm in all directions. The position of all mitochondrial centers was determined by finding local fluorescence maxima of the blurred 3-D stack of images. Subsarcolemmal mitochondria and mitochondria around the nucleus (perinuclear mitochondria) were filtered out as judged by the eye. A space around each mitochondrial center was divided into 14 sectors: 2 sectors in the *y*-direction along the myofibril, 2 sectors in the *x*-direction across the myofibril in the image plane, 2 sectors in the *z*-direction across the myofibril perpendicular to the image plane, 4 diagonal sectors in the *xy*-direction, and 4 diagonal sectors in the *yz*-direction (Fig. 1). For each mitochondrial center, we found the closest neighboring mitochondrial center in each of these sectors, as shown in Fig. 1. Finally, the relative position of these neighboring mitochondrial centers was analyzed by finding the probability density function and cumulative probability distribution, as in Ref. 4.

For statistical analysis, we found for each cell separately the cumulative distribution function for the nearest neighboring mitochondria in each direction. The averaged results of the distance at 25%, 50%, and 75% of the distribution function for R and R_{XZ} (notation from Fig. 5) were compared for WT and GAMT$^{-/-}$ cardiomyocytes, as detailed in the RESULTS.

Respirometer recordings. Respirometer recordings were used to determine *1*) the respiration kinetics of permeabilized cells stimulated by stepwise increases in ADP or ATP and *2*) the inhibition of ATP-stimulated respiration by a competitive assay consisting of phosphoenol pyruvate (PEP; 5 mM) and PK (20 IU/ml). For this, we used a Strathkelvin RC 650 respirometer equipped with six 1302 O_2 electrodes connected via a 929 Oxygen System interface (all from Strathkelvin Instruments) to a computer. The respirometer was thermostatted to 25°C (Julabo F12-ED, JULABO Labortechnik). The O_2 tension in each chamber was recorded by the software provided by Strathkelvin and our homemade software, which immediately calculated the rate of O_2 consumption as well. The latter is open-source software and is freely available at http://code.google.com/p/iocbio/wiki/IOCBioStrathKelvin.

For recordings of ADP kinetics, a 15- to 20-μl cell suspension was added to the respiration chamber containing 2 ml Cr and PCr-free respiration solution (see composition below). Cells were allowed at least 5 min to permeabilize before the steady-state basal respiration rate (V_0) was recorded. ADP was added to the respirometer chamber using a Hamilton syringe (801RN, Hamilton Bonaduz). The ADP concentration was increased in steps, and the respiration rate was allowed to reach steady state for at least 2 min before the addition of more ADP. Recordings of ATP kinetics were carried out in a similar way except that a 30- to 50-μl cell suspension was added to the chamber and ATP was added instead of ADP. To record how a competitive ADP-trapping assay consisting of PEP and PK competes with mitochondria for the consumption of ADP from ATPases, a 30- to 60-μl cell suspension was added to the respirometer chamber. After recording V_0, 2 mM ATP was added to stimulate ATPases. Initially, this endogenously produced ADP was exclusively consumed by the mitochondria and stimulated respiration ($V_{2\ mM\ ATP}$). The addition of 5 mM PEP (no. P-7002, Sigma-Aldrich) activated endogenous PK to compete with mitochondria for the consumption of ADP and the lowered respiration rate (V_{PEP}). Further addition of 20 U/ml exogenous PK (no.

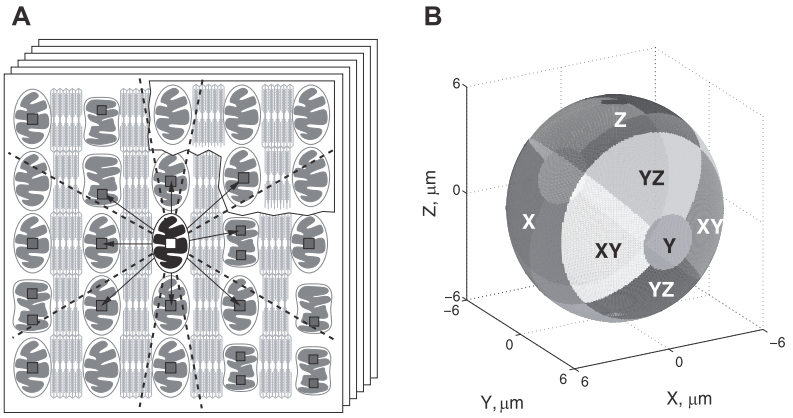

Fig. 1. Method used to analyze distribution of mitochondria in cardiomyocytes, taken from Ref. 4. *A*: first, a series of *Z*-stack confocal images of mitochondria in nonpermeabilized cardiomyocytes was acquired (scheme). Second, the local fluorescence maxima (small squares) were found. As indicated in the scheme, the maxima were not always on the same image in the stack. Note that sometimes two fluorescence maxima seem to be found per mitochondrion (as shown in *A*). Next, the closest neighbors were found for each mitochondrion, one per sector (the projections of the sector borders in two dimensions are shown by the dashed lines). In this scheme, the mitochondrion, in which neighbors are sought, is highlighted, and the closest neighbors to this mitochondrion are indicated by arrows. Note that the closest mitochondria in some sectors are not always from the same image in the stack. The relative coordinates of the closest neighbors, i.e., the coordinates relative to the highlighted mitochondria, were stored and further analyzed. *B*: division of three-dimensional space into the sectors, with sectors shown by the different levels of gray. The mitochondrion for which neighbors are sought is positioned at the origin of coordinate system. Here, the coordinate *y*-axis corresponds to the fiber orientation. The sector names are shown in the scheme.

Downloaded from journals.physiology.org/journal/ajpheart (193.040.253.082) on June 1, 2022.

10109045001, Roche), lowered the respiration rate ($V_{PEP + PK}$) even more.

Spectrophotometer recordings. ATP kinetics of ATPases and ADP kinetics of endogenous PK were recorded using an Evolution 600 spectrophotometer (Thermo Fisher Scientific) equipped with a Peltier water-cooled cell changer (SPE 8 W, Thermo Fisher Scientific) to maintain temperature at 25°C. ADP production by ATPases in permeabilized cardiomyocytes was recorded in 2 ml respiration solution using a coupled assay consisting of 5 mM PEP (no. P-7002, Sigma-Aldrich), 0.3 mM NADH (no. 10128015001, Roche), 7.2 U/ml LDH (no. 61311, Sigma-Aldrich), and 20 U/ml PK (no. 10109045001, Roche). To avoid ADP consumption by mitochondria, respiration was inhibited by 5 mM NaCN (no. 205222, Sigma-Aldrich) and 10 μM oligomycin (no. 75351, Sigma-Aldrich). The basal ATPase rate was first recorded in the absence of ATP and then at increasing concentrations of ATP. Rates were recorded for 3 min after each addition, and steady state was verified for each step. NADH was replenished as needed to keep absorbance between 1.7 and 0.7 (the linear range of NADH consumption as verified by preliminary experiments; data not shown). The ADP kinetics of endogenous PK were recorded using the same coupled assay (where only 5 mM NaCN, 10 μM oligomycin, 5 mM PEP, 0.3 mM NADH, and 7.2 U/ml LDH were added), and PK activity was recorded at increasing ADP concentrations.

For normalization, the protein content was measured with a Nanodrop 2000 (Thermo Fisher Scientific).

Mathematical model. For a detailed description of the model, see Ref. 45. In brief, models of different complexity were considered (Fig. 2). All models included three separate compartments: extracellular solution, cytoplasm, and intermembrane space (IMS). *Models 3* and *4* also included a fourth compartment (*compartment 4*) with PK and ATPase to describe coupling between glycolysis and ATPases, as described in Ref. 45. The processes considered in the models were diffusion between compartments restricted by diffusion barriers, the reactions of ATPases, oxidative phosphorylation, and the reactions of endogenous PK. The models containing two groups of ATPases (2, 3, and 4) were also considered in a simplified form (2s, 3s, and 4s) with both groups of ATPases having the same affinities for ATP and ADP.

For simplicity, ATP synthesis in mitochondria was described by the simple phenomenological Michaelis-Menten-type equation involving the concentrations of ATP and ADP only in the IMS, as shown in Fig. 2. Note that this approach is possible due to high concentrations of P_i, oxygen, and substrates, as used in our experiments. This simplification allowed us to simulate diffusion and reactions in the intracellular compartments only (cytoplasm, IMS, and *compartment 4*) and thus allowed us to ignore the details of the reactions involved in the respiratory chain. The same approach has been applied by us earlier and used to estimate the compartmentation of ATPases and intracellular diffusion restrictions in two dimensions (52), three dimensions (36), and simplified multicompartment (45) analysis of the intracellular environment.

To compare the models, the goodness of fit was evaluated using Akaike information criteria (AIC), corrected AIC (AIC_c), and Bayesian information criteria (BIC), which were calculated for each model. For all three criteria, the best-fitting model is the one with the minimum criterion value. Those criteria take into account the goodness of fit and number of parameters in the model. Using AIC_c and BIC, a larger number of parameters is penalized more than in AIC. Multiple goodness criteria were used to ensure that the conclusions would not depend on the selection of one particular criterion.

In addition, models were compared by an *F*-test for nested models, which allows comparison of *models 1* and *2* with *model 3* as well as *models 1* and *2* with *model 4*. The *F*-test takes the number of parameters into account so that statistical significance indicates that the more complicated model fits the data better irrespective of the number of parameters.

Next, the *F*-test was used to evaluate confidence intervals for each of the fitted model parameters. Confidence intervals were calculated using an *F*-test and show the range where the fit is worse than an optimal fit but with a *P* value larger than 0.05 (in terms of extra sum of squares), as in Ref. 45.

Finally, to test whether the data recorded in WT and GAMT$^{-/-}$ cardiomyocytes were significantly different from each other, the data were fit either separately for different types of cardiomyocytes or by fitting both sets with the same model parameters (pooled data set). The *F*-test was applied to test whether an increased number of parameters induced by fitting the experiments separately was justified or whether the better fits were due to chance. For this test, a fit of pooled data by a single set of model parameters can be considered as a simplified version of fitting the data separately using two sets of model parameters: one for WT cardiomyocytes and one for GAMT$^{-/-}$ cardiomyocytes.

For a detailed model description, numeric methods, and statistical analysis, see Ref. 45.

Recordings of NADH and Fp autofluorescence. Recordings of NADH and Fp autofluoresence were performed as described in Ref. 22. In brief, microscope experiments were performed on an inverted Nikon Eclipse Ti-U microscope (Nikon, Tokyo, Japan; objective CFI Super Plan Fluor ELWD ×20/0.45 NA) equipped with two tiers of motorized filter turrets for simultaneous acquisition of transmission and fluorescence images. For images of NADH and Fp autofluorescence, respectively, light from a Prior Lumen 200 with a 200-W metal halide lamp with extended wavelength (Prior Scientific, Cambridge, UK) was passed via an optical fiber into the upper filter turret. For NADH recordings, the light was passed through a 340/26-nm excita-

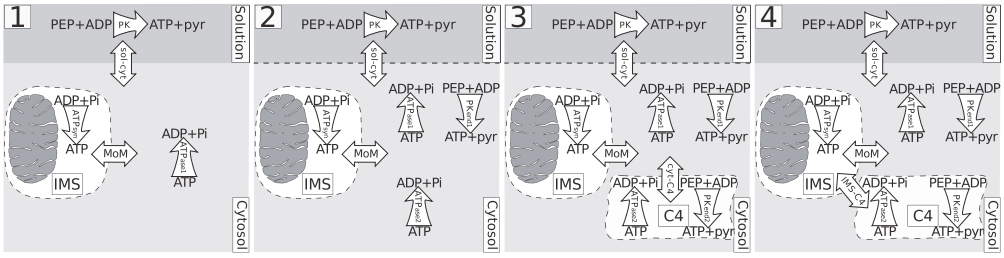

Fig. 2. Schematic diagrams of *models 1–4*. Compartments are indicated by dashed lines, reactions by single-headed curved arrows, and exchange between compartments by double-headed straight arrows. All models have compartments representing the solution, cytosol, and mitochondrial intermembane space (IMS). *Models 3* and *4* include a fourth compartment (C4). The reactions considered are mitochondrial ATP synthesis in the mitochondrial matrix leading to the conversion of ADP to ATP in the mitochondrial IMS (ATP_{syn}), ATP consumption by ATPases (ATPase1 and ATPase2), and ATP synthesis by endogenous pyruvate kinase (PK; PKend1 and PKend2) and exogenous PK. The following exchanges between compartments were calculated: solution and cytosol (sol-cyt), IMS and cytosol through the outer mitochondrial membrane (MoM), cytosol and C4 (cyt-C4), and IMS and C4 (IMS-C4). PEP, phosphoenol pyruvate.

Downloaded from journals.physiology.org/journal/ajpheart (193.040.253.082) on June 1, 2022.

tion filter onto a 400-nm long-pass dichroic mirror, which deflected the light onto the specimen. Light emitted from the specimen passed back through the upper filter cube to a 510 XR dichroic in the lower filter cube and reflected through a 460/80-nm emission filter to an Andor Ixon EMCCD camera (Andor Technologies, Belfast, UK). For Fp recordings, the light was passed through a 465/30-nm excitation filter onto a 510-nm dichroic mirror, which deflected the light onto the specimen. Light emitted from the specimen passed back through the upper filter cube to a 560 XR dichroic in the lower filter cube and reflected through a 525/50-nm emission filter. All filters were purchased from AHF Analysentechnik. For each filter, the first number describes the mode wavelength and the second number describes the total bandwidth at half-maximum transparency (half-minimum optical density). This means that a 340/26-nm filter mainly passes light between 327 and 356 nm. Filter specifications, including plots of their optical density at different wavelengths, can be found on the suppliers website (http://www.ahf.de). Transmission images together with images of NADH or Fp autofluorescence were acquired every 30 s. To reduce photobleaching, a Uniblitz shutter (VCM-D1, Vincent Associates, Rochester, NY) timed the light exposure with the acquisition.

Immediately before each experiment, a new batch of cells was permeabilized for 5 min with gentle mixing in an Eppendorf tube with respiration solution containing 25 μg/ml saponin and 50 μM ADP. A fraction of the permeabilized cells was put into a diamond-shaped fast-exchange chamber (15 × 6 mm, RC-24N, Warner Instruments, Harvard Apparatus, March-Hugstetten, Germany) on the microscope. Cells were allowed to sediment for 5–10 min before the superfusion was started with respiration solution containing different concentrations of ADP. Only cells located in the middle of the chamber were used for measurements. According to the manufacturer, the geometry of the chamber provided laminar flow of solutions during experiments at the used flow rate of ≈0.5 ml/min and was laminar in our conditions, as confirmed by mathematical model of the flow (22). The ADP concentration was increased stepwise from 50 to 100, 300, 500, 1,000, and 2,000 μM, and cells were superfused for at least 4.5 min at each step.

Fluorescence signal intensity from microscope single cell experiments was analyzed using ImageJ software. Both regions containing each cell and background regions were selected, and corresponding average fluorescence signal intensities were determined with the ImageJ plug-in "measure stack." Background fluorescence was then subtracted from cell fluorescence, and the data were plotted on a timescale. From the latter plot, average fluorescence was found for each condition to which the cell was exposed (ADP concentration, uncoupling or block of oxidative phosphorylation). To enable comparison between cells, signals were normalized to maximum and minimum fluorescence recorded under fully reduced (respiration inhibited with oligomycin and cyanide) or oxidized (mitochondria uncoupled with FCCP) conditions.

Solutions. The wash solution consisted of (in mM) 117 NaCl (no. 71379, Sigma-Aldrich), 5.7 KCl (no. P-5405, Sigma-Aldrich), 1.5 KH_2PO_4 (no. P-0662, Sigma-Aldrich), 4.4 $NaHCO_3$ (no. S-6014, Sigma-Aldrich), 1.7 $MgCl_2$ (no. 63068, Sigma-Aldrich), 21 HEPES (no. H-3375, Sigma-Aldrich), 20 taurine (no. 86329, Sigma-Aldrich), and 11.7 glucose (no. 158968, Sigma-Aldrich). pH was adjusted to 7.4 with NaOH.

For the collagenase solution, 0.25 mg/ml collagenase P (no. 11213873001, Roche) and 3 mg/ml BSA (no. 10775835001, Roche) was added to 40 ml of the wash solution.

For the sedimentation solution, 2 mM pyruvate (no. P-2256, Sigma-Aldrich), 10 μM leupeptin (no. 11034626001, Roche), 2 μM soybean trypsin inhibitor (no. 93619, Sigma-Aldrich), and 3 mg/ml BSA (no. 10775835001, Roche) were added to 60 ml of the wash solution.

The respiration solution contained (in mM) 110 sucrose (no. S-1888, Sigma-Aldrich), 60 K-lactobionic acid (no. L-2398, Sigma-Aldrich), 3 KH_2PO_4 (no. P-0662, Sigma-Aldrich), 3 $MgCl_2$ (no. 63068, Sigma-Aldrich), 20 HEPES (no. H-3375, Sigma-Aldrich), 20 taurine (no. 86329, Sigma-Aldrich), 0.5 EGTA (no. 71379, Sigma-Aldrich), 0.5 DTT (no. D-0632, Sigma-Aldrich), 2 malate (no. M-6413, Sigma-Aldrich), and 5 glutamate (no. 49449, Sigma-Aldrich). pH was adjusted to 7.1 with KOH. Immediately before use, 5 mg/ml BSA (no. 10775835001, Roche) and 20 μg/ml saponin (no. 47036, Sigma-Aldrich) were added.

The ADP stock solution contained 200 mM ADP (no. A-2754, Sigma-Aldrich) and 60 mM $MgCl_2$ (no. 63068, Sigma-Aldrich). pH was adjusted to 7.1 with KOH.

The ATP stock solution contained (in mM) 200 ATP (no. 10127531001, Roche), 200 Mg-acetate (no. M-5661, Sigma-Aldrich), and 20 HEPES (no. H-3375, Sigma-Aldrich). pH was adjusted to 7.1 with KOH.

Concentrations of the uncoupler and respiration blockers were as follows: FCCP (10 μM, no. Asc-081, Ascent Scientific), oligomycin A (10 μM, no. 579-13-5, Tebu-bio), and sodium cyanide (5 mM, no. 205222, Sigma-Aldrich).

Statistics. Raw data were analyzed using homemade software. Values are given as means ± SD.

RESULTS

Characteristics of WT and GAMT$^{-/-}$ mice. Genotypes of the mice were confirmed by PCR. The results are shown in Fig. 3.

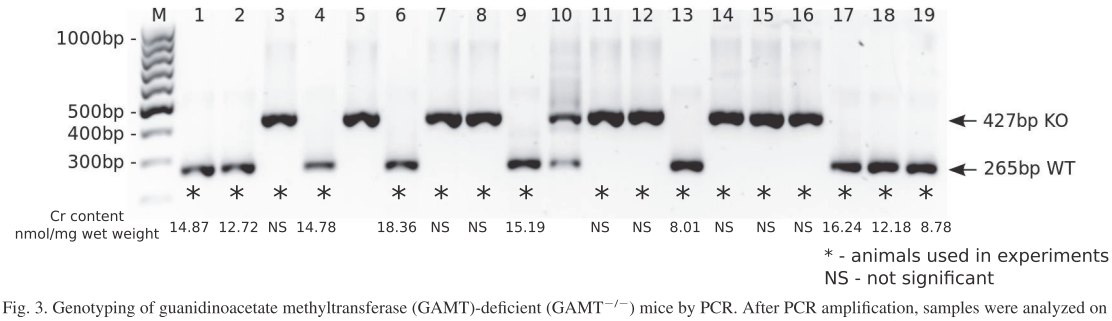

Fig. 3. Genotyping of guanidinoacetate methyltransferase (GAMT)-deficient (GAMT$^{-/-}$) mice by PCR. After PCR amplification, samples were analyzed on 1% agarose gel stained with ethidium bromide along with a DNA ladder (*lane M*: GeneRuler 100-bp DNA Ladder). The 265- and 427-bp-long PCR products corresponded to wild-type (WT) GAMT (GAMT$^{+/+}$) or homozygous GAMT knockout (GAMT$^{-/-}$ KO) genotypes, respectively. *Animals that were used in experiments. Total skeletal muscle creatine (Cr) content (expressed as nmol/mg wet wt) is shown under each mouse used in the experiments, respectively. The levels of Cr in GAMT$^{-/-}$ mice were statistically not significant (NS).

Downloaded from journals.physiology.org/journal/ajpheart (193.040.253.082) on June 1, 2022.

GAMT$^{-/-}$ mice had a lower body weight than their WT littermates [female WT: 24.2 ± 3.8 g vs. female GAMT$^{-/-}$: 17.5 ± 2.6 g ($P < 0.05$); male WT: 34.5 ± 5.3 g vs. male GAMT$^{-/-}$: 23.0 ± 2.7 g ($P < 0.01$)]. In female mice, tibial length was also shorter in GAMT$^{-/-}$ than WT mice [female WT: 21.8 ± 0.2 mm vs. female GAMT$^{-/-}$: 21.1 ± 0.6 mm ($P < 0.05$); male WT: 22.6 ± 0.6 mm vs. male GAMT$^{-/-}$: 21.7 ± 0.8 mm ($P = 0.1330$)]. This is in agreement with previous observations (19, 41).

Total Cr content was measured enzymatically in GAMT$^{-/-}$ and WT mice used in the experiments. Skeletal muscle Cr content was 13.46 ± 3.40 nmol/mg wet wt in WT control mice ($n = 9$) and undetectable in GAMT$^{-/-}$ mice ($n = 8$) (Fig. 3). This was confirmed statistically with a paired t-test showing no significant difference in the Cr content between the GAMT$^{-/-}$ sample and the corresponding blank ($P > 0.05$) and a significant difference between the WT sample and the corresponding blank ($P < 0.05$).

Mitochondrial positioning. Visual inspection of the confocal images showed similar mitochondrial distribution in GAMT$^{-/-}$ and WT cardiomyocytes. This was confirmed by quantitative analysis of the relative positioning of the mitochondrial centers (Figs. 4 and 5). Figure 4 shows the probability densities of the closest mitochondrial centers found in the different sectors. There was no difference between GAMT$^{-/-}$ and WT cardiomyocytes. Figure 5 shows plots of the cumulative distribution functions. The graphs for WT and GAMT$^{-/-}$ cardiomyocytes were overlapping or were very close in all directions (Fig. 5).

For statistical analysis, we found the averaged distances R and R_{XZ} (notation from Fig. 5) at 25%, 50%, and 75% of the cumulative distribution function (Table 1). There was no significant

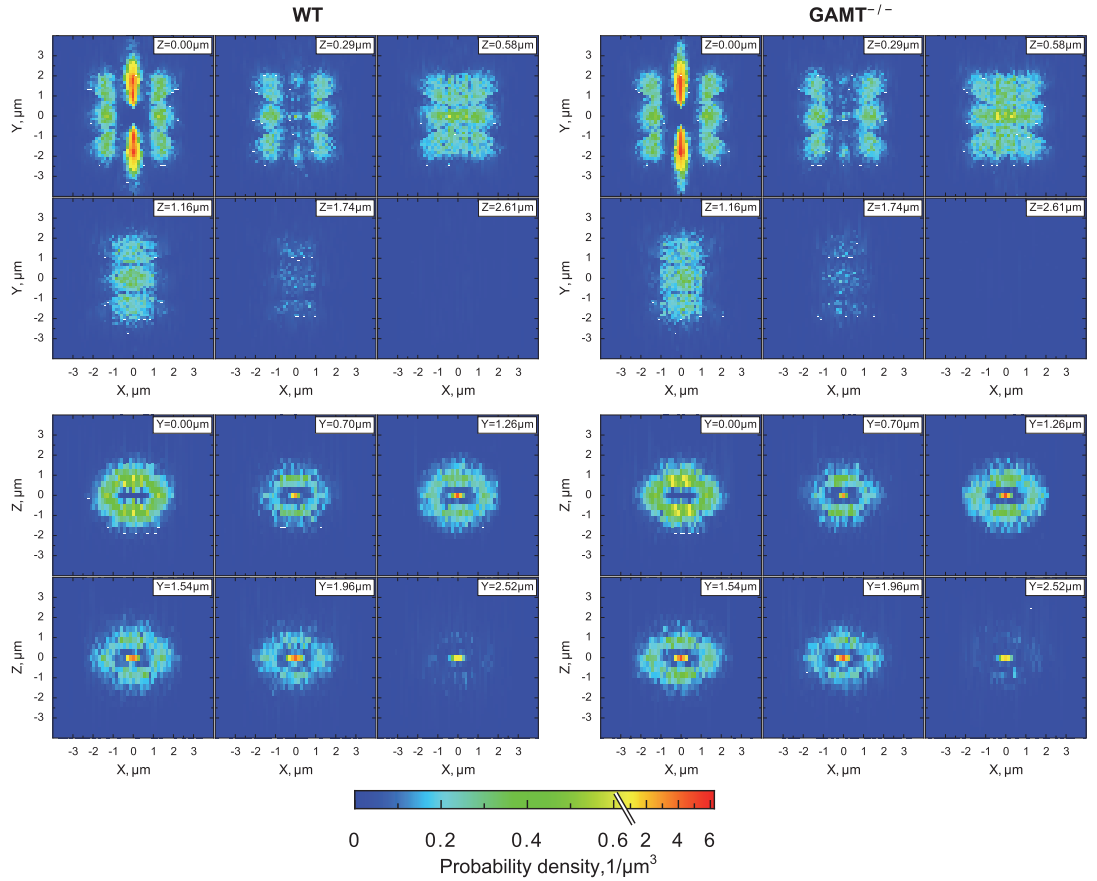

Fig. 4. Probability density of the closest mitochondrial centers in each of the directions in WT (*left*) and GAMT$^{-/-}$ (*right*) cardiomyocytes. A total of 24,588 (WT) and 23,405 (GAMT$^{-/-}$) mitochondria from 6 cells were analyzed. Each mitochondrial center was considered to be in the origin (0, 0). The space around was divided into 14 sectors, and the distribution of the closest mitochondrial centers in each sector was analyzed. Results from sectors with the same direction were pooled. Here, and in the following analysis, the y-direction was taken along the myofibrills and x- and z-directions were transversal directions at and perpendicular to the image planes, respectively. The xy- and yz-directions were diagonal directions. Two-dimensional probability density is shown at different planes perpendicular to the z-axis (XY-planes; *top*) or the y-axis (XZ-planes; *bottom*) at different distances from the origin as indicated at the *top right* corner of each plane. Note how similar the mitochondrial distributions were in GAMT$^{-/-}$ and WT cardiomyocytes.

Downloaded from journals.physiology.org/journal/ajpheart (193.040.253.082) on June 1, 2022.

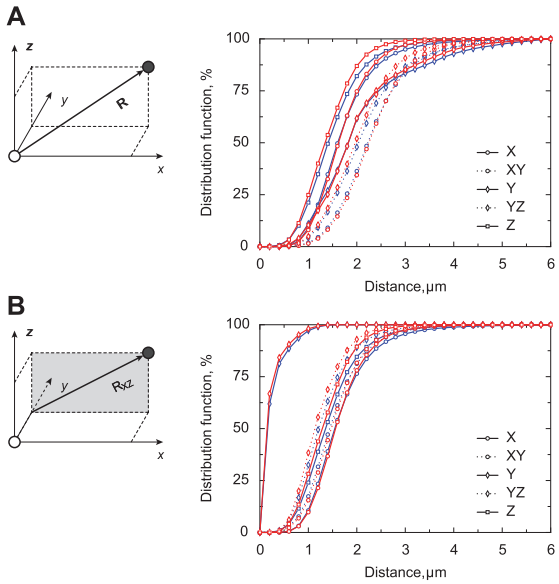

Fig. 5. Cumulative distribution function of the distance between centers of neighboring mitochondria in different directions. The distribution functions for the following distances were calculated: distance (R) from the origin to the nearest mitochondrion in each direction (A) and distance (R_{XZ}) from the y-axis through the origin to the nearest mitochondrion in each direction (B). The differences in the corresponding distances are highlighted on the schemes shown in A and B, *left*. If the rows of mitochondria were parallel, R_{XZ} would be the same in the X- and XY-directions and Z- and YZ-directions. Indeed, their distribution functions were very close. For parallel rows, R_{XZ} in the Y-sector would be 0. Note in both A and B that the distribution functions for the WT (blue) and GAMT$^{-/-}$ (red) groups were either overlapping or very close to each other.

difference in the distances between WT and GAMT$^{-/-}$ cardiomyocytes as analyzed with mixed-design ANOVA. In this statistical test, the between-subject variables were mouse genotypes (2 levels: WT or GAMT$^{-/-}$) and the within-subject variables were directions for R and R_{XZ} (5 directions for each, 10 levels in total) and percentile points (3 levels). On the basis of ANOVA, we concluded that there was no significant main effect of genotype, $P = 0.28$. No significant differences in the distances were found when we compared the distances obtained at all directions and all percentile points for WT and GAMT$^{-/-}$ cardiomyocytes using Welch's t-test and correcting for multiple comparisons using the Šidák correction.

From this analysis, we conclude that the distances between mitochondrial centers in WT and GAMT$^{-/-}$ cardiomyocytes were not significantly different. Furthermore, we did not observe any compensation in mitochondrial positioning to the lack of a functional CK shuttle in GAMT$^{-/-}$ cardiomyocytes.

Kinetic recordings. In the respirometer, we recorded the kinetics of ADP- and ATP-stimulated respiration in permeabilized cardiomyocytes. ADP directly stimulates respiration, whereas ATP is first hydrolyzed by ATPases to ADP, which diffuses to the mitochondria and stimulates respiration (Fig. 6, A and B). In addition, we recorded how ATP-stimulated respiration is affected by a competitive ADP-trapping system consisting of PEP activating endogenous PK and PEP activating additional 20 U/ml exogenous PK (Table 2). The respiration data were complemented by spectrophotometric recordings of the kinetics of ATP-stimulated ATPase activity and ADP-stimulated endogenous PK activity using a coupled assay (Fig. 6, C and D).

Analysis of kinetic data by mathematical models. The experimental data were fitted by several mathematical models with different levels of compartmentation (Fig. 2). The model fits were compared with the measurements shown in Fig. 6 and Table 2. To analyze the data obtained from WT and GAMT$^{-/-}$ mouse cardiomyocytes, we first fitted the data separately. The data were then pooled together and fitted (parameters shown in Table 3). As expected, the fit was better when the models were allowed to fit the WT and GAMT$^{-/-}$ data separately (quantified by sum of squares in least-squares fitting). However, according to the extra sum-of-squares F-test (F-test), the increased number of parameters induced by fitting the experiments separately was not justified, and the better fits were due to chance (depending on the model, P was from 0.37 to 0.99). From this, we concluded that the kinetic recordings in WT and GAMT$^{-/-}$ mouse cardiomyocytes were not significantly different and that the two cases could be described by a single set of a model parameters.

Table 1. *Distances at 25%, 50%, and 75% of the distribution function for R_{XYZ} and R_{XZ}*

	25%		50%		75%	
Direction	WT	GAMT$^{-/-}$	WT	GAMT$^{-/-}$	WT	GAMT$^{-/-}$
R_{XYZ}						
X	1.28 ± 0.04	1.31 ± 0.08	1.61 ± 0.04	1.64 ± 0.07	2.07 ± 0.09	2.06 ± 0.09
XY	1.81 ± 0.08	1.88 ± 0.12	2.25 ± 0.07	2.29 ± 0.11	2.76 ± 0.10	2.78 ± 0.13
Y	1.35 ± 0.15	1.39 ± 0.18	1.83 ± 0.08	1.82 ± 0.09	2.56 ± 0.29	2.39 ± 0.15
YZ	1.61 ± 0.08	1.57 ± 0.10	2.08 ± 0.11	2.01 ± 0.11	2.65 ± 0.23	2.48 ± 0.11
Z	1.07 ± 0.05	0.99 ± 0.08	1.43 ± 0.08	1.35 ± 0.08	1.89 ± 0.19	1.75 ± 0.08
R_{XZ}						
X	1.23 ± 0.03	1.27 ± 0.08	1.55 ± 0.04	1.58 ± 0.07	2.00 ± 0.09	2.00 ± 0.10
XY	1.12 ± 0.03	1.17 ± 0.07	1.45 ± 0.02	1.50 ± 0.08	1.88 ± 0.05	1.90 ± 0.10
Y	0.08 ± 0.01	0.07 ± 0.02	0.16 ± 0.03	0.12 ± 0.04	0.32 ± 0.09	0.24 ± 0.06
YZ	0.92 ± 0.04	0.86 ± 0.07	1.23 ± 0.05	1.14 ± 0.08	1.68 ± 0.15	1.54 ± 0.10
Z	1.03 ± 0.05	0.95 ± 0.08	1.38 ± 0.08	1.29 ± 0.08	1.82 ± 0.20	1.68 ± 0.09

Values (in μm) are means ± SD; $n = 6$ wild-type (WT) cardiomyocytes and 6 guanidinoacetate methyltransferase (GAMT)-deficient (GAMT$^{-/-}$) cardiomyocytes. R_{XYZ}, distance from the origin to the nearest mitochondrion; R_{XZ}, distance from the y-axis through the origin to the nearest mitochondrion.

Downloaded from journals.physiology.org/journal/ajpheart (193.040.253.082) on June 1, 2022.

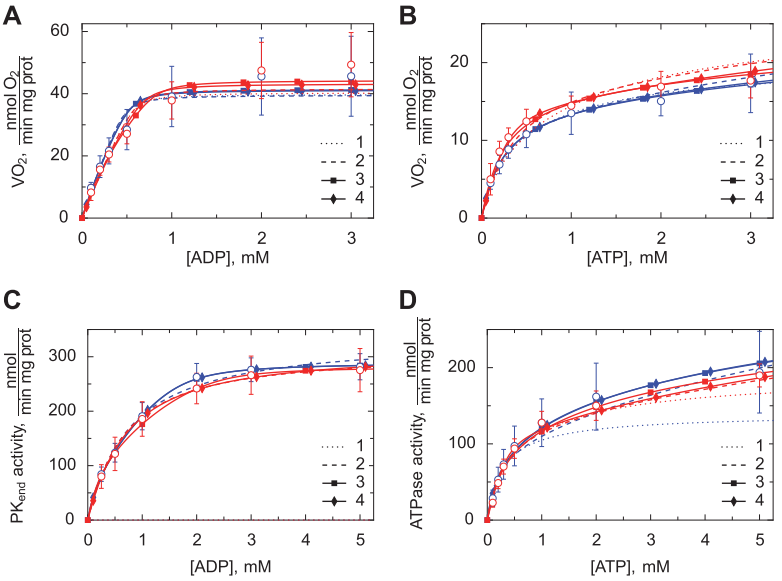

Fig. 6. Kinetic analysis of permeabilized cardiomyocytes from WT (blue) and GAMT$^{-/-}$ (red) mice. Measurements were performed in respiration solution containing 2 mM malate and 5 mM glutamate to support ADP-stimulated respiration. The experimental results are shown as means ± SD (open circles). These were compared with the solutions from *models 1–4*. Fits from simplified *model 2s*, *3s*, and *4s* were excluded for simplicity. *A*: respiration rate as a function of the ADP concentration added to the respirometer chamber (n = 6 and 5 for WT and GAMT$^{-/-}$ cardiomyocytes, respectively). *B*: respiration rate as a function of ATP (n = 7 and 5 for WT and GAMT$^{-/-}$ cardiomyocytes, respectively). *C*: endogenous PK activity as a function of ADP in the spectrophotometer cuvette (n = 8 and 7 for WT and GAMT$^{-/-}$ cardiomyocytes, respectively). *D*: ATPase activity as a function of ATP in the spectrophotometer cuvette (n = 9 and 7 for WT and GAMT$^{-/-}$ cardiomyocytes, respectively). Note that the fits from *models 3* and *4* were either very close or overlapping in all cases. V_{O_2}, O_2 consumption.

As previously found for rat cardiomyocytes (45), the fits obtained by *models 1*, *2*, and *2s* were considerably worse than the fits with the other models, as shown by statistical analysis using an F-test of the nested models (Table 4). However, when information criteria were used, only *model 1* was considerably worse than the other models (AIC_c and BIC). By comparing the results from multiple goodness-of-fit criteria, we can conclude that solutions of all models, except for *model 1*, can be considered reasonable. The main difference between *model 2* and *models 3*, *3s*, *4*, and *4s* is the introduction of a coupling between a part of endogenous PK and ATPases. Thus, while the *F*-test strongly suggests that a part of endogenous PK is coupled to ATPases ($P < 0.05$), the information criteria analysis was not conclusive, and further studies are needed. In addition, considerable diffusion restriction was identified at the level of the mitochondrial outer membrane and at the level of intracellular diffusion restrictions separating mitochondria from the surrounding solution.

As explained above, when analyzing the model parameters obtained by fitting the data, we have to consider the pooled case only (Table 3). In the models, all reaction rates were simulated using Michaelis-Menten kinetics with the apparent kinetic constants V_{max} and K_m. ATPases were considered to be inhibited competitively by ADP (where $K_{iATPase}$ is the apparent inhibition constant). The diffusion restrictions are described via exchange coefficients between the compartments (where $C_{compartment\ 1\text{-}compartment\ 2}$ is the exchange coefficient between *compartment 1* and *compartment 2*). Table 3 shows the parameters used for each model. According to our simulation results using the pooled data set, the diffusion restrictions that separate the surrounding solution from mitochondria were similar to the diffusion restrictions

Table 2. *$V_{2\ mM\ ATP}$, V_{PEP}, and $V_{PEP\ +\ PK}$ for experimental data and the various models*

		Models						
	Experimental Data	*1*	*2*	*2s*	*3*	*3s*	*4*	*4s*
WT								
$V_{2\ mM\ ATP}$	14.48 ± 4.24	15.98	16.14	16.72	15.71	15.33	15.79	15.51
V_{PEP}	11.15 ± 3.73	17.23	11.45	11.73	8.88	11.15	9.1	11.53
$V_{PK\ +\ PEP}$	4.84 ± 2.02	5.53	4.42	5.68	6.5	6.87	6.15	6.43
GAMT$^{-/-}$								
$V_{2\ mM\ ATP}$	14.07 ± 3.02	18.12	17.97	19.08	17.14	16.58	17.14	17
V_{PEP}	10.86 ± 2.53	19.69	12.36	12.82	9.81	11.29	11.52	13.07
$V_{PK\ +\ PEP}$	5.21 ± 2.18	8.16	7.16	7.62	9.22	9.9	6.46	10.43
Pooled								
$V_{2\ mM\ ATP}$	14.30 ± 3.64	17.66	17.31	18.4	16.6	16.04	16.5	16.55
V_{PEP}	11.02 ± 3.16	19.06	12.06	12.69	9.19	11.07	11.26	12.25
$V_{PK\ +\ PEP}$	5.00 ± 2.03	7.13	6.04	7.07	8.4	8.95	5.61	9.01

Values are in nmol·min^{-1}·mg protein^{-1}; n = 8 WT cardiomyocytes, 7 GAMT$^{-/-}$ cardiomyocytes, and 15 pooled cardiomyocytes. Experimental data were compared with simulation results obtained by *models 1–4* and their simplified versions (*models 2s*, *3s*, and *4s*). $V_{2\ mM\ ATP}$, ATP-stimulated respiration rate; V_{PEP}, inhibition of ATP-stimulated respiration rate by endogenous pyruvate kinase (PK); $V_{PEP\ +\ PK}$, inhibition of ATP-stimulated respiration rate by endogenous PK; PEP, phosphoenol pyruvate.

Downloaded from journals.physiology.org/journal/ajpheart (193.040.253.082) on June 1, 2022.

Table 3. *Model parameters found by fitting the pooled data obtained from WT and GAMT$^{-/-}$ cardiomyocytes*

	Models						
	1	*2 s*	*2*	*3 s*	*3*	*4 s*	*4*
$V_{maxATPsyn}$, nmol·min^{-1}·mg protein^{-1}							
Optimal value	233	248	243	257	262	255	254
Confidence intervals	62–720	174–335	172–330	191–332	193–344	182–338	190–327
$C_{sol\text{-}cyt}$, nmol·mM^{-1}·min^{-1}·mg protein^{-1}							
Optimal value	1,461	1,017	1,295	409	299	493	1,234
Confidence intervals	175 to >10^5	562–2031	606–3,062	249–651	199–426	273–893	635–2,464
C_{MoM}, nmol·mM^{-1}·min^{-1}·mg protein^{-1}							
Optimal value	646	676	612	1,132	2,362	950	517
Confidence intervals	222–2,231	530–875	481–791	786–1,788	1,264–7,394	662–1,479	425–635
$C_{IMS\text{-}C4}$, nmol·mM^{-1}·min^{-1}·mg protein^{-1}							
Optimal value						8.39	366
Confidence intervals						1.72–16	261–544
$C_{cyto\text{-}C4}$, nmol·mM^{-1}·min^{-1}·mg protein^{-1}							
Optimal value				0.005	156		
Confidence intervals				0.003–0.009	81–343		
$V_{maxATPase1}$, nmol·min^{-1}·mg protein^{-1}							
Optimal value	181	177	614	119	89	105	742
Confidence intervals	90–298	156–198	322–954	108–130	79–99	93–117	474–1,045
$K_{mATPase1}$, Mm							
Optimal value	0.21	0.271	10	0.235	0.201	0.201	10
Confidence intervals	0.06–0.834	0.206–0.358	≥10	0.187–0.294	0.147–0.276	0.143–0.279	6.91 to >10
$K_{iATPase1}$, mM							
Optimal value	0.051	0.102	0.05	9.62	10	10	0.051
Confidence intervals	0.05 to >10	0.056–0.228	0.05 to >10	0.208 to >10	≥10	0.229 to >10	0.05–0.09
$V_{maxATPase2}$, nmol·min^{-1}·mg protein^{-1}							
Optimal value			107	119	278	127	95
Confidence intervals			92–122	75–169	186–391	42–4,500	82–108
$K_{mATPase2}$, mM							
Optimal value			0.194		3.77		0.051
Confidence intervals			0.131–0.286		2.47–6.26		0.05–0.1
$K_{iATPase2}$, mM							
Optimal value			10		0.053		10
Confidence intervals			0.142 to >10		0.05–0.147		0.166 to >10
$V_{maxPKend1}$, nmol·min^{-1}·mg protein^{-1}							
Optimal value		322	327	235	68	284	327
Confidence intervals		282–362	287–368	204–267	42–94	244–325	293–361
$K_{mPKend1}$, mM							
Optimal value		0.546	0.621	0.33	0.05	0.596	0.616
Confidence intervals		0.366–0.809	0.424–0.904	0.208–0.502	0.05–0.112	0.414–0.852	0.448–0.845
$V_{maxPKend2}$, nmol·min^{-1}·mg protein^{-1}							
Optimal value				356	217	47	0.118
Confidence intervals				111–7199	180–258	23–72	0.053–29

induced by mitochondrial outer membrane. This is clear from a comparison of the exchange coefficients $C_{sol\text{-}cyt}$ and C_{mom} for all the models that provided reasonable fits (Table 3). Namely, while for some models (*models 2*, *2s*, and *4*) the diffusion restriction induced by the mitochondrial outer membrane was larger than the one separating the surrounding solution from mitochondria, the opposite was true for the other models (*models 3*, *3s*, and *4s*). However, we should note that for all models, with the exception of *model 3*, those diffusion restrictions were of the same order of magnitude, suggesting that they are similar. Note that the description of ATPases and endogenous PK interaction in *compartment 4* is a phenomenological one and that all the model parameters obtained for this compartment, including the exchange coefficient, are phenomenological coefficients and may not represent the interaction between ATPases and PK in a mechanistic way (as discussed in Ref. 45). As such, the obtained low exchange coefficient for *compartment 4* is a part of a general description of coupling between PK and ATPases and cannot be compared directly with the other exchange coefficients found by the model.

Autofluorescence of single, permeabilized cardiomyocytes during ADP titration. To verify that diffusion restrictions were not due to clumping of the cells, we recorded NADH and Fp autofluorescence responses to the change in ADP at the single cell level (Fig. 7). The mainly mitochondrial origin of NADH and Fp fluorescence signals allowed us to relate fluorescence to the state of oxidative phosphorylation. NADH and Fp signals decreased and increased, respectively, as the concentration of ADP in the surrounding solution was increased (Fig. 7). We compared the normalized NADH and Fp fluorescence at each ADP concentration and found no statistically significant difference between cardiomyocytes from WT and GAMT$^{-/-}$ mice (P from 0.09 to 0.95 by Welch's t-test; Fig. 7, *C* and *D*).

Downloaded from journals.physiology.org/journal/ajpheart (193.040.253.082) on June 1, 2022.

Table 4. *Statistical analysis of the fits*

				F-Tests					
	AIC	AIC_c	BIC	*Model 2s*	*Model 2*	*Model 3s*	*Model 3*	*Model 4s*	*Model 4*
WT cardiomyocytes									
Model 1	98.39	102.2	590.48	<0.0001	<0.0001	<0.0001	<0.0001	<0.0001	<0.0001
Model 2s	−23.1	−15.9	34.47		0.124	<0.05	<0.05	<0.05	<0.05
Model 2	−26.13	−10.61	42.56				<0.05		<0.05
Model 3s	−32.68	−17.15	41.44				0.113		
Model 3	−36.58	−12.32	47.13						
Model 4s	−30.43	−14.9	41.8						<0.05
Model 4	−37.7	−13.44	47.0						
GAMT$^{-/-}$ cardiomyocytes									
Model 1	77.59	81.41	298.61	<0.0001	<0.0001	<0.0001	<0.0001	<0.0001	<0.0001
Model 2s	7.75	14.95	48.76		0.139	<0.01	<0.01	<0.05	<0.001
Model 2	5.14	20.67	53.25				<0.01		<0.001
Model 3s	−11.33	4.2	46.23				0.583		
Model 3	−9.28	14.98	52.37						
Model 4s	0.55	16.08	50.88						<0.01
Model 4	−16.84	7.43	50.4						
Pooled WT and *GAMT*$^{-/-}$ cardiomyocytes									
Model 1	167.94	169.59	877.59	<0.0001	<0.0001	<0.0001	<0.0001	<0.0001	<0.0001
Model 2s	−15.07	−12.13	66.43		<0.01	<0.0001	<0.0001	<0.001	<0.0001
Model 2	−27.04	−21.3	69.56				<0.0001		<0.0001
Model 3s	−47.47	−41.73	62.17				0.052		
Model 3	−51.09	−42.82	68.14						
Model 4s	−33.13	−27.4	67.08						<0.0001
Model 4	−54.96	−46.68	67.15						

Fits were analyzed by calculating Akaike information criteria (AIC), corrected AIC (AIC_c), and Bayesian information criteria (BIC). For all three criteria, the best-fitting model was the one with the minimum criterion value. Note that for AIC_c and BIC, a larger number of parameters is penalized more than in AIC. *F*-tests of the nested models are shown, with the simpler model (rows) compared with the nested, more complicated model (columns). The analysis was performed for fits of the data recorded from WT and GAMT$^{-/-}$ mouse cardiomyocytes separately as well as for pooled data.

Because no statistically significant difference was found when we performed multiple comparisons separately, no additional correction for multiple tests or ANOVA analysis was required to check whether the difference in autofluorescence between cardiomyocytes from WT and GAMT$^{-/-}$ mice was significant. Thus, on the basis of our results, diffusion from the solution to the mitochondrial inner membrane is restricted to the same extent.

DISCUSSION

The present study shows that inactivation of the CK system by GAMT deficiency due to lack of Cr is not associated with any changes in cardiomyocyte mitochondrial organization or stimulated respiration or its regulation by exogenous and endogenous ADP-supply. In addition, according to our modeling results, there was no change in intracellular compartmentation when cells were in a relaxed state. This indicates that inactivation of the CK system by GAMT deficiency does not induce cytoarchitectural changes.

The CK system is considered an important temporal and spatial energy buffer in the heart. In all muscle types, CK is present near sites of ATP consumption and sites of ATP production. In white, glycolytic skeletal muscle, CK is present near the myofibrillar I-band and functionally coupled to glycolytic enzymes (26). In oxidative skeletal muscle and the heart, mitochondrial CK is bound to the outer side of the inner mitochondrial membrane (25) and functionally coupled to respiration (59). Cytosolic CK is localized at the myofibrillar M-band, which is favorable for the regeneration of ATP for myosin ATPase (58). Also, it is bound near and functionally coupled to SERCA (33), sarcolemmal ATP-sensitive K^+ channels (9), and Na^+-K^+-ATPase (13). The "spatial energy buffer" or "energy transport" function of CK has mainly been ascribed to tissues such as the heart, where a relatively large fraction of the CK activity is of mitochondrial origin (56, 59). Mitochondrial CK activity is tissue specific and relates to oxidative capacity (56). This relationship can also be observed during cardiac maturation (12, 16). Facilitation of ADP/ATP transport may seem particularly important in oxidative muscles, where ADP/ATP diffusion is restricted (28, 40, 56) and mitochondrial energy production, although more efficient than glycolysis, is more distant and physically separated from ATPases by the mitochondrial membranes. In terms of energy transport, the CK system provides a parallel energy circuit between sites of production and consumption. PCr and Cr are smaller molecules than ATP and ADP and thus diffuse faster (32). Another advantage is that they are present in higher concentrations, allowing the build up of larger gradients of Cr than ADP. For example, whereas the Cr concentration is in the order of 10 mM, the ADP concentration is ~50 μM. Since diffusion is driven by the absolute difference in concentration, the same gradient for ADP would require 10 mM/50 μM = 20 × larger relative difference in concentration than for Cr.

The importance of CK has been the subject of debate for a long time, with sometimes vague hypotheses used to define the role of CK, precluding testing of the hypotheses using a strong inference approach (3). An alternative view has been proposed that the high transport via PCr and Cr is simply a consequence of the CK reaction being close to equilibrium (32). After making some assumptions on the relative concentrations of ATP, ADP, PCr, and Cr, it has been shown that CK is expected to facilitate energy transfer, leading to most of the energy

Downloaded from journals.physiology.org/journal/ajpheart (193.040.253.082) on June 1, 2022.

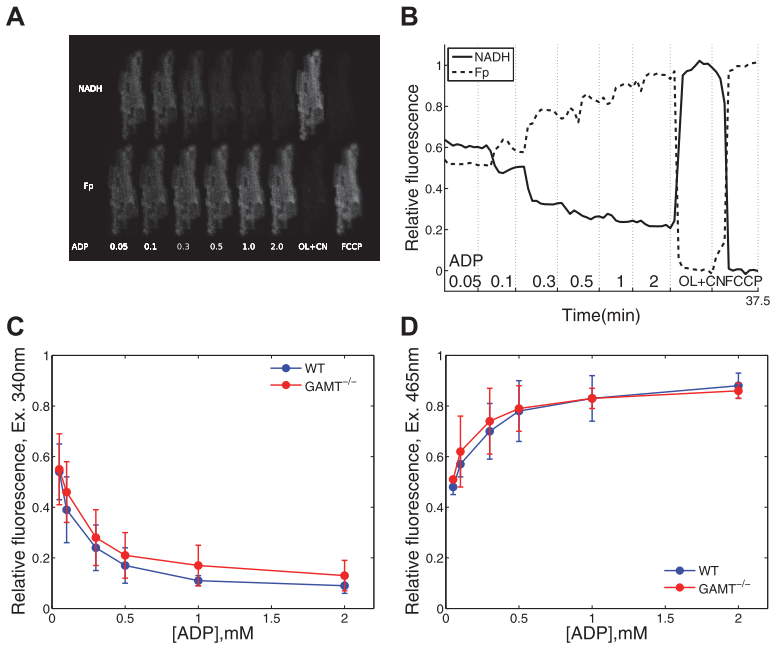

Fig. 7. Autofluorescence response of a permeabilized cardiomyocytes to changes in solution. *A*: representative example of NADH and flavoprotein (Fp) fluorescence from a GAMT$^{-/-}$ cardiomyocyte exposed to different concentrations of ADP, oligomycin and NaCN (OL + CN), and FCCP, as indicated at the *bottom*. *B*: normalized integrated fluorescence of the cardiomyocyte shown in *A*. *C* and *D*: comparison of NADH (*C*) and Fp (*D*) autofluorescence responses in permeabilized cardiomyocytes from WT (blue; n = 6) and GAMT$^{-/-}$ (red; n = 6) cardiomyocytes to the changes in exogenous ADP.

transfer to occur through PCr and Cr diffusion. In addition, for small diffusion distances, such as in cardiac muscle, the absence of an active CK system should not have any significant functional consequences (32). The latter was demonstrated assuming that there are no significant diffusion restrictions on the diffusion path of molecules between ATPases and mitochondria. Recently, on the basis of analysis of raster image correlation spectroscopy recordings, we (21) suggested that rat cardiomyocytes are split into smaller compartments with lattice-like barriers. The location of the barriers and the intracellular structures forming them are still unknown and would have different physiological consequences depending on whether the barriers are between ATPases and mitochondria or not. The lack of adaptation to inactive CK reported by us is in agreement with the mechanism of CK operation suggested by Meyer et al. (32) in their analysis.

If we assume the importance of the CK system as an additional energy transport system in the heart, it seems intuitive that disruption of this shuttle by genetic knockout of cytosolic and mitochondrial CK would lead to changes in the ultrastructure and regulation of mitochondrial respiration. In cardiomyocytes from CK$^{-/-}$ mice, rows of myofilaments were split into thinner myofilaments by mitochondria wedging into the branching points, as if to compensate for a lack of energy transfer by diminishing intracellular diffusion distances (23). In addition, permeabilized fibers from CK$^{-/-}$ mice have a higher ADP affinity of respiration than WT control mice, indicating smaller intracellular diffusion restrictions imposed on the molecules (23). Such changes in morphology and ADP affinity were consistent with the viewpoint that CK regulates the local ATP-to-ADP ratio and "compensatory mechanisms should be operating in CK$^{-/-}$ mouse heart to overcome diffusion limitation and to preserve cardiac function at least at moderate levels of activity" (23). It was therefore surprising to find no difference between cardiomyocytes from GAMT$^{-/-}$ and their WT littermates. Both had parallel rows of mitochondria with the same distances between mitochondrial centers (Figs. 4 and 5 and Table 1). In permeabilized cardiomyocytes, ADP sensitivity was similar at the population level (Fig. 6) as well as at the single cell level (Fig. 7). Finally, intracellular compartmentation, as assessed by kinetic measurements and mathematical modeling, was found to be the same in both WT and GAMT$^{-/-}$ cardiomyocytes. These findings are in agreement with and extend the observations of a recent study (30) that failed to identify any adaptational changes when left ventricular proteomes, adenylate kinase activity, or mitochondrial respiration were compared.

The difference between our results and those from CK$^{-/-}$ mice might be explained by differences in the genetic background (CK$^{-/-}$ mice on a mixed C57BL/6 and S129 background were compared with WT C57BL/6 mice) and genetic drift. This has been shown to play a role in a study (31) of mice deficient in mitochondrial CK (Mt-CK$^{-/-}$ mice). In the present study, we compared GAMT$^{-/-}$ mice with their WT littermates. Alternatively, the different outcomes may be the result of different genetic modifications. Indeed, CK is a structural as well as catalytic protein. Muscle-type CK is an integral part of the myofibrillar M-band (17, 18, 49), where it serves as an efficient ATP-regenerating system for myosin ATPase located on both sides of the M-band (58). Mt-CK in the mitochondria seems to play a structural role in addition to ADP regeneration. It has been suggested that the octameric form induces the formation of contact sites between the inner and outer mitochondrial membranes (46), where it is involved in lipid transfer

Downloaded from journals.physiology.org/journal/ajpheart (193.040.253.082) on June 1, 2022.

between the two membranes (11). In another study (29), the structural role of Mt-CK has been demonstrated by finding that it stabilizes specific contact sites between inner and outer mitochondrial membranes. It must be noted that these findings are not from cardiac muscle. It remains to be verified whether the lack of Mt-CK in cardiac muscle affects mitochondrial organization. However, an increase citrate synthase activity does suggest an increased mitochondrial volume in cardiac muscle of Mt-CK$^{-/-}$ mice (31). As CK is expressed to the same extent in GAMT$^{-/-}$ mice as in WT mice (19), these other roles of (especially) Mt-CK are preserved in GAMT$^{-/-}$ mice, and our results reflect only the catalytic role of CK.

It is tempting to speculate that guanidinoacetate (GA) may be used by CK in a similar manner as Cr. Indeed, although GAMT$^{-/-}$ mice have undetectable levels of total Cr, as shown in Fig. 3, they have a considerable amount of phosphorylated (p-)GA. In the heart, the p-GA concentration in a GAMT$^{-/-}$ mouse is ~2/3 of the PCr concentration in a WT mouse (19). However, phosphotransfer from ATP to p-GA was undetectable in GAMT$^{-/-}$ mice (29), and it has been shown that the reactivity of muscle-type CK with GA is ~100 times smaller than with Cr (5). This reactivity is sufficient to dephosphorylate p-GA at the induction of ischemia (24) or cyanide inhibition of oxidative phosphorylation (5). However, for energy transfer between mitochondria and ATPases, Mt-CK must convert ATP into PCr or its analog. When ATP-stimulated respiration on isolated mitochondria or on permeabilized fibers was analyzed, Mt-CK reactivity in the presence of GA was negligible and ADP synthesis from GA and ATP was not able to stimulate respiration (5). Taking into account the inability of Mt-CK to react with GA as well as undetectable levels of total Cr, the contribution of the CK shuttle to energy transfer is expected to be negligible in GAMT$^{-/-}$ cardiomyocytes. Thus, in contrast to the suggestion cited above from Ref. 23, the present results suggest that disruption of CK shuttle does not necessarily lead to compensatory changes in mitochondrial arrangement and intracellular compartmentation.

Applied methods and study limitations. In this study, we used confocal microscopy to estimate the intracellular mitochondrial positioning in WT and GAMT$^{-/-}$ cardiomyocytes. The analysis was based on a method that we have previously applied on rat and trout cardiomyocytes (4, 50). Compared with traditional electron microscopy, there are several differences that ought to be considered when interpreting the data obtained by our method. Analysis of confocal images allowed us to use live cells. Thus, there are no histological artifacts that may be introduced by the fixation and dehydration of cells during their preparation for electron microscopy (38). In addition, the distances between the centers of mitochondria estimated by our method can be analyzed in three dimensions (Fig. 1) with an estimation based on a large number of mitochondria. In this study, >20,000 mitochondria were analyzed for each of the genotypes. Collecting a similar amount of data using electron microscopy is possible but would probably not be feasible when time and monetary costs are considered. Taking into account that most of the SDs of the percentile points shown in Table 1 are below 100 nm, the method can be considered precise and should be able to identify subtle changes in mitochondrial positioning. Note that those deviations include variability between cells as well. Such precision can be attributed to sub-Airy disk accuracy in finding centers of the objects in optical microscopy. However, in contrast to electron microscopy, confocal microscopy images do not allow us to determine relative distances between the borders of the objects, such as the distance between membranes of neighboring mitochondria, due to the limits induced by diffraction. As a result, in our study, such distances cannot be analyzed accurately and have not been reported. A further consideration is the isolation procedure, which is of great importance in obtaining a high yield of viable cardiomyocytes with unaltered morphological characteristics. The dissociation of a heart into a single cell suspension involves several critical factors such as excision and cannulation for perfusion, collagenase quality and activity, the length of enzyme digestion, and the Ca^{2+} concentration in the perfusion solution. To control for these variables, we used several criteria to check the quality of the isolation procedure, for example, contraction of cardiomyocytes upon electrical field stimulation, indicating that cells are Ca^{2+} tolerant, and checking for the prevalence of rod-shaped cells with clear striations and well-delineated membranes. However, even with those tests, we cannot exclude a possibility that there are some morphological changes introduced during the isolation procedure that may influence the analysis of mitochondrial positioning.

It is important to keep in mind the limitations of this study. For the functional assays, we studied cardiomyocytes with the sarcolemma permeabilized by saponin. Because the surrounding solution contained low free Ca^{2+}, cells were kept in a resting state. We stimulated mitochondrial respiration and endogenous PK and ATPases by adding ADP or ATP to the solution outside the cells. Thus, these compounds had to cross an unstirred layer around the cells (22) as well as the intracellular diffusion obstacles, which partition cardiomyocytes into smaller compartments (21, 23, 45), before reaching the mitochondria. In contrast, in intact, working cells, there is a circuit of ADP/ATP between adjacent ATPases and mitochondria significantly reducing the diffusion distances and obstacles that influence the energy transfer if compared with the permeabilized cardiomyocyte experiments. In addition, the level of intracellular compartmentation induced by diffusion restrictions is not known in working heart muscle cells. While an analysis of raster image correlation spectroscopy measurements on relaxed rat cardiomyocytes suggested lattice-like intracellular diffusion barriers separating the cardiomyocytes into smaller compartments (21), it is not clear whether such compartmentation persists in the contracting cell. Mitochondrial respiration was stimulated to the maximal rate by very high concentrations of ADP in the presence of a high concentration of P_i, which is also an important regulator of mitochondrial respiration (7, 39, 61). Thus, the changes induced by GAMT deficiency have not been probed in the same conditions as in vivo experiments. However, on the basis of our analysis, we can conclude that the mitochondrial organization and intracellular compartmentation, as observed in our experiments, are unchanged in GAMT$^{-/-}$ mice.

Disruption of the CK system may be compensated for by other mechanisms that were not measured in this study. For example, upregulation of alternative phosphotransfer systems, such as adenylate kinase, has been observed in CK$^{-/-}$ mice (34), and upregulation of other glycolytic enzymes is observed after heart failure (2). Upregulation of these alternative phosphotransfer systems may serve to compensate for both the

Downloaded from journals.physiology.org/journal/ajpheart (193.040.253.082) on June 1, 2022.

temporal and spatial buffer functions of the CK system. However, the change after heart failure may also simply reflect a change of phenotype induced by reverting to a fetal gene expression (37). Metabolically, this includes an upregulation of glycolytic enzymes and a downregulation of mitochondrial enzymes (48, 54). Clearly, further studies are needed to determine how disruption of the CK system by GAMT deficiency affects the cardiac phenotype.

Our kinetic recordings, such as mitochondrial respiration and ATPase activities, were performed in the absence of Cr in solution. This was done to determine whether intracellular compartmentation and mitochondrial respiration capacity changed during adaptation of the cells to Cr deficiency in GAMT$^{-/-}$ mice. As we have previously demonstrated (45), this information can be obtained using kinetic recordings without Cr. Thus, while we know on the basis of earlier studies that the total Cr content is too low to be determined in GAMT$^{-/-}$ mice leading to inactivation of the CK shuttle system in GAMT$^{-/-}$ mice, the kinetic properties of CK isoforms, their distribution, and coupling to mitochondrial respiration is not known and cannot be predicted on the basis of our measurements.

Physiological implications. The lack of compensatory changes in GAMT$^{-/-}$ mice prompts a careful consideration of the role of the CK system in cardiomyocytes. At the whole heart level, both CK$^{-/-}$ and GAMT$^{-/-}$ mice show almost no changes in basal contractile performance (6, 42), but they fail to perform at inotropically stimulated high workload and are more susceptible to ischemia-reperfusion injury (10, 19, 47). Clearly, the CK system is indispensable when the heart is exposed to a severe energetic challenge. But how important is it as an energy transport system? It is well established that a significant fraction of energy transport occurs via the CK system in the heart, and this is severely diminished in the failing heart (20). However, Meyer et al. (32) suggested that CK-facilitated energy transfer is merely a consequence of the existence of the CK system and is not required for cardiac function, if the diffusion distances are taken into account. Its main role is to buffer temporal fluctuations in the ADP-to-ATP ratio during situations, when energy demand is higher than energy production (32). A recent analysis of ^{31}P NMR data suggested that the contribution of the CK shuttle to overall energy transfer between mitochondria and ATPases can depend on the workload and could reduce with an increase in workload or in pathological conditions (53). While our results are by no means conclusive, they raise questions regarding the importance of CK as an energy transport system at low and moderate workloads.

In conclusion, our results suggest that the healthy heart is able to preserve cardiac function at a basal level in the absence of CK-facilitated energy transfer without compromising intracellular organization and the regulation of mitochondrial energy homeostasis.

ACKNOWLEDGMENTS

The authors acknowledge Prof. Dirk Isbrandt (University of Hamburg, Hamburg, Germany) for generating the strain of GAMT-deficient mice as well as Merle Mandel and Adele Puusalu (Institute of Cybernetics, Tallinn University of Technology, Tallinn, Estonia) for technical assistance.

GRANTS

This work was funded by The Wellcome Trust Fellowship WT081755MA, the European Union through the European Regional Development Fund, Estonian Science Foundation Grant ETF8041 (PhD stipends for J. Branovets, N. Jepihhina, and N. Sokolova), and British Heart Foundation Grant RG/10/002/28187.

DISCLOSURES

No conflicts of interest, financial or otherwise, are declared by the author(s).

AUTHOR CONTRIBUTIONS

Author contributions: J.B., S.K., N.J., N.S., and D.A. performed experiments; J.B., M.S., S.K., N.J., and M.V. analyzed data; J.B., M.S., M.V., and R.B. interpreted results of experiments; J.B., M.S., and M.V. prepared figures; C.A.L., S.N., M.V., and R.B. conception and design of research; C.A.L., S.N., M.V., and R.B. edited and revised manuscript; C.A.L., S.N., M.V., and R.B. approved final version of manuscript; R.B. drafted manuscript.

REFERENCES

1. **Abraham MR, Selivanov VA, Hodgson DM, Pucar D, Zingman LV, Wieringa B, Dzeja PP, Alekseev AE, Terzic A.** Coupling of cell energetics with membrane metabolic sensing. *J Biol Chem* 277: 24427–24434, 2002.
2. **Aksentijević D, Lygate CA, Makinen K, Zervou S, Sebag-Montefiore L, Medway D, Barnes H, Schneider JE, Neubauer S.** High-energy phosphotransfer in the failing mouse heart: role of adenylate kinase and glycolytic enzymes. *Eur J Heart Fail* 12: 1282–1289, 2010.
3. **Beard DA, Kushmerick MJ.** Strong Inference for Systems Biology. *PLoS Comput Biol* 5: e1000459, 2009.
4. **Birkedal R, Shiels HA, Vendelin M.** Three-dimensional mitochondrial arrangement in ventricular myocytes: from chaos to order. *Am J Physiol Cell Physiol* 291: C1148–C1158, 2006.
5. **Boehm EA, Radda GK, Tomlin H, Clark JF.** The utilisation of creatine and its analogues by cytosolic and mitochondrial creatine kinase. *Biochim Biophys Acta* 1274: 119–128, 1996.
6. **Bonz AW, Kniesch S, Hofmann U, Küllmer S, Bauer L, Wagner H, Ertl G, Spindler M.** Functional properties and $[Ca^{2+}]_i$ metabolism of creatine kinase–KO mice myocardium. *Biochem Biophys Res Commun* 298: 163–168, 2002.
7. **Bose S, French S, Evans FJ, Joubert F, Balaban RS.** Metabolic network control of oxidative phosphorylation. *J Biol Chem* 278: 39155–39165, 2003.
8. **Braissant O, Henry H, Béard E, Uldry J.** Creatine deficiency syndromes and the importance of creatine synthesis in the brain. *Amino Acids* 40: 1315–1324, 2011.
9. **Crawford RM, Ranki HJ, Botting CH, Budas GR, Jovanovic A.** Creatine kinase is physically associated with the cardiac ATP-sensitive K^+ channel in vivo. *FASEB J* 16: 102–104, 2002.
10. **Crozatier B, Badoual T, Boehm E, Ennezat PV, Guenoun T, Su J, Veksler V, Hittinger L, Ventura-Clapier R.** Role of creatine kinase in cardiac excitation-contraction coupling: studies in creatine kinase-deficient mice. *FASEB J* 16: 653–660, 2002.
11. **Epand RF, Schlattner U, Wallimann T, Lacombe ML, Epand RM.** novel lipid transfer property of two mitochondrial proteins that bridge the inner and outer membranes. *Biophys J* 92: 126–137, 2007.
12. **Fischer A, ten Hove M, Sebag-Montefiore L, Wagner H, Clarke K, Watkins H, Lygate CA, Neubauer S.** Changes in creatine transporter function during cardiac maturation in the rat. *BMC Dev Biol* 10: 70, 2010.
13. **Grosse R, Spitzer E, Kupriyanov VV, Saks VA, Repke KR.** Coordinate interplay between (Na^+ + K^+)-ATPase and creatine phosphokinase optimizes (Na^+/K^+)-antiport across the membrane of vesicles formed from the plasma membrane of cardiac muscle cell. *Biochim Biophys Acta* 603: 142–156, 1980.
14. **Gudbjarnason S, Mathes P, Ravens KG.** Functional compartmentation of ATP and creatine phosphate in heart muscle. *J Mol Cell Cardiol* 1: 325–339, 1970.
15. **Gupta A, Akki A, Wang Y, Leppo MK, Chacko VP, Foster DB, Caceres V, Shi S, Kirk JA, Su J, Lai S, Paolocci N, Steenbergen C, Gerstenblith G, Weiss RG.** Creatine kinase-mediated improvement of function in failing mouse hearts provides causal evidence the failing heart is energy starved. *J Clin Invest* 122: 291–302, 2012.

Downloaded from journals.physiology.org/journal/ajpheart (193.040.253.082) on June 1, 2022.

16. **Hoerter JA, Ventura-Clapier R, Kuznetsov A.** Compartmentation of creatine kinases during perinatal development of mammalian heart. *Mol Cell Biochem* 133–134: 277–286, 1994.
17. **Hornemann T, Kempa S, Himmel M, Hayeß K, Fürst DO, Wallimann T.** Muscle-type creatine kinase interacts with central domains of the M-band proteins myomesin and M-protein. *J Mol Biol* 332: 877–887, 2003.
18. **Hornemann T, Stolz M, Wallimann T.** Isoenzyme-specific interaction of muscle-type creatine kinase with the sarcomeric M-line is mediated by NH_2-terminal lysine charge-clamps. *J Cell Biol* 149: 1225–1234, 2000.
19. **Hove ten M, Lygate CA, Fischer A, Schneider JE, Sang AE, Hulbert K, Sebag-Montefiore L, Watkins H, Clarke K, Isbrandt D, Wallis J, Neubauer S.** Reduced inotropic reserve and increased susceptibility to cardiac ischemia/reperfusion injury in phosphocreatine-deficient guanidinoacetate-*N*-methyltransferase-knockout mice. *Circulation* 111: 2477–2485, 2005.
20. **Ten Hove M, Neubauer S.** MR spectroscopy in heart failure-clinical and experimental findings. *Heart Fail Rev* 12: 48–57, 2007.
21. **Illaste A, Laasmaa M, Peterson P, Vendelin M.** Analysis of molecular movement reveals latticelike obstructions to diffusion in heart muscle cells. *Biophys J* 102: 739–748, 2012.
22. **Jepihhina N, Beraud N, Sepp M, Birkedal R, Vendelin M.** Permeabilized rat cardiomyocyte response demonstrates intracellular origin of diffusion obstacles. *Biophys J* 101: 2112–2121, 2011.
23. **Kaasik A, Veksler V, Boehm E, Novotova M, Minajeva A, Ventura-Clapier R.** Energetic crosstalk between organelles: architectural integration of energy production and utilization. *Circ Res* 89: 153–159, 2001.
24. **Kan HE, Renema WKJ, Isbrandt D, Heerschap A.** Phosphorylated guanidinoacetate partly compensates for the lack of phosphocreatine in skeletal muscle of mice lacking guanidinoacetate methyltransferase. *J Physiol* 560: 219–229, 2004.
25. **Karo J, Peterson P, Vendelin M.** Molecular dynamics simulations of creatine kinase and adenine nucleotide translocase in mitochondrial membrane patch. *J Biol Chem* 287: 7467–7476, 2012.
26. **Kraft T, Hornemann T, Stolz M, Nier V, Wallimann T.** Coupling of creatine kinase to glycolytic enzymes at the sarcomeric I-band of skeletal muscle: a biochemical study in situ. *J Muscle Res Cell Motil* 21: 691–703, 2000.
27. **Kümmel L.** Ca, Mg-ATPase activity of permeabilised rat heart cells and its functional coupling to oxidative phosphorylation of the cells. *Cardiovasc Res* 22: 359–367, 1988.
28. **Kuznetsov AV, Tiivel T, Sikk P, Kaambre T, Kay L, Daneshrad Z, Rossi A, Kadaja L, Peet N, Seppet E, Saks VA.** Striking differences between the kinetics of regulation of respiration by ADP in slow-twitch and fast-twitch muscles in vivo. *Eur J Biochem* 241: 909–915, 1996.
29. **Lenz H, Schmidt M, Welge V, Kueper T, Schlattner U, Wallimann T, Elsässer HP, Wittern KP, Wenck H, Staeb F, Blatt T.** Inhibition of cytosolic and mitochondrial creatine kinase by siRNA in HaCaT- and HeLaS3-cells affects cell viability and mitochondrial morphology. *Mol Cell Biochem* 306: 153–162, 2007.
30. **Lygate CA, Aksentijevic D, Dawson D, ten Hove M, Phillips D, de Bono JP, Medway DJ, Sebag-Montefiore L, Hunyor I, Channon KM, Clarke K, Zervou S, Watkins H, Balaban RS, Neubauer S.** Living without creatine: unchanged exercise capacity and response to chronic myocardial infarction in creatine-deficient mice. *Circ Res* 112: 945–955, 2013.
31. **Lygate CA, Hunyor I, Medway D, de Bono JP, Dawson D, Wallis J, Sebag-Montefiore L, Neubauer S.** Cardiac phenotype of mitochondrial creatine kinase knockout mice is modified on a pure C57BL/6 genetic background. *J Mol Cell Cardiol* 46: 93–99, 2009.
32. **Meyer RA, Sweeney HL, Kushmerick MJ.** A simple analysis of the "phosphocreatine shuttle". *Am J Physiol Cell Physiol* 246: C365–C377, 1984.
33. **Minajeva A, Ventura-Clapier R, Veksler V.** Ca^{2+} uptake by cardiac sarcoplasmic reticulum ATPase in situ strongly depends on bound creatine kinase. *Pflügers Arch* 432: 904–912, 1996.
34. **Momken I, Lechêne P, Koulmann N, Fortin D, Mateo P, Doan BT, Hoerter J, Bigard X, Veksler V, Ventura-Clapier R.** Impaired voluntary running capacity of creatine kinase-deficient mice. *J Physiol* 565: 951–964, 2005.
35. **Nahrendorf M, Streif JU, Hiller KH, Hu K, Nordbeck P, Ritter O, Sosnovik D, Bauer L, Neubauer S, Jakob PM, Ertl G, Spindler M, Bauer WR.** Multimodal functional cardiac MRI in creatine kinase-deficient mice reveals subtle abnormalities in myocardial perfusion and mechanics. *Am J Physiol Heart Circ Physiol* 290: H2516–H2521, 2006.
36. **Ramay HR, Vendelin M.** Diffusion restrictions surrounding mitochondria: a mathematical model of heart muscle fibers. *Biophys J* 97: 443–452, 2009.
37. **Razeghi P, Young ME, Alcorn JL, Moravec CS, Frazier OH, Taegtmeyer H.** Metabolic gene expression in fetal and failing human heart. *Circulation* 104: 2923–2931, 2001.
38. **Roy RR, Pierotti DJ, Edgerton VR.** Skeletal muscle fiber cross-sectional area: effects of freezing procedures. *Acta Anat (Basel)* 155: 131–135, 1996.
39. **Saks VA, Kongas O, Vendelin M, Kay L.** Role of the creatine/phosphocreatine system in the regulation of mitochondrial respiration. *Acta Physiol Scand* 168: 635–641, 2000.
40. **Saks V, Kuznetsov A, Andrienko T, Usson Y, Appaix F, Guerrero K, Kaambre T, Sikk P, Lemba M, Vendelin M.** Heterogeneity of ADP diffusion and regulation of respiration in cardiac cells. *Biophys J* 84: 3436–3456, 2003.
41. **Schmidt A, Marescau B, Boehm EA, Renema WK, Peco R, Das A, Steinfeld R, Chan S, Wallis J, Davidoff M, Ullrich K, Waldschutz R, Heerschap A, De Deyn PP, Neubauer S, Isbrandt D.** Severely altered guanidino compound levels, disturbed body weight homeostasis and impaired fertility in a mouse model of guanidinoacetate *N*-methyltransferase (GAMT) deficiency. *Hum Mol Genet* 13: 905–921, 2004.
42. **Schneider JE, Stork LA, Bell JT, Hove ten M, Isbrandt D, Clarke K, Watkins H, Lygate CA, Neubauer S.** Cardiac structure and function during ageing in energetically compromised guanidinoacetate *N*-methyltransferase (GAMT)-knockout mice–a one year longitudinal MRI study. *J Cardiovasc Magn Reson* 10: 9, 2008.
43. **Schulze A.** Creatine deficiency syndromes. *Mol Cell Biochem* 244: 143–150, 2003.
44. **Seppet EK, Kaambre T, Sikk P, Tiivel T, Vija H, Tonkonogi M, Sahlin K, Kay L, Appaix F, Braun U, Eimre M, Saks VA.** Functional complexes of mitochondria with Ca,MgATPases of myofibrils and sarcoplasmic reticulum in muscle cells. *Biochim Biophys Acta* 1504: 379–395, 2001.
45. **Sepp M, Vendelin M, Vija H, Birkedal R.** ADP compartmentation analysis reveals coupling between pyruvate kinase and ATPases in heart muscle. *Biophys J* 98: 2785–2793, 2010.
46. **Speer O, Bäck N, Buerklen T, Brdiczka D, Koretsky A, Wallimann T, Eriksson O.** Octameric mitochondrial creatine kinase induces and stabilizes contact sites between the inner and outer membrane. *Biochem J* 385: 445, 2005.
47. **Spindler M, Meyer K, Strömer H, Leupold A, Boehm E, Wagner H, Neubauer S.** Creatine kinase-deficient hearts exhibit increased susceptibility to ischemia-reperfusion injury and impaired calcium homeostasis. *Am J Physiol Heart Circ Physiol* 287: H1039–H1045, 2004.
48. **Taegtmeyer H, Wilson CR, Razeghi P, Sharma S.** Metabolic energetics and genetics in the heart. *Ann NY Acad Sci* 1047: 208–218, 2005.
49. **Turner DC, Wallimann T, Eppenberger HM.** A protein that binds specifically to the M-line of skeletal muscle is identified as the muscle form of creatine kinase. *Proc Natl Acad Sci USA* 70: 702–705, 1973.
50. **Vendelin M, Béraud N, Guerrero K, Andrienko T, Kuznetsov AV, Olivares J, Kay L, Saks VA.** Mitochondrial regular arrangement in muscle cells: a "crystal-like" pattern. *Am J Physiol Cell Physiol* 288: C757–C767, 2005.
51. **Vendelin M, Birkedal R.** Anisotropic diffusion of fluorescently labeled ATP in rat cardiomyocytes determined by raster image correlation spectroscopy. *Am J Physiol Cell Physiol* 295: C1302–C1315, 2008.
52. **Vendelin M, Eimre M, Seppet E, Peet N, Andrienko T, Lemba M, Engelbrecht J, Seppet EK, Saks VA.** Intracellular diffusion of adenosine phosphates is locally restricted in cardiac muscle. *Mol Cell Biochem* 256–257: 229–241, 2004.
53. **Vendelin M, Hoerter JA, Mateo P, Soboll S, Gillet B, Mazet JL.** Modulation of energy transfer pathways between mitochondria and myofibrils by changes in performance of perfused heart. *J Biol Chem* 285: 37240–37250, 2010.
54. **Ventura-Clapier R, Garnier A, Veksler V.** Energy metabolism in heart failure. *J Physiol* 555: 1–13, 2004.
55. **Ventura-Clapier R, Kuznetsov AV, d' Albis A, Deursen van J, Wieringa B, Veksler VI.** Muscle creatine kinase-deficient mice. I. Alterations in myofibrillar function. *J Biol Chem* 270: 19914–19920, 1995.

Downloaded from journals.physiology.org/journal/ajpheart (193.040.253.082) on June 1, 2022.

56. **Ventura-Clapier R, Kuznetsov A, Veksler V, Boehm E, Anflous K.** Functional coupling of creatine kinases in muscles: species and tissue specificity. *Mol Cell Biochem* 184: 231–247, 1998.
57. **Ventura-Clapier R, Mekhfi H, Vassort G.** Role of creatine kinase in force development in chemically skinned rat cardiac muscle. *J Gen Physiol* 89: 815–837, 1987.
58. **Wallimann T, Schlosser T, Eppenberger HM.** Function of M-line-bound creatine kinase as intramyofibrillar ATP regenerator at the receiving end of the phosphorylcreatine shuttle in muscle. *J Biol Chem* 259: 5238–5246, 1984.
59. **Wallimann T, Wyss M, Brdiczka D, Nicolay K, Eppenberger H.** Intracellular compartmentation, structure and function of creatine kinase isoenzymes in tissues with high and fluctuating energy demands: the "phosphocreatine circuit" for cellular energy homeostasis. *Biochem J* 281: 21–40, 1992.
60. **Weiss JN, Korge P.** The cytoplasm: no longer a well-mixed bag. *Circ Res* 89: 108–110, 2001.
61. **Wu F, Zhang EY, Zhang J, Bache RJ, Beard DA.** Phosphate metabolite concentrations and ATP hydrolysis potential in normal and ischaemic hearts. *J Physiol* 586: 4193–4208, 2008.

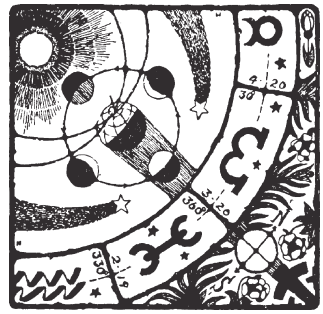

Downloaded from journals.physiology.org/journal/ajpheart (193.040.253.082) on June 1, 2022.

Appendix 2

Publication II

Branovets J, Karro N, Barsunova K, Laasmaa M, Lygate CA, Vendelin M, Birkedal R

Cardiac expression and location of hexokinase changes in a mouse model of pure creatine deficiency.

Am J Physiol Heart Circ Physiol. 2021 Feb 1;320(2):H613-H629. doi: 10.1152/ajpheart.00188.2020.

AMERICAN JOURNAL OF PHYSIOLOGY
HEART AND CIRCULATORY PHYSIOLOGY

Am J Physiol Heart Circ Physiol 320: H613–H629, 2021.
First published December 18, 2020; doi:10.1152/ajpheart.00188.2020

RESEARCH ARTICLE

Energetics and Metabolism

Cardiac expression and location of hexokinase changes in a mouse model of pure creatine deficiency

Jelena Branovets,[1] Niina Karro,[1] Karina Barsunova,[1] Martin Laasmaa,[1] Craig A. Lygate,[2] Marko Vendelin,[1] and Rikke Birkedal[1]

[1]*Laboratory of Systems Biology, Institute of Cybernetics, Tallinn University of Technology, Tallinn, Estonia and* [2]*Division of Cardiovascular Medicine, Radcliffe Department of Medicine, University of Oxford, Oxford, United Kingdom*

Abstract

Creatine kinase (CK) is considered the main phosphotransfer system in the heart, important for overcoming diffusion restrictions and regulating mitochondrial respiration. It is substrate limited in creatine-deficient mice lacking L-arginine:glycine amidinotransferase (AGAT) or guanidinoacetate *N*-methyltranferase (GAMT). Our aim was to determine the expression, activity, and mitochondrial coupling of hexokinase (HK) and adenylate kinase (AK), as these represent alternative energy transfer systems. In permeabilized cardiomyocytes, we assessed how much endogenous ADP generated by HK, AK, or CK stimulated mitochondrial respiration and how much was channeled to mitochondria. In whole heart homogenates, and cytosolic and mitochondrial fractions, we measured the activities of AK, CK, and HK. Lastly, we assessed the expression of the major HK, AK, and CK isoforms. Overall, respiration stimulated by HK, AK, and CK was ~25, 90, and 80%, respectively, of the maximal respiration rate, and ~20, 0, and 25%, respectively, was channeled to the mitochondria. The activity, distribution, and expression of HK, AK, and CK did not change in GAMT knockout (KO) mice. In AGAT KO mice, we found no changes in AK, but we found a higher HK activity in the mitochondrial fraction, greater expression of HK I, but a lower stimulation of respiration by HK. Our findings suggest that mouse hearts depend less on phosphotransfer systems to facilitate ADP flux across the mitochondrial membrane. In AGAT KO mice, which are a model of pure creatine deficiency, the changes in HK may reflect changes in metabolism as well as influence mitochondrial regulation and reactive oxygen species production.

NEW & NOTEWORTHY In creatine-deficient AGAT$^{-/-}$ and GAMT$^{-/-}$ mice, the myocardial creatine kinase system is substrate limited. It is unknown whether subcellular localization and mitochondrial ADP channeling by hexokinase and adenylate kinase may compensate as alternative phosphotransfer systems. Our results show no changes in adenylate kinase, which is the main alternative to creatine kinase in heart. However, we found increased expression and activity of hexokinase I in AGAT$^{-/-}$ cardiomyocytes. This could affect mitochondrial regulation and reactive oxygen species production.

adenylate kinase; cardiac energetics; creatine-deficient mice; creatine kinase; hexokinase

INTRODUCTION

The creatine kinase (CK) system is considered a crucial phosphotransfer system in the heart, ensuring adequate energy transfer to fuel cardiac mechanical work. Indeed, loss of CK and its functional coupling to mitochondrial respiration is a hallmark of cardiac ischemia-reperfusion (I-R) injury (1–4), and it is potentially a major culprit of the compromised function in energy-starved, failing hearts (4–6). The latter is supported by the finding that overexpression of CK ameliorates cardiac dysfunction after I-R injury and in failing hearts (7–9). However, studies on transgenic mice lacking both the cytosolic and mitochondrial CK (Mi-CK) isoforms in muscle [CK knockout (KO) mice] have been equivocal (10). Cardiac performance is near-normal at low to moderate workloads and is blunted at high workloads (11), but the development of chronic heart failure following myocardial infarction is not exacerbated (12). CK KO mice do eventually develop spontaneous congestive heart failure but only in aging males on an appropriate genetic background (13).

The intracellular environment of cardiomyocytes is densely packed with structures forming lattice-like barriers causing anisotropic diffusion (14–16). In rat cardiomyocytes, half of the diffusion restriction is at the level of the outer mitochondrial membrane (17). Cardiomyocytes have multiple, integrated phosphotransfer systems formed by adenylate kinase (AK) and glycolytic enzymes such as hexokinase (HK) (18). CK, AK, and HK are all involved in metabolic sensing

Correspondence: R. Birkedal (e-mail: rikke@sysbio.ioc.ee).
Submitted 17 March 2020 / Revised 10 November 2020 / Accepted 3 December 2020

0363-6135/21 Copyright © 2021 the American Physiological Society

Downloaded from journals.physiology.org/journal/ajpheart by Rikke Birkedal (086.110.032.113) on March 18, 2021.

and regulation, and their activities and extent of mitochondrial association vary between tissues (19). However, the CK system, with mitochondrial CK located in the mitochondrial intermembrane space, is believed to be critical for conveying metabolic signals from the ATPases across the diffusion barriers to the adenine nucleotide translocase (ANT) in the mitochondria, ensuring that ATP production by respiration meets demand (20–26). Hearts from CK KO mice exhibit several changes that may enable normal cardiac function at moderate workloads. The mitochondria are reorganized, and the apparent ADP-affinity of mitochondria is higher, retaining the functional coupling between mitochondria and ATPases (27). Furthermore, there is a compensatory increase in both AK- and HK-catalyzed phosphotransfer (28).

Creatine-deficient mice are alternative models to study the role of the CK system. For the CK system to function, creatine is either taken up via the food or synthesized in the body. The two enzymes involved in creatine synthesis are L-arginine:glycine amidinotransferase (AGAT; EC 2.1.4.1) and guanidinoacetate *N*-methyltransferase (GAMT; EC 2.1.1.2). The cardiac phenotype of GAMT KO mice is remarkably mild. Similar to CK KO mice, they exhibit a reduced contractile reserve, and recovery of cardiac function is compromised following acute ischemia (29). However, their exercise capacity and response to surgically induced chronic heart failure are similar to those in wild-type mice (29, 30). The other creatine-deficient model, AGAT KO, exhibits impaired cardiac contractility even at baseline, but this is driven by the combined lack of creatine and homoarginine (31), which is another AGAT product and a marker of overall cardiac health (32). Hearts from both GAMT and AGAT KO mice have similar respiration capacity and total AK activity as their wild-type littermates (30, 31).

As AK and HK take on a more prominent role in the hearts of CK KO mice (28), we speculated whether the expression and mitochondrial association of these two enzymes is upregulated in hearts from GAMT and AGAT KO mice. Changes in the intracellular distribution of HK may occur without changes in the overall activity (33), and it is conceivable this could also be the case for AK. Therefore, the present study was undertaken to determine *1*) the stimulation of mitochondrial respiration by activating HK, AK, and CK in permeabilized cardiomyocytes, *2*) the intracellular distribution of HK, AK, and CK between cytosol and mitochondria separated by fractionation of whole tissue homogenate, and *3*) the expression of the major isoforms of HK (isoforms I and II), AK (isoforms 1 and 2), and CK (MM-CK and sarcomeric mitochondrial CK) in hearts from AGAT and GAMT, KO and WT, and male and female mice. CK was included in the measurements as its overall activity and isoform distribution is similar in AGAT KO and wild-type mice and with no or only minor changes in GAMT KO mice (29–31).

MATERIALS AND METHODS

All animal procedures were carried out according to directive 2010/63/EU of the European Parliament and had been approved by the Project Authorisation Committee for Animal Experiments in the Estonian Ministry of Rural Affairs.

Animals

GAMT (34) and AGAT (32) heterozygous mice on a pure C57BL/6J genetic background (backcrossed for >10 generations) were originally from The Wellcome Trust Center for Human Genetics (Oxford, UK). The animals were kept and bred in the animal facility of Tallinn University of Technology at an ambient temperature of 22–22.8°C and a 12:12-h light-dark cycle. They had free access to water and food (naturally creatine-free V1534-000 Rat/mouse maintenance from Ssniff Spezialdiäten GmbH, Germany). As the AGAT KO mice were small and weak, they were housed in groups whenever possible, given moistened food at the bottom of the cage, and had longer cages with a heating lamp at one end to allow for behavioral thermoregulation. Breeding was performed with heterozygous mating to obtain KO and WT littermates. Both GAMT and AGAT KO mice were housed separately from their WT and heterozygous littermates to avoid accumulating creatine via coprophagia (34).

Genotyping

GAMT mice were genotyped by PCR as previously described (35). AGAT mice were genotyped by PCR according to the following protocol. Genomic DNA was extracted from tissue samples by SDS/proteinase K (Bioline, London, UK) digestion followed by isopropanol precipitation. PCR amplification of the DNA fragments was performed using the following specific primers: 5′-AGCCCCTCTATTTCCCTTTTCATT-3′ and 5′-TTCCACTGCGTCATTCTCCTGTAA-3′. PCRs were carried out in a 25-μL volume containing 1× PCR buffer (Bioline Immobuffer, Bioline, London, UK), 0.5 mM dNTP mixture (Bioline, London, UK), 1.2 mM $MgCl_2$, 0.5 pmol·μL^{-1} of each primer (TAG Copenhagen, Copenhagen, Denmark), 5% DMSO, 1 M betaine, 0.06 U·μL^{-1} IMMOLASE DNA polymerase (Bioline, London, UK), and 5 μL template DNA. The touchdown PCR protocol was as follows: an initial denaturation at 95°C for 5 min was followed by 10 cycles at 94°C for 60 s, 65°C (0.5°C decrease per cycle) for 60 s, 72°C for 30 s, then another 35 cycles at 95°C for 60 s, 60°C for 60 s, 72°C for 30 s, and a final extension step was carried out at 72°C for 2 min. This was done in a thermal cycler (Bio-Rad DNA Engine, Bio-Rad Laboratories, Hercules, CA, or Eppendorf Mastercycler, Eppendorf, Hamburg, Germany). PCR products were electrophoresed on a 1% agarose gel with ethidium bromide in 0.5× Tris-borate-EDTA. Amplification of a single 522-bp product or a 277-bp PCR product corresponded to AGAT WT or homozygous AGAT knockout (AGAT KO) genotype, respectively. Simultaneous amplification of a 522- and 277-bp fragments corresponded to a heterozygous AGAT genotype.

Isolation of Cardiomyocytes

Cardiomyocytes were isolated using slightly modified version of a method described previously (35). Mice were anaesthetized with ketamine/dexmedetomidine mixture (150 mg·kg^{-1} and 0.5 mg·kg^{-1}, respectively) and received an injection of 250 U of heparin to prevent blood coagulation. When the toe-pinch reflex was absent, the animal was euthanized by cervical dislocation. The heart was excised and immediately placed in ice-cold wash solution consisting of the following (in mM): 117 NaCl, 5.7 KCl, 1.5 KH_2PO_4, 4.4 $NaHCO_3$, 1.7 $MgCl_2$, 21 HEPES, 20 taurine,

Downloaded from journals.physiology.org/journal/ajpheart by Rikke Birkedal (086.110.032.113) on March 18, 2021.

11.7 glucose, and 10 2,3-butanedione monoxime (pH was adjusted to 7.4 with NaOH). It was cannulated via the aorta on a Langendorff perfusion system. The heart was first perfused with wash solution at 38.5°C at a constant pressure of 80 cmH_2O for 5 min with a flow rate of 2–3 mL·min^{-1}. After the heart was washed free of blood, the perfusion was switched to a digestion solution, which consisted of wash solution containing additional 0.2–0.25 mg·mL^{-1} Liberase DL and 1.36 mg·mL^{-1} of dispase II. After 10–20 min perfusion, when the heart was soft, the ventricles were cut into four pieces, transferred into digestion solution, and incubated further at 37°C with gentle shaking until the tissue started falling apart. Cells were further dissociated with a pasteur pipette. As a result, the cell suspension was a mix of isolated cardiomyocytes from the left and right ventricles. Cells were harvested several times during postdigestion and filtered through a 100-μm cell strainer (EASYstrainer Cell Strainer, Greiner Bio-One) into a glass tube, which contained glucose-free sedimentation solution consisting of wash solution (without glucose and 2,3-butanedione monoxime) containing additional 2 mM pyruvate, 10 μM leupeptin, 2 μM soybean trypsin inhibitor, and 3 mg·mL^{-1} BSA. Each time, additional digestion solution was added to the undigested cells. Then, the viable cells were separated by sedimentation or by centrifugation at 300 rpm for 2 min. First, extracellular Ca^{2+} was gradually increased to 2 mM to ensure Ca^{2+} tolerance of the cells. After this, extracellular Ca^{2+} was washed out again by washing the cells three times with 5 mL of sedimentation solution. Isolated cells were stored in this solution at room temperature until use within 3 h.

Respirometer Recordings

Respiration of saponin-permeabilized cardiomyocytes was determined at 25°C with a Strathkelvin RC 650 respirometer equipped with six 1302 O_2 electrodes connected via a 929 Oxygen System interface (all from Strathkelvin Instruments, Glasgow, UK) to a computer. The O_2 tension in each chamber was recorded by the software provided by Strathkelvin Instruments and our homemade software, which immediately calculated the rate of O_2 consumption as well. The latter is open-source software and is freely available at https://iocbio.gitlab.io/kinetics.

To start the respiration experiments, 5 to 40 μL cell suspension was added to the respiration chamber containing 2 mL of respiration solution consisting of 110 mM sucrose, 60 mM K-lactobionic acid, 3 mM KH_2PO_4, 3 mM $MgCl_2$, 20 mM HEPES, 20 mM taurine, 0.5 mM EGTA, 0.5 mM dithiothreitol (DTT), 2 mM malate, 5 mM glutamate, 5 mg·mL^{-1} BSA, and 25 μg·mL^{-1} saponin (pH was adjusted to 7.1 with KOH). For HK, AK, and CK experiments, different amounts of cells were added to get a good resolution without running out of oxygen during the experiment. As the activity of HK is relatively low, we added 30–40 μL of cell suspension to the chambers, where HK function was assessed. In contrast, the activity of AK was very high, and we added 5–20 μL of cell suspension to the chambers, where AK function was assessed. Cells were allowed at least 5 min to permeabilize before the steady-state basal respiration rate, V_0, was recorded. After that, 2 mM ATP were added to stimulate nonspecific ATPase activity. After reaching steady state, we added 10 mM glucose to stimulate HK or 1 mM AMP to stimulate AK. To stimulate CK, 20 mM creatine were present in the respirometer chamber from the beginning, before the cells were added, and the addition of 2 mM ATP activated CK as well as other ATPases. However, the experiments with HK and AK demonstrated that the nonspecific ATPase rate was relatively low as is to be expected in quiescent cardiomyocytes. At first, endogenous ADP from HK, AK, or CK was exclusively consumed by the mitochondria and stimulated respiration. Then, the addition of 5 mM phosphoenolpyruvate (PEP) induced a decrease in respiration rate due to activated endogenous pyruvate kinase (PK) that competed with mitochondria for the consumption of ADP. Finally, by the addition of 20 U·mL^{-1} exogenous PK, we assessed the fraction of the ADP flux that was channeled directly from the kinase to the mitochondria.

In parallel, in another chamber, cells were stimulated first with ATP to stimulate ATPases and then with 10 mM glucose to stimulate HK or 1 mM AMP to stimulate AK. Again, to stimulate CK, 20 mM creatine were present in the respirometer chamber from the beginning, before the cells were added, and the addition of 2 mM ATP activated CK as well as other ATPases. Finally, the respiration rate was stimulated to maximal, V_{max}, by the addition of 2 mM ADP. This allowed us to assess the capacity of HK, AK, and CK relative to V_{max}, as well as to determine the coupling efficiency, defined as $(V_{max} - V_0)/V_{max}$ (36).

The ADP stock solution contained the following (in mM): 200 ADP and 60 $MgCl_2$ (pH adjusted to 7.1 with KOH).

The ATP stock solution contained the following (in mM): 200 ATP, 160 Mg-acetate, and 20 HEPES (pH adjusted to 7.1 with KOH). The ATP stock solution was prepared with Mg-acetate instead of $MgCl_2$, as this prolonged its storage life. As 2 mM ATP were added to all experiments, any impact acetate may have had as a mitochondrial substrate was the same in all experiments.

Fractionation

The mouse was anesthetized and euthanized as described above for the isolation of cardiomyocytes. The heart was quickly removed and immediately transferred to a glass beaker with ice-cold isolation solution. The heart was trimmed of any obvious fat and connective tissue, gently blotted to remove excess fluids, and weighed before transfer to an ice-cold glass plate. All subsequent procedures were carried out on ice. The heart tissue was minced with scissors into very small pieces and suspended in 8 mL ice-cold homogenization buffer per gram tissue (33). The homogenization buffer contained the following (in mM): 250 sucrose, 20 HEPES, and 1 DTT and protease inhibitors (1 tablet cOmplete mini per 10 mL of buffer). Next, the heart was homogenized in a prechilled 15 mL Potter-Elvehjem homogenizer. From this homogenate, 200 μL were taken aside for assays on whole tissue homogenate. The remaining homogenate was centrifuged at 1,000 *g* for 3 min at 4°C to pellet tissue debris. The pellet was discarded, and the supernatant was transferred to a new Eppendorf and centrifuged at 10,000 *g* for 1 h at 4°C. The resulting supernatant represented the cytosolic

Downloaded from journals.physiology.org/journal/ajpheart by Rikke Birkedal (086.110.032.113) on March 18, 2021.

fraction, and the pellet represented the mitochondrial fraction. The supernatant was transferred to a new Eppendorf, and the remaining liquid from the pellet was carefully removed with blotting paper. The mitochondrial pellet was resuspended in 200 μL homogenization buffer. The supernatant (cytosolic fraction) was cleaned once more by centrifugation at 11,000 *g* for 10 min at 4°C. Fifty microliters of whole tissue homogenate and cytosolic and mitochondrial fraction were taken aside for protein measurements. The whole tissue homogenate and mitochondrial suspension were incubated on ice for at least 30 min with Triton-X 100 at a final concentration of 0.5%. All suspensions were stored at −80°C until recording of their enzyme activities.

Enzyme Activities

Enzyme activities were measured with coupled enzyme assays using an Evolution 600 spectrophotometer (Thermo Fisher Scientific) equipped with a Peltier water-cooled cell changer (SPE 8 W, Thermo Fisher Scientific) to maintain temperature at 25°C.

Citrate synthase (CS) activity was recorded in a total volume of 1 mL CS buffer containing the following (in mM): 100 Tris·HCl buffer (pH 8.1), 0.1 5,5′-dithiobis(2-nitrobenzoic acid), and 0.3 acetyl-CoA. The assay was started by the addition of 10 μL of diluted (1:10) fraction (mitochondrial or cytosolic fraction or whole tissue homogenate). The change in absorbance was recorded for 2 min at 412 nm before (for reference) and after addition of 0.5 mM oxaloacetate. The activity was calculated using the extinction coefficient for thionitrobenzoate, which is 14,150 $M^{-1}\cdot cm^{-1}$ at 25°C (37).

Activities of creatine kinase (CK) and adenylate kinase (AK) were measured in a total volume of 1 mL AK/CK buffer containing the following (in mM): 20 HEPES, 20 glucose, 5 Mg acetate, 0.5 DTT, 0.6 NADP, and 1.2 ADP. pH was adjusted to 7.4 with KOH. Immediately before use, we added 5 $U\cdot mL^{-1}$ hexokinase and 5 $U\cdot mL^{-1}$ glucose-6-phosphate dehydrogenase. The assay was started by the addition of 10 μL of diluted (1:10) fraction. The absorbance was measured for 2 min at 340 nm before (AK activity) and after addition of 10 mM creatine phosphate (CK activity + AK activity).

Hexokinase (HK) activity was measured in 1 mL HK buffer containing the following (in mM): 20 HEPES, 20 glucose, 5 Mg acetate, 0.5 DTT, 0.6 NADP, and 2 ATP. pH was adjusted to 7.4 with KOH. Immediately before use, we added 5 $U\cdot mL^{-1}$ glucose-6-phosphate dehydrogenase. The assay was started by the addition of 10 μL of nondiluted fraction, and the reduction of NADP was followed at 340 nm for 2 min.

Lactate dehydrogenase activity (LDH) was measured in 1 mL LDH buffer containing the following (in mM): 34.1 K_2HPO_4, 7.35 KH_2PO_4, 0.35 sodium pyruvate, and 0.3 NADH (pH was adjusted to 7.5 with K_2HPO_4/KH_2PO_4). The assay was started by the addition of 10 μL of nondiluted fraction, and the reaction was monitored for 2 min at 340 nm.

The activities of AK, CK, HK, and LDH were calculated using the extinction coefficient for NADH/NADPH ($\varepsilon 340 = 6220\ M^{-1}\cdot cm^{-1}$). All measurements were performed in triplicate, and the results were averaged.

Western Blotting

Frozen hearts were homogenized in a glass homogenizer at a concentration of 20 mg tissue/mL of extraction buffer containing the following (in mM): 50 Tris, 150 NaCl, 2% SDS, and 1 DTT and 1 tablet each of cOmplete Mini and PhosSTOP protease and phosphatase inhibitor cocktails, respectively, per 10 mL. The protein concentration was determined spectrophotometrically (see Determination of Protein Content). Ten micrograms of protein were loaded onto SDS-PAGE gels (4% stacking gel, 10 or 12% separating gel), which were run at 60 V for ~35 min followed by 120 V for 50–55 min in a Mini-PROTEAN Tetra System using a PowerPac HC power supply (Bio-Rad Laboratories, Hercules, CA). The separated proteins were transferred onto a nitrocellulose membrane overnight at 4°C at 90 mA. The protein loading was assessed by staining with a 0.1% Ponceau S solution followed by two washes with ultra-pure water. After imaging the Ponceau staining, the membranes were blocked with 5% BSA, incubated with primary antibody, and incubated with secondary antibody in a Tris-buffered saline with 0.1% Tween-20 (TBST) for 1 h at room temperature. Between each step, the membranes were washed two times for 10 min in TBST. The antibodies were detected with the Bio-Rad Clarity Western ECL substrate. Both Ponceau and antibody staining were imaged in an Image Quant LAS 400 imager.

The primary antibodies were from Cell Signaling Technology (CST), Abcam, or ThermoFisher Scientific (TFS): hexokinase I (C35C4) [CST, product no 2024, Research Resource Identifier (RRID):AB_2116996, 1:1,000)], hexokinase II (C64G5) (CST, product no. 2867, RRID:AB_2232946, 1:1,000), adenylate kinase 1 (TFS, product no. PA5-89246, RRID:AB_2805440, 1:1,000), adenylate kinase 2 (Abcam, product no. ab166901, RRID:AB_2877142, 1:1,000), creatine kinase MM (MM-CK; Abcam, product no. ab198235, RRID:AB_2877143, 1:8,000), creatine kinase mitochondrial (TFS, product no. PA5-106347, RRID:AB_2854023, 1:7,000), and cytochrome oxidase (COX IV) (CST, product no 4844, RRID:AB_2085427, 1:5,000). The secondary antibody was HRP-Conjugated Goat Anti-Rabbit IgG (H + L) (Jackson ImmunoResearch Laboratories Inc.), which was diluted in TBST with 5% BSA and used at a dilution of 1:10,000 for detection of HK I, HK II, AK 1, and AK 2, 1:50,000 for detection of COX IV, 1:70,000 for detection of Mi-CK, and 1:80,000 for detection of MM-CK. The amount of protein loaded on the gel and the dilutions of the primary and secondary antibodies had been optimized in preliminary experiments, where proportionality of the staining intensity to protein concentration had been verified.

The Western blots for COX IV, HK, AK, and MM-CK were straightforward, showing single bands near the expected molecular weight. However, Mi-CK had three bands. To test the specificity of these bands, we used liver as a negative control and gastrocnemius, which has lower levels of Mi-CK than the heart. In liver, the lowermost band was faint, but visible, suggesting that this band was nonspecific. In gastrocnemius, the top band was fainter than in heart, whereas there were two strongly stained bands in the middle, suggesting that only the top band was specific for Mi-CK. Therefore, we analyzed only the top band, and only the first half of the intensity profile to avoid any impact from the middle band.

Downloaded from journals.physiology.org/journal/ajpheart by Rikke Birkedal (086.110.032.113) on March 18, 2021.

For the analysis, the samples were split into two groups: AGAT (WT and KO) and GAMT (WT and KO). As a single gel was insufficient to measure all samples in a group, one or two lanes were used for a reference sample that was a mix of all the samples in the group and used throughout the study. The tissue samples were distributed in a random order and were measured two to three times.

The staining intensity was determined using the free software, GelAnalyzer 19.1 (www.gelanalyzer.com). For the Ponceau staining images, the background was determined and subtracted using ImageJ. The staining intensities were entered into the database using IOCBIO WebDB (https://gitlab.com/iocbio/webdb).

For each gel, the intensities of Ponceau, HK/AK/CK, and COX IV were normalized first to the amount of protein in the lane and then normalized to the corresponding intensity per protein of the reference lane. If the reference sample was loaded into multiple lanes, the mean intensity per protein for the reference lanes was used for normalization. For the statistical analysis, the signal of the protein of interest (HK/AK/CK) was normalized to protein content, Ponceau staining, and, in the case of HK and AK, COX IV intensity. For each tissue sample, the average of the normalized intensity was used for statistical analysis.

Determination of Protein Content

Protein content was determined spectrophotometrically. Fifty microliters of sample were incubated with 2.5 μL of 30% sodium dodecyl sulfate (SDS) at 80°C for 30 min, except for the Western blotting tissue extract, which already contained SDS and was incubated directly at 80°C for 30 min. After heating, the transparent solution was frozen until determination of their protein content in a BioSpec-nano or a NanoDrop 200c spectrophotometer (Shimadzu Scientific Instruments Inc., Columbia, MD, and ThermoFisher Scientific, Waltham, MA), which recorded the absorption spectra from 220–800 nm. The protein content of each sample was measured at least three times, and the results were averaged. The absorption at 280 nm was background corrected by subtracting the absorption at 330 nm, and protein content was calculated using the molecular weight and extinction coefficient of BSA (66 400 g·mol^{-1} and 43,824 M^{-1}·cm^{-1}, respectively). For isolated cardiomyocytes, the protein content of each cell suspension was corrected for the protein content of the corresponding sedimentation solution. For homogenate, cytosolic and mitochondrial fractions, and for Western blotting tissue extract, the protein content was corrected for that of the homogenization buffer.

Chemicals

If not specified otherwise, the chemicals were from Merck or VWR.

Statistics

Values are given as means ± SE. If not stated otherwise, data are plotted using the Tukey box plot notation. Statistical tests and analysis were performed in R, using Bayesian ANOVA with the statistical models considering changes induced by phenotype (WT vs. KO), gender (male vs. female), and interaction between these factors. For Bayes Factor (BF) interpretation, common evidence categories were used (38), with BF > 10 considered to be statistically significant.

RESULTS

We assessed the activity and mitochondrial association of HK, AK, and CK in creatine-deficient mice in several ways. On permeabilized cardiomyocytes, we assessed how much their ATPase activity stimulates respiration. To complement these measurements, we assessed the intracellular distribution of HK, AK, and CK in experiments, where whole tissue homogenate was centrifuged to separate the cytosolic and mitochondrial fractions. Lastly, we used Western blotting to assess the expression of the major isoforms of HK, AK, and CK in the heart.

Animals

Table 1 shows the morphological data of the animals used for these experiments. As we could not measure the heart weight of the mice used for cardiomyocyte isolation, the heart weight is only reported for the mice used for fractionation and Western blotting. For both AGAT and GAMT mice, the body weight, tibial length and heart weight were significantly affected by both genotype and sex (BF > 100, extreme evidence). For the body weight of AGAT mice, there was also a significant interaction between genotype and sex (BF > 30, very strong evidence), because the body weight of males was more affected than that of females. The body weight of AGAT and GAMT KO mice was ~60% and ~75%, respectively, of the body weight of WT littermates. As a result, the relative heart weight (HW/BW) was higher in both AGAT and GAMT KO (BF > 100, extreme evidence) but did not differ between males and females.

Mitochondrial Respiration Capacity, Citrate Synthase, and Lactate Dehydrogenase Activities

For the experiments recording the respiration of isolated, permeabilized cardiomyocytes, the stimulation of respiration by endogenous ADP generated by HK, AK, or CK was determined relative to the maximal respiration rate as recorded in the presence of 2 mM ADP, V_{max}. When normalized to the protein content of the cell suspension, there was no effect of genotype or sex on V_{max}, which was 129 ± 9 and 106 ± 7 nmol O_2·min^{-1}·mg protein^{-1} in AGAT KO and WT, respectively, and 108 ± 6 and 127 ± 14 nmol O_2·min^{-1}·mg protein^{-1} in GAMT KO and WT, respectively.

To determine the overall activities and intracellular distribution of CK, AK, and HK, we prepared cardiac whole tissue homogenates, from which a part was separated by differential centrifugation into a cytosolic and mitochondrial fraction. The activities of lactate dehydrogenase (LDH) and citrate synthase (CS) were used as markers of cytosol and mitochondria (33). Figure 1 shows the total activities of LDH (Fig. 1, *A* and *B*) and CS (Fig. 1, *C* and *D*) in whole tissue homogenate, the cytosolic fraction, and the mitochondrial fraction from AGAT and GAMT, WT and KO, and males and females. When analyzed by Bayesian ANOVA, there was no effect of genotype or sex in any of the measurements.

The activities in Fig. 1 are normalized to the protein content. For whole tissue homogenate, we also calculated the

Downloaded from journals.physiology.org/journal/ajpheart by Rikke Birkedal (086.110.032.113) on March 18, 2021.

Table 1. *Characteristics of the mice used in the experiments*

Genotype/Sex	*n*	Age, days	BW, g	TL, cm	HW, mg	HW/BW, mg/g
AGAT WT						
F	29 (18)	199 ± 9	24.7 ± 0.7	2.17 ± 0.01	103 ± 3	4.2 ± 0.1
M	23 (13)	209 ± 9	31.5 ± 0.7	2.26 ± 0.01	129 ± 3	4.0 ± 0.1
AGAT KO						
F	23 (13)	211 ± 11	15.4 ± 0.4	2.08 ± 0.01	80 ± 2	5.5 ± 0.1
M	23 (14)	200 ± 10	17.7 ± 0.4	2.10 ± 0.01	93 ± 2	5.4 ± 0.1
Genotype			***	***	***	***
Sex			***	***	***	
Interaction			**			
GAMT WT						
F	19 (12)	258 ± 16	26.6 ± 0.8	2.21 ± 0.01	114 ± 3	4.0 ± 0.1
M	19 (12)	260 ± 16	31.9 ± 1.0	2.24 ± 0.01	137 ± 4	4.0 ± 0.1
GAMT KO						
F	17 (11)	246 ± 18	19.2 ± 0.5	2.13 ± 0.02	96 ± 3	4.9 ± 0.1
M	20 (14)	250 ± 16	24.2 ± 0.4	2.20 ± 0.01	119 ± 2	4.9 ± 0.1
Genotype			***	***	***	***
Sex			***	***	***	
Interaction						

Values are means ± SE. We report the age, bodyweight (BW), tibial length (TL), absolute heart weight (HW), and relative heart weight (HW/BW). The total number of animals is shown in column *n*. As we could not weigh the hearts used for cardiomyocyte isolation, the heart weight (HW and HW/BW) is reported for a smaller number of animals, indicated in parenthesis. AGAT, L-arginine:glycine amidinotransferase (AGAT); GAMT, *N*-guanidinoacetate methyltranferase. Below each genotype, we show the results of the statistical analysis by a two-way Bayesian ANOVA assessing the effect of genotype, sex, and their interaction. **Indicates 30 < Bayesian factor (BF) ≤100, strong evidence; ***indicates BF >100, extremely strong evidence.

enzyme activities normalized to the wet weight. These results are shown in Table 2. The number of experiments for each of the groups shown in Table 2 is the same for all measurements related to the study of intracellular distribution by fractionation. When the activities of CS and LDH were normalized to the wet weight, there was also no effect of genotype or sex.

Hexokinase Stimulation of Respiration, Activity, and Distribution

To assess the activity and distribution of HK, we stimulated respiration via HK, which resides in the cytosol, but has a fraction bound on the outside of mitochondria. As shown schematically in Fig. 2*A*, the addition of ATP and glucose to the solution with permeabilized cardiomyocytes stimulates HK to produce endogenous ADP. This ADP enters mitochondria via voltage-dependent anion channel (VDAC) and stimulates respiration. This can be measured as the reduction in oxygen concentration in the solution as shown in the representative experimental trace in Fig. 2*B*. Subsequent addition of PEP activates endogenous PK, which competes with mitochondrial respiration for ADP produced by endogenous ATPases, such as HK. Further addition of exogenous PK ensures that any ADP diffusing from the ATPases into solution is immediately converted to ATP. Only ADP, which is channeled directly from HK to the mitochondria, stimulates respiration. This is due to the large overall activity of PK in the solution surrounding the cardiomyocytes compared with the overall activity of ATPases in cardiomyocytes. In the second half of Fig. 2*B* trace, the reduction in respiration rate after the addition of PEP and subsequent addition of PK is shown. In parallel with the described experiment, we performed, with the same cardiomyocyte suspension, an experiment in which we added 2 mM ADP to the solution instead of PEP and PK. This allowed us to determine the respiration stimulated by HK (V_{HK}) relative to the maximal respiration rate (V_{max}) under our conditions.

The statistical analysis of all experiments is summarized in Fig. 2, *C*–*F*. Figure 2, *C* and *D*, shows the averaged results from the respiration experiments with AGAT and GAMT mice, respectively. The *left* shows the respiration rate in the presence of ATP and glucose, V_{HK}, as a fraction of V_{max} obtained with 2 mM ADP. In AGAT mice, V_{HK}/V_{max} was moderately lower in KO than in WT (17.5 ± 0.7% and 25.2 ± 1.4%, respectively; BF > 100, extreme evidence). In GAMT mice, V_{HK}/V_{max} was 22.4 ± 1.6% and 27.3 ± 3.0% in KO and WT, respectively, and this was not significantly different. The coupling efficiency of respiration was 92.6 ± 0.4% and 91.4 ± 0.4% for AGAT and GAMT mice, respectively. The relative inhibition by PEP and PK was the same irrespective of genotype or sex, and they lowered the respiration rate to 16.1 ± 1.8% in AGAT and 24.5 ± 2.6% in GAMT.

The total activity of HK was much lower than for the other enzymes (AK and CK; Table 2). Figure 2, *E* and *F*, shows the averaged HK activities recorded in the three different fractions. AGAT KO mice had a slightly higher HK activity in the mitochondrial fraction (Fig. 2*E*; BF > 30, very strong evidence). In GAMT mice, there was no effect of genotype or sex (Fig. 2*F*).

Adenylate Kinase Stimulation of Respiration, Activity, and Distribution

As for HK, we assessed how ADP generated by the AK reaction stimulates respiration and is inhibited by PEP and PK. In contrast to HK, which is exclusively cytosolic, AK has cytosolic as well as mitochondrial isoforms (Fig. 3*A*). Respiration, in this case, was stimulated by ATP and AMP and resulted in a large increase in respiration rate (Fig. 3*B*). This respiration rate (V_{AK}) was almost fully inhibited by the addition of PEP and PK, as illustrated in representative experiment (Fig. 3*B*). Figure 3, *C* and *D*, shows the averaged results from the

Downloaded from journals.physiology.org/journal/ajpheart by Rikke Birkedal (086.110.032.113) on March 18, 2021.

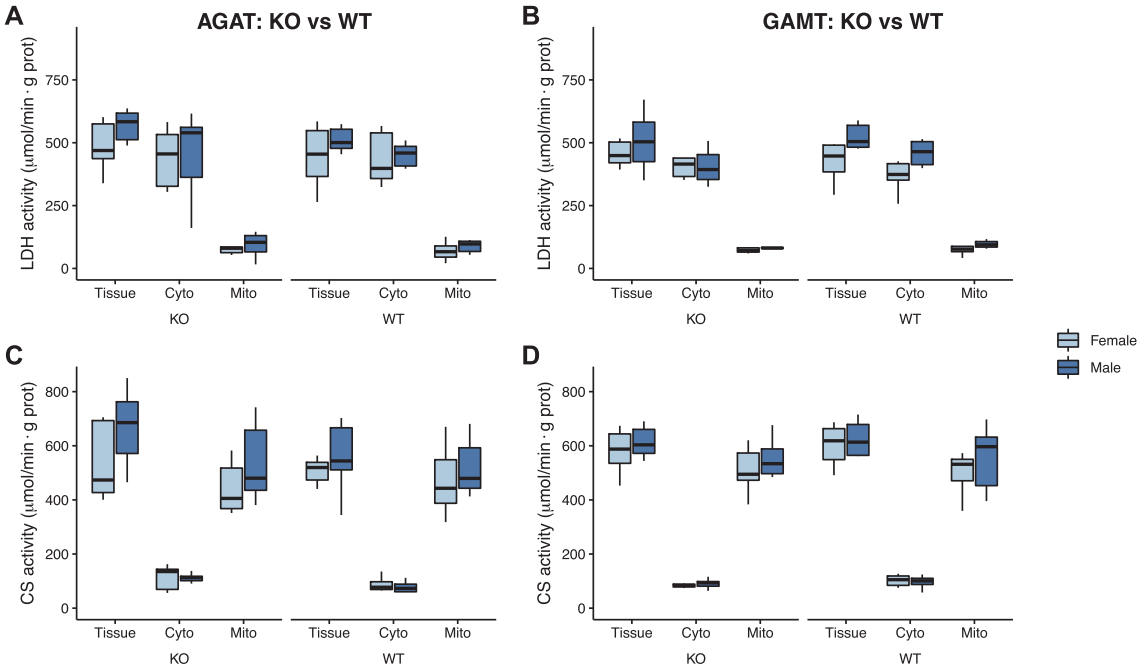

Figure 1. The overall activity and intracellular distribution of lactate dehydrogenase (LDH) and citrate synthase (CS) in L-arginine:glycine amidinotransferase (AGAT) and guanidinoacetate *N*-methyltranferase (GAMT) mice. The activities of LDH (*A* and *B*) and CS (*C* and *D*) in whole tissue homogenate (tissue) and the cytosolic (cyto) and the mitochondrial (mito) fraction in hearts from AGAT and GAMT wild-type (WT) and knockout (KO) mice. The number of experimental animals in each group is the same as in Table 2. The effects of genotype, sex, and their interaction were assessed by a two-way Bayesian ANOVA. There was no effect of genotype or sex in any of these measurements.

respiration experiments with AGAT and GAMT mice, respectively. There was no effect of genotype or sex, and the pooled V_{AK}/V_{max} was 85.9 ± 2.1% and 95.4 ± 1.0 in AGAT and GAMT, respectively. The coupling efficiency of respiration was 92.3 ± 0.6% and 91.5 ± 0.5% for AGAT and GAMT mice, respectively. The addition of PEP and PK lowered the respiration rate to an average of 4.2 ± 1.2 and −1.0 ± 0.5% of V_{AK} in AGAT and GAMT, respectively.

Table 2 shows the average AK activity in whole tissue homogenate normalized to the tissue wet weight. Figure 3, *E* and *F*, shows the averaged AK activities recorded in the three different fractions. Most of the AK activity was found in the cytosolic fraction. There was no effect of genotype or sex in any of the measurements related to AK.

Creatine Kinase Stimulation of Respiration, Activity, and Distribution

CK resides in cytosol and in the mitochondrial intermembrane space. In contrast to AK, CK has been shown to be functionally coupled to adenine nucleotide translocase through direct transfer of ADP between proteins (39). The direct transfer is not expected to be for all ADP produced by mitochondrial CK, as illustrated in Fig. 4*A*. The respiration stimulated by addition of ATP (with creatine present in the medium) (V_{CK}) was significant, with some of the respiration remaining after addition of PEP and PK (Fig. 4*B*).

Figure 4, *C* and *D*, shows the averaged results from the respiration measurements with AGAT and GAMT mice, respectively. In AGAT mice, V_{CK}/V_{max} was moderately lower in KO than in WT (66.2 ± 2.2% and 79.8 ± 2.5%, respectively; BF > 100, extreme evidence). In GAMT mice, V_{CK}/V_{max} was 75.7 ± 1.1% and 82.3 ± 2.5% in KO and WT, respectively, and this was not significantly different. The coupling efficiency of respiration was 90.0 ± 0.5% and 90.2 ± 0.6% for AGAT and GAMT mice, respectively. The addition of PEP and PK lowered respiration rate to an average of 18.6 ± 1.9 and 27.7 ± 2.6% of V_{CK} in AGAT and GAMT, respectively. These data are pooled because there was no effect of genotype or sex.

The total CK activity was close to the AK activity but slightly lower (Fig. 4 and Table 2). AGAT KO mice had a slightly lower CK activity than WT (Table 2, BF > 10, strong evidence). In contrast, for GAMT mice, the CK activity difference between KO and WT littermates was not statistically significantly different, as the model assuming differences being due to genotype had a BF of 3.2. Figure 4, *E* and *F*, shows the averaged CK activities recorded in the three different fractions from AGAT and GAMT mice, respectively. The CK activity was distributed ~50:50 between the cytosolic

Downloaded from journals.physiology.org/journal/ajpheart by Rikke Birkedal (086.110.032.113) on March 18, 2021.

Table 2. *Enzyme activities in the whole tissue homogenate normalized to the wet weight*

	n	LDH	CS	CK	AK	HK
AGAT						
WT						
F	7	137 ± 13	153 ± 11	238 ± 21	271 ± 19	6.78 ± 0.79
M	7	156 ± 8	176 ± 12	267 ± 25	308 ± 19	7.28 ± 0.63
KO						
F	13	131 ± 7	142 ± 12	208 ± 14*	271 ± 15	7.55 ± 0.7
M	7	137 ± 17	174 ± 14	171 ± 12*	244 ± 22	6.65 ± 1.03
GAMT						
WT						
F	6	124 ± 16	163 ± 10	228 ± 22	272 ± 13	5.77 ± 0.54
M	8	149 ± 11	170 ± 10	215 ± 17	281 ± 28	6.58 ± 0.46
KO						
F	6	139 ± 9	163 ± 5	185 ± 30	257 ± 16	6.11 ± 0.32
M	6	145 ± 12	176 ± 6	160 ± 8	232 ± 15	6.07 ± 0.47

Values are means ± SE in μmol·min^{-1}·g wet wt^{-1}, and *n* denotes the number of animals. AGAT, L-arginine:glycine amidinotransferase; GAMT, *N*-guanidinoacetate methyltranferase; LDH, lactate dehydrogenase; CK, creatine kinase; HK, hexokinase; AK, adenylate kinase; KO, knockout; WT, wild type; F, female; M, male. The effects of genotype, sex, and their interaction were assessed by a two-way Bayesian ANOVA. *In AGAT mice, the CK activity was slightly but significantly lower in KO than in WT (Bayesian factor >10, strong evidence).

and the mitochondrial fraction. Bayesian ANOVA showed no effect of genotype or sex.

Expression of HK, AK, and CK Isoforms

The expression of cytochrome oxidase (COX IV), HK I and II, AK 1 and 2, MM-CK, and mitochondrial CK was assessed by Western blotting. The results are shown in Fig. 5. In GAMT mice, there was no effect of genotype or sex in any of the expression patterns (Fig. 5*B*). However, in AGAT mice, we saw a significant increase in the expression of HK I (Fig. 5*C*). The level of significance (BF > 100, extreme evidence) was independent of whether the HK I signal was normalized to *1*) the amount of protein loaded, *2*) Ponceau protein staining, or *3*) the COX IV signal.

DISCUSSION

Whereas we found no changes in the overall activity and mitochondrial association of CK, AK, or HK in hearts from GAMT KO mice, AGAT KO mice, which are considered a model of pure creatine deficiency (40), exhibited a higher HK activity associated with the mito-chondria, consistent with increased protein expression of HK I. However, since AGAT KO mice had lower HK-stimulated respiration, our results suggest that adaptive changes in HK I in the hearts of creatine-deficient AGAT mice do not to compensate for changes in overall energy transfer but are related to other activities and functions of HK.

The mitochondrial association of HK, AK, and CK was assessed in multiple ways. First, we recorded in permeabilized cardiomyocytes how much respiration was stimulated by their respective ATPase activity. These cardiomyocytes are quiescent and do not represent the situation in vivo, where energy fluxes are dynamic, but the preparation allowed us to assess the relative capacities of the HK, AK, and CK phosphotransfer systems. The cardiomyocytes were permeabilized with saponin, which only perforates the sarcolemma, but leaves intracellular structures intact (41). Consequently, cytosolic proteins in solution (such as LDH and the nonbound fractions of HK, AK, and CK) can diffuse out of the cells but will retain their catalytic function in the surrounding solution. When the ATPase activity of HK, AK, or CK was activated with ATP and glucose, AMP, or creatine, respectively, this represents the total ATPase activity of soluble as well as bound fractions of the enzymes. In one chamber, the kinase ATPase activity was related to the maximal respiration rate assessed by addition of 2 mM ADP (V_{kinase}/V_{max}). The maximal respiration rate of permeabilized cardiomyocytes was not affected by genotype or sex. This is in agreement with other studies (30, 31, 35, 42, 43). In another chamber, the ADP-flux from the kinase to the mitochondria was inhibited by the addition of PEP and PK, functioning as a competitive ADP trap. These experiments show how much of the endogenously generated ADP is channeled directly to the mitochondria. Note, that for AK and CK, which have isoforms in the mitochondrial intermembrane space, the channeling depends on the association between enzymes as well as the permeability of the outer mitochondrial membrane.

In addition to the respiration experiments, we assessed the distribution of HK, AK, and CK between the cytosol and mitochondria. CS activity is a marker of mitochondrial volume (44), and for the study of intracellular enzyme distribution, CS and LDH were used as markers of mitochondria and cytosol, respectively, as in Ref. 33. Indeed, the majority of LDH was found in the cytosol, and the majority of CS was found in the mitochondrial fraction (Fig. 1). There was a small cross-contamination between the fractions, which was consistent between groups. CS in the cytosol could be due to some of the mitochondria being damaged and ruptured during the homogenization and fractionation process (33). The presence of LDH in the mitochondrial fraction indicates a small contamination from the cytosolic fraction. Although great care was taken during the experiments, some contamination could occur due to the small amounts of tissue used in this work.

The enzyme activities shown in Fig. 1–4 are normalized to the protein concentration. However, the outcome of protein measurements depends on the assay as well as the exact protocol (45), which complicates comparisons between studies. Therefore, we also report the enzyme activities in the whole tissue homogenate normalized to wet weight (Table 2). When taking into account differences in assay temperature, the activities of CS and LDH reported in the present study were close to those found by others (27, 46–48). In agreement with the similar V_{max} respiration rates and other studies of GAMT and AGAT mice, we found no differences in the cardiac CS activity (Fig. 1 and Table 2) (29, 31).

Lastly, we assessed the expression of the major isoforms of HK, AK, and CK. Their expression was related to either the amount of protein, to the amount of protein estimated by Ponceau staining, or (for HK and AK) to the expression of the mitochondrial protein COX IV. COX IV expression was not affected by genotype or sex, which again is in agreement with the similar V_{max} and CS activity.

Downloaded from journals.physiology.org/journal/ajpheart by Rikke Birkedal (086.110.032.113) on March 18, 2021.

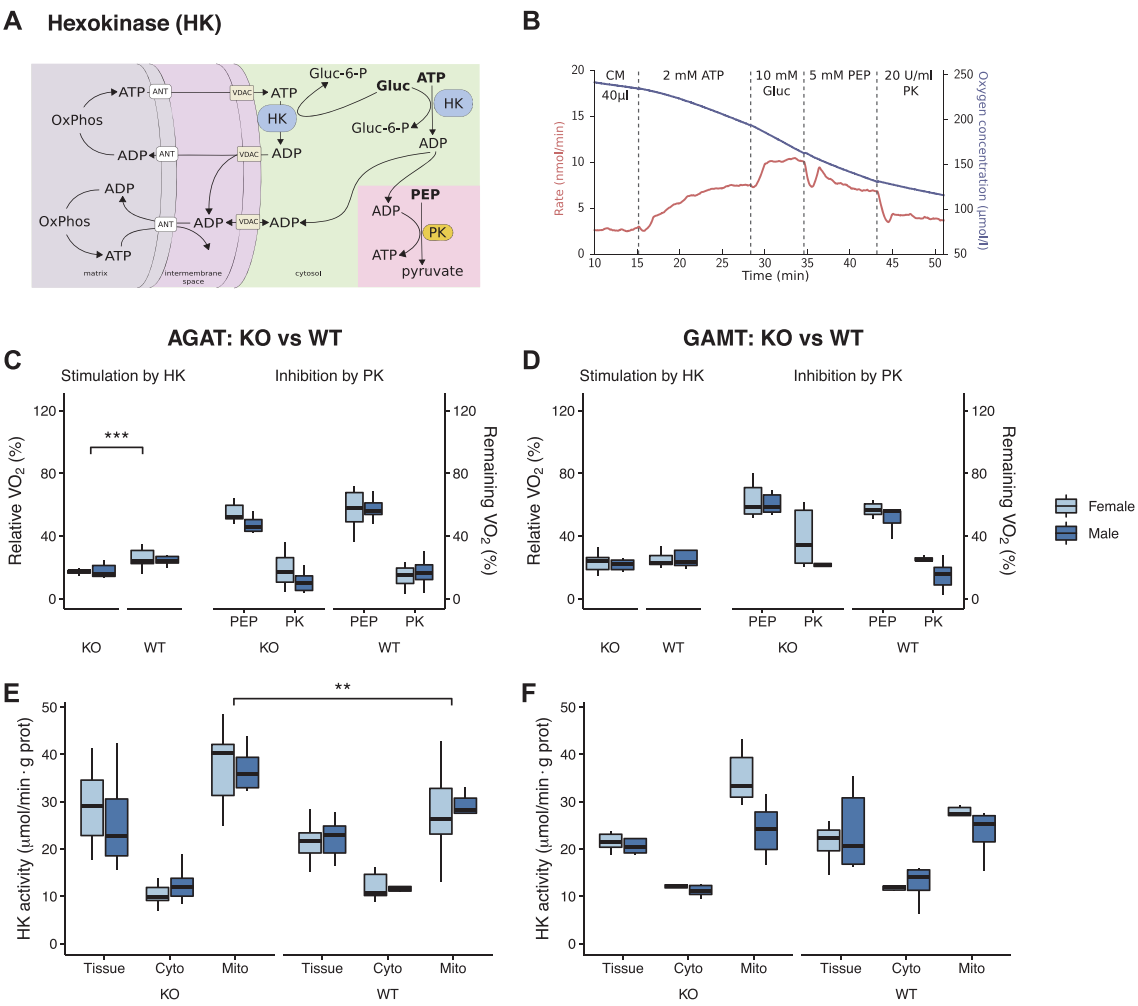

Figure 2. Hexokinase (HK) coupling to respiration and intracellular distribution in L-arginine:glycine amidinotransferase (AGAT) and *N*-guanidinoacetate methyltranferase (GAMT) mice. *A*: schematic representation of reactions studied in permeabilized cardiomyocytes (see the main text for details). *B*: representative example of respirometer recording. The volume of cardiomyocyte suspension (CM) is indicated. *C* and *D*: averaged results of the respiration experiments in AGAT (*C*) and GAMT (*D*) mice. The number of animals in each group, GAMT and AGAT, wild-type (WT) and knockout (KO), and male and female was $n = 5–10$. *Left*: respiration stimulated by HK/maximal respiration rate (V_{HK}/V_{max}). *Right*: fractional lowering by phosphoenolpyruvate (PEP) and pyruvate kinase (PK). *E* and *F*: the intracellular distribution of HK in AGAT (*E*) and GAMT (*F*). The number of experimental animals in each group was the same as in Table 2. The effects of genotype, sex, and their interaction were assessed by a two-way Bayesian ANOVA. **Bayes factor (BF) > 30 and ***BF > 100, significant effect of genotype.

HK Expression, Distribution, and Stimulation of Respiration Change in AGAT KO Hearts

HK catalyzes the first step in glycolysis. Adult mammalian hearts mainly express HK isoforms I and II, of which II is predominant (49). Whereas HK I is associated with the mitochondria, the location of HK II is dynamic and depends on metabolism. HK II functions as a metabolic switch directing the fate of glucose (50, 51), and mitochondrial associated HK plays a crucial role in cardiac protection (52–56).

In the present study, the HK activity in mouse heart (Fig. 2 and Table 2) was similar to the activity in rat heart (46, 57). Overall, the ATPase activity of HK stimulated respiration to ~25% of V_{max} (Fig. 2). The majority of HK was found in the mitochondrial fraction (Fig. 2, *E* and *F*). Other studies have found 30–60% of HK in the mitochondrial fraction (33, 52). Mitochondrially associated HK is bound on the cytosolic side of the mitochondrial outer membrane (58) and is able to channel ADP to the matrix (59–61). This channeling was confirmed in the present study, where PEP and PK did not fully inhibit the respiration but lowered the rate to 16–25% (Fig. 2, *C* and *F*).

Downloaded from journals.physiology.org/journal/ajpheart by Rikke Birkedal (086.110.032.113) on March 18, 2021.

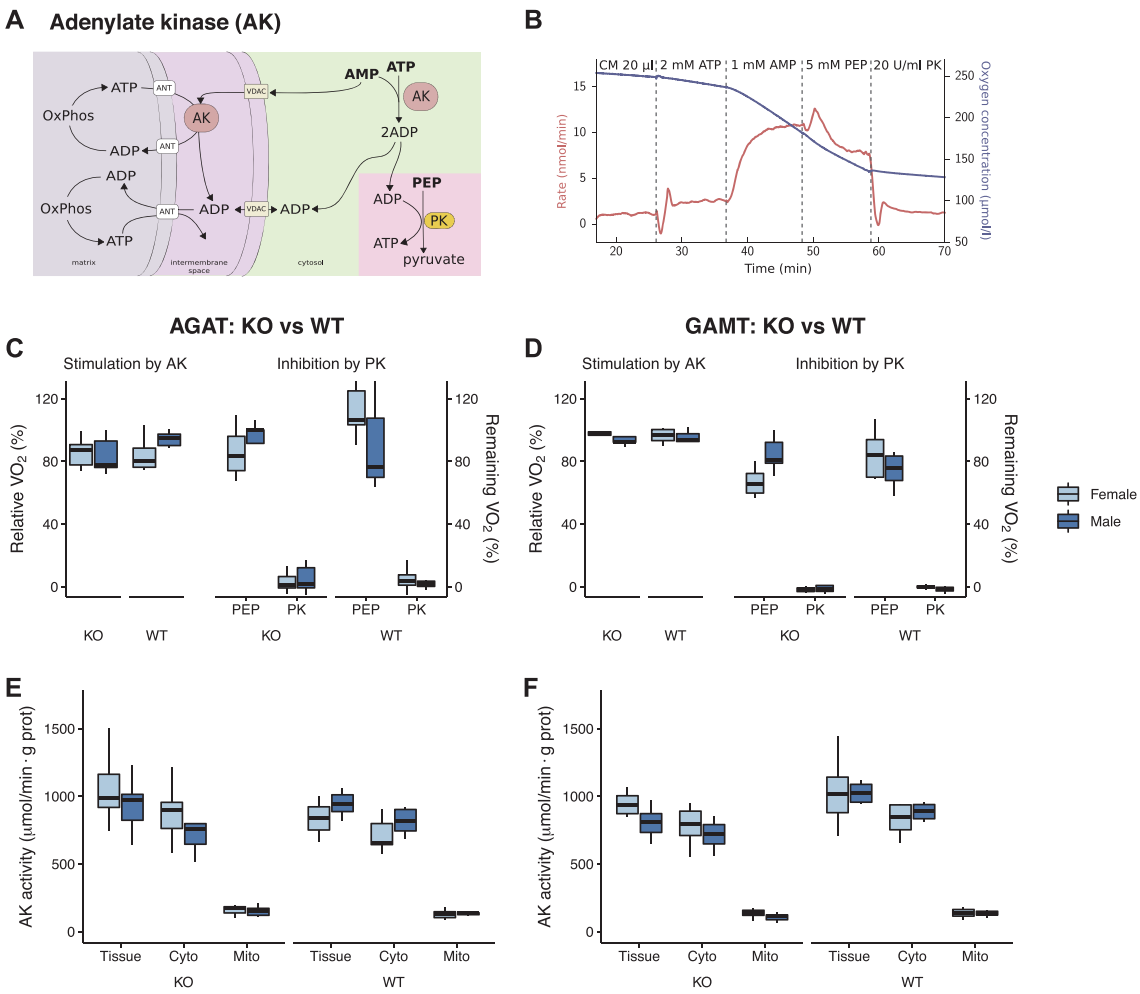

Figure 3. Adenylate kinase (AK) coupling to respiration and intracellular distribution in L-arginine:glycine amidinotransferase (AGAT) and *N*-guanidinoacetate methyltranferase (GAMT) mice. *A*: schematic representation of reactions studied in permeabilized cardiomyocytes (see the main text for details). *B*: representative example of respirometer recording. The volume of cardiomyocyte suspension (CM) is indicated. *C* and *D*: averaged results of the respiration experiments in AGAT (*C*) and GAMT (*D*) mice. The number of animals in each group (AGAT and GAMT, wild-type (WT) and knockout (KO), and male and female) was $n = 5$–9. *Left*: respiration stimulated by AK/maximal respiration rate (V_{AK}/V_{max}). *Right*: fractional lowering by phosphoenolpyruvate (PEP) and pyruvate kinase (PK). *E* and *F*: the intracellular distribution of AK in AGAT (*E*) and GAMT (*F*). The number of experimental animals in each group was the same as in Table 2. The effects of genotype, sex, and their interaction were assessed by a two-way Bayesian ANOVA. There was no effect of genotype or sex in any of the measurements.

In GAMT mice, the HK activity, distribution, and stimulation of respiration did not differ between KO and WT. However, AGAT KO mice had a slightly higher HK activity in the mitochondrial fraction (Fig. 2*E*) and greater expression of HK I (Fig. 5), although the total HK activity did not differ between KO and WT (Fig. 4 and Table 2). It may seem counterintuitive that mitochondrially associated HK activity increases, whereas the ADP feedback from HK to stimulate respiration decreases (Fig. 2*C*). However, HK I binding to VDAC promotes closure of the channel (62). This would limit respiration at submaximal ADP concentrations, as generated endogenously by HK in the presence of glucose and ATP but not at saturating ADP concentrations as in the presence of 2 mM exogenous ADP. The influence of HK on the regulation of oxygen consumption has been observed previously, where acute, but not chronic, detachment of HK II from mitochondria increased oxygen consumption in the perfused heart (63). Taken together with the present results, this suggests that HK is involved in regulating the gating of the mitochondrial outer membrane. This is an interesting topic that deserves attention in future studies.

Our results are in agreement with a study on the cardiac transcriptome of AGAT KO and WT hearts, where a greater expression of HK I and a smaller expression of HK II was

Downloaded from journals.physiology.org/journal/ajpheart by Rikke Birkedal (086.110.032.113) on March 18, 2021.

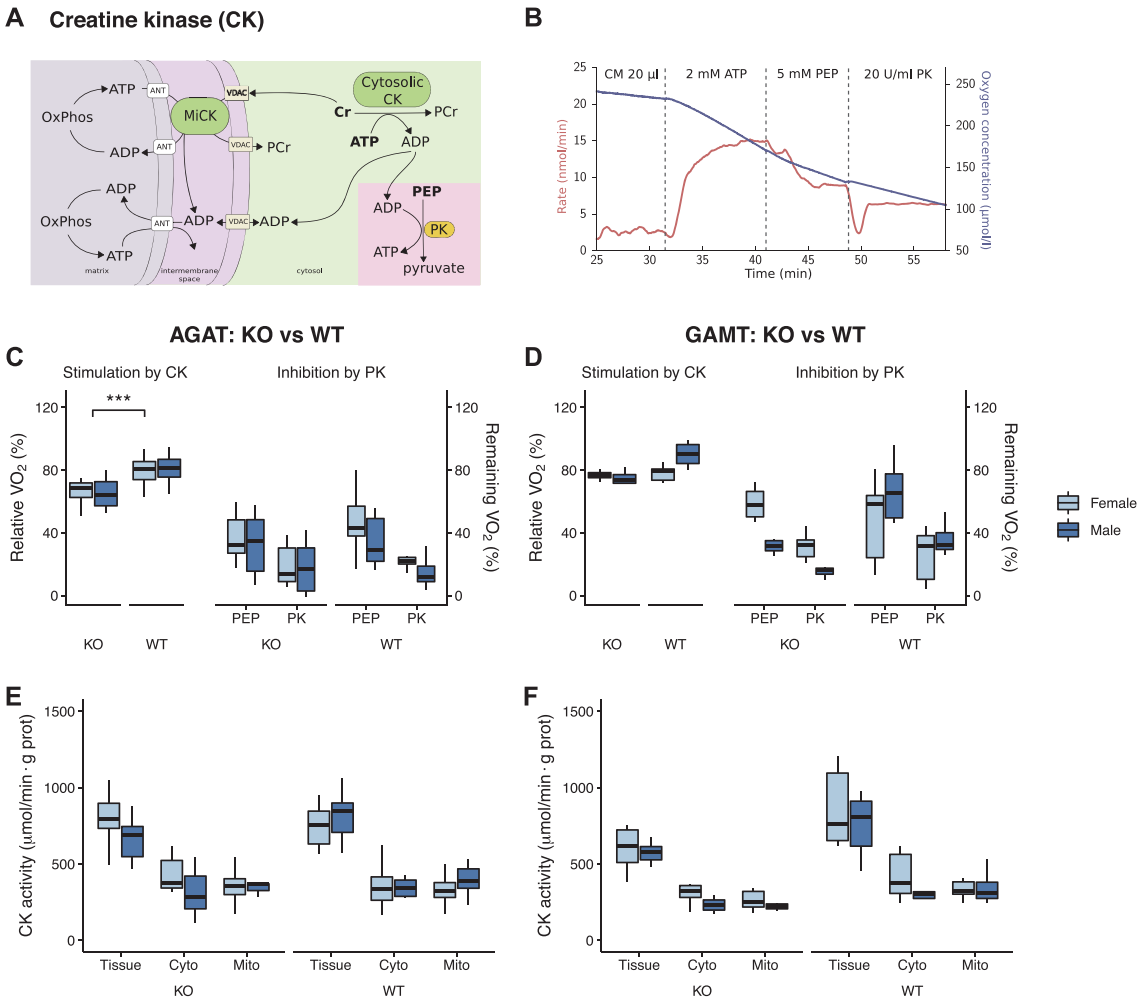

Figure 4. Creatine kinase (CK) coupling to respiration and intracellular distribution in L-arginine:glycine amidinotransferase (AGAT) or *N*-guanidinoacetate methyltranferase (GAMT) mice. *A*: schematic representation of reactions studied in permeabilized cardiomyocytes (see the main text for details). *B*: representative example of respirometer recording. The volume of cardiomyocyte suspension (CM) is indicated. *C* and *D*: averaged results of the respiration experiments in AGAT (*C*) and GAMT (*D*) mice. The number of animals in each group (AGAT and GAMT, wild-type (WT) and knockout (KO), and male and female) was $n = 4–10$. *Left*: respiration stimulated by CK/maximal respiration rate (V_{CK}/V_{max}). *Right*: fractional lowering by phosphoenolpyruvate (PEP) and pyruvate kinase (PK). *E* and *F*: the intracellular distribution of CK in AGAT (*E*) and GAMT (*F*). The number of experimental animals in each group was the same as in Table 2. The effects of genotype, sex, and their interaction were assessed by a two-way Bayesian ANOVA. ***Bayes factor (BF) > 100, significant effect of genotype.

found (64). Although we did not see any difference in HK II at the protein expression level, the greater expression of HK I was clear (Fig. 5). As noted above, HK I binds to the mitochondria, and the higher HK activity near mitochondria and the higher expression of HK I may confer several advantages. First, due to differences in isoform kinetics, the greater proportion of HK I may be an advantage for AGAT KO mouse hearts, which have elevated levels of inorganic phosphate, P_i (31). P_i counters the product inhibition of HK I (by glucose-6-phosphate), whereas it may even aggravate the product inhibition of HK II (65). Although this is complex, as the sensitivity to glucose-6-phosphate decreases upon binding to the mitochondria, the shift toward more HK I could be to balance the regulation of overall HK activity. Second, as mitochondrially associated CK and HK are both involved in the buffering of mitochondrial ROS production (66–68), a greater proportion of mitochondrially associated HK I could compensate for the substrate limitation of mitochondrial CK.

We cannot say whether the change in cardiac HK is compensatory or metabolically related. AGAT KO mice are resistant to metabolic syndrome due to chronic activation of

Downloaded from journals.physiology.org/journal/ajpheart by Rikke Birkedal (086.110.032.113) on March 18, 2021.

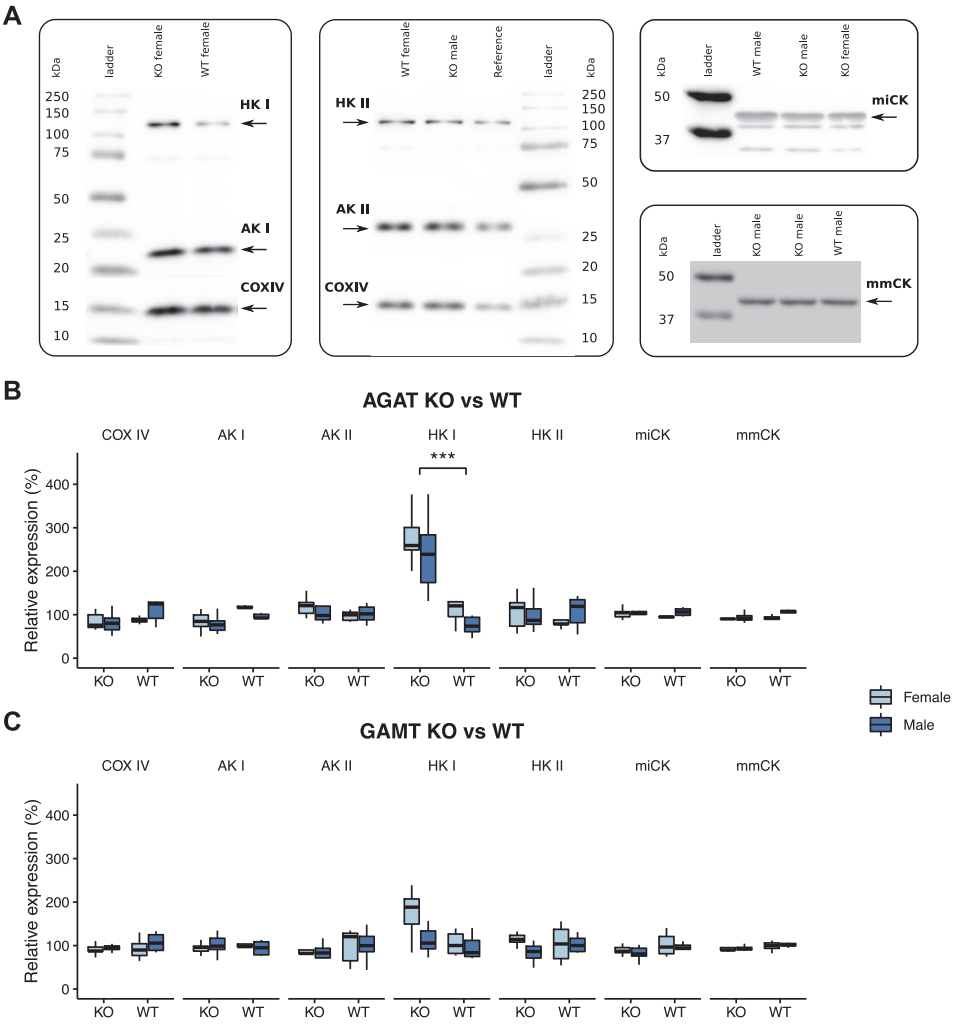

Figure 5. Western blots to assess the expression of the main isoforms of hexokinase (HK), adenylate kinase (AK), and creatine kinase (CK). *A*: representative raw images of Western blots. Here, we show only blots from L-arginine:glycine amidinotransferase (AGAT) mice as indicated above each lane. The reference sample was a mix of all samples from this group of mice (see MATERIALS AND METHODS for details). For cytochrome oxidase (COX IV), HK, AK, and MM-CK, there was a single band near the expected molecular weight. For mitochondrial (Mi)-CK, preliminary experiments showed that only the uppermost band was specific (see MATERIALS AND METHODS for details). *B* and *C*: the averaged expression normalized to Ponceau staining (used as a loading control) from AGAT (*B*) and *N*-guanidinoacetate methyltranferase (GAMT; *C*) mice. The number of animals in each group [AGAT and GAMT, wild-type (WT) and knockout (KO), and male and female] was $n = 5–6$. The effects of genotype, sex, and their interaction were assessed by a two-way Bayesian ANOVA. ***Bayes factor (BF) > 100, significant effect of genotype. Note the significantly higher expression of HK I in AGAT KO compared with WT littermates. This was the only protein expression that was affected by genotype. Protein expression was not affected by sex in any of the measurements.

AMPK in their fat, skeletal muscles and hypothalamus of the brain (69). Although the heart has a distinct phenotype and no chronic AMPK activation (31), chronic AMPK activation in other tissues may have systemic effects, because the nutritional uptake by fat and skeletal muscles may indirectly affect that of other tissues, including the heart, and/or the hypothalamus has a central role in the regulating whole body metabolism. The expression of HK is modified by diet and thus nutrient uptake (49). Furthermore, it has been suggested that mitochondrial HK is committed to glycolysis, whereas cytosolic HK promotes anabolic pathways such as glycogen synthesis and the pentose phosphate pathway (65). Thus the shift toward more mitochondrially associated HK I is in agreement with an overall reduction of anabolism and promotion of catabolism in AGAT KO mice.

Downloaded from journals.physiology.org/journal/ajpheart by Rikke Birkedal (086.110.032.113) on March 18, 2021.

A comparison of AGAT and GAMT KO mice does not provide further clues regarding the cause of the change in HK, as the phenotype of GAMT KO mice is generally milder. Compared with AGAT KO mice, they have more grip strength and smaller changes in skeletal muscle mass and metabolic marker enzymes (34, 40, 70, 71). This is likely due to GAMT mice accumulating guanidinoacetate, which may substitute for creatine in the CK reaction albeit at reduced reaction rates (72). In the hearts of GAMT KO, no increase in P_i is reported (29), and so HK regulation by Pi is likely unaltered. Furthermore, as Mi-CK buffers mitochondrial ROS production with μM amounts of creatine (67), it is likely that guanidinoacetate is a sufficient substitute.

AK and CK Phosphotransfer Systems in Hearts from AGAT and GAMT Mice

AK is considered the second major phosphotransfer system after CK, and it has been hypothesized that mitochondrial and cytosolic AK isoforms can facilitate energy transfer much in the same way (73, 74). Several studies have addressed the role of mitochondrial AK in the compartmentalization of adenine nucleotides in the mitochondrial intermembrane space (19, 61, 75).

In the present study, AK had the highest activity of the kinases (Table 2). The activity was at the high end of the spectrum but close to that reported by others (27, 47). In agreement with previous studies, the total AK activity was not upregulated in GAMT and AGAT KO (30, 31). Only as GAMT KO mice get older is an upregulation of the AK activity observed (42).

The present results show that the intracellular distribution of AK and its coupling to respiration were also not affected by creatine deficiency. Endogenous ADP produced by AK stimulated the respiration rate almost to the maximum, but this was basically abolished in the presence of PEP and PK (Fig. 3, *C* and *D*). This suggests that almost all AK was situated in the cytosol and fully accessible for PEP and PK to consume ADP, before it reached the mitochondria. The respiration data were corroborated by the fractionation data, which showed that almost all AK activity was found in the cytosol (Fig. 3, *E* and *F*). Others have also reported that AK is mainly cytosolic in mouse heart (76). Both AK 1 and AK 2 were readily detected by Western blotting, which showed that their overall expression was not affected by genotype or sex (Fig. 5).

The activity, distribution, and coupling of CK were included in this study as a control, because others have shown that the overall activity and isoform distribution of CK in the heart do not change in AGAT mice (31) and only little in GAMT KO mice (29, 30). When taking differences in assay temperature into account (assuming a Q_{10} of 2.5 as in Ref. 77), the total CK activity was 25–35% lower than reported in some studies (27, 47) but similar to that reported by Veksler et al. (48) for control mice.

When respiration was stimulated by the ATPase activity of CK, the response was smaller in AGAT KO than in WT (Fig. 4*C*). This is in agreement with the lower total CK activity in AGAT KO (Table 2). However, the MM-CK and Mi-CK protein expression was not different (Fig. 5), suggesting that either the changes were not resolved by Western blotting, the specific activity had changed, or any differences were due to changes in the expression of brain-CK (B-CK). Another study of AGAT mice found no difference in the CK activity and isoform distribution (31). There can, however, be some variation between studies. In GAMT mice, we found no difference in the CK activity as in (29), whereas another study found a slightly lower CK activity in GAMT KO (30).

In AGAT WT and GAMT mice, the activation of CK stimulated the respiration rate to ~80% of V_{max}. The fraction of ADP from CK that is accessible to PEP + PK depends on two factors: the fraction of CK within the mitochondria and the permeability of the outer mitochondrial membrane. Approximately half of the CK activity was found in the mitochondrial fraction (Fig. 4, *E* and *F*). Acknowledging a small contamination from the cytosolic fraction, this is in agreement with the fraction of mitochondrial CK estimated by gel electrophoresis being in the range of 20–40% (9, 30, 31, 47, 48, 78, 79). PEP + PK reduced the respiration rate to ~25% (Fig. 4, *C* and *D*). This could suggest that some ADP from mitochondrial CK was accessible to PEP + PK. Mitochondrial CK and ANT are functionally coupled with direct transfer contributing to about half of the flux (39). However, the other half of the flux is through ADP that is released into the intermembrane space by mitochondrial CK. If the outer mitochondrial membrane is permeable to ADP, some of it will diffuse into the cytosol to be accessible for PEP + PK. This suggests, in turn, that diffusion restriction by the mitochondrial outer membrane is less than expected from measurements on rat cardiomyocytes (17).

The physiological role of CK and other phosphotransfer systems in the heart depends on their isoform distribution, the permeability of the outer mitochondrial membrane, and their ADP flux capacity relative to that of the mitochondria. Several papers on rat hearts have shown that mitochondrial CK alone is able to stimulate respiration to maximal (20, 80, 81), and in permeabilized cardiomyocytes, PEP and PK do not reduce the respiration rate stimulated by ATP and creatine (80, 81). This is consistent with the strong coupling of mitochondrial CK to ANT (39) and significant diffusion restriction by the outer mitochondrial membrane due to the very small fraction of open VDACs (17). The high ADP flux through CK and the significant diffusion restriction at the level of the outer mitochondrial membrane suggest a prominent role of the CK system in facilitating energy transfer between ATPases and mitochondria and regulating mitochondrial respiration (18, 21–25, 73, 82).

In contrast, the present results clearly demonstrate that in the hearts from AGAT and GAMT WT mice, even cytosolic and mitochondrial CK together cannot supply ADP to sustain maximal respiration. Activation of all CK in the cells only stimulated the respiration rate to ~80% of V_{max}. The reduction by PEP and PK suggests that mitochondrial CK alone supports ~25% of V_{max} through direct transfer to ANT (Fig. 4, *C* and *D*). At first, we speculated whether mice and rats differ in terms of the relative rates of CK activity and respiration. Indeed, although not specified in the paper, one study shows that CK activity relative to the maximal respiration rate is lower in mice than in rats (25). However, the present data are in agreement with a study on rat cardiac fibers, where ATP and creatine in the presence of PEP and PK stimulated respiration to ~20% of the maximal respiration

Downloaded from journals.physiology.org/journal/ajpheart by Rikke Birkedal (086.110.032.113) on March 18, 2021.

with ADP (83). There is a similar discrepancy between studies of mitochondrial AK. In the present experiments, AK stimulated the respiration rate to near maximal (Fig. 3), but our results suggest that it is mainly situated in the cytosol, and its phosphotransfer across the outer mitochondrial membrane is negligible. This is in agreement with one study on rat heart, which found very little AK in mitochondria (84), whereas another one study found that mitochondrial AK stimulates respiration to maximal and is able to channel approximately one third of ADP to ANT in the presence of PEP + PK (75). We are unable to explain this variation between studies. In the present study, the coupling efficiency of respiration ranged from 90 to 92%, which corresponds to an acceptor coupling ratio of 10–13. This indicates that our preparation was sound. The discrepancy between studies has to be investigated further, as there is no clear and obvious cause for it. Taken together, the low capacity of mitochondrial CK and the near absence of mitochondrial AK suggests that, in the hearts of AGAT and GAMT WT mice, the phosphotransfer systems are not developed to facilitate energy transfer by overcoming diffusion restriction at the level of the outer mitochondrial membrane. This may explain the relatively mild cardiac phenotype of AGAT and GAMT KO mice (30, 31, 35, 42).

In perspective, there is no question that the CK system is important. It is elaborate with different isoforms expressed in a tissue-dependent manner, and it has evolved several times (85). For wild animals, predator as well as prey, physical performance is a matter of life and death. However, laboratory mice are relatively sedentary. Indeed, wild mice sprint much faster (2.4–3.3 $m \cdot s^{-1}$) than laboratory mice (0.9–1.7 $m \cdot s^{-1}$) (86). The present results suggest that in the hearts of healthy individuals in a laboratory setting, the CK system is not crucial for energy transfer between ATPases and mitochondria. However, the severe substrate limitation of CK in AGAT KO mice leads to changes in HK expression and mitochondrial association.

ACKNOWLEDGMENTS

We acknowledge Dirk Isbrandt (University of Cologne, Germany) for generating the strains of L-arginine:glycine amidinotransferase (AGAT) or guanidinoacetate *N*-methyltranferase (GAMT)-deficient mice.

GRANTS

This work was supported by the European Union through the European Regional Development Fund (CENS Estonian Center of Excellence in Research) and Estonian Research Council (IUT33-7). C.L. acknowledges funding from British Heart Foundation Programme Grant (RG/18/12/34040).

DISCLOSURES

No conflicts of interest, financial or otherwise, are declared by the authors.

AUTHOR CONTRIBUTIONS

M.V. and R.B. conceived and designed research; J.B., N.K., K.B., and R.B. performed experiments; J.B., N.K., M.L., M.V., and R.B. analyzed data; M.V. and R.B. interpreted results of experiments; J.B., M.L., and M.V. prepared figures; R.B. drafted manuscript; C.A.L., M.V., and R.B. edited and revised manuscript; J.B., N.K., M.L., C.A.L., M.V., and R.B. approved final version of manuscript.

REFERENCES

1. **Boudina S**, **Laclau MN**, **Tariosse L**, **Daret D**, **Gouverneur G**, **Bonoron-Adele S**, **Saks VA**, **Santos PD.** Alteration of mitochondrial function in a model of chronic ischemia in vivo in rat heart. *Am J Physiol Heart Circ Physiol* 282: H821–H831, 2002. doi:10.1152/ajpheart.00471.2001.
2. **De Sousa E**, **Veksler V**, **Minajeva A**, **Kaasik A**, **Mateo P**, **Mayoux E**, **Hoerter J**, **Bigard X**, **Serrurier B**, **Ventura-Clapier R.** Subcellular creatine kinase alterations. Implications in heart failure. *Circ Res* 85: 68–76, 1999. doi:10.1161/01.RES.85.1.68.
3. **Laclau MN**, **Boudina S**, **Thambo JB**, **Tariosse L**, **Gouverneur G**, **Bonoron-Adele S**, **Saks VA**, **Garlid KD**, **Santos PD.** Cardioprotection by ischemic preconditioning preserves mitochondrial function and functional coupling between adenine nucleotide translocase and creatine kinase. *J Mol Cell Cardiol* 33: 947–956, 2001. doi:10.1006/jmcc.2001.1357.
4. **Ventura-Clapier R**, **Garnier A**, **Veksler V**, **Joubert F.** Bioenergetics of the failing heart. *Biochim Biophys Acta* 1813: 1360–1372, 2011. doi:10.1016/j.bbamcr.2010.09.006.
5. **Ingwall JS.** Energy metabolism in heart failure and remodelling. *Cardiovasc Res* 81: 412–419, 2008 doi:10.1093/cvr/cvn301.
6. **Ingwall JS**, **Weiss RG.** Is the failing heart energy starved? *Circ Res* 95: 135–145, 2004. doi:10.1161/01.RES.0000137170.41939.d9.
7. **Akki A**, **Su J**, **Yano T**, **Gupta A**, **Wang Y**, **Leppo MK**, **Chacko VP**, **Steenbergen C**, **Weiss RG.** Creatine kinase overexpression improves ATP kinetics and contractile function in postischemic myocardium. *Am J Physiol Heart Circ Physiol* 303: H844–H852, 2012. doi:10.1152/ajpheart.00268.2012.
8. **Gupta A**, **Akki A**, **Wang Y**, **Leppo MK**, **Chacko VP**, **Foster DB**, **Caceres V**, **Shi S**, **Kirk JA**, **Su J**, **Lai S**, **Paolocci N**, **Steenbergen C**, **Gerstenblith G**, **Weiss RG.** Creatine kinase–mediated improvement of function in failing mouse hearts provides causal evidence the failing heart is energy starved. *J Clin Invest* 122: 291–302, 2012. doi:10.1172/JCI57426.
9. **Whittington HJ**, **Ostrowski PJ**, **McAndrew DJ**, **Cao F**, **Shaw A**, **Eykyn TR**, **Lake HA**, **Tyler J**, **Schneider JE**, **Neubauer S**, **Zervou S**, **Lygate CA.** Over-expression of mitochondrial creatine kinase in the murine heart improves functional recovery and protects against injury following ischaemia-reperfusion. *Cardiovasc Res* 114: 858–869, 2018. doi:10.1093/cvr/cvy054.
10. **Lygate CA**, **Neubauer S.** The myocardial creatine kinase system in the normal, ischaemic and failing heart. In: *Cardiac Energy Metabolism in Health and Disease*, edited by Lopaschuk GD, Dhalla NS. New York: Springer, 2014, p. 155–168.
11. **Crozatier B**, **Badoual T**, **Boehm E**, **Ennezat PV**, **Guenoun T**, **Su J**, **Veksler V**, **Hittinger L**, **Ventura-Clapier R.** Role of creatine kinase in cardiac excitation-contraction coupling: studies in creatine kinase-deficient mice. *FASEB J* 16: 653–660, 2002. doi:10.1096/fj.01-0652com.
12. **Nahrendorf M**, **Spindler M**, **Hu K**, **Bauer L**, **Ritter O**, **Nordbeck P**, **Quaschning T**, **Hiller KH**, **Wallis J**, **Ertl G**, **Bauer WR**, **Neubauer S.** Creatine kinase knockout mice show left ventricular hypertrophy and dilatation, but unaltered remodeling post-myocardial infarction. *Cardiovasc Res* 65: 419–427, 2005. doi:10.1016/j.cardiores.2004.10.006.
13. **Lygate CA**, **Medway DJ**, **Ostrowski PJ**, **Aksentijevic D**, **Sebag-Montefiore L**, **Hunyor I**, **Zervou S**, **Schneider JE**, **Neubauer S.** Chronic creatine kinase deficiency eventually leads to congestive heart failure, but severity is dependent on genetic background, gender and age. *Basic Res Cardiol* 107: 276–286, 2012. doi:10.1007/s00395-012-0276-2.
14. **Illaste A**, **Laasmaa M**, **Peterson P**, **Vendelin M.** Analysis of molecular movement reveals lattice-like obstructions to diffusion in heart muscle cells. *Biophys J* 102: 739–748, 2012 doi:10.1016/j.bpj.2012.01.012.
15. **Jepihhina N**, **Beraud N**, **Sepp M**, **Birkedal R**, **Vendelin M.** Permeabilized rat cardiomyocyte response demonstrates intracellular origin of diffusion obstacles. *Biophys J* 101: 2112–2121, 2011. doi:10.1016/j.bpj.2011.09.025.

Downloaded from journals.physiology.org/journal/ajpheart by Rikke Birkedal (086.110.032.113) on March 18, 2021.

16. **Vendelin M**, **Birkedal R.** Anisotropic diffusion of fluorescently labeled atp in rat cardiomyocytes determined by raster image correlation spectroscopy. *Am J Physiol Cell Physiol* 295: C1302–C1315, 2008. doi:10.1152/ajpcell.00313.2008.
17. **Simson P**, **Jepihhina N**, **Laasmaa M**, **Peterson P**, **Birkedal R**, **Vendelin M.** Restricted ADP movement in cardiomyocytes: cytosolic diffusion obstacles are complemented with a small number of open mitochondrial voltage-dependent anion channels. *J Mol Cell Cardiol* 97: 197–203, 2016. doi:10.1016/j.yjmcc.2016.04.012.
18. **Dzeja PP**, **Terzic A.** Phosphotransfer networks and cellular energetics. *J Exp Biol* 206: 2039–2047, 2003. doi:10.1242/jeb.00426.
19. **Clark JF**, **Kuznetsov AV**, **Radda GK.** ADP-regenerating enzyme systems in mitochondria of guinea pig myometrium and heart. *Am J Physiol Cell Physiol* 272: C399–C404, 1997. doi:10.1152/ajpcell.1997.272.2.C399.
20. **Gellerich F**, **Saks VA.** Control of heart mitochondrial oxygen consumption by creatine kinase: the importance of enzyme localization. *Biochem Biophys Res Commun* 105: 1473–1481, 1982. doi:10.1016/0006-291X(82)90954-8.
21. **Kay L**, **Nicolay K**, **Wieringa B**, **Saks V**, **Wallimann T.** Direct evidence for the control of mitochondrial respiration by mitochondrial creatine kinase in oxidative muscle cells in situ. *J Biol Chem* 275: 6937–6944, 2000. doi:10.1074/jbc.275.10.6937.
22. **Saks VA**, **Belikova YO**, **Kuznetsov AV.** In vivo regulation of mitochondrial respiration in cardiomyocytes: specific restrictions for intracellular diffusion of ADP. *Biochim Biophys Acta* 1074: 302–311, 1991. doi:10.1016/0304-4165(91)90168-G.
23. **Saks VA**, **Kuznetsov AV**, **Khuchua ZA**, **Vasilyeva EV**, **Belikova JO**, **Kesvatera T**, **Tiivel T.** Control of cellular respiration in vivo by mitochondrial outer membrane and by creatine kinase. A new speculative hypothesis: possible involvement of mitochondrial-cytoskeleton interactions. *J Mol Cell Cardiol* 27: 625–645, 1995. doi:10.1016/S0022-2828(08)80056-9.
24. **Saks VA**, **Vasil'eva E**, **Belikova Y**, **Kuznetsov AV**, **Lyapina S**, **Petrova L**, **Perov NA.** Retarded diffusion of ADP in cardiomyocytes: possible role of mitochondrial outer membrane and creatine kinase in cellular regulation of oxidative phosphorylation. *Biochim Biophys Acta* 1144: 134–148, 1993. doi:10.1016/0005-2728(93)90166-D.
25. **Ventura-Clapier R**, **Kuznetsov A**, **Veksler V**, **Boehm E**, **Anflous K.** Functional coupling of creatine kinases in muscles: species and tissue specificity. *Mol Cell Biochem* 184: 231–247, 1998. doi:10.1023/A:1006840508139.
26. **Wallimann T**, **Wyss M**, **Brdiczka D**, **Nicolay K**, **Eppenberger HM.** Intracellular compartmentation, structure and function of creatine kinase isoenzymes in tissues with high and fluctuating energy demands: the "phosphocreatine circuit" for cellular energy homeostasis. *Biochem J* 281: 21–40, 1992. doi:10.1042/bj2810021.
27. **Kaasik A**, **Veksler V**, **Boehm E**, **Novotova M**, **Minajeva A**, **Ventura-Clapier R.** Energetic crosstalk between organelles: architectural integration of energy production and utilization. *Circ Res* 89: 153–159, 2001. doi:10.1161/hh1401.093440.
28. **Dzeja PP**, **Hoyer K**, **Tian R**, **Zhang S**, **Nemutlu E**, **Spindler M**, **Ingwall JS.** Rearrangement of energetic and substrate utilization networks compensate for chronic myocardial creatine kinase deficiency. *J Physiol* 589: 5193–5211, 2011. doi:10.1113/jphysiol.2011.212829.
29. **ten Hove M**, **Lygate CA**, **Fischer A**, **Schneider JE**, **Sang AE**, **Hulbert K**, **Sebag-Montefiore L**, **Watkins H**, **Clarke K**, **Isbrandt D**, **Wallis J**, **Neubauer S.** Reduced inotropic reserve and increased susceptibility to cardiac ischemia/reperfusion injury in phosphocreatine-deficient guanidinoacetate-N-methyltransferase-knockout mice. *Circulation* 111: 2477–2485, 2005. doi:10.1161/01.CIR.0000165147.99592.01.
30. **Lygate CA**, **Aksentijevic D**, **Dawson D**, **Hove M. T**, **Phillips D**, **Bono J. D**, **Medway DJ**, **Sebag-Montefiore L**, **Hunyor I**, **Channon KM**, **Clarke K**, **Zervou S**, **Watkins H**, **Balaban RS**, **Neubauer S.** Living without creatine unchanged exercise capacity and response to chronic myocardial infarction in creatine-deficient mice. *Circ Res* 112: 945–955, 2013. doi:10.1161/CIRCRESAHA.112.300725.
31. **Faller KM**, **Atzler D**, **McAndrew DJ**, **Zervou S**, **Whittington HJ**, **Simon JN**, **Aksentijevic D**, **Hove M. T**, **Choe C**, **Isbrandt D**, **Casadei B**, **Schneider JE**, **Neubauer S**, **Lygate CA.** Impaired cardiac contractile function in AGAT knockout mice devoid of creatine is rescued by homoarginine but not creatine. *Cardiovasc Res* 114: 417–430, 2017. doi:10.1093/cvr/cvx242.
32. **Choe C**, **Atzler D**, **Wild PS**, **Carter AM**, **Böger RH**, **Ojeda F**, **Simova O**, **Stockebrand M**, **Lackner K**, **Nabuurs C**, **Marescau B**, **Streichert T**, **Müller C**, **Lüneburg N**, **Deyn PP**, **Benndorf RA**, **Baldus S**, **Gerloff C**, **Blankenberg S**, **Heerschap A**, **Grant PJ**, **Magnus T**, **Zeller T**, **Isbrandt D**, **Schwedhelm E.** Homoarginine levels are regulated by l-arginine:glycine amidinotransferase and affect stroke outcome results from human and murine studies. *Circulation* 128: 1451–1461, 2013. doi:10.1161/CIRCULATIONAHA.112.000580.
33. **Zuurbier CJ**, **Eerbeek O**, **Meijer AJ.** Ischemic preconditioning, insulin, and morphine all cause hexokinase redistribution. *Am J Physiol Heart Circ Physiol* 289: H496–H499, 2005. doi:10.1152/ajpheart.01182.2004.
34. **Schmidt A**, **Marescau B**, **Boehm EA**, **Renema WK**, **Peco R**, **Das A**, **Steinfeld R**, **Chan S**, **Wallis J**, **Davidoff M**, **Ullrich K**, **Waldschutz R**, **Heerschap A**, **De Deyn PP**, **Neubauer S**, **Isbrandt D.** Severely altered guanidino compound levels, disturbed body weight homeostasis and impaired fertility in a mouse model of guanidinoacetate N-methyltransferase (GAMT) deficiency. *Hum Mol Genet* 13: 905–921, 2004. doi:10.1093/hmg/ddh112.
35. **Branovets J**, **Sepp M**, **Kotlyarova S**, **Jepihhina N**, **Sokolova N**, **Aksentijevic D**, **Lygate CA**, **Neubauer S**, **Vendelin M**, **Birkedal R.** Unchanged mitochondrial organization and compartmentation of high-energy phosphates in creatine-deficient GAMT−/− mouse hearts. *Am J Physiol Heart Circ Physiol* 305: H506–H520, 2013. doi:10.1152/ajpheart.00919.2012.
36. **Gnaiger E.** *Mitochondrial Pathways and Respiratory Control. An Introduction to OXPHOS Analysis* (4th ed.) (Online). Axams, Austria: Steiger Druck GmbH. www.bioblast.at/index.php/Gnaiger_2014_MitoPathways. [2014].
37. **Eyer P**, **Worek F**, **Kiderlen D**, **Sinko G**, **Stuglin A**, **Simeon-Rudolf V**, **Reiner E.** Molar absorption coefficients for the reduced Ellman reagent: reassessment. *Anal Biochem* 312: 224–227, 2003. doi:10.1016/S0003-2697(02)00506-7.
38. **Lee MD**, **Wagenmakers EJ.** *Bayesian Cognitive Modeling: a Practical Course*. Cambridge, UK: Cambridge University Press, 2014.
39. **Vendelin M**, **Lemba M**, **Saks VA.** Analysis of functional coupling: mitochondrial creatine kinase and adenine nucleotide translocase. *Biophys J* 87: 696–713, 2004. doi:10.1529/biophysj.103.036210.
40. **Nabuurs CI**, **Choe CU**, **Veltien A**, **Kan HE**, **van Loon LJ**, **Rodenburg RJ**, **Matschke J**, **Wieringa B**, **Kemp GJ**, **Isbrandt D**, **Heerschap A.** Disturbed energy metabolism and muscular dystrophy caused by pure creatine deficiency are reversible by creatine intake. *J Physiol* 591: 571–592, 2013. doi:10.1113/jphysiol.2012.241760.
41. **Saks VA**, **Veksler VI**, **Kuznetsov AV**, **Kay L**, **Sikk P**, **Tiivel T**, **Tranqui L**, **Olivares J**, **Winkler K**, **Wiedemann F**, **Kunz WS.** Permeabilized cell and skinned fiber techniques in studies of mitochondrial function in vivo. *Mol Cell Biochem* 184: 81–100, 1998. doi:10.1023/A:1006834912257.
42. **Aksentijević D**, **Zervou S**, **Eykyn TR**, **McAndrew DJ**, **Wallis J**, **Schneider JE**, **Neubauer S**, **Lygate CA.** Age-dependent decline in cardiac function in guanidinoacetate-N-methyltransferase knockout mice. *Front Physiol* 10: 1535, 2020. doi:10.3389/fphys.2019.01535.
43. **Karro N**, **Laasmaa M**, **Vendelin M**, **Birkedal R.** Respiration of permeabilized cardiomyocytes from mice: no sex differences, but substrate-dependent changes in the apparent ADP affinity. *Sci Rep* 9: 1–11, 2019. doi:10.1038/s41598-018-37186-2.
44. **Larsen S**, **Nielsen J**, **Hansen CN**, **Nielsen LB**, **Wibrand F**, **Stride N**, **Schroder HD**, **Boushel R**, **Helge JW**, **Dela F**, **Hey-Mogensen M.** Biomarkers of mitochondrial content in skeletal muscle of healthy young human subjects. *J Physiol* 590: 3349–3360, 2012. doi:10.1113/jphysiol.2012.230185.
45. **Lu TS**, **Yiao SY**, **Lim K**, **Jensen RV**, **Hsiao LL.** Interpretation of biological and mechanical variations between the Lowry versus Bradford method for protein quantification. *N Am J Med Sci* 2: 325–328, 2010. doi:10.4297/najms.2010.2325.
46. **Crabtree B**, **Newsholme EA.** The activities of phosphorylase, hexokinase, phosphofructokinase, lactate dehydrogenase and the glycerol 3-phosphate dehydrogenases in muscles from vertebrates and invertebrates. *Biochem J* 126: 49–58, 1972. doi:10.1042/bj1260049.
47. **Momken I**, **Lechêne P**, **Koulmann N**, **Fortin D**, **Mateo P**, **Doan BT**, **Hoerter J**, **Bigard X**, **Veksler V**, **Ventura-Clapier R.** Impaired voluntary running capacity of creatine kinase-deficient mice. *J Physiol (Lond)* 565: 951–964, 2005. doi:10.1113/jphysiol.2005.086397.

Downloaded from journals.physiology.org/journal/ajpheart by Rikke Birkedal (086.110.032.113) on March 18, 2021.

48. **Veksler VI**, **Kuznetsov AV**, **Anflous K**, **Mateo P**, **van Deursen J**, **Wieringa B**, **Ventura-Clapier R.** Muscle creatine kinase-deficient mice. II. Cardiac and skeletal muscles exhibit tissue-specific adaptation of the mitochondrial function. *J Biol Chem* 270: 19921–19929, 1995. doi:10.1074/jbc.270.34.19921.
49. **Postic C**, **Leturque A**, **Printz RL**, **Maulard P**, **Loizeau M**, **Granner DK**, **Girard J.** Development and regulation of glucose transporter and hexokinase expression in rat. *Am J Physiol Endocrinol Metab* 266: E548–E559, 1994. doi:10.1152/ajpendo.1994.266.4.E548.
50. **John S**, **Weiss JN**, **Ribalet B.** Subcellular localization of hexokinases I and II directs the metabolic fate of glucose. *PLoS One* 6: e17674, 2011. doi:10.1371/journal.pone.0017674.
51. **Mergenthaler P**, **Kahl A**, **Kamitz A**, **van Laak V**, **Stohlmann K**, **Thomsen S**, **Klawitter H**, **Przesdzing I**, **Neeb L**, **Freyer D**, **Priller J**, **Collins TJ**, **Megow D**, **Dirnagl U**, **Andrews DW**, **Meisel A.** Mitochondrial hexokinase II (HKII) and phosphoprotein enriched in astrocytes (PEA15) form a molecular switch governing cellular fate depending on the metabolic state. *Proc Natl Acad Sci U S A* 109: 1518–1523, 2012. doi:10.1073/pnas.1108225109.
52. **Gürel E**, **Smeele KM**, **Eerbeek O**, **Koeman A**, **Demirci C**, **Hollmann MW**, **Zuurbier CJ.** Ischemic preconditioning affects hexokinase activity and HKII in different subcellular compartments throughout cardiac ischemia-reperfusion. *J Appl Physiol* 106: 1909–1916, 2009. doi:10.1152/japplphysiol.90537.2008.
53. **Halestrap AP**, **Pereira GC**, **Pasdois P.** The role of hexokinase in cardioprotection – mechanism and potential for translation. *Br J Pharmacol* 172: 2085–2100, 2015. doi:10.1111/bph.12899.
54. **McCommis KS**, **Douglas DL**, **Krenz M**, **Baines CP.** Cardiac-specific hexokinase 2 overexpression attenuates hypertrophy by increasing pentose phosphate pathway flux. *J Am Heart Assoc* 2: e000355, 2013. jaha.113.000355
55. **Roberts DJ**, **Miyamoto S.** Hexokinase II integrates energy metabolism and cellular protection: Acting on mitochondria and TORCing to autophagy. *Cell Death Differ* 22: 248–257, 2015 [Erratum in *Cell Death Differ* 22: 364, 2015]. doi:10.1038/cdd.2014.173.
56. **Southworth R**, **Davey KA**, **Warley A**, **Garlick PB.** A reevaluation of the roles of hexokinase I and II in the heart. *Am J Physiol Heart Circ Physiol* 292: H378–H386, 2007. doi:10.1152/ajpheart.00664.2006.
57. **Shoubridge EA**, **Challiss RA**, **Hayes DJ**, **Radda GK.** Biochemical adaptation in the skeletal muscle of rats depleted of creatine with the substrate analogue beta-guanidinopropionic acid. *BiochemJ* 232: 125–131, 1985. doi:10.1042/bj2320125.
58. **Brdiczka DG**, **Zorov DB**, **Sheu SS.** Mitochondrial contact sites: their role in energy metabolism and apoptosis. *Biochim Biophys Acta* 1762: 148–163, 2006. doi:10.1016/j.bbadis.2005.09.007.
59. **Gellerich FN**, **Schlame M**, **Bohnensack R**, **Kunz W.** Dynamic compartmentation of adenine nucleotides in the mitochondrial intermembrane space of rat-heart mitochondria. *Biochim Biophys Acta* 890: 117–126, 1987. doi:10.1016/0005-2728(87)90012-0.
60. **Veer FD**, **Gellerich FN**, **Nicolay K.** Macromolecules increase the channeling of ADP from externally associated hexokinase to the matrix of mitochondria. *Eur J Biochem* 232: 569–577, 1995. doi:10.1111/j.1432-1033.1995.569zz.x.
61. **Laterveer FD**, **Nicolay K**, **Gellerich FN.** Experimental evidence for dynamic compartmentation of ADP at the mitochondrial periphery: coupling of mitochondrial adenylate kinase and mitochondrial hexokinase with oxidative phosphorylation under conditions mimicking the intracellular colloid osmotic pressure. *Mol Cell Biochem* 174: 43–51, 1997. doi:10.1023/A:1006899621926.
62. **Azoulay-Zohar H**, **Israelson A**, **Abu-Hamad S**, **Shoshan-Barmatz V.** In self-defence: hexokinase promotes voltage-dependent anion channel closure and prevents mitochondria-mediated apoptotic cell death. *Biochem J* 377: 347–355, 2004. doi:10.1042/bj20031465.
63. **Nederlof R**, **Denis S**, **Lauzier B**, **Rosiers CD**, **Laakso M**, **Hagen J**, **Argmann C**, **Wanders R**, **Houtkooper RH**, **Hollmann MW**, **Houten SM**, **Zuurbier CJ.** Acute detachment of hexokinase II from mitochondria modestly increases oxygen consumption of the intact mouse heart. *Metabolism* 72: 66–74, 2017. doi:10.1016/j.metabol.2017.04.008.
64. **Jensen M**, **Müller C**, **Choe C**, **Schwedhelm E**, **Zeller T.** Analysis of L-arginine:glycine amidinotransferase-, creatine- and homoarginine-dependent gene regulation in the murine heart. *Sci Rep* 10: 4821, 2020. doi:10.1038/s41598-020-61638-3.
65. **Calmettes G**, **Ribalet B**, **John S**, **Korge P**, **Ping P**, **Weiss JN.** Hexokinases and cardioprotection. *J Mol Cell Cardiol* 78: 107–115, 2015. doi:10.1016/j.yjmcc.2014.09.020.
66. **da-Silva WS**, **Gómez-Puyou A**, **Gómez-Puyou M. D**, **Moreno-Sanchez R**, **Felice FGD**, **Meis L. D**, **Oliveira MF**, **Galina A.** Mitochondrial bound hexokinase activity as a preventive antioxidant defense: steady-state ADP formation as a regulatory mechanism of membrane potential and reactive oxygen species generation in mitochondria. *J Biol Chem* 279: 39846–39855, 2004. doi:10.1074/jbc.M403835200.
67. **Meyer LE**, **Machado LB**, **Santiago AP**, **da-Silva WS**, **Felice FG**, **Holub O**, **Oliveira MF**, **Galina A.** Mitochondrial creatine kinase activity prevents reactive oxygen species generation: antioxidant role of mitochondrial kinase-dependent ADP re-cycling activity. *J Biol Chem* 281: 37361–37371, 2006. doi:10.1074/jbc.M604123200.
68. **Santiago AP**, **Chaves EA**, **Oliveira MF**, **Galina A.** Reactive oxygen species generation is modulated by mitochondrial kinases: correlation with mitochondrial antioxidant peroxidases in rat tissues. *Biochimie* 90: 1566–1577, 2008. doi:10.1016/j.biochi.2008.06.013.
69. **Choe C**, **Nabuurs C**, **Stockebrand MC**, **Neu A**, **Nunes P**, **Morellini F**, **Sauter K**, **Schillemeit S**, **Hermans-Borgmeyer I**, **Marescau B**, **Heerschap A**, **Isbrandt D.** l-arginine:glycine amidinotransferase deficiency protects from metabolic syndrome. *Hum Mol Genet* 22: 110–123, 2013 [Erratum in *Hum Mol Genet* 22: 4030, 2013]. doi:10.1093/hmg/dds407.
70. **Barsunova K**, **Vendelin M**, **Birkedal R.** Marker enzyme activities in hindleg from creatine-deficient AGAT and GAMT KO mice–differences between models, muscles, and sexes. *Sci Rep* 10: 1–9, 2020. doi:10.1038/s41598-019-56847-4.
71. **Sasani A**, **Hornig S**, **Grzybowski R**, **Cordts K**, **Hanff E**, **Tsikas D**, **Böger R**, **Gerloff C**, **Isbrandt D**, **Neu A**, **Schwedhelm E**, **Choe C.** Muscle phenotype of AGAT- and GAMT-deficient mice after simvastatin exposure. *Amino Acids* 52: 73–85, 2020. doi:10.1007/s00726-019-02812-4.
72. **Kan HE**, **Renema WK**, **Isbrandt D**, **Heerschap A.** Phosphorylated guanidinoacetate partly compensates for the lack of phosphocreatine in skeletal muscle of mice lacking guanidinoacetate methyltransferase. *J Physiol (Lond)* 560: 219–229, 2004. doi:10.1113/jphysiol.2004.067926.
73. **Dzeja PP**, **Zeleznikar RJ**, **Goldberg ND.** Adenylate kinase: kinetic behavior in intact cells indicates it is integral to multiple cellular processes. *Mol Cell Biochem* 184: 169–182, 1998. doi:10.1023/A:1006859632730.
74. **Zeleznikar RJ**, **Dzeja PP**, **Goldberg ND.** Adenylate kinase-catalyzed phosphoryl transfer couples ATP utilization with its generation by glycolysis in intact muscle. *J Biol Chem* 270: 7311–7319, 1995. doi:10.1074/jbc.270.13.7311.
75. **Gellerich FN.** The role of adenylate kinase in dynamic compartmentation of adenine nucleotides in the mitochondrial intermembrane space. *FEBS Lett* 297: 55–58, 1992. doi:10.1016/0014-5793(92)80326-C.
76. **Noma T.** Dynamics of nucleotide metabolism as a supporter of life phenomena. *J Med Invest* 52: 127–136, 2005. doi:10.2152/jmi.52.127.
77. **Christensen M**, **Hartmund T**, **Gesser H.** Creatine kinase, energy-rich phosphates and energy metabolism in heart muscle of different vertebrates. *J Comp Physiol B* 164: 118–123, 1994. doi:10.1007/BF00301652.
78. **Anflous K**, **Veksler V**, **Mateo P**, **Samson F**, **Saks V**, **Ventura-Clapier R.** Mitochondrial creatine kinase isoform expression does not correlate with its mode of action. *Biochem J* 322: 73–78, 1997. doi:10.1042/bj3220073.
79. **Lygate CA**, **Hunyor I**, **Medway D**, **de Bono JP**, **Dawson D**, **Wallis J**, **Sebag-Montefiore L**, **Neubauer S.** Cardiac phenotype of mitochondrial creatine kinase knockout mice is modified on a pure C57BL/6 genetic background. *J Mol Cell Cardiol* 46: 93–99, 2009. doi:10.1016/j.yjmcc.2008.09.710.
80. **Guzun R**, **Timohhina N**, **Tepp K**, **Monge C**, **Kaambre T**, **Sikk P**, **Kuznetsov AV**, **Pison C**, **Saks V.** Regulation of respiration controlled by mitochondrial creatine kinase in permeabilized cardiac cells in situ: Importance of system level properties. *Biochim Biophys Acta* 1787: 1089–1105, 2009. doi:10.1016/j.bbabio.2009.03.024.

Downloaded from journals.physiology.org/journal/ajpheart by Rikke Birkedal (086.110.032.113) on March 18, 2021.

81. **Tepp K**, **Shevchuk I**, **Chekulayev V**, **Timohhina N**, **Kuznetsov AV**, **Guzun R**, **Saks V**, **Kaambre T.** High efficiency of energy flux controls within mitochondrial interactosome in cardiac intracellular energetic units. *Biochim Biophys Acta* 1807: 1549–1561, 2011 doi:10.1016/j.bbabio.2011.08.005.
82. **Kuznetsov AV**, **Tiivel T**, **Sikk P**, **Kaambre T**, **Kay L**, **Daneshrad Z**, **Rossi A**, **Kadaja L**, **Peet N**, **Seppet E**, **Saks VA.** Striking differences between the kinetics of regulation of respiration by ADP in slow-twitch and fast-twitch muscles in vivo. *Eur J Biochem* 241: 909–915, 1996. doi:10.1111/j.1432-1033.1996.00909.x.
83. **Power AS**, **Pham T**, **Loiselle DS**, **Crossman DH**, **Ward ML**, **Hickey AJ.** Impaired ADP channeling to mitochondria and elevated reactive oxygen species in hypertensive hearts. *Am J Physiol Heart Circ Physiol* 310: H1649–H1657, 2016. doi:10.1152/ajpheart.00050.2016.
84. **Jacobus WE**, **Lehninger AL.** Creatine kinase of rat heart mitochondria. Coupling of creatine phosphorylation to electron transport. *J Biol Chem* 248: 4803–4810, 1973. doi:10.1016/S0021-9258(19)43737-X.
85. **Ellington WR.** Evolution and physiological roles of phosphagen systems. *Annu Rev Physiol* 63: 289–325, 2001. doi:10.1146/annurev.physiol.63.1.289.
86. **Garland T**, **Gleeson TT**, **Aronovitz BA**, **Richardson CS**, **Dorm MR.** Maximal sprint speeds and muscle fiber composition of wild and laboratory house mice. *Physiol Behav* 58: 869–876, 1995. doi:10.1016/0031-9384(95)00148-C.

Downloaded from journals.physiology.org/journal/ajpheart by Rikke Birkedal (086.110.032.113) on March 18, 2021.

Appendix 3

Publication III
Branovets J, Vendelin M, Birkedal R

Intracellular compartmentalization shapes energy transfer – differences between adenylate kinase activities in homogenate and permeabilized cardiomyocytes.

(manuscript)

The rules of the publisher prevent publication of the manuscript of Publication III prior to the acceptance. Official committee members and opponents will be given a copy of the manuscript to enable them to carry out a judicious review of the dissertation.

Appendix 4

Publication IV

Laasmaa M, **Branovets J** *, Barsunova K*, Karro N, Lygate CA, Birkedal R, Vendelin M

Altered calcium handling in cardiomyocytes from arginine-glycine amidinotransferase-knockout mice is rescued by creatine.

Am J Physiol Heart Circ Physiol. 2021 Feb 1;320(2):H805-H825. doi: 10.1152/ajpheart.00300.2020

* Equal contribution

AMERICAN JOURNAL OF PHYSIOLOGY
HEART AND CIRCULATORY PHYSIOLOGY

Am J Physiol Heart Circ Physiol 320: H805–H825, 2021.
First published December 4, 2020; doi:10.1152/ajpheart.00300.2020

RESEARCH ARTICLE

Cardiac Excitation and Contraction

Altered calcium handling in cardiomyocytes from arginine-glycine amidinotransferase-knockout mice is rescued by creatine

Martin Laasmaa,[1] Jelena Branovets,[1*] Karina Barsunova,[1*] Niina Karro,[1] Craig A. Lygate,[2] Rikke Birkedal,[1] and Marko Vendelin[1]

[1]*Laboratory of Systems Biology, Department of Cybernetics, School of Science, Tallinn University of Technology, Tallinn, Estonia; and* [2]*Division of Cardiovascular Medicine, Radcliffe Department of Medicine, and the British Heart Foundation Centre of Research Excellence, University of Oxford, Tallinn, United Kingdom*

Abstract

The creatine kinase system facilitates energy transfer between mitochondria and the major ATPases in the heart. Creatine-deficient mice, which lack arginine-glycine amidinotransferase (AGAT) to synthesize creatine and homoarginine, exhibit reduced cardiac contractility. We studied how the absence of a functional CK system influences calcium handling in isolated cardiomyocytes from AGAT-knockouts and wild-type littermates as well as in AGAT-knockout mice receiving lifelong creatine supplementation via the food. Using a combination of whole cell patch clamp and fluorescence microscopy, we demonstrate that the L-type calcium channel (LTCC) current amplitude and voltage range of activation were significantly lower in AGAT-knockout compared with wild-type littermates. Additionally, the inactivation of LTCC and the calcium transient decay were significantly slower. According to our modeling results, these changes can be reproduced by reducing three parameters in knockout mice when compared with wild-type: LTCC conductance, the exchange constant of Ca^{2+} transfer between subspace and cytosol, and SERCA activity. Because tissue expression of LTCC and SERCA protein were not significantly different between genotypes, this suggests the involvement of posttranslational regulatory mechanisms or structural reorganization. The AGAT-knockout phenotype of calcium handling was fully reversed by dietary creatine supplementation throughout life. Our results indicate reduced calcium cycling in cardiomyocytes from AGAT-knockouts and suggest that the creatine kinase system is important for the development of calcium handling in the heart.

NEW & NOTEWORTHY Creatine-deficient mice lacking arginine-glycine amidinotransferase exhibit compromised cardiac function. Here, we show that this is at least partially due to an overall slowing of calcium dynamics. Calcium influx into the cytosol via the L-type calcium current (LTCC) is diminished, and the rate of the sarcoendoplasmic reticulum calcium ATPase (SERCA) pumping calcium back into the sarcoplasmic reticulum is slower. The expression of LTCC and SERCA did not change, suggesting that the changes are regulatory.

arginine:glycine amidinotransferase knockout; calcium; creatine kinase; heart; membrane currents

INTRODUCTION

Creatine kinase (CK) is expected to play a major role in energy transfer between mitochondria and ATPases in the heart (1, 2). This energy transfer starts in the mitochondrial intermembrane space, where mitochondrial CK is tightly coupled to the adenine nucleotide translocase (3, 4), allowing it to synthesize phosphocreatine (PCr) from ATP, partially using the mitochondrial membrane potential as a driving force (5). PCr diffuses within the cell and is, through CK and ATPase coupling, used to locally regenerate ATP next to ATPases. It buffers local ATP/ADP levels in a thermodynamically favorable way and reduces oscillations during a heartbeat (6).

CK is bound near the major ATPases involved in excitation-contraction (e-c) coupling. To briefly recapitulate, the e-c coupling starts with an action potential exciting the sarcolemma and opening L-type Ca^{2+} channels (LTCCs), resulting in an inward Ca^{2+} current (I_{LTCC}). The I_{LTCC} triggers Ca^{2+}-induced Ca^{2+} release (CICR) through ryanodine receptors in the sarcoplasmic reticulum (SR). Together, these Ca^{2+} fluxes form the Ca^{2+} transient, i.e., the transient increase in cytosolic Ca^{2+}. Ca^{2+} binding to tropomyosin exposes the myosin-binding sites on actin, and the mechanical work of

* J. Branovets and K. Barsunova contributed equally to this article.
Correspondence: M. Vendelin (markov@sysbio.ioc.ee).
Submitted 28 April 2020 / Revised 30 October 2020 / Accepted 23 November 2020

0363-6135/21 Copyright © 2021 the American Physiological Society

Downloaded from journals.physiology.org/journal/ajpheart by Rikke Birkedal (086.110.032.113) on March 18, 2021.

myosin ATPase causes the myofilaments to slide along each other and the cell to contract. For relaxation to occur, Ca^{2+} is removed from the cytosol mainly by the sarcoplasmic reticulum Ca^{2+} ATPase (SERCA), pumping it back into the SR. In addition, Ca^{2+} is transported out of the cell via the Na^+/Ca^{2+} exchanger (NCX). Na^+, in turn, is transported out of the cell by the Na^+/K^+ ATPase. The action potential duration and, as a consequence, the Ca^{2+} transient are modulated, among other K^+ outward currents, by K_{ATP} channel. Key components in the described e-c coupling system are affected by CK; a local, energetic coupling between ATPases and CK have been demonstrated for SERCA (7), actomyosin ATPase (8), and the Na^+/K^+ ATPase (9). In addition, it has been suggested to transform the K_{ATP} channel from an ATP sensor to a PCr sensor (10). Therefore, it is conceivable that compromising the function of the CK system may affect e-c coupling and hence, the contractile performance of the heart.

To study the role of CK in energy transfer in the heart, several animal models with compromised CK function have been used. In the earlier studies, CK-knockout (KO) mice (lacking the sarcomeric mitochodnrial and cytosolic CK isoforms) have been associated with large changes in morphological organization of mitochondria in skeletal (11) and heart (12) muscles when compared to the wild-type (WT) controls. In skeletal muscle, accompanied with these morphological abnormalities, CK-KO mice had slower Ca^{2+} uptake and release, suggesting a link between CK and calcium handling (11). The most recent models are deficient in one of the two enzymes involved in creatine synthesis: L-arginine-glycine amidinotransferase or AGAT (EC 2.1.4.1) and guanidinoacetate *N*-methyltransferase or GAMT (EC 2.1.1.2). These are global knockout models, as AGAT and GAMT are predominantly expressed in kidney and liver, respectively, for creatine and homoargenine supply of the organs via circulation (13). Creatine-deficient mice exhibit reduced body weight (see RESULTS for data on AGAT-KO) and skeletal muscle mass (14). However, these models have shown surprisingly small adaptations in the heart. With creatine synthesis altered through GAMT-KO, the voluntary and forced exercise was unaltered (15), there were no signs of hypertrophy, and the systolic and diastolic function was similar at baseline (16). Differences between GAMT-WT and -KO animals were only observed when studying heart function during inotropic stimulation with KO animals exhibiting a smaller contractile reserve (16). At the same time, there were no changes recorded in energy transfer such as respiration activity and intracellular diffusion restriction (17). In contrast to earlier studies on CK-KO mice (12), we observed unchanged intracellular distribution of mitochondria in GAMT-KO mice cardiomyocytes, indicating that diffusion distances encountered by ATP and ADP are not prohibitive for cell function (17).

When creatine synthesis has been altered through AGAT, the mice are not only deficient in creatine but avoid the accumulation of guanidinoacetate, as is the case in the GAMT-KO. This has an advantage, as guanidinoacetate can participate, at lower activity, as a substitute of creatine in the CK reaction (18). However, AGAT-KO also have low levels of homoarginine (19), which is an indicator of cardiovascular health (20). In AGAT-KO mice, the changes in heart function were, in general, also rather mild, and there were no metabolic adaptations in the heart. However, the contractility of the heart was reduced in AGAT-KO mice (21). The present study was conducted to assess whether changes in calcium handling could be involved in the changes in contractility. For that, we used a combination of electrophysiological experiments and analysis with a mathematical model. The experiments recorded I_{LTCC} and the Ca^{2+} transient, and the model allowed us to pinpoint the potential changes in calcium handling that could account for our experimental observations. To focus on the changes that are caused by possible remodeling of AGAT-KO cardiomyocytes, we ensured that the intracellular environment was similar in all experiments, including acute energy provision via the CK system. The study was conducted taking into account differences between male and female animals in terms of the e-c coupling (22, 23) by considering male and female animals as separate groups. Finally, we tested whether lifelong creatine supplementation through food can rescue the changes in calcium handling in AGAT-KO animals (AGAT-KO + Cr).

METHODS

Animals

All animal procedures were approved by the Project Authorisation Committee for Animal Experiments in the Estonian Ministry of Rural Affairs.

For the experiments, arginine-glycine amidinotransferase (AGAT) gene-knockout (KO) and wild-type (WT) mice were used. The animals were back-crossed for more than 10 generations with C57BL/6JOlaHsd (Envigo). The animals were bred and kept at our local animal facility, with free access to water and food (V1534-000 rat/mouse maintenance from Ssniff Spezialdiaten GmbH; free of creatine), an ambient temperature of 22–23°C, and a 12:12-h light-dark cycle. KO were separated from WT to prevent creatine ingestion via copraphagia. Because the AGAT-KO animals were skinny, but active, they were housed in groups whenever possible, given moistened food at the bottom of the cage, and had longer cages with a heating lamp at one end to allow for behavioral thermoregulation. All animals were fed the same chow (R/M-H complete maintenance diet for rats and mice; Ssniff, Soest, Germany). For the creatine-supplemented KO animals, the diet contained additional creatine (R/M-H complete maintenance diet for rats and mice with 5 g/kg creatine monohydrate, Ssniff, Soest, Germany) from the time of being separated from their littermates (KO + Cr group). As shown earlier (21), this housing and diet arrangement led to the absence of cardiac creatine in KO animals and normal creatine levels in KO + Cr animals.

The animals used in the study for electrophysiological measurements were 6.5–16.5 mo for the WT and KO + Cr groups and 6–7.5 mo for the KO group. For animal groups with larger age spans (WT and KO + Cr), we tested whether any of the reported measurement values were age dependent within the age span of the used animals (see RESULTS). For Western blotting, we used separate animals that were 7–9 mo (WT and KO groups).

Genotyping

AGAT mice were genotyped by polymerase chain reaction (PCR) according to the following protocol. Genomic DNA

Downloaded from journals.physiology.org/journal/ajpheart by Rikke Birkedal (086.110.032.113) on March 18, 2021.

was extracted from tissue samples by SDS/proteinase K (Bioline, London, UK) digestion, followed by isopropanol precipitation. PCR amplification of the DNA fragments was performed using the following specific primers: 5′-AGCCCCTCTATTTCCCTTTTCATT-3′ and 5′-TTCCACTGCGTCATTCTCCTGTAA-3′. PCRs were carried out in a 25-μL volume containing 1× PCR buffer (Bioline Immobuffer, Bioline, London, UK), 0.5 mM dNTP mixture (Bioline, London, UK), 1.2 mM $MgCl_2$, 0.5 pmol/μL of each primer (TAG Copenhagen, Copenhagen, Denmark), 5% DMSO, 1 M betaine, 0.06 U/μL IMMOLASE DNA polymerase (Bioline, London, UK), and 5 μL of template DNA. The touchdown PCR protocol was as follows. An initial denaturation at 95°C for 5 min was followed by 10 cycles at 94°C for 60 s, 65°C (0.5°C decrease/cycle) for 60 s, and 72°C for 30 s and then another 35 cycles at 95°C for 60 s, 60°C for 60 s, and 72°C for 30 s, and a final extension step was carried out at 72°C for 2 min. This was done in a thermal cycler (Bio-Rad DNA Engine; Bio-Rad Laboratories, Hercules, CA, or Eppendorf Mastercycler; Eppendorf, Hamburg, Germany). PCR products were electrophoresed on a 1% agarose gel with ethidium bromide in 0.5× Tris-borate-EDTA. Amplification of a single 522-bp product or a 277-bp PCR product corresponded to AGAT WT or homozygous AGAT-knockout (AGAT-KO) genotype, respectively. Simultaneous amplification of a 522- and 277-bp fragments corresponded to a heterozygous AGAT genotype. See Fig. 1, for example.

Solutions

For the isolation of cardiomyocytes, the wash solution consisted of (in mM) 117 NaCl, 5.7 KCl, 1.5 KH_2PO_4, 4.4 $NaHCO_3$, 1.7 $MgCl_2$, 21 HEPES, 20 taurine, 11.7 glucose, and 10 2,3-butanedione monoxime. pH was adjusted to 7.4 with NaOH.

For the digestion solution, 0.2–0.25 mg/mL Liberase DL and 1.36 mg/mL Dispase II were added to 20 mL of the wash solution.

For the sedimentation solution, 2 mM pyruvate, 10 μM leupeptin (Merck), 2 μM soybean trypsin inhibitor, and 3 mg/mL BSA (Roche) were added to 40 mL of the wash solution.

For electrophysiological recordings, the bath solution consisted of (in mM): 150 NaCl, 5.4 CsCl, 0.33 NaH_2PO_4, 1 $MgCl_2$, 1.13 $CaCl_2$, 20 TEA-Cl, 10 glucose, and 10 HEPES. pH was adjusted to 7.4 with NaOH. To inhibit sodium channels, we used 10 μM tetrodotoxin (TTX) citrate (TOCRIS, Abingdon, UK) in the bath solution. Note that cells were patch clamped in the absence of TTX; otherwise TTX was always present. For β-adrenergic stimulation and SR Ca^{2+} content estimation, 50 nM isoprenaline (ISO) and 10 mM caffeine, respectively, were added to the bath solution. Ca^{2+} concentration was selected according to ionized Ca^{2+} concentration in blood (24), similar to that used previously (25), and sodium according to Fox et al. (26).

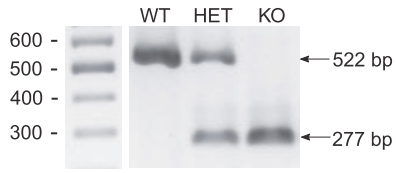

Figure 1. Representative gel with arginine-glycine amidinotransferase (AGAT) genotyping results. The genotype of the mice was determined by isolating DNA from ear notches and using PCR to amplify specific DNA sequences using appropriate primers pairs (described in METHODS). Amplification of a single 522-bp product or a 277-bp PCR product corresponded to AGAT-wild-type (WT) or homozygous AGAT-knockout (KO) genotype, respectively. Simultaneous amplification of a 522- and 277-bp fragments corresponded to a heterozygous AGAT genotype.

The pipette solution contained (in mM) 150 CsCl, 1 $MgCl_2$, 20 TEA-Cl, 5.5 Na_2PCr, 5 MgATP, 0.03 Na_2GTP, and 10 HEPES. pH was adjusted to 7.2 with CsOH. For Ca^{2+} imaging, an additional 25 μM of Fluo-4 pentapotassium salt (F14200; Invitrogen) was added to the pipette solution.

The protein extraction buffer for Western blotting contained (in mM) 50 Tris, 150 NaCl, 2% SDS, 1 DTT, and one tablet each of cOmplete Mini and PhosSTOP protease and phosphatase inhibitor cocktails, respectively, per 10 mL.

All chemicals were obtained from Merck if not mentioned otherwise.

Western Blot Analysis

Frozen hearts were homogenized in a glass homogenizer at a concentration of 20 mg tissue/mL of extraction buffer. The protein concentration was determined spectrophotometrically. Fifty microliters of Western blotting tissue extract, which already contained SDS, was incubated at 80°C for 30 min. After heating, the transparent solution was diluted 1:10 and the protein content determined in a BioSpec-nano or a NanoDrop 2000c spectrophotometer (Shimadzu Scientific Instruments, Inc., and ThermoFisher Scientific). The protein content of each sample was measured at least three times, and the results were averaged. The absorption at 280 nm was background corrected by subtracting the absorption at 330 nm, and protein content was calculated using the molecular weight and extinction coefficient of BSA (66 400 $g \cdot mol^{-1}$ and 43 824 $M^{-1} \cdot cm^{-1}$, respectively). The protein content was corrected for that of the extraction buffer.

Ten micrograms of protein was loaded onto SDS-PAGE gels (4% stacking gel, 6 or 10% separating gel), which were run at 60 V for ~35 min, followed by 120 V for 50–55 min in a Mini-PROTEAN Tetra System using a PowerPac HC power supply (Bio-Rad Laboratories). The separated proteins were transferred onto a nitrocellulose membrane overnight at 4°C and 90 mA. The protein loading was assessed by staining with a 0.1% Ponceau S solution, followed by two washes with ultrapure water. After imaging the Ponceau staining, the membranes were blocked with 5% BSA, incubated with primary antibody, and incubated with secondary antibody in a Tris-buffered saline with 0.1% Tween-20 (TBST) for 1 h at room temperature. Between each step, the membranes were washed two times for 10 min in TBST. The antibodies were detected with the Bio-Rad Clarity Western ECL substrate. Both Ponceau and antibody staining were imaged in an Image Quant LAS 400 imager (GE Healthcare, Chicago, IL).

The following primary antibodies were used; anti-CACNA1C (product no. ab58552, RRID:AB_879800, 1:200; Abcam) and anti-SERCA2 ATPase (product no. ab3625, RRID:AB_303961, dilution 1:2,500; Abcam) were used to assess LTCC and SERCA expression, respectively. Anti-GAPDH (14C10) (product no 2118, RRID:AB_561053, dilution 1:4,000; Cell Signaling Technology) was used to assess the

Downloaded from journals.physiology.org/journal/ajpheart by Rikke Birkedal (086.110.032.113) on March 18, 2021.

expression of GAPDH, which is a commonly used housekeeping protein. The secondary antibody was a horseradish peroxidase (HRP)-conjugated goat anti-rabbit IgG (H + L) (Jackson ImmunoResearch Laboratories, Inc.), which was used at a dilution of 1:10,000 for detection of LTCC, 1:20,000 for detection of SERCA, and 1:40,000 for detection of GAPDH.

The antibodies were tested on mouse heart, liver, and skeletal muscle. For anti-CACNA1C, liver was used as a negative control and showed no signal. Anti-CACNA1C gave a strong signal in gastrocnemius, suggesting that this antibody may bind to other LTCC isoforms as well. Others have shown colocalization of anti-CACNA1C staining with sarcolemma and t-tubules in myocardium, in agreement with the expected location of LTCC (27). The SERCA antibody showed several bands. In the heart, the double band observed in the region of the expected size was used in the analysis. A similar double band was observed in the muscle study (28). When used in immunocytochemistry, the SERCA2 antibody was used to stain endoplasmic reticulum in neonatal rat cardiomyocytes (29).

Because a single gel was insufficient to measure all samples in a group (AGAT-KO, WT, females and males separately), one or two lanes were used for a reference sample that was a mix of all the samples in the group and used throughout the study. The tissue samples were distributed in a random order and were measured two to three times.

The staining intensity was determined using GelAnalyzer 19.1 (www.gelanalyzer.com). For the Ponceau staining images, the background was determined and subtracted using ImageJ. The staining intensities were entered into the database using IOCBIO WebDB (https://gitlab.com/iocbio/webdb).

For each gel, the intensities of Ponceau, the protein of interest (SERCA or LTCC), and GAPDH (housekeeping) were normalized first to the amount of protein in the lane and then to the corresponding intensity per protein of the reference lane. If the reference sample was loaded into multiple lanes, the mean intensity per protein for the reference lanes was used for normalization. For the statistical analysis, the signal of the protein of interest was normalized to *1*) protein content, *2*) Ponceau staining, or *3*) GAPDH intensity. For each tissue sample, the average of the normalized intensity was used for statistical analysis.

Cardiomyocyte Isolation

Cardiomyocytes were isolated using the same protocol as described (30). The mice received two intraperitoneal injections: one with 250 U heparin to prevent blood coagulation and one with an anesthetic mixture of ketamine-dexmedetomidine (150 mg/kg and 0.5 mg/kg, respectively). When the toe-pinch reflex was absent, the animal was euthanized by cervical dislocation. The heart was excised, cannulated via the aorta on a Langendorff perfusion system, and perfused with wash solution. When it was rinsed free of blood, the perfusion was switched to a digestion solution containing 0.2–0.25 mg/mL Liberase DL and 1.36 mg/mL of dispase II. The pressure was monitored continuously for 10–20 min until the pressure had decreased to 30–40% of the initial, and the heart was soft. After perfusion, the ventricles were cut into smaller pieces and incubated further at 37°C in a beaker with digestion solution. During this postdigestion, cells were harvested with a Pasteur pipette several times and filtered through a 100-μm mesh. The viable cells were separated by sedimentation. First, extracellular Ca^{2+} was gradually increased to 2 mM to ensure Ca^{2+} tolerance of the cells. After this, extracellular Ca^{2+} was washed out again by washing the cells three times with 5 mL of sedimentation solution. The isolated cells were stored in this solution at room temperature until use within 3 h.

Experimental Equipment

The experimental setup was the same as described earlier (31). In short, a Nikon Eclipse Ti-U microscope (Nikon) was equipped with an Andor Ixon EMCCD camera (Andor Technologies, Belfast, UK) for measuring Fluo-4-induced fluorescence. Fluo-4 was excited at wavelengths of 482 ± 18 nm and emission collected at 536 ± 20 nm. The EMCCD camera image was binned 4 × 4, gain was set to 100, and images were acquired at 85 fps. Imaging was done through a ×40 objective (CFI Super Plan Fluor ELWD 40xC NA 0.60; Nikon). For electrophysiological measurements, we used an Optopatch patch clamp amplifier (Cairn Research) connected to a computer via NI PCIe-6353 data acquisition board (National Instruments). Data were recorded at 10 kHz using custom-made software. Patch pipettes, with resistance of 1.5–2.5 MΩ, were made from thin borosilicate glass capillaries (TW150F-3; WPI, Sarasota, FL) using a Narishige PC-10 pipette puller (Narishige). All electrophysiological recordings were conducted in the whole cell voltage clamp configuration at room temperature (23°C, temperature controlled by air conditioner).

Experimental Protocol

First, a batch of cells was placed under the microscope in a RC-24N chamber (Warner Instruments, Hamden, CT) containing the bath solution. Cells were allowed to attach to the coverslip bottom for 5–10 min before perfusion of the chamber was started with the bath solution at a flow rate of ~0.5 mL/min. Then, a cell in the middle of the chamber was selected for patch clamping. After gigaseal formation and successful rupturing of the cell's membrane, membrane capacitance and series resistance were noted. Then, solutions were switched from patching solution to control the experiment solution containing TTX.

Each cell was subjected to several protocols in sequence to record different datasets characterizing Ca^{2+} handling (Fig. 2*A*). The experiments started with inhibition of the fast sodium channels. Next, the SR was loaded with Ca^{2+} using the SR loading protocol, and the current-voltage relationship was determined. After the addition of isoprenaline (ISO), the SR was again loaded and the current-voltage relationship was determined in the presence of ISO. After recording the current-voltage relationships, we ran the third SR Ca^{2+} loading protocol. Some cells were then ruptured to determine maximal Ca^{2+}-induced Fluo-4 fluorescence, and some cells were studied further. The cells that were studied further were exposed to caffeine to determine SR Ca^{2+} content. After that, the SR loading protocol was applied a last time, and maximal Ca^{2+}-induced Fluo-4 fluorescence

Downloaded from journals.physiology.org/journal/ajpheart by Rikke Birkedal (086.110.032.113) on March 18, 2021.

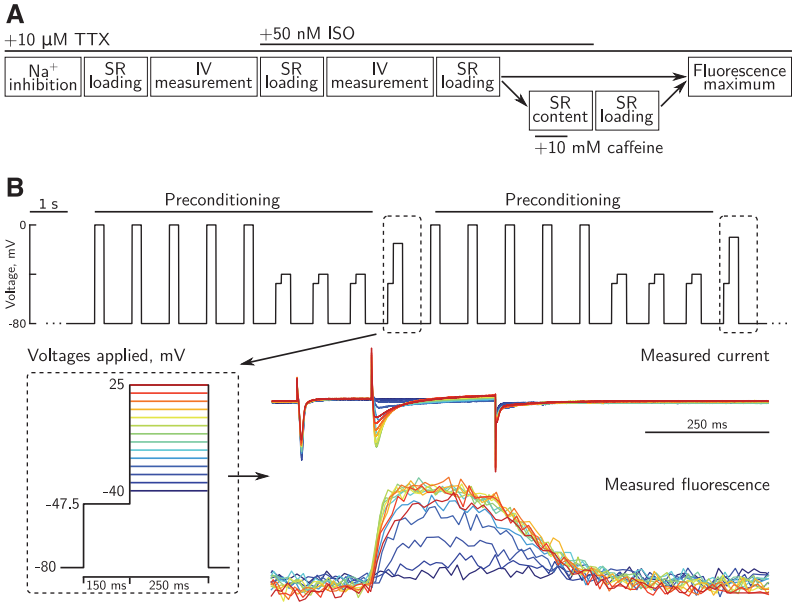

Figure 2. Overview of the experimental protocol (*A*) and the sequence used to measure voltage-current relationship (*B*). *A*: protocol stages applied to a single cell. Current-voltage (*I-V*) measurements consisted of sequences as shown in *B*. *B*: sequence of pulses used to measure current-voltage relationship and Fluo-4 Ca^{2+}-induced transients for different voltage steps. Each pulse used for recordings, marked by a dashed box, was preceded by 5 stimulations with rectangular pulses and 3 stimulations with staircase pulses, as shown at *top*. The used staircase pulses are shown at *bottom left*. An example recording is shown on the *bottom right*, depicting changes in current and fluorescence. ISO, isoprenaline; SR, sarcoplasmic reticulum; TTX, tetrodotoxin citrate. See METHODS for details.

was determined. Below, each part of the experiment is described in detail.

The inhibition of fast sodium channels by TTX was followed for 90 s, with periodic depolarizations of the cell from −80 to −45 mV for 250 ms at 1 Hz.

The SR Ca^{2+} loading protocol consisted of a series of 250-ms depolarization pulses from −80 to 0 mV, and it was applied at 1 Hz for 30 s or more to ensure that the SR was loaded with Ca^{2+}. The latter was judged by following the Fluo-4 fluorescence transients and waiting for their stabilization.

To determine the current-voltage relationship of L-type Ca^{2+} channels and record the corresponding changes in Fluo-4 fluorescence, we used the sequence of pulses shown in Fig. 2*B*. The sequence included several pulses (preconditioning sequence) applied before the pulse used for measurements. The preconditioning sequence consisted of five rectangular pulses that depolarized the cell to 0 mV for 250 ms (as used during SR loading protocol), followed by three staircase pulses with the same profile as the measurement pulse (Fig. 2*B*, *bottom left*) and depolarization voltages of −47.5 mV and −40 mV. For the measurements, the second stair voltage was varied from −40 mV to +25 mV. This approach allowed us to avoid interference between measurements at different voltages and ensured that the cells were in the same state before the measurement pulse was applied. In the measurements, we recorded the currents and fluorescence changes. Recordings of the current-voltage relationship were performed once per each voltage step.

After 50 nM ISO was added to the bath solution, the cell was subject to another Ca^{2+} loading protocol for ≥60 s until Ca^{2+} transients reached steady state, as judged by following the Fluo-4 fluorescence transients. Then, the current-voltage relationship was determined in the presence of ISO.

For SR Ca^{2+} content estimation, we kept the cell for 90 s at −80 mV. Within this period, ~10 s from its start, perfusion with bath solution containing an additional 10 mM caffeine was started. This induced Ca^{2+} release from SR and its subsequent efflux from the cell by NCX. The state of the cell was followed by measuring the transmembrane current and Fluo-4 fluorescence. After Fluo-4 fluorescence and measured current were stabilized (10–20 s), caffeine was washed out, and the SR Ca^{2+} loading protocol was applied to refill SR with Ca^{2+}.

Maximal Ca^{2+}-induced Fluo-4 fluorescence was determined by inducing Ca^{2+} influx from extracellular solution into the cell. The influx was induced by applying brief suction by the patch pipette, leading to disruption of the seal and establishment of the pathway for Ca^{2+} movement between cytosol and extracellular solution. Changes in Ca^{2+}-induced Fluo-4 fluorescence were recorded, and the maximum was determined for normalization purposes.

Data Analysis

Current-voltage relationship.

We fitted the current-voltage relationship data obtained from each cell with a Boltzmann equation:

$$I = \frac{G_{max}(V - V_{rev})}{1 + \exp[(V_{half} - V)/k]} \quad (1)$$

where G_{max} is maximal conductance, V_{rev} reversal potential, V_{half} is activation midpoint potential, and k is the slope factor. Additionally, using the equation and fitted parameters, we calculated maximal current and a corresponding potential.

Calcium transients.

Ca^{2+} transients were found by subtracting average fluorescence signals from regions that contained cell and only the

Downloaded from journals.physiology.org/journal/ajpheart by Rikke Birkedal (086.110.032.113) on March 18, 2021.

background per each captured frame, respectively. For the Ca^{2+} transient decay time, we used time difference between time moments where the transient was decreased from 75% to 25% from its peak value. To find the time constant h that describes Ca^{2+} transient recovery after caffeine washout, we fitted Ca^{2+} transient amplitudes using the least-squares method with the Hill equation in following form:

$$\mathrm{FCa}(T) = A \cdot \frac{T^n}{(h^n + T^n)} + b, \quad (2)$$

where FCa(T) is measured Ca^{2+} transient maximum at pulse T, A is the fitted amplitude, n is the Hill coefficient, and b is baseline fluorescence.

Mathematical Modeling

To interpret the experimental results, we performed a parameter scan on a mathematical model of action potential of mouse ventricular myocytes by Bondarenko et al. (32) that was slightly modified (see below). Two different parameter scan scenarios were considered that correspond to *1*) LTCC current-voltage relationship measurement at 0 mV and *2*) recovery after caffeine-induced Ca^{2+} release. For that, to imitate voltage clamp protocols, the solution for membrane potential was replaced with voltage pulse used in the experiments. In the first scenario, the same square pulse was applied as for preconditioning and SR loading at 1 Hz for 60 s to let the model to reach a steady-state solution in our conditions. After that, a staircase pulse was applied from −80 to −47.5 (for 150 ms) to 0 mV (for 250 ms) (Fig. 2*B*, *bottom left*). In the second scenario, again, the preconditioning pulse at 1 Hz for 60 s was used first, followed by 100 s of simulated caffeine Ca^{2+}-release (see below). Then, the model solution was calculated for 0.1 ms at −80 mV, after which 17 SR loading pulses were applied at 1 Hz.

Modified constants.

To match intracellular and extracellular concentrations, the following constants were modified (in mM): $[Na^+]_i$ = 11.0, $[Na^+]_o$ = 150.0, $[Ca^{2+}]_o$ = 1.13. Also, Ca^{2+} half-saturation constant for calmodulin was set to 2.38 μM (33–36).

Fluo-4 Ca^{2+} buffering.

Intracellular Ca^{2+} flux to Fluo-4 (J_{FCa}) was is described with the following equation:

$$J_{FCa} = k_{on}(F_{TOT} - FCa)\,Ca_i - k_{off}FCa, \quad (3)$$

where Ca_i is intracellular Ca^{2+} concentration, FCa is Ca^{2+} bound Fluo-4, F_{TOT} is total concentration of Fluo-4 that was taken equal to 25 μM as in the patch pipette, and k_{on} and k_{off} are Fluo-4 reaction rate constants (k_{on} = 0.1 $\mu M^{-1}\cdot ms^{-1}$, k_{off} = 0.11 ms^{-1}, as in (Ref. 37). FCa was calculated as

$$\frac{dFCa}{dt} = J_{FCa}, \quad (4)$$

The term J_{FCa} was included in *equation A2* in Ref. 32 as

$$\frac{d[Ca^{2+}]_i}{dt} = B_i\{J_{leak} + J_{xfer} - J_{up} - J_{trpn} - J_{FCa} - (I_{Cab} - 2I_{NaCa} + I_{p(Ca)})\,A_{cap}\,C_m/(2V_{myo}F)\}. \quad (5)$$

Caffeine Release

To simulate Ca^{2+} release from SR by caffeine, the membrane potential was kept at −80 mV, and the original equation (A9 in Ref. 32) was

$$J = v_1(P_{O1} + P_{O2})(Ca_{JSR} - Ca_{SS})P_{RyR}, \quad (6)$$

which describes the Ca^{2+} release from SR by RyRs that was replaced by

$$J_{rel} = v_1(Ca_{JSR} - Ca_{SS}), \quad (7)$$

where v_1 is maximum RyR channel Ca^{2+} permeability, and Ca_{JSR} and Ca_{ss} are junctional SR and subspace Ca^{2+} concentration, respectively.

Parameter Scan

The model solutions were calculated by varying the following constant values: *1*) SR Ca^{2+}-ATPase maximum pump rate (v_3 in equation no. A13 in Ref. 32), *2*) maximum conductance for L-type Ca^{2+} channel (G_{CaL} in equation no. A22 in Ref. 32), and *3*) exchange constant of Ca^{2+} transfer between subspace and cytosol ($1/\tau_{xfer}$, where τ_{xfer} is time constant for Ca^{2+} transfer from subspace to cytosol in equation no. A11 in Ref. 32). Each scanned parameter was scaled in the range of [0.25, 1.0] with the step of 0.0375, i.e., 21 values for each parameter, totaling 9,261 cases.

Numerical Methods

All the numerical calculations where done in Python. The initial model source code was downloaded from the CellML website (www.cellml.org). The model calculations at different parameter values were executed in parallel using a command-line tool, the GNU Parallel (38), and the model equations were solved using a Real-Valued Variable-coefficient Ordinary Differential Equation solver from SciPy sub module scipy.integrate.

For least-square fitting, we used the SciPy function scipy.optimize.least_squares.

Statistics

If not stated otherwise, statistics is reported using means ± SE.

Statistical tests were performed using JASP, using Bayesian ANOVA or Bayesian repeated-measures ANOVA tests. In the tests, ISO effect was included into the null model. These tests evaluated hierarchy of models of different complexity, with the most complex one consisting of interactions between all studied factors, lower-order of interactions, and the studied factors separately. The model with the largest odds against null model [largest Bayes factor (BF)] is shown in the statistics results (ND if the null model had the odds larger than assumed significant for alternative hypothesis; see below) together with the model-averaged inclusion Bayes factor, using matched models approach for the interactions (39).

For Bayes factor (BF) interpretation, common evidence categories were used (40). For analysis with JASP, SQL and Python scripts were written to fetch the data from the database into a file in the format suitable for JASP input.

Downloaded from journals.physiology.org/journal/ajpheart by Rikke Birkedal (086.110.032.113) on March 18, 2021.

RESULTS

To analyze cardiomyocyte Ca^{2+} handling, we looked into the characteristics of I_{LTCC} and Ca^{2+} uptake by the SR using several approaches. The experiments were performed on cardiomyocytes isolated from three groups of mice: AGAT-WT, AGAT-KO, and creatine-supplemented AGAT KO + Cr.

Animals

The characteristics of the animals used for electrophysiological recordings are given in Table 1. AGAT-KO mice had significantly lower body weight and tibial length than AGAT-WT and AGAT-KO + Cr (BF ≫ 100, extreme evidence). Creatine supplementation throughout life led to a normal body weight and tibial length; i.e., there was no difference between WT and KO + Cr. In AGAT-WT and AGAT-KO + Cr, males had a higher body weight than females (BF ≫ 100, extreme evidence), whereas in AGAT-KO the body weight was not statistically significantly different between males and females.

LTCC Current Characteristics Are Altered in AGAT-KO

The current-voltage relationship of I_{LTCC} was measured in the absence and presence of isoprenaline (ISO; Fig. 2*B*). Representative traces of the recorded current and fluorescence from AGAT-KO and WT mice are shown in Fig. 3, *A* and *B*, and clearly demonstrate the difference in I_{LTCC} current and calcium-induced fluorescence.

The maximal current at different test pulses was determined for all combinations of phenotype and sex (Fig. 3*C*). For statistical analysis of I_{LTCC} maxima, we fitted the current-voltage relationship with the Boltzmann equation (see METHODS) and analyzed the differences in the fitted equation parameters (Fig. 4). Statistical analysis was performed using a hierarchy of statistical models as defined in Bayesian ANOVA (see METHODS). According to our data, AGAT-KO mice exhibited a smaller I_{LTCC} maximal current (Fig. 4*B*) as well as voltage range of activation (Fig. 4, *C*, *D*, *E*, and *F*). All of these changes were reversed by feeding with creatine, as we found no difference between KO + Cr and WT in Fig. 4.

I_{LTCC} Inactivation is Slower in AGAT-KO in the Absence of Isoprenaline

Individual I_{LTCC} traces recorded at −5 mV were analyzed further to determine the inactivation dynamics of I_{LTCC}. We determined the time constants at which the current was reduced to 25, 50, and 75% of the maximal current (T_{25}, T_{50}, and T_{75}, respectively, as defined in Fig. 5*A*). From the statistical analysis of the time constants from AGAT-KO, WT, and KO + Cr, we observed very strong to extreme interactions between phenotype (creatine deficient or not), ISO, and time constant. The interaction between phenotype and ISO was due to the time constants being different in the absence, but not in the presence of ISO. The interaction with time constant was due to differences being observed only for T_{75} and T_{50}, but not T_{25}. As shown in Fig. 5, T_{50} and T_{75} were, under control conditions, significantly higher for KO animals compared with WT and KO + Cr. This was confirmed by further analysis of the time constants in the absence of ISO, where extreme statistical difference was found between KO and WT as well as KO and KO + Cr, attributed to either phenotype (KO and WT comparison) or phenotype and time constant interaction (both comparisons). In contrast, in the presence of ISO, no statistically significant differences were observed. The slower I_{LTCC} inactivation in AGAT-KO was fully reversed by creatine supplementation, as shown in the statistical tests comparing WT and KO + Cr.

SR Ca^{2+} Uptake is Slower in AGAT-KO

Simultaneously with the currents, we recorded changes in Ca^{2+}-induced Fluo-4 fluorescence in the cells. In mammalian cardiomyocytes, in contrast to some other animals (31), it is expected that most of the Ca^{2+} cycling is through SR. Thus, the decay of the Ca^{2+} transient would be strongly influenced by SERCA, one of the main ATPases in the cells. To characterize the Ca^{2+} transient decay, we measured the time interval, τ, between the moments at which fluorescence was 75% and 25% of its maximum (as defined in Fig. 6*A*). For a better statistical power, we averaged τ determined from the traces recorded at −5 mV, 0 mV, and +5 mV. This was done since no significant influence of voltage on the fluorescence decay time was found at this range (results not shown). As shown in Fig. 6*B*, τ is significantly higher, i.e., it takes a longer time to reduce Ca^{2+}-induced fluorescence, in cardiomyocytes from AGAT-KO compared with WT or KO + Cr. In addition, the effect of ISO was considerably larger in AGAT-KO cardiomyocytes, as indicated by the significant interaction in the statistical model Fig. 6*B*. No difference was found between WT and KO + Cr.

The peak amplitudes of the Ca^{2+} transients (relative to the maximal fluorescence recorded at the end of the experiments) was close in all groups. The only statistically significant difference in maximal fluorescence between KO and WT animals was induced by a larger increase of the maximal fluorescence by ISO treatment in KO when compared to WT. This is indicated by the significance of the interaction factor in Fig. 6*C*.

SR Ca^{2+} Content

We looked into SR Ca^{2+} content by exposing the cardiomyocytes to caffeine and recording NCX current through the membrane. From the recorded current (Fig. 7*A*), we

Table 1. *Body weight and tibial length of animals in different groups*

	AGAT-KO		AGAT-WT		AGAT-KO + Cr	
	Male	Female	Male	Female	Male	Female
No. of animals	6	7	12	8	5	8
Weight, g	18.0 ± 1.6	17.6 ± 1.3	34.3 ± 1.5	26.6 ± 1.9	31.6 ± 3.6	26.9 ± 2.6
Tibial length, cm	2.12 ± 0.03	2.09 ± 0.05	2.28 ± 0.04	2.23 ± 0.07	2.24 ± 0.02	2.19 ± 0.04

Values are means ± SD. AGAT, arginine-glycine amidinotransferase; KO, knockout; WT, wild type; Cr, creatine.

Downloaded from journals.physiology.org/journal/ajpheart by Rikke Birkedal (086.110.032.113) on March 18, 2021.

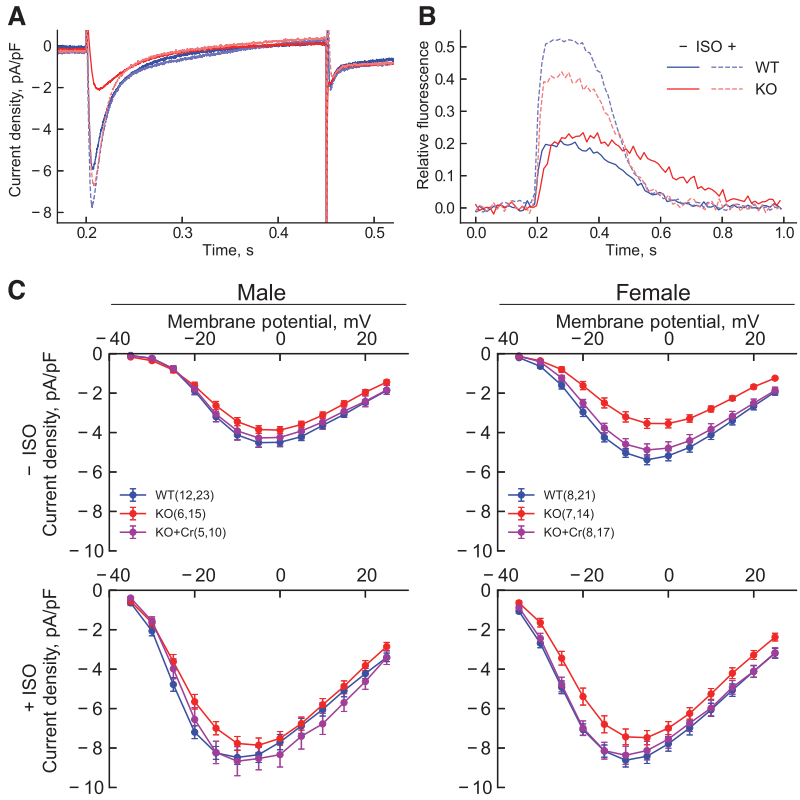

Figure 3. Cardiomyocyte response to the voltage-clamp protocol. *A* and *B*: representative traces of I_{LTCC} current and calcium fluorescence, respectively, from female wild-type (WT) and creatine-deficient (KO) mice in the absence and presence of isoprenaline (ISO). Traces are shown from current-voltage relationship recordings at 0 mV. Notice the smaller I_{LTCC} and slower decline in fluorescence in cardiomyocytes from arginine-glycine amidinotransferase (AGAT)-knockout (KO) animals. *C*: current-voltage relationship for wild-type (WT), KO, and creatine supplemented (KO + Cr) animals in the presence and absence of ISO. Notice how the currents measured in AGAT-KO animals are smaller than in WT. This effect of creatine deficiency on the current is reversible through creatine supplementation.

calculated the transferred charge and compared it between the groups (Fig. 7*B*). Although there were no significant differences in SR Ca^{2+} content statistically, on average, SR Ca^{2+} content in KO group was smaller compared with WT and KO + Cr, as indicated in Fig. 7.

Loading of Ca^{2+} to Empty SR

After the exposure to caffeine was stopped, the SR was reloaded with Ca^{2+} by repeated stimulation, as described in METHODS. Under these conditions, at the beginning of the loading protocol, it is expected that a large fraction of Ca^{2+} entering the cell through LTCCs will be stored in the SR until Ca^{2+} content in SR is recovered. With the recovery of the Ca^{2+} content in SR, I_{LTCC} will be increasingly inhibited by CICR. Consistent with this, I_{LTCC} of the first pulse was the largest, and the following currents gradually became smaller (Fig. 8*A*). Simultaneously, Ca^{2+}-induced fluorescence showed a significant increase and stabilized over several pulses (Fig. 8*B*). The time constant of SR Ca^{2+} loading was found by fitting the fluorescence peaks by the Hill function and finding the time moment corresponding to the half-saturation (Fig. 8*B*). Although the charge transfer recorded during the first pulse in this protocol was significantly smaller for cardiomyocytes from KO than from WT mice (Fig. 8*C*), no difference was found for the time constant describing recovery of Ca^{2+}-induced fluorescence during Ca^{2+} loading (Fig. 8*D*). Thus, the time course of SR Ca^{2+} loading was similar in KO, WT, and KO + Cr.

Impact of Aging on WT and KO + Cr Groups

We have used animals with a large age span for the WT and KO + Cr groups. Within these groups, we could divide the animals into younger (6.5–10 mo) and older (14–16.5 mo) subgroups, with the younger subgroup having a similar age as the AGAT-KO used in the study. The distribution of sexes within these subgroups was insufficient to test interaction between age and sex. So, the tests were performed considering either animals of both sexes as one group or younger and older animals within the same sex. All of the experimental data presented above were analyzed as shown in Fig. 9.

We found that the ISO response of the LTCC current inactivation was blunted in older mice (Fig. 10). This impact was found in both groups (WT and KO + Cr) either with the sexes pooled together or among males (WT) or females (KO + Cr). Taking into account that we used younger animals in the AGAT-KO group, we tested whether our conclusions from the data in Fig. 5 would hold, when only data from younger animal groups (WT and KO + Cr) were used for comparison. When comparing KO and WT, the same factors were found to be significant, with the evidence ranging

Downloaded from journals.physiology.org/journal/ajpheart by Rikke Birkedal (086.110.032.113) on March 18, 2021.

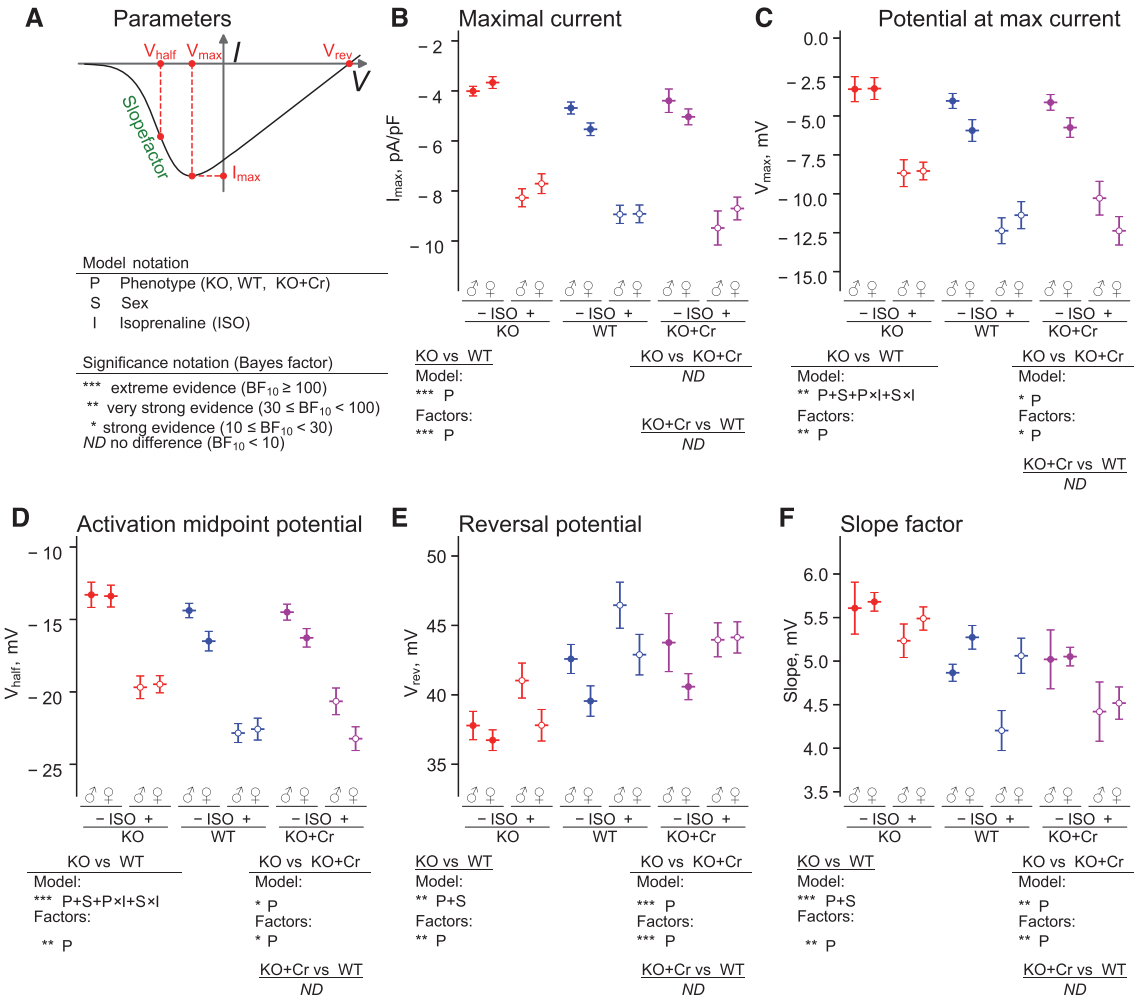

Figure 4. Statistical analysis of the current-voltage relationships. The current-voltage relationships were described through the set of parameters indicated on the scheme (*A*). *A*, *bottom*: statistical models considered differences in phenotype (P), sex (S), and the presence of isoprenaline (I) with the significance levels, as indicated in the notations. *B–F*: for each parameter, the comparison was performed with the best statistical model, its significance, and significant model parameters shown below each subplot. Parameters are shown using means ± SE. Notice how most of the analyzed parameters changed in the creatine-deficient animals (KO) with the change reversed by creatine feeding (KO + Cr). Whereas the best models sometimes included multiple factors and their interactions, the only significant factor found in the case of the differences was the phenotype. No. of animals and cells used in the experiments were as follows (reported in animals/cells notation): KO male (6/15), KO female (7/14), WT male (12/23), WT female (8/21), KO + Cr male (5/11), KO + Cr female (8/17). Statistical analysis was performed using Bayesian repeated-measures ANOVA.

from very strong to extreme. When comparing KO and KO + Cr, the significant difference was imposed between the groups through interaction between phenotype and time constant (extreme evidence), but, and in contrast to Fig. 5, there was no significance attributed to the interaction between phenotype and isoprenaline treatment. When comparing younger animal data only, creatine feeding abolished all of the differences between KO and WT, with no statistically significant difference found when comparing data from KO + Cr and WT groups. Thus, the overall conclusion remained the same; creatine deficiency had a significant effect on LTCC inactivation, and creatine supplementation of KO animals is able to restore their phenotype.

Among all other possible combinations tested, only the reversal potential of the LTCC current-voltage relationship was found to be impacted by age. Namely, among male WT mice, the statistical model $A + A \times I$ had a Bayes factor of 12 (strong evidence). However, none of the other groups (WT, both sexes pooled, KO + Cr groups) had any indication of such an impact, with the second largest BF being 1.3 for the

Downloaded from journals.physiology.org/journal/ajpheart by Rikke Birkedal (086.110.032.113) on March 18, 2021.

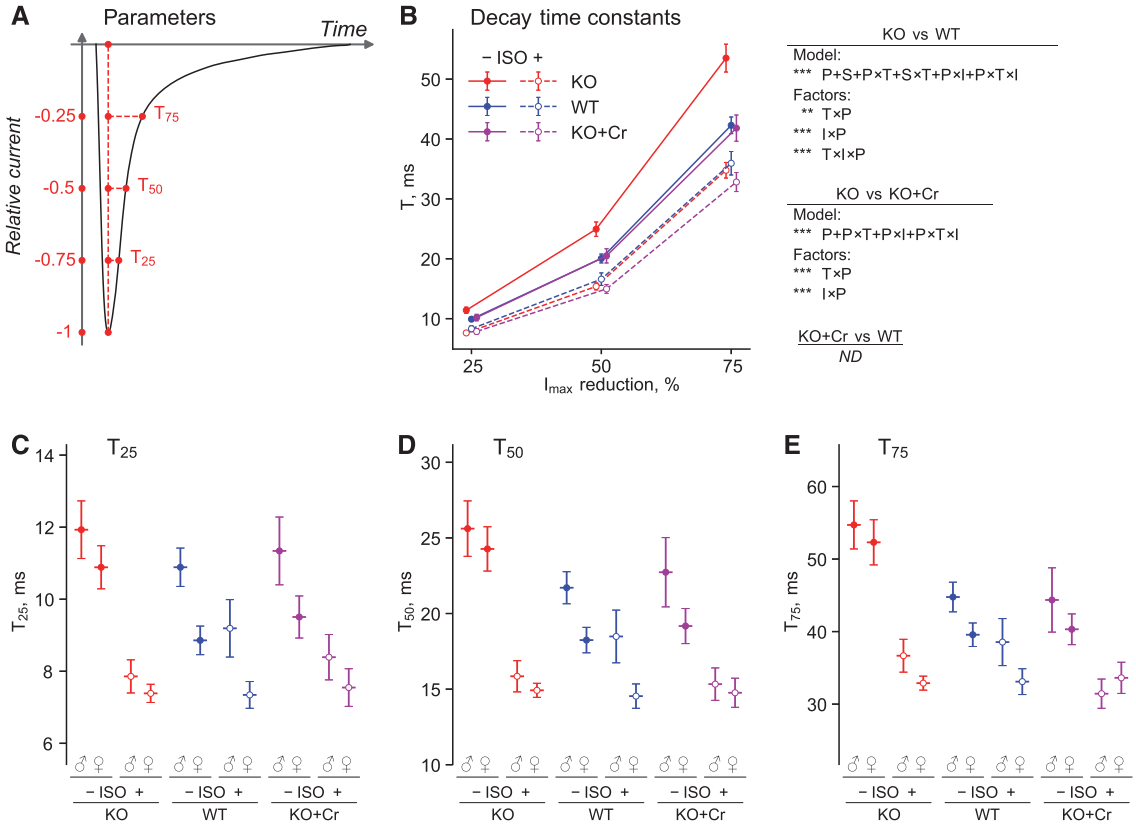

Figure 5. Statistical analysis of L-type calcium channel (LTCC) current inactivation. Here, the currents recorded at the measurement pulse with −5 mV step were analyzed. *A*: decay of LTCC current was described using 3 time constants corresponding to the duration required for the current to be reduced by 25%, 50%, and 75%. *B*: decay time constants (*x*-axis) for the current are shown for all animal groups, and the data from males and females are pooled and shown using means ± SE. On the *right*, statistical analysis is shown using the same notation as in Fig. 4, with the additional factor *T* (time constant). Notice the strong interaction between isoprenaline (ISO) and phenotype when creatine-deficient arginine-glycine amidinotransferase (AGAT)-knockout (KO) data are compared with WT and KO + Cr. *C*, *D*, and *E*: plots with the analyzed measurements shown for each of the factor combinations separately. To accurately show the data, different scales were used. Here, the same notation is used as in the plots on Fig. 4. No. of animals and cells used in the experiments was as in Fig. 4, with exception of KO female, where 1 cell less was used. Statistical analysis was performed using Bayesian repeated-measures ANOVA.

reversal potential. Taking into account that none of the factors of that model (A or A × I) were found to be significant separately, we did not consider that difference further.

Within the performed analysis, the number of experiments performed on the older group was rather limited when considering SR Ca^{2+} content and loading of Ca^{2+} into SR. Because the number of measurements were low in some groups, the statistical analysis should be considered as nonconclusive in this case and is only shown here for completeness within the context of this study.

Summary of Patch Clamping Results

Overall, the experimental data showed that creatine deficiency in AGAT-KO mice is associated with a reduction in I_{LTCC}, its voltage range of activation, and its rate of inactivation (Fig. 4). Furthermore, the decay of the Ca^{2+} transient was slower (Fig. 6). In all our measurements, there was no statistically significant difference between males and females, and creatine supplementation in the food reversed the phenotype.

Use of Mathematical Model to Analyze the Experimental Data

For further interpretation of our measurements, we carried out a set of simulations using a mathematical model of the action potential of mouse cardiomyocytes. The modeling part was based on the model of Bondarenko et al. (32), with an extension to include Fluo-4, adjustment of ion concentrations according to the used solutions, and other modifications, as described in METHODS.

We looked into how the model reproduces our measurements while pacing the cells with a periodic, rectangular

AJP-Heart Circ Physiol • doi:10.1152/ajpheart.00300.2020 • www.ajpheart.org
Downloaded from journals.physiology.org/journal/ajpheart by Rikke Birkedal (086.110.032.113) on March 18, 2021.

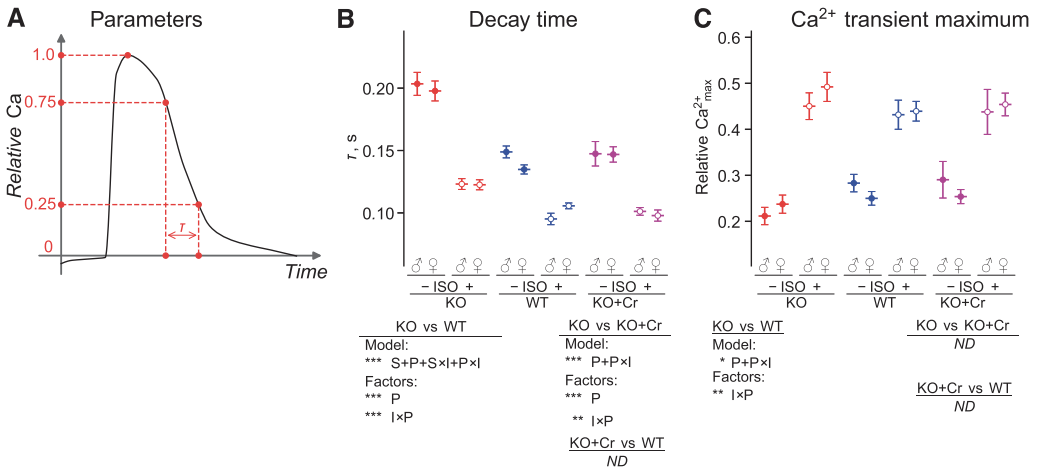

Figure 6. Analysis of Ca^{2+}-sensitive fluorescence transients (Ca^{2+} transients) recorded while stimulating the cell with the measurement pulse to 0 mV. Here, Ca^{2+} transient decay and amplitude are compared. *A*: the transient decay and amplitude are shown schematically. *B*: Ca^{2+} decay was significantly different for creatine-deficient (KO) animals when compared with controls [wild type (WT)] and creatine-fed (KO + Cr) animals. This difference was attributed mainly to the difference in phenotype and phenotype interaction with isoprenaline (ISO) presence. *C*: for Ca^{2+} transient maximum, the difference between KO and WT was found and attributed to the interaction between phenotype and isoprenaline presence. Notice, that in contrast to the decay, the maximum was not significantly different between KO and KO + Cr groups. In all parameters, feeding arginine-glycine amidinotransferase (AGAT)-KO with creatine restored the phenotype. The same notation is used as in Fig. 4. No. of animals and cells used in the experiments was as in Fig. 4. Statistical analysis was performed using Bayesian repeated-measures ANOVA.

pulse train. When compared with the measurements, calculated changes in Ca^{2+}-induced fluorescence have a somewhat sharper peak (Fig. 11*A*) than that recorded in the experiment (Fig. 3*B*). At the peak, only I_{LTCC} contributed significantly to the total current, suggesting that the measurements in Fig. 3*C* correspond to the peak I_{LTCC}. After reaching the peak current, the total Ca^{2+} current calculated by the model had a significant contribution of plasma membrane Ca^{2+} ATPase (PMCA), which induced a small bump. This bump was not observed in our recordings. As to the calculated fluorescence traces, the model solution did not stabilize at the end of each pulse (Fig. 11*B*). In contrast, in the experiment, fluorescence was stable at the end of each pulse (Fig. 8*B*). We took these limitations into account by analyzing the model solutions and looking into the overall behavior of the system without requiring a perfect fit to the experimental data.

Validation of the Model: Reproducing Changes in Ca^{2+} Fluxes During Ca^{2+} Loading into Depleted SR

To verify that the model was able to reproduce our data, we calculated the response of a cardiomyocyte to pacing with rectangular pulses after depletion of its SR from Ca^{2+}. This is similar to our measurements during Ca^{2+} loading after caffeine-induced SR Ca^{2+} release. Our simulations show the same stepwise increase in Fluo-4 fluorescence amplitude and changes in the shape of the total current (Fig. 11*B*), as observed in our experiments (Fig. 8*A* and *B*). The total current, in this case, is predominantly due to LTCC.

The dynamics of intracellular Ca^{2+} fluxes during a pulse predicted by the model was rather complex and involved binding and unbinding of Ca^{2+} from buffers, troponin C, and Fluo-4. To study what can be learned from the experiments involving the loading of Ca^{2+} after SR Ca^{2+} depletion, we integrated the intracellular Ca^{2+} fluxes and examined their distribution (Fig. 11*C*). In this plot, all sarcolemmal fluxes and intracellular processes are shown in blue and red tones, respectively. Notice that during the first beats, most of the Ca^{2+}, which enters the cell through the sarcolemma, is not extruded out of the cell. This is clear from comparing the influx of Ca^{2+} through LTCC, NCX, and background Ca^{2+} current (I_{BCa}) with the efflux through PMCA and NCX. This is in contrast to the steady-state behavior, where all transmembrane fluxes are in balance and most of the fluxes are through the SR (pulse 100 in Fig. 11*C*).

When looking into the first pulse dynamics, we identified the main net contributors to Ca^{2+} fluxes as LTCCs and SERCA (Fig. 11*D*). On the net influx side, LTCCs provide most of the Ca^{2+}, with I_{BCa} 5× and net contribution by intracellular buffers 7× smaller than of I_{LTCC}. On the efflux side, SERCA is able to pump back most of the Ca^{2+} from the cytosol to the SR. The only other net efflux contributor, PMCA, was (11×) smaller (Fig. 11*D*).

Reduced LTCC Conductance, SERCA Activity, and Ca^{2+} Transfer Between Subspace and Cytosol in AGAT-KO

We used our model to determine the extent of the changes in I_{LTCC}, SERCA, and Ca^{2+} transfer between the subsarcolemmal space [subspace (41)] and cytosol. A change in the rate of Ca^{2+} transfer from the subspace to the cytosol could be due to a smaller and/or slower CICR, which we were unable to resolve with our fluorescence measurements (Fig. 6*C*). We looked for changes in the corresponding rate constants of the model that would allow us to reproduce the

Downloaded from journals.physiology.org/journal/ajpheart by Rikke Birkedal (086.110.032.113) on March 18, 2021.

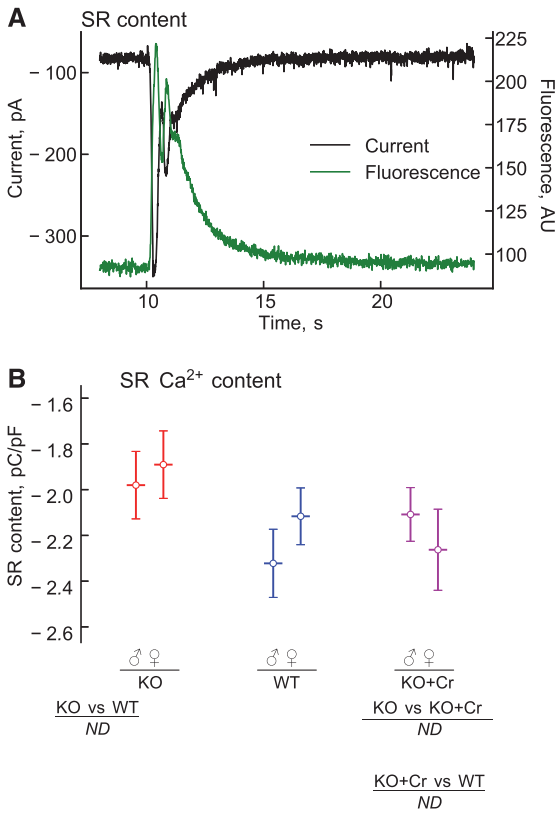

Figure 7. Estimation of sarcoplasmic reticulum (SR) Ca^{2+} content in the presence of isoprenaline. *A*: example measurement traces are shown, with the current (in black) and corresponding Fluo-4 fluorescence (green) after application of caffeine started at 10 s. *B*: SR Ca^{2+} content was estimated by integration of the current. Although there is a trend of having smaller SR Ca^{2+} content in knockout (KO) than in the other groups, there are no statistically significant differences between the groups. The same notation is used as in Fig. 4. No. of animals and cells used in the experiments were as follows (reported in animals/cell notation): KO male (2/6), KO female (3/6), wild-type (WT) male (5/8), WT female (3/6), KO + creatine (Cr) male (5/10), KO + Cr female (3/8). Statistical analysis was performed using Bayesian ANOVA.

experimentally determined changes induced by creatine deficiency. For that, we looked for model parameters that would satisfy the determined changes in relatively large ranges. Specifically, we looked for the model solutions that would have *1*) a reduction in calculated maximal I_{LTCC} of 15 ± 10% (Fig. 4*D*), *2*) a reduction in LTCC charge influx by 20 ± 10% during Ca^{2+} loading (Fig. 8*C*), and *3*) a slowing of the Ca^{2+} transient fluorescence decay by 22.5 ± 10% (Fig. 6*A*) while *4*) keeping the Ca^{2+} transient maximum unchanged or with a reduction smaller than 20% or 30% (Fig. 6*B*).

The simulations were performed for a large number of parameter combinations. Here, LTCC maximum conductance (LTCC conductance), the exchange constant of Ca^{2+} transfer between subspace and cytosol (Ca^{2+} transfer), and activity of SERCA were reduced up to 25% of their original value, with all combinations of reductions tested in simulations. As shown in Fig. 12*A*, there is a set of model parameters that can reproduce the data. Most of the model solutions suggested a reduction of Fluo-4 Ca^{2+}-induced fluorescence maximum, when reducing any of the studied fluxes. Although we have not observed any significant reduction, only a slight tendency, in Fluo-4 fluorescence (Fig. 6*C*), we allowed some changes in fluorescence peak in the model solution while considering it to satisfy the conditions. As shown in Fig. 12*A*, the number of successful simulations strongly depends on the allowed reduction of Fluo-4 transient (compare blue and orange histograms). However, qualitatively, the interpretation of the measured data is the same. In addition to the reduction of SERCA activity in AGAT-KO cardiomyocytes, the data point toward a simultaneous reduction of LTCC conductance and Ca^{2+} transfer between subspace and cytosol.

The reduction of LTCC conductance and Ca^{2+} transfer found by the simulations are not independent of each other. As it is demonstrated in Fig. 12*B*, at least one of the flux rates has to be reduced with the sum of the reductions staying relatively constant (all solutions align along a line on the *left* subplot of Fig. 12*B*). The reduction in SERCA activity is related to the sum of the reductions on the Ca^{2+} influx pathway and not to the separate fluxes involved in the influx (Fig. 12*B*). Thus, when considering Ca^{2+} dynamics in cytosol, AGAT-KO cardiomyocytes exhibit reduced Ca^{2+} influx and efflux rates (Fig. 12*C*).

Reduction of Ca^{2+} Transfer between Subspace and Cytosol and Reduction in LTCC Conductance Reproduce Different Aspects of I_{LTCC} Changes in AGAT-KO

To test whether we can distinguish between the effects of reducing LTCC conductance and Ca^{2+} transfer between subspace and cytosol, we analyzed the changes in current-voltage relationships and I_{LTCC} inactivation characteristics and compared them with our experimental data (Figs. 4 and 5). As pointed out above, the model does not fit our data perfectly, so we were looking for trends and not absolute values to avoid overinterpretation of the modeling results.

Because of the dynamic nature of Ca^{2+} concentration changes in subspace, LTCC Ca^{2+}-dependent inactivation, and CICR, changes in LTCC conductance and in Ca^{2+} transfer have different impacts on the macroscopic properties of the current amplitude (experimental data in Fig. 4). According to our simulations, reduction of both Ca^{2+} transfer and LTCC conductance reduced the I_{LTCC} amplitude, but Ca^{2+} transfer reduced the current amplitude significantly less than LTCC conductance (Fig. 13, *A* and *B*). However, their reduction had different effects on the parameters that define the shape of the LTCC current-voltage relationship: the potential corresponding to the maximal current (Fig. 13*C*), activation midpoint potential (Fig. 13*D*), and the slope (Fig. 13*F*). As shown in (Fig. 4), AGAT-KO exhibited a reduction in I_{LTCC} amplitude, an increase in the potential at maximal current, activation midpoint potential, and the slope factor, whereas the reversal potential had a tendency to reduce. All of these changes were in agreement with a reduction in Ca^{2+} transfer and opposite to the trends observed

Downloaded from journals.physiology.org/journal/ajpheart by Rikke Birkedal (086.110.032.113) on March 18, 2021.

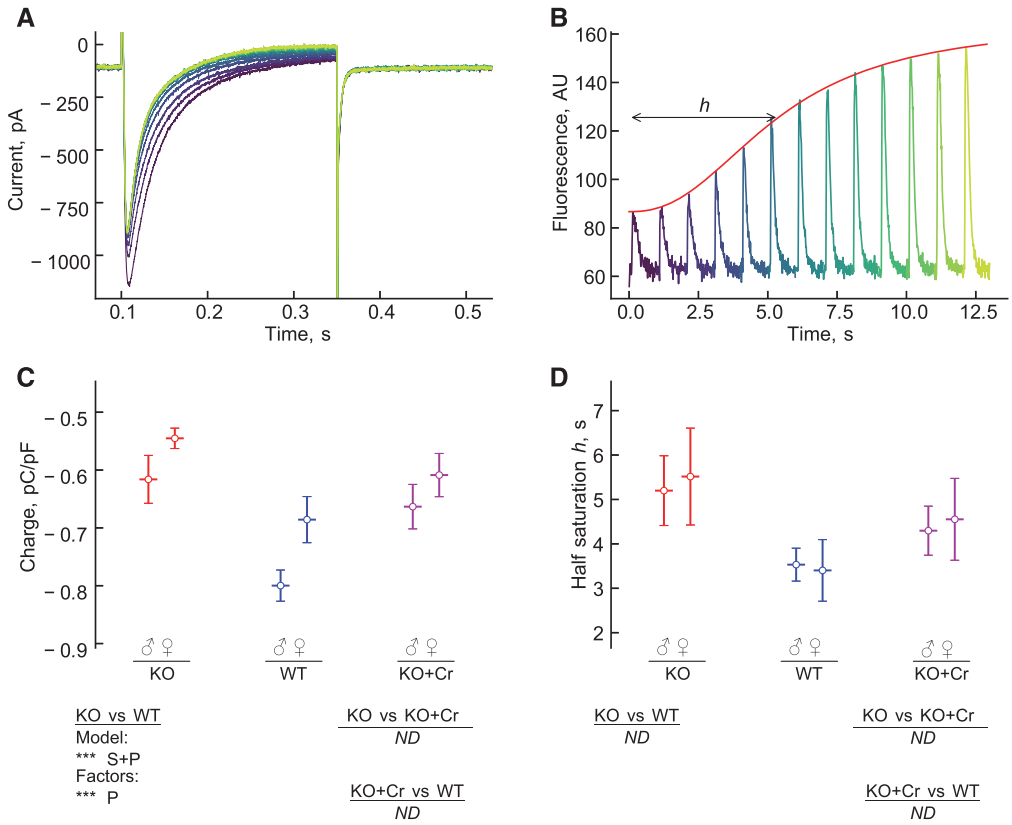

Figure 8. Sarcoplasmic reticulum (SR) recovery after Ca^{2+} depletion by caffeine. Current (*A*) and Fluo-4 fluorescence (*B*) were measured during recovery, with the pulses shown in different color, as in *B*. We analyzed the charge carried during the first pulse (*C*) and the time constant *h* for Ca^{2+} recovery (*D*). Although the charge (*C*) found for creatine-deficient animals was significantly smaller than for control animals, there were no statistically significant differences found for the time constant (*D*). Here, the same notation is used as in Fig. 4. No. of animals and cells used in the experiments were as follows (reported in animals/cells notation): knockout (KO) male (2/6), KO female (3/6), wild-type (WT) male (5/8), WT female (3/6), KO + creatine (Cr) male (5/10), KO + Cr female (3/8). Statistical analysis was performed using Bayesian ANOVA.

when reducing LTCC conductance in the model (Fig. 13, *C*, *D*, and *F*).

Neither reduction in Ca^{2+} transfer nor in LTCC conductance was able to reproduce the reduction in the reversal potential (compare Fig. 4*E* and Fig. 13*E*). Out of the two mechanisms considered, reduction of Ca^{2+} transfer was closer to the experimental data, leading to no changes in the beginning of the studied range, as opposed to the immediate increase in potential induced by reduction in LTCC conductance (Fig. 13*E*).

The influence of LTCC conductance and the Ca^{2+} transfer was analyzed further by analyzing the time constant of the LTCC current inactivation, T_{50}. According to our simulations, a reduction of the Ca^{2+} transfer is associated with an unchanged or faster decay of I_{LTCC} (Fig. 13*G*), whereas a reduction of LTCC conductance increased T_{50}. In this case, the latter is consistent with our experimental results, where I_{LTCC} inactivation is slower in the absence of ISO (Fig. 5).

In summary, a reduction of the exchange constant of Ca^{2+} transfer between subspace and cytosol was able to reproduce most of the trends in changes of the LTCC current-voltage characteristics in AGAT-KO mice. However, the analysis of LTCC inactivation time constants points toward a reduction of LTCC conductance.

Expression of LTCC and SERCA

We assessed the expression of LTCC and SERCA in AGAT-KO and WT mice by Western blotting (Fig. 14). According to our data, the expression of LTCC, SERCA, and GAPDH in AGAT-KO mice was not statistically different from the expression in WT. There was also no statistically significant difference in expression of these proteins between males and females nor interaction between sex and phenotype. No difference was found regardless of whether we normalized to *1*) the amount of protein in each lane, *2*) the protein level detected by Ponceau staining of the membrane, or *3*) for SERCA, normalization to the GAPDH signal.

Downloaded from journals.physiology.org/journal/ajpheart by Rikke Birkedal (086.110.032.113) on March 18, 2021.

Animals	Sex	n_Y	n_O	Analyzed Factors	Analyzed Null	Parameter	Fig	Significant Factors	Significance
LTCC current-voltage									
WT	both	34	10	A, I	I	Maximal current	4B	–	
WT	male	16	7			Potential at max current	4C		
KO+Cr	both	16	12			Act. midpoint potential	4D		
KO+Cr	female	5	12			Reversal potential	4E		
						Slope factor	4F		
LTCC current inactivation									
WT	both	34	10	A, I, T	I+T+I×T	Time constants	5	A×I	**
WT	male	16	7					A×I	**
KO+Cr	both	16	12					A×I	***
KO+Cr	female	5	12					A×I	***
Calcium transient									
WT	both	34	10	A, I	I	Decay time	6B	–	
WT	male	16	7			Transient maximum	6C		
KO+Cr	both	16	12						
KO+Cr	female	5	12						
Sarcoplasmic reticulum: calcium content and recovery after calcium depletion									
KO+Cr	both	15	3	A	–	Calcium content	7	–	
KO+Cr	female	5	3						
KO+Cr	both	14	2	A	–	First pulse charge	8C	–	
KO+Cr	female	5	2			Recovery time constant	8D		

Figure 9. Contribution of age difference on measured parameters analyzed statistically with the significance levels indicated on the *right*. The contribution of aging (*factor A*) was tested only for the groups with a significant number of measurements in younger (n_Y) and older (n_O) individuals, as discussed in the text. The factor notations were the same as in the figures referred to (see column figure for figure number). For cases with multiple analyzed factors, we considered a hierarchy of statistical models starting from the null model and adding factors separately until the model included all factors and their interactions. Note that the effect of isoprenaline (ISO) on the L-type calcium channel (LTCC) current inactivation was influenced by age in all groups. See the text for discussion regarding 1 case determined as significant by analysis in LTCC current-voltage relationship.

DISCUSSION

To our knowledge, this is the first electrophysiological study of cardiomyocytes from AGAT-KO mice, their WT littermates, and AGAT KO + Cr mice receiving creatine-supplemented food. We found that AGAT-KO mice had a smaller I_{LTCC} peak and voltage range of activation and a slower I_{LTCC} inactivation rate. Furthermore, the rate of Ca^{2+} transient decay was slower, suggesting a reduction in SERCA activity. According to our modeling results, these changes can be reproduced by reducing three parameters: LTCC conductance, the exchange constant of Ca^{2+} transfer between subspace and cytosol, and SERCA activity (Fig. 12*C*). These differences were recorded in the presence of PCr (in the patch pipette) and were thus due to differences in structure, expression, and/or regulation of the proteins involved in e-c coupling rather than acute absence of energy transfer pathways. According to our measurements, LTCC and SERCA protein expression was not different in KO and WT, suggesting that regulatory mechanisms likely account for the observed changes, and these changes were prevented by lifelong creatine supplementation via the food.

Dissecting Chronic Adaptations from Acute Energy Provision

In vivo, it is expected that cardiomyocytes from AGAT-KO have altered calcium handling due to the absence of CK catalyzed energy transfer. However, in this work, we show that they exhibit a long-term reorganization of calcium handling in the cell. To exclude effects caused by differences in energy transfer and focus on the long-term reorganization, we did our measurements with the same pipette solution for all groups. Because solution components diffuse from the patch pipette into the cell, the intracellular environment is expected to be similar in the all cells studied regardless of phenotype. Because the CK activity and isoform distribution are not different in wild-type and AGAT-KO hearts (21), the experimental inclusion of PCr reconstitutes the CK system such that differences between AGAT-KO and WT in the present study are unlikely due to differences in CK energy transfer.

In our experiments, we set the PCr concentration of the pipette solution roughly in between the values expected in AGAT-WT and KO cardiomyocytes (PCr values from Ref. 21).

Downloaded from journals.physiology.org/journal/ajpheart by Rikke Birkedal (086.110.032.113) on March 18, 2021.

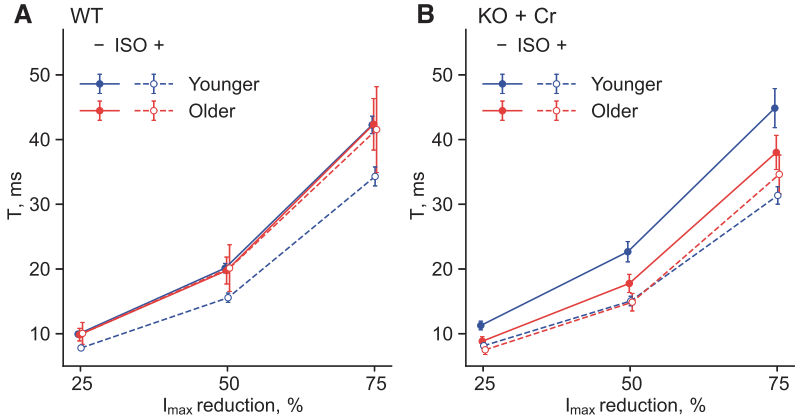

Figure 10. Statistical analysis of L-type calcium channel (LTCC) current inactivation among different age groups. As in Fig. 5*B*, decay time constants are plotted against current reduction (*x*-axis). Here, younger and older groups are compared within wild-type (WT; *A*) and knockout (KO) + creatine (Cr) (*B*) animals. Notice that isoprenaline (ISO) has a smaller effect on cardiomyocytes from older compared with younger mice. Data from males and females are pooled and shown using means ± SE.

This was to reduce the differences between recorded and in vivo conditions experienced by the cells. Thus, we expect that the recorded differences in calcium handling are smaller in our measurements than those experienced by the phenotypes in vivo. However, these experimental conditions allowed us to pinpoint the long-term adaptation to creatine deficiency in the heart in terms of the changes in calcium-handling system.

On the other side, an adaptation that we cannot rule out in our design is a physical disassociation between CK and SR leading to the reduction of functional coupling between CK and SERCA in AGAT-KO. It is possible that, in part, reduction in SERCA activity can be explained by changes in CK-SERCA coupling while keeping the same CK isoform distribution as reported (21).

AGAT-KO Cardiomyocytes Exhibit a Slowing of Ca^{2+} Fluxes

The Ca^{2+} increase in cytosol was impaired by multiple changes in I_{LTCC} (Figs. 3*C* and 4) in AGAT-KO. In addition to the reduction of maximal I_{LTCC}, there were changes in activation midpoint potential, reversal potential, and the slope factor (Fig. 4). All these changes were toward a reduction of transsarcolemmal Ca^{2+} influx: reduction of maximal rate and its activation in a smaller range of membrane potentials (Fig. 12*C*, *left*).

In addition to the reduction in I_{LTCC}, our modeling results demonstrated that the exchange constant of Ca^{2+} transfer between the dyadic subspace and cytosol was reduced (Fig. 13, *B*–*F*), leading to the reduction of the exchange (J_{xfer}; Fig. 12*C*, *left*). To explain the changes in Ca^{2+} transfer from the subspace to the cytosol, it is important to take into account that the intracellular environment consists of multiple compartments, where local ion and metabolite concentrations are different from those in the bulk cytosol. Roughly 80% of the LTCC channels are located in the transverse tubules [t-tubules (42)], where they are organized in dyadic clefts with ryanodine receptors by junctophilin-2 and amphiphysin-2 (BIN-1) (43). Within the dyadic cleft, the sarcolemma with LTCCs and the SR membrane with ryanodine receptors are so close that a subspace is formed (Fig. 12*C*, *left*), where the Ca^{2+} influx through LTCCs results in a brief pulse of Ca^{2+}, which reaches much higher concentrations than Ca^{2+} in the bulk cytosol (32). The I_{LTCC} alone contributes only little to the Ca^{2+} transient in mouse cardiomyocytes (Ref. 44 and Fig. 11), but it triggers a rapid Ca^{2+} release from the SR, which is steeply graded with the size of the stimulus (45). Ca^{2+} from both I_{LTCC} and CICR diffuses from the subspace to the cytosol, where it initiates contraction. If the rate of Ca^{2+} transfer out of the subspace is reduced, it could indicate that either Ca^{2+} efflux from the subspace is more restricted, or the gradient of Ca^{2+} between subspace and the cytosol is smaller. The gradient, in turn, could be smaller due to Ca^{2+} being released from the SR in smaller amounts and/or at a slower rate.

A Smaller CICR in AGAT-KO is in Line with the Fact That a Smaller I_{LTCC} Would Trigger a Smaller CICR

Furthermore, SR Ca^{2+} release affects the Ca^{2+}-dependent inactivation of I_{LTCC} in the t-tubules, where LTCCs and ryanodine receptors are closely positioned (42). Thus, a smaller CICR could explain why the inactivation of I_{LTCC} is slower in AGAT-KO (Fig. 5). It is also possible that AGAT-KO exhibit a slower SR Ca^{2+} release. A slower, dysynchronous Ca^{2+} release is exhibited by "orphaned" ryanodine receptors, which are not close to LTCCs in the dyadic cleft. These are observed in cardiomyocytes from developing and failing hearts (46–48). Whether AGAT-KO cardiomyocytes exhibit ultrastructural changes affecting ion channel communication should be studied further.

From our analysis of the Ca^{2+} transients associated with contraction, we observed a significant increase in the transient decay time in AGAT-KO mice (Fig. 6*B*). Our model demonstrated the best fit of the data, when SERCA activity was reduced by ~20% (Fig. 12, *A* and *C*, *right*). The Ca^{2+} influx and efflux rates were reduced to similar extents (Fig. 12*B*), demonstrating a fine flux balance between the two systems as required to achieve steady-state conditions (49).

Taken together, our results show that in AGAT-KO cardiomyocytes, the Ca^{2+} influx to the cytosol is reduced and

Downloaded from journals.physiology.org/journal/ajpheart by Rikke Birkedal (086.110.032.113) on March 18, 2021.

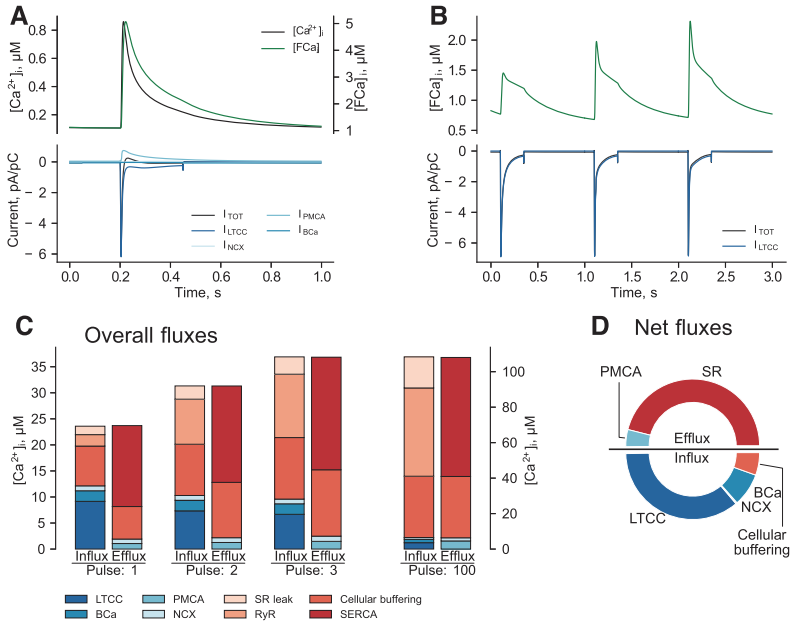

Figure 11. Estimation of Ca^{2+} fluxes using mathematical modeling. *A*: cardiomyocyte response to periodic stimulation by a 2-step voltage pulse, as in the experiments with the 2nd step at 0 mV. Here, the cytosolic Ca^{2+} concentration and corresponding Fluo-4 with bound Ca^{2+} (FCa) concentration is shown at the *top*, and transmembrane currents are shown at the *bottom*. The considered currents were as follows: total (TOT), L-type calcium channel (LTCC), Na^{+}/Ca^{2+} exchanger (NCX), plasma membrane Ca^{2+} ATPase (PMCA), and background Ca^{2+} (BCa). *B*: cardiomyocyte response to stimulation with the rectangular pulse (0 mV) after sarcoplasmic reticulum (SR) depletion of Ca^{2+}, corresponding to the experimental conditions during loading of cardiomyocytes with Ca^{2+} after caffeine treatment. Here, the model solution for the first 3 pulses is shown using the same notation as in *A*. Note that the scale of FCa is different in *A* and *B*. *C*: distribution of overall fluxes during 1 beat while loading cardiomyocyte with Ca^{2+}, as in *B*. The fluxes are classified as "influx" and "efflux" from following Ca^{2+} in the cytosol; i.e., processes bringing Ca^{2+} to the cytosol are classified under influx and processes removing Ca^{2+} from the cytosol are classified under efflux. Cellular buffering is including binding to troponin C and calmodulin. During a beat, Ca^{2+} is first bound to the buffers and later released; hence, buffers contribute to influx and efflux when overall fluxes are considered. Note that the steady-state solution (pulse 100) is shown using a different scale than the first 3 pulses. *D*: distribution of net fluxes during the 1st beat when loading cardiomyocyte with Ca^{2+}. Here, SR, when accounting for the difference in uptake through sarcoendoplasmic reticulum calcium ATPase (SERCA) and Ca^{2+} release through RyR and leak, is the main contributor in removing Ca^{2+} from the cytosol. The main Ca^{2+} provider is LTCC, with net contribution of buffers and Ca^{2+} leak through sarcolemma next in the contributions. The net contribution of Na^{+}/Ca^{2+} exchanger (NCX) to the influx of Ca^{2+} during the first beat was too small to show on the chart. See the main text for the discussion of these modeling results.

slowed down; I_{LTCC} is reduced (Figs. 3*C* and 4), as is the rate of Ca^{2+} transfer between the subspace and the cytosol (Figs. 12*B* and 13). The slower Ca^{2+}-dependent inactivation of I_{LTCC} speaks in favor of that at least part of the slowed Ca^{2+} transfer is due to a smaller CICR. In addition, Ca^{2+} efflux is slowed down (Fig. 6*B*) through a reduction in SERCA (Fig. 12). These results are in agreement with the impaired rates of contraction and relaxation in AGAT-KO mice recorded in vivo (21).

Effects of Adrenergic Stimulation

β-Adrenergic stimulation of the cardiomyocytes with isoprenaline affected the parameters of the I_{LTCC} current-voltage relationship to a similar extent in the three animal groups (Fig. 4). Thus, LTCCs in AGAT-KO exhibited a full β-adrenergic response, but their current remained smaller than that of WT and KO + Cr.

ISO enhanced SR function to a greater extent in AGAT-KO than in AGAT-WT and AGAT-KO + Cr. ISO had a larger effect on the Ca^{2+} transient decay time in AGAT KO (Fig. 6*B*), and it abolished the genotype differences in I_{LTCC} inactivation time constants (Fig. 5*B*). The latter suggests that ISO enhanced CICR via the ryanodine receptors. This is in agreement with the fact that ISO also had a greater effect on the Ca^{2+} transient maximum in AGAT-KO (Fig. 6*C*). Despite a greater effect of ISO in AGAT-KO, the Ca^{2+} transient decay was still slower in AGAT-KO cardiomyocytes under all conditions (Fig. 6*B*). This is consistent with hemodynamic measurements, where contractility was slower in AGAT-KO animals with and without adrenergic stimulation (21).

LTCC and SERCA Expression

The overall slowing of calcium fluxes was not due to changes in protein expression of LTCC or SERCA (Fig. 14). This suggests that regulatory mechanisms and/or changes in the expression of regulatory proteins are involved. In the case of SERCA, ultrastructural changes in AGAT-KO cardiomyocytes affecting its colocalization with CK could also affect the function.

Our Western blotting results are in agreement with a study on gene expression in AGAT-KO and WT hearts (50), where

Downloaded from journals.physiology.org/journal/ajpheart by Rikke Birkedal (086.110.032.113) on March 18, 2021.

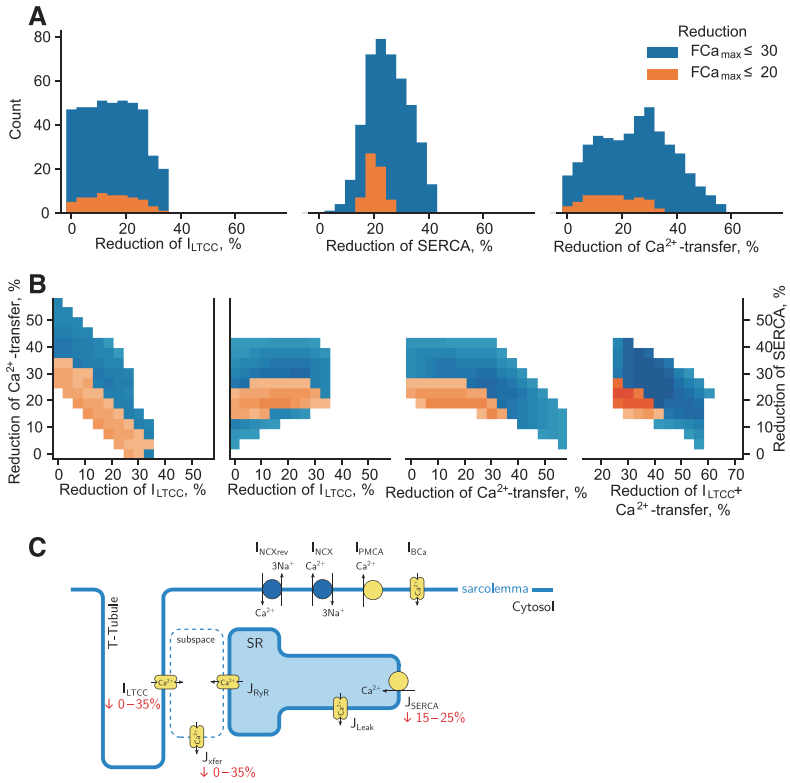

Figure 12. Changes in calcium handling induced by creatine deficiency as predicted by the mathematical model. *A*: set of parameters (*x*-axis) satisfying the imposed conditions. The histograms show distributions of successful simulation counts as a function of a parameter value. Two cutoffs for Fluo-4 Ca^{2+}-induced fluorescence maximum reduction in cardiomyocytes of creatine-deficient mice were used: 30% (blue) and 20% (orange). *B*: correlation between the set of parameters satisfying the imposed conditions. Here, the color tone was proportional to the no. of successful simulations, with blue and orange tones used to distinguish the reduction of Ca^{2+}-induced fluorescence maximum, as in *A*. Notice that at least one of the processes on the influx pathway has to be reduced (the *left* subplot). Sarcoendoplasmic reticulum calcium ATPase (SERCA) uptake rate reduction can be related to the sum of the reductions of L-type Ca^{2+} channels (LTCCs) conductance and the Ca^{2+} transfer (the *right* subplot) and not to the specific reduction of LTCC or the Ca^{2+} transfer (the subplots in the middle). *C*: expected reduction in LTCC conductance, the exchange constant of Ca^{2+} transfer between subspace and cytosol, and SERCA activity are shown on the basis of the model simulation results in *A*.

the most relevant reported changes were in the conduction system of the heart in the expression of *Scn4a*, *Scn4b*, and *Cacna1s*. However, the isoforms of sodium- and L-type calcium channel encoded by these genes ($Na_v1.4$ and $Ca_v1.1$) are not the predominant forms in the heart, where the main channels are $Na_v1.5$ (*Scn5a*) and $Ca_v1.2$ (*Cacna1c*) (51, 52). No changes in *Cacna1c* or SERCA were reported (50), so we assume there was no differential regulation found. This is in line with our protein expression measurements (Fig. 14).

There are several gene regulation studies performed on AGAT-KO to study changes in gene expression in skeletal muscle, brain, and heart (50, 53, 54). Multiple changes in gene expression were found in all these studies. Taking into account that there were 485 affected genes (50), it demonstrates that the absence of a functional CK system in the heart does interfere significantly with cardiomyocyte development, in agreement with our patch clamp results. Furthermore, our data point to changes being induced by the absence of CK that have significant functional consequences and induce physiologically relevant adaptations in the heart.

Female and Male Mice Are Affected Equally by Creatine-Deficiency

In our study, we looked into possible sex differences. In some of the comparisons (Figs. 4, *B*, *C*, *E*, and *F*, 6*B*, and 8*C*), sex was one of the parameters in the highest-scoring statistical models. However, when analyzed further, we did not find a single case where sex contribution would be considered statistically significant, either separately or through interaction with the other parameters. Therefore, we conclude that the phenotype of AGAT-KO cardiomyocytes was similar for female and male mice.

Rescue by Creatine Supplementation

The changes observed in AGAT-KO mice were fully rescued by lifelong supplementation of creatine in the food, as observed in the KO + Cr group. This includes recovery of LTCC current-voltage relationship, I_{LTCC} inactivation, and Ca^{2+} uptake by SR during a test pulse. The recovery was full under control conditions and during β-adrenergic stimulation with ISO.

The present results may at first seem to contrast those of Faller et al. (21), where they found that homoarginine, but not creatine, rescued cardiac contractility in AGAT-KO mice. Whereas creatine supplementation in AGAT-KO mice is shown to recover the creatine content in skeletal muscle and brain (55) as well as in the heart (21), the level of homoarginine, the product of the second reaction catalyzed by AGAT (19), remains low. Faller et al. (21) found that when AGAT-KO were given supplements of homoarginine or creatine later in life, only homoarginine supplementation rescued the phenotype. However, there are notable differences between the

Downloaded from journals.physiology.org/journal/ajpheart by Rikke Birkedal (086.110.032.113) on March 18, 2021.

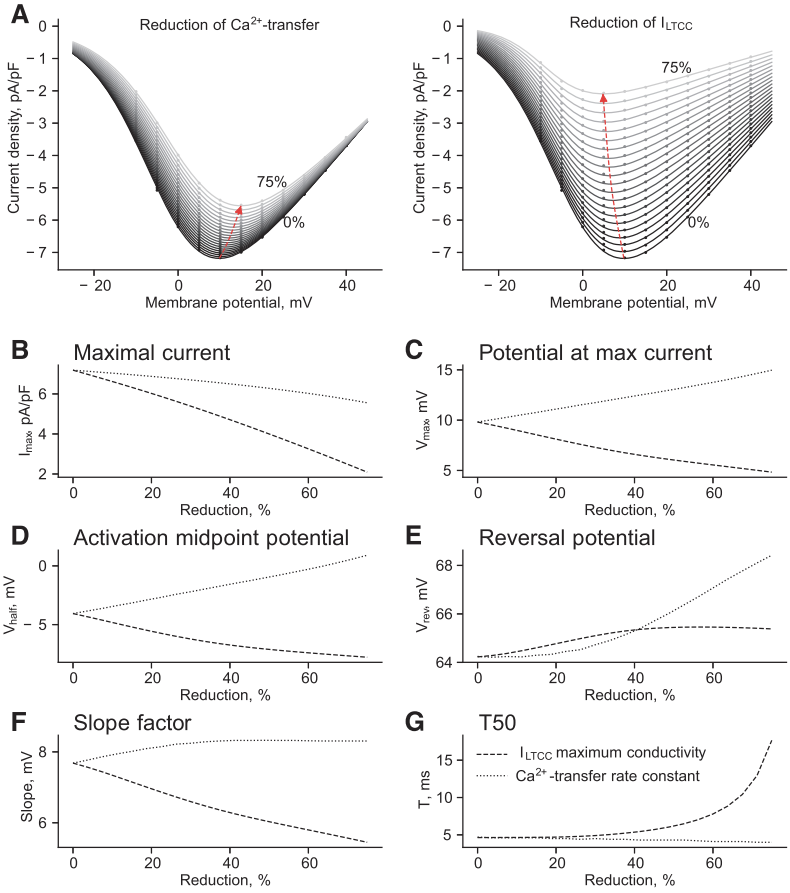

Figure 13. Analysis of the effects of reducing of L-type Ca^{2+} channel (LTCC) conductance or Ca^{2+} transfer between subspace and cytosol on I_{LTCC} properties. *A*: simulated changes in I_{LTCC} induced by reduction of Ca^{2+} transfer (*left*) or reduction in LTCC conductance (*right*). LTCC conductance and Ca^{2+} transfer were reduced from the original value by varying degree from 0 to 75%, as indicated by the arrows on the subplots. Here, the simulations were performed with the same potential steps as in the experiment, and the results (dots) were fitted (lines) as the experimental data in Fig. 3 to compare the fit parameters obtained in from experimental and simulated data in the subsequent subplots. *B–F*: changes in the parameters describing the calculated *I-V* curves associated with the reduction of Ca^{2+} transfer between subspace and cytosol (dotted line) and LTCC conductance (dashed line). *G*: I_{LTCC} inactivation time constant T_{50} as a function of the reduction in Ca^{2+} transfer between subspace and cytosol and LTCC conductance. See the text for the description and comparison with the experimental data.

preparations. First, the present study focused on the Ca^{2+} dynamics of LTCC and CICR using patch clamp, where the intracellular environment is affected by the pipette solution and the cardiomyocytes are stimulated by rectangular pulses. Faller et al. (21) recorded contractility of the whole heart and intact cells. Thus, in their preparation, contractility was affected by the shape of the action potentials, Ca^{2+} flux through NCX, which may be important in mouse cardiomyocytes (56), as well as cross-bridge kinetics and Ca^{2+} binding and unbinding to troponin (57, 58). Secondly, the rescue experiments in Faller et al. (21) were performed after the mice had experienced a period of creatine deficiency, and the mice did not recover their body weight. In the present study, the AGAT KO + Cr mice received creatine-supplemented food from the time of separation from their littermates, and their body weight was similar to that of AGAT-WT. Thus, the timing of creatine supplementation is important. In fact, our results are well in agreement with those of Faller et al. (21), who found that lifelong creatine supplementation led to similar Ca^{2+} transients in WT and KO, whereas contractility remained slower. Thus, creatine supplementation throughout life can rescue LTCC and CICR Ca^{2+} dynamics in AGAT-KO. But for rescue of contractility, supplementation with homoarginine is required.

The Impact of Creatine Deficiency on e-c Coupling

According to our results, creatine deficiency in AGAT-KO mice had a significant impact on LTCC and SR Ca^{2+} dynamics in cardiomyocytes. It is uncertain whether it relates to a compromised CK energy transfer per SE. Cardiomyocytes have intracellular, lattice-like diffusion barriers (59–61). In the mitochondria, most of the VDAC channels are inaccessible for ADP coming from the cytosol (62) either through closure of VDAC (63) or its shielding by intracellular structures (64, 65). The CK system has been suggested to play a crucial role in cardiomyocytes, overcoming these barriers and ensuring an adequate energy transfer and thus adequate performance of the e-c coupling system (66). However, a study on isolated hearts suggested that energy transfer is, at least under some conditions, carried out through diffusion of ATP and ADP rather than creatine and phosphocreatine (67). So far, the studies on AGAT- and GAMT-KO hearts demonstrate

Downloaded from journals.physiology.org/journal/ajpheart by Rikke Birkedal (086.110.032.113) on March 18, 2021.

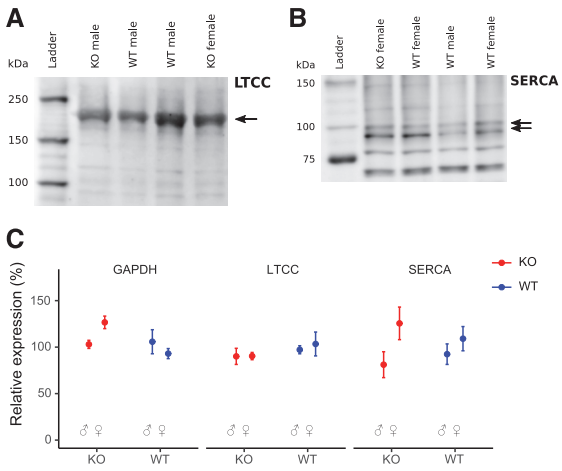

Figure 14. L-type Ca^{2+} channel (LTCC) and sarcoplasmic reticulum Ca^{2+} ATPase (SERCA) expression levels were similar in arginine-glycine amidinotransferase (AGAT) knockout (KO) and wild type (WT). *A* and *B*: representative Western blots for LTCC (*A*) and SERCA (*B*) with the random distribution of the samples as indicated at *top*. The ladder is shown in the 1st lane of the blots, and the arrows indicate the analyzed peaks. *C*: LTCC, SERCA, and GAPDH expression levels normalized by protein staining were related to the mean expression of WT (both sexes pooled). Expression levels are shown as means ± SE. Note that none of the studied proteins showed a statistically significant difference between WT and KO. No. of animals used for expression analysis is shown as female/male: LTCC: KO 5/6 and WT 5/6; SERCA: KO 6/7 and WT 5/6; GAPDH: KO 6/6 and WT 5/6.

that the energy transfer through diffusion of ATP and ADP can support the cell function. In GAMT-KO, no changes suggesting reorganization of diffusion barriers on VDAC or cytosolic barriers have been recorded, nor has adaptation in terms of mitochondrial reorganization (17). Thus, there is a contradiction between expected dominance of CK system in energy transfer on the basis of large fractions of closed VDACs in the heart mitochondria and the data from GAMT-KO. This contradiction and establishing whether cardiomyocytes in AGAT-KO have changes in energy transfer system as well as intracellular diffusion restrictions is the subject of further studies.

A comparison with studies on other mouse models with an inactivated CK system provides important information. Isolated heart muscle from CK-knockout mice lacking both mitochondrial and cytoplasmic CK have similar Ca^{2+} transients and force development at different stimulation conditions as in wild-type mice (68). Furthermore, creatine-deficient GAMT mice, which have high levels of homoarginine (19), exhibit normal contractility at low to moderate workloads (15). This suggests that the changes in LTCC and SR Ca^{2+} dynamics observed in AGAT-KO mice do not relate to a compromised energy transfer per SE. Only the combined effect of creatine and homoarginine deficiency affects Ca^{2+} dynamics under baseline conditions.

Because our results point to a reduced SERCA activity combined with a reduced Ca^{2+} influx due to reduced LTCC and conductance between dyadic space and cytosol, we can speculate that Ca^{2+} influx is tuned to match Ca^{2+} efflux capacity of the cardiomyocytes during the development of the heart. Interestingly, this is done in addition to functional coupling between Ca^{2+} influx and efflux via feedback mechanisms (49). This matching could explain why Ca^{2+} influx was reduced while not being coupled to ATPase activity directly as LTCC opening and diffusion from dyadic space are. Looking at the bigger picture, such matching would make sense. It will allow the heart to optimize expression of the involved proteins and possibly make the feedback regulation for matching Ca^{2+} influx and efflux faster to respond to out-of-balance cardiac cycles. As a result, that would allow the heart to resist Ca^{2+} overload and all possible complications arising from it, such as arrhythmia and mitochondrial damage. However, the precise mechanism behind such matching of proteins and organization of the compartments responsible for Ca^{2+} influx and efflux is the subject of further studies.

In summary, we have demonstrated that creatine deficiency in AGAT-KO mice leads to changes in LTCC and SR Ca^{2+} handling in cardiomyocytes. Because these changes can be prevented by lifelong creatine supplementation through the food, we conclude that a functional CK system is involved in developing normal Ca^{2+} handling in the heart.

DATA AVAILABILITY

Data are available on request from the authors.

ACKNOWLEDGMENTS

We acknowledge Prof. Dirk Isbrandt (University of Hamburg, Hamburg, Germany) for generating the strain of AGAT-deficient mice.

GRANTS

This work was supported by Estonian Research Council (IUT33-7) and British Heart Foundation grants (RG/18/12/34040) to C.A.L.

Downloaded from journals.physiology.org/journal/ajpheart by Rikke Birkedal (086.110.032.113) on March 18, 2021.

DISCLOSURES

No conflicts of interest, financial or otherwise, are declared by the authors.

AUTHOR CONTRIBUTIONS

M.L., C.A.L., R.B. and M.V. conceived and designed research; M.L., J.B., K.B. and N.K. performed experiments; M.L., K.B. and M.V. analyzed data; M.L., C.A.L., R.B. and M.V. interpreted results of experiments; M.L. prepared figures; M.L., R.B. and M.V. drafted manuscript; M.L., C.A.L., R.B. and M.V. edited and revised manuscript; M.L., J.B., N.K., C.A.L., R.B. and M.V. approved final version of manuscript.

REFERENCES

1. **Bessman SP**, **Geiger PJ.** Transport of energy in muscle: the phosphorylcreatine shuttle. *Science* 211: 448–452, 1981. doi:10.1126/science.6450446.
2. **Wallimann T**, **Wyss M**, **Brdiczka D**, **Nicolay K**, **Eppenberger HM.** Intracellular compartmentation, structure and function of creatine kinase isoenzymes in tissues with high and fluctuating energy demands: the 'phosphocreatine circuit' for cellular energy homeostasis. *Biochem J* 281: 21–40, 1992. doi:10.1042/bj2810021.
3. **Jacobus WE**, **Lehninger AL.** Creatine kinase of rat heart mitochondria. coupling of creatine phosphorylation to electron transport. *J Biol Chem* 248: 4803–4810, 1973. doi:10.1016/S0021-9258(19)43737-X.
4. **Saks VA**, **Chernousova GB**, **Gukovsky DE**, **Smirnov VN**, **Chazov EI.** Studies of energy transport in heart cells. mitochondrial isoenzyme of creatine phosphokinase: kinetic properties and regulatory action of mg2 + ions. *Eur J Biochem* 57: 273–290, 1975. doi:10.1111/j.1432-1033.1975.tb02299.x.
5. **Vendelin M**, **Lemba M**, **Saks VA.** Analysis of functional coupling: mitochondrial creatine kinase and adenine nucleotide translocase. *Biophys J* 87: 696–713, 2004. doi:10.1529/biophysj.103.036210.
6. **Vendelin M**, **Kongas O**, **Saks V.** Regulation of mitochondrial respiration in heart cells analyzed by reaction-diffusion model of energy transfer. *Am J Physiol Cell Physiol* 278: C747–C764, 2000. doi:10.1152/ajpcell.2000.278.4.C747.
7. **De Sousa E**, **Veksler V**, **Minajeva A**, **Kaasik A**, **Mateo P**, **Mayoux E**, **Hoerter J**, **Bigard X**, **Serrurier B**, **Ventura-Clapier R.** Subcellular creatine kinase alterations. *Circ Res* 85: 68–76, 1999. doi:10.1161/01.RES.85.1.68.
8. **Veksler VI**, **Lechene P**, **Matrougui K**, **Ventura-Clapier R.** Rigor tension in single skinned rat cardiac cell: role of myofibrillar creatine kinase. *Cardiovasc Res* 36: 354–362, 1997. doi:10.1016/S0008-6363(97)00178-8.
9. **Grosse R**, **Spitzer E**, **Kupriyanov VV**, **Saks VA**, **Repke KR.** Coordinate interplay between (na + + k +)-atpase and creatine phosphokinase optimizes (na + /k +)-antiport across the membrane of vesicles formed from the plasma membrane of cardiac muscle cell. *BBA* 603: 142–156, 1980. doi:10.1016/0005-2736(80)90397-1.
10. **Abraham MR**, **Selivanov V**, **Hodgson D**, **Pucar D**, **Zingman L**, **Wieringa B**, **Dzeja P**, **Alekseev A**, **Terzic A.** Coupling of cell energetics with membrane metabolic sensing. *J Biol Chem* 277: 24427–24434, 2002. doi:10.1074/jbc.M201777200.
11. **Steeghs K**, **Benders A**, **Oerlemans F**, **de Haan A**, **Heerschap A**, **Ruitenbeek W**, **Jost C**, **van Deursen J**, **Perryman B**, **Pette D**, **Bruckwilder M**, **Koudijs J**, **Jap P**, **Veerkamp J**, **Wieringa B.** Altered ca2 + responses in muscles with combined mitochondrial and cytosolic creatine kinase deficiencies. *Cell* 89: 93–103, 1997. doi:10.1016/S0092-8674(00)80186-5.
12. **Kaasik A**, **Veksler V**, **Boehm E**, **Novotova M**, **Minajeva A**, **Ventura-Clapier R.** Energetic crosstalk between organelles: Architectural integration of energy production and utilization. *Circ Res* 89: 153–159, 2001. doi:10.1161/hh1401.093440.
13. **Brosnan M**, **Edison E**, **da Silva R**, **Brosnan J.** New insights into creatine function and synthesis. *Adv Enzyme Regul* 47: 252–260, 2007. doi:10.1016/j.advenzreg.2006.12.005.
14. **Barsunova K**, **Vendelin M**, **Birkedal R.** Marker enzyme activities in hindleg from creatine-deficient agat and gamt ko mice – differences between models, muscles, and sexes. *Sci Rep* 10: 7956, 2020. doi:10.1038/s41598-020-64740-8.
15. **Lygate C**, **Aksentijevic D**, **Dawson D**, **ten Hove M**, **Phillips D**, **de Bono J**, **Medway D**, **Sebag-Montefiore L**, **Hunyor I**, **Channon K**, **Clarke K**, **Zervou S**, **Watkins H**, **Balaban R**, **Neubauer S.** Living without creatine: unchanged exercise capacity and response to chronic myocardial infarction in creatine-deficient mice. *Circ Res* 112: 945–955, 2013. doi:10.1161/CIRCRESAHA.112.300725.
16. **ten Hove M**, **Lygate CA**, **Fischer A**, **Schneider JE**, **Sang AE**, **Hulbert K**, **Sebag-Montefiore L**, **Watkins H**, **Clarke K**, **Isbrandt D**, **Wallis J**, **Neubauer S.** Reduced inotropic reserve and increased susceptibility to cardiac ischemia/reperfusion injury in phosphocreatine-deficient guanidinoacetate-n-methyltransferase-knockout mice. *Circulation* 111: 2477–2485, 2005. doi:10.1161/01.CIR.0000165147.99592.01.
17. **Branovets J**, **Sepp M**, **Kotlyarova S**, **Jepihhina N**, **Sokolova N**, **Aksentijevic D**, **Lygate C**, **Neubauer S**, **Vendelin M**, **Birkedal R.** Unchanged mitochondrial organization and compartmentation of high-energy phosphates in creatine-deficient gamt−/− mouse hearts. *Am J Physiol Heart Circ Physiol* 305: H506–H520, 2013. doi:10.1152/ajpheart.00919.2012.
18. **Kan H**, **Renema WK**, **Isbrandt D**, **Heerschap A.** Phosphorylated guanidinoacetate partly compensates for the lack of phosphocreatine in skeletal muscle of mice lacking guanidinoacetate methyltransferase. *J Physiol (Lond)* 560: 219–229, 2004. doi:10.1113/jphysiol.2004.067926.
19. **Choe C**, **Atzler D**, **Wild P**, **Carter A**, **Böger R**, **Ojeda F**, **Simova O**, **Stockebrand M**, **Lackner K**, **Nabuurs C**, **Marescau B**, **Streichert T**, **Müller C**, **Lüneburg N**, **Deyn PD**, **Benndorf R**, **Baldus S**, **Gerloff C**, **Blankenberg S**, **Heerschap A**, **Grant P**, **Magnus T**, **Zeller T**, **Isbrandt D**, **Schwedhelm E.** Homoarginine levels are regulated by l-arginine:glycine amidinotransferase and affect stroke outcome results from human and murine studies. *Circulation* 128: 1451–1461, 2013. doi:10.1161/CIRCULATIONAHA.112.000580.
20. **März W**, **Meinitzer A**, **Drechsler C**, **Pilz S**, **Krane V**, **Kleber ME**, **Fischer J**, **Winkelmann BR**, **BöHm BO**, **Ritz E**, **Wanner C**, Homoarginine, cardiovascular risk, and mortality**.** *Circulation* 122: 967–975, 2010. doi:10.1161/CIRCULATIONAHA.109.908988.
21. **Faller KE**, **Atzler D**, **Mcandrew D**, **Zervou S**, **Whittington H**, **Simon J**, **Aksentijevic D**, **ten Hove M**, **Choe C**, **Isbrandt D**, **Casadei B**, **Schneider J**, **Neubauer S**, **Lygate C.** Impaired cardiac contractile function in arginine:glycine amidinotransferase knockout mice devoid of creatine is rescued by homoarginine but not creatine. *Cardiovasc Res* 114: 417–430, 2018. doi:10.1093/cvr/cvx242.
22. **Farrell S**, **Ross J**, **Howlett S.** Sex differences in mechanisms of cardiac excitation-contraction coupling in rat ventricular myocytes. *Am J Physiol Heart Circ Physiol* 299: H36–H45, 2010. doi:10.1152/ajpheart.00299.2010.
23. **Parks R**, **Howlett S.** Sex differences in mechanisms of cardiac excitation–contraction coupling. *Pflugers Arch - Eur J Physiol* 465: 747–763, 2013. doi:10.1007/s00424-013-1233-0.
24. **Tordoff M**, **Bachmanov A**, **Reed D.** Forty mouse strain survey of voluntary calcium intake, blood calcium, and bone mineral content. *Physiol Behav* 91: 632–643, 2007. doi:10.1016/j.physbeh.2007.03.027.
25. **Yao A**, **Su Z**, **Nonaka A**, **Zubair I**, **Lu L**, **Philipson K**, **Bridge JB**, **Barry W.** Effects of overexpression of the na + -ca2 + exchanger on [ca2 +]i transients in murine ventricular myocytes. *Circ Res* 82: 657–665, 1998. doi:10.1161/01.RES.82.6.657.
26. **Fox J**, **Barthold S**, **Davisson M**, **Newcomer C**, **Quimby F**, **Smith A.** *The Mouse in Biomedical Research, Volume 3: Normative Biology, Husbandry, and Models*. Academic Press, 2006.
27. **Seidel T**, **Navankasattusas S**, **Ahmad A**, **Diakos NA**, **Xu WD**, **Tristani-Firouzi M**, **Bonios MJ**, **Taleb I**, **Li DY**, **Selzman CH**, **Drakos SG**, **Sachse FB.** Sheet-like remodeling of the transverse tubular system in human heart failure impairs excitation-contraction coupling and functional recovery by mechanical unloading. *Circulation* 135: 1632–1645, 2017. doi:10.1161/CIRCULATIONAHA.116.024470.
28. **Ferretti R**, **Marques M**, **Khurana T**, **Santo Neto H.** Expression of calcium-buffering proteins in rat intrinsic laryngeal muscles. *Physiol Rep* 3: e12409, 2015. doi:10.14814/phy2.12409.
29. **Shintani Y**, **Kapoor A**, **Kaneko M**, **Smolenski RT**, **D'Acquisto F**, **Coppen SR**, **Harada-Shoji N**, **Lee HJ**, **Thiemermann C**, **Takashima S**, **Yashiro K**, **Suzuki K.** mediates cellular protection by modulating

Downloaded from journals.physiology.org/journal/ajpheart by Rikke Birkedal (086.110.032.113) on March 18, 2021.

energy metabolism in cardiomyocytes and neurons. *PNAS* 110: 5109–5114, 2013. doi:10.1073/pnas.1219243110.
30. **Laasmaa M**, **Karro N**, **Birkedal R**, **Vendelin M.** Iocbio sparks detection and analysis software. *PeerJ* 7: e6652, 2019. doi:10.7717/peerj.6652.
31. **Laasmaa M**, **Birkedal R**, **Vendelin M.** Revealing calcium fluxes by analyzing inhibition dynamics in action potential clamp. *J Mol Cell Cardiol* 100: 93–108, 2016. doi:10.1016/j.yjmcc.2016.08.015.
32. **Bondarenko V**, **Szigeti G**, **Bett GL**, **Kim S**, **Rasmusson R.** Computer model of action potential of mouse ventricular myocytes. *Am J Physiol Heart Circ Physiol* 287: H1378–H1403, 2004. doi:10.1152/ajpheart.00185.2003.
33. **Greenstein J**, **Winslow R.** An integrative model of the cardiac ventricular myocyte incorporating local control of ca2+ release. *Biophys J* 83: 2918–2945, 2002. doi:10.1016/S0006-3495(02)75301-0.
34. **Koivumäki J**, **Takalo J**, **Korhonen T**, **Tavi P**, **Weckström M.** Modelling sarcoplasmic reticulum calcium atpase and its regulation in cardiac myocytes. *Phil Trans R Soc A* 367: 2181–2202, 2009. doi:10.1098/rsta.2008.0304.
35. **Pandit S**, **Clark R**, **Giles W**, **Demir S.** A mathematical model of action potential heterogeneity in adult rat left ventricular myocytes. *Biophys J* 81: 3029–3051, 2001. doi:10.1016/S0006-3495(01)75943-7.
36. **Winslow RL**, **Rice J**, **Jafri S**, **Marbán E**, **O'Rourke B.** Mechanisms of altered excitation-contraction coupling in canine tachycardia-induced heart failure, ii: model studies. *Circ Res* 84: 571–586, 1999. . doi:10.1161/01.RES.84.5.571.
37. **Walker MA**, **Williams GSB**, **Kohl T**, **Lehnart S**, **Jafri MS**, **Greenstein J**, **Lederer WJ**, **Winslow R.** Superresolution modeling of calcium release in the heart. *Biophys J* 107: 3018–3029, 2014. doi:10.1016/j.bpj.2014.11.003.
38. **Tange O.** *Gnu parallel - the command-line power tool.; login: The USENIX Magazine* 36: 42–47, 2011.
39. **Gershman S**, **Blei D.** A tutorial on bayesian nonparametric models. *arXiv:11062697 [stat]*, 2011.
40. **Lee M**, **Wagenmakers E.** *Bayesian Cognitive Modeling: A Practical Course*. Cambridge University Press, 2014.
41. **Cheng H**, **Lederer WJ.** Calcium sparks. *Physiol Rev* 88: 1491–1545, 2008. doi:10.1152/physrev.00030.2007.
42. **Brette F**, **Sallé L**, **Orchard C.** Differential modulation of l-type ca2+ current by sr ca2+ release at the t-tubules and surface membrane of rat ventricular myocytes. *Circ Res* 95: e1–7, 2004.
43. **Jones P**, **Macquaide N**, **Louch W.** Dyadic plasticity in cardiomyocytes. *Front Physiol* 9, 2018.
44. **Bers DM.** *Excitation-Contraction Coupling and Cardiac Contractile Force*. Kluwer Academic Publishers, 2001.
45. **Trafford AW**, **Díaz ME**, **Sibbring GC**, **Eisner DA.** Modulation of cicr has no maintained effect on systolic ca2+: simultaneous measurements of sarcoplasmic reticulum and sarcolemmal ca2+ fluxes in rat ventricular myocytes. *J Physiol (Lond)* 522: 259–270, 2000. . doi:10.1111/j.1469-7793.2000.t01-2-00259.x.
46. **Caldwell J**, **Smith CR**, **Taylor R**, **Kitmitto A**, **Eisner D**, **Dibb K**, **Trafford A.** Dependence of cardiac transverse tubules on the bar domain protein amphiphysin ii (bin-1). *Circ Res* 115: 986–996, 2014. doi:10.1161/CIRCRESAHA.116.303448.
47. **Lipsett DB**, **Frisk M**, **Aronsen JM**, **Nordén ES**, **Buonarati OR**, **Cataliotti A**, **Hell JW**, **Sjaastad I**, **Christensen G**, **Louch WE.** Cardiomyocyte substructure reverts to an immature phenotype during heart failure. *J Physiol* 597: 1833–1853, 2019. doi:10.1113/JP277273.
48. **Louch WE**, **Mørk HK**, **Sexton J**, **Strømme TA**, **Laake P**, **Sjaastad I**, **Sejersted OM.** T-tubule disorganization and reduced synchrony of ca2+ release in murine cardiomyocytes following myocardial infarction. *J Physiol* 574: 519–533, 2006. doi:10.1113/jphysiol.2006.107227.
49. **Eisner D**, **Caldwell J**, **Kistamás K**, **Trafford A.** Calcium and excitation-contraction coupling in the heart. *Circ Res* 121: 181–195, 2017. doi:10.1161/CIRCRESAHA.117.310230.
50. **Jensen M**, **Müller C**, **Choe C**, **Schwedhelm E**, **Zeller T.** Analysis of l-arginine:glycine amidinotransferase-, creatine- and homoarginine-dependent gene regulation in the murine heart. *Sci Rep* 10: 4821, 2020. doi:10.1038/s41598-020-61638-3.
51. **Striessnig J**, **Pinggera A**, **Kaur G**, **Bock G**, **Tuluc P.** L-type ca2+ channels in heart and brain. *WIREs Membr Transp Signal* 3: 15–38, 2014. doi:10.1002/wmts.102.
52. **Zimmer T**, **Haufe V**, **Blechschmidt S.** Voltage-gated sodium channels in the mammalian heart. *Global Cardiol Sci Pract* 2014: 58–2015, 2014. doi:10.5339/gcsp.2014.58.
53. **Jensen M**, **Müller C**, **Schwedhelm E**, **Arunachalam P**, **Gelderblom M**, **Magnus T**, **Gerloff C**, **Zeller T**, **Choe C.** Homoarginine- and creatine-dependent gene regulation in murine brains with l-arginine:glycine amidinotransferase deficiency. *IJMS* 21: 1865, 2020. doi:10.3390/ijms21051865.
54. **Stockebrand M**, **Nejad A**, **Neu A**, **Kharbanda K**, **Sauter K**, **Schillemeit S**, **Isbrandt D**, **Choe C.** Transcriptomic and metabolic analyses reveal salvage pathways in creatine-deficient agat−/− mice. *Amino Acids* 48: 2025–2039, 2016. doi:10.1007/s00726-016-2202-7.
55. **Nabuurs CI**, **Choe CU**, **Veltien A**, **Kan HE**, **van Loon LJC**, **Rodenburg RJT**, **Matschke J**, **Wieringa B**, **Kemp GJ**, **Isbrandt D**, **Heerschap A.** Disturbed energy metabolism and muscular dystrophy caused by pure creatine deficiency are reversible by creatine intake. *J Physiol* 591: 571–592, 2013. doi:10.1113/jphysiol.2012.241760.
56. **Larbig R**, **Torres N**, **Bridge J**, **Goldhaber J**, **Philipson K.** Activation of reverse na+–ca2+ exchange by the na+ current augments the cardiac ca2+ transient: evidence from ncx knockout mice. *J Physiol (Lond)* 588: 3267–3276, 2010. doi:10.1113/jphysiol.2010.187708.
57. **Biesiadecki B**, **Davis J**, **Ziolo M**, **Janssen PML.** Tri-modal regulation of cardiac muscle relaxation; intracellular calcium decline, thin filament deactivation, and cross-bridge cycling kinetics. *Biophys Rev* 6: 273–289, 2014. doi:10.1007/s12551-014-0143-5.
58. **Davis J**, **Tikunova SB.** Ca2+ exchange with troponin c and cardiac muscle dynamics. *Cardiovasc Res* 77: 619–626, 2007. doi:10.1093/cvr/cvm098.
59. **Illaste A**, **Laasmaa M**, **Peterson P**, **Vendelin M.** Analysis of molecular movement reveals latticelike obstructions to diffusion in heart muscle cells. *Biophys J* 102: 739–748, 2012. doi:10.1016/j.bpj.2012.01.012.
60. **Jepihhina N**, **Beraud N**, **Sepp M**, **Birkedal R**, **Vendelin M.** Permeabilized rat cardiomyocyte response demonstrates intracellular origin of diffusion obstacles. *Biophys J* 101: 2112–2121, 2011. doi:10.1016/j.bpj.2011.09.025.
61. **Vendelin M**, **Eimre M**, **Seppet E**, **Peet N**, **Andrienko T**, **Lemba M**, **Engelbrecht J**, **Seppet E**, **Saks VA.** Intracellular diffusion of adenosine phosphates is locally restricted in cardiac muscle. *Mol Cell Biochem* 256: 229–241, 2004. doi:10.1023/B:MCBI.0000009871.04141.64.
62. **Simson P**, **Jepihhina N**, **Laasmaa M**, **Peterson P**, **Birkedal R**, **Vendelin M.** Restricted adp movement in cardiomyocytes: Cytosolic diffusion obstacles are complemented with a small number of open mitochondrial voltage-dependent anion channels. *J Mol Cell Cardiol* 97: 197–203, 2016. doi:10.1016/j.yjmcc.2016.04.012.
63. **Rostovtseva TK**, **Sheldon KL**, **Hassanzadeh E**, **Monge C**, **Saks V**, **Bezrukov SM**, **Sackett DL.** Tubulin binding blocks mitochondrial voltage-dependent anion channel and regulates respiration. *PNAS* 105: 18746–18751, 2008. doi:10.1073/pnas.0806303105.
64. **Birkedal R**, **Laasmaa M**, **Vendelin M.** The location of energetic compartments affects energetic communication in cardiomyocytes. *Front Physiol* 5: 376, 2014.
65. **Ramay HR**, **Vendelin , M.** Diffusion restrictions surrounding mitochondria: A mathematical model of heart muscle fibers. *Biophys J* 97: 443–452, 2009. doi:10.1016/j.bpj.2009.04.062.
66. **Saks VA**, **Belikova YO**, **Kuznetsov AV.** In vivo regulation of mitochondrial respiration in cardiomyocytes: specific restrictions for intracellular diffusion of adp. *BBA* 1074: 302–311, 1991.
67. **Vendelin M**, **Hoerter JA**, **Mateo P**, **Soboll S**, **Gillet B**, **Mazet JL.** Modulation of energy transfer pathways between mitochondria and myofibrils by changes in performance of perfused heart. *J Biol Chem* 285: 37240–37250, 2010. doi:10.1074/jbc.M110.147116.
68. **Bonz A**, **Kniesch S**, **Hofmann U**, **Küllmer S**, **Bauer L**, **Wagner H**, **Ertl G**, **Spindler M.** Functional properties and [ca2+]i metabolism of creatine kinase–ko mice myocardium. *Biochem Biophys Res Commun* 298: 163–168, 2002. doi:10.1016/S0006-291X(02)02402-6.

Downloaded from journals.physiology.org/journal/ajpheart by Rikke Birkedal (086.110.032.113) on March 18, 2021.

Appendix 5

Publication V

Branovets J, Kalda M, Laasmaa M, Stolova J, Shen X, Balodis MJ, Grahv C, Hendrikson E, Louch WE, Birkedal R, Vendelin M

Compromised creatine kinase energy transfer leads to adaptations in cardiac excitation-contraction coupling that are distinct from changes associated with heart failure.

(manuscript)

The rules of the publisher prevent publication of the manuscript of Publication V prior to the acceptance. Official committee members and opponents will be given a copy of the manuscript to enable them to carry out a judicious review of the dissertation.

Curriculum vitae

Personal data

Name:	Jelena Branovets
Date of birth:	09.06.1984
Place of birth:	Tallinn, Estonia
Citizenship:	Estonia

Contact data

E-mail:	jelena@sysbio.ioc.ee

Education

2009–2022	Tallinn University of Technology, PhD
2006–2008	Tallinn University of Technology, MSC (gene technology)
2003–2006	Tallinn University of Technology, BSC (gene technology)
1991–2003	Tallinn Central Russian Gymnasium

Language competence

Russian	Native
Estonian	Fluent
English	Fluent

Professional employment

2009–…	Tallinn University of Technology, Department of Cybernetics, engineer
2008–2009	The National Institute for Health Development, researcher

Scholarships and awards

2016	Archimedes/Kristjan Jaak scholarship to attend Biophysical Society 60th Annual Meeting
2013	The best scientific publication of a young scientist at the Institute of Cybernetics at TUT

Courses and conferences

February 2016	Biophysical Society 60th Annual Meeting, Los Angeles, California, USA; poster presentation "The influence of alternative energy transfer systems on respiration in creatine-deficient mouse cardiomyocytes".
February 2016	Competence course of Laboratory Animal Science II in the Estonian University of Life Sciences, AU.452
September 2015	44th European Muscle Conference 2015, Warsaw, Poland; poster presentation "The influence of adenylate kinase and hexokinase on respiration in creatine-deficient GAMT -/- and AGAT -/- mouse cardiomyocytes".
August 2015	Competence course of Laboratory Animal Science I in the Estonian University of Life Sciences, AU.441
February 2015	Biophysical Society 59th Annual Meeting, Baltimore, Maryland, USA; poster presentation "The influence of adenylate kinase and hexokinase on respiration in creatine-deficient GAMT -/- mouse cardiomyocytes".
July 2013	37th International Congress of Physiological Sciences (IUPS 2013), Birmingham, UK; poster presentation "Unaltered mitochondrial

organization and compartmentation in creatine deficient GAMT-/- mouse cardiomyocytes".

February 2013 Biophysical Society 57th Annual Meeting, Philadelphia, Pennsylvania, USA; poster presentation "Unchanged mitochondrial organization and compartmentation in creatine deficient GAMT-/- mouse heart".

Supervised dissertation

Lucia Jaska Master's Degree, 2021, (sup) Rikke Birkedal Nielsen; (co-sup) Jelena Branovets, Comparing respiration of isolated cardiomyocytes from young and old, guanidinoacetate N-methyltransferase (GAMT) knockout and wild type mice, Tallinn University of Technology, Department of Cybernetics.

Publications

Laasmaa, Martin; Branovets, Jelena*; Barsunova, Karina*; Karro, Niina; Lygate, Craig A.; Birkedal, Rikke; Vendelin, Marko (2021). Altered calcium handling in cardiomyocytes from arginine-glycine amidinotransferase-knockout mice is rescued by creatine. American Journal of Physiology-Heart and Circulatory Physiology, 3230 (2), H805−H825. DOI: 10.1152/ajpheart.00300.2020.

Vendelin, Marko; Laasmaa, Martin; Kalda, Mari; Branovets, Jelena; Karro, Niina; Barsunova, Karina; Birkedal, Rikke (2020). IOCBIO Kinetics: An open-source software solution for analysis of data traces. PLoS Computational Biology, 16 (12), e1008475. DOI: 10.1371/journal.pcbi.1008475.

Branovets, Jelena; Karro, Niina; Barsunova, Karina; Laasmaa, Martin; Lygate, Craig A.; Vendelin, Marko; Birkedal, Rikke (2020). Cardiac expression and location of hexokinase changes in a mouse model of pure creatine deficiency. American Journal of Physiology-Heart and Circulatory Physiology, 320 (2), H613−H629. DOI: 10.1152/ajpheart.00188.2020.

Branovets, Jelena; Sepp, Mervi; Kotlyarova, Svetlana; Jepihhina, Natalja; Sokolova, Niina; Aksentijevic, Dunja; Lygate, Craig A.; Neubauer, Stefan; Vendelin, Marko; Birkedal, Rikke (2013). Unchanged mitochondrial organization and compartmentation of high-energy phosphates in creatine-deficient GAMT (-/-) mouse hearts. American Journal of Physiology-Heart and Circulatory Physiology, 305 (4), H506−H520. DOI: 10.1152/ajpheart.00919.2012.

Smorodin, Eugeniy; Kurtenkov, Oleg; Sergeyev, Boris; Branovets, Jelena; Izotova, Jelena; Formanovsky, Andrey (2011). Specificity of serum anti-A(di) IgG antibodies from patients with gastrointestinal cancer. Journal of Immunoassay and Immunochemistry, 32, 170−190.

Kaer Kristel, Branovets Jelena, Hallikma Anni, Nigumann Pilvi and Speek Mart (2011). Intronic L1 retrotransposons and nested genes cause transcriptional interference by inducing intron retention, exonization and cryptic polyadenylation. PLoS ONE, 6(10): e26099. Epub 2011 Oct 13. DOI: 10.1371/journal.pone.0026099.

* Equal contribution

Elulookirjeldus

Isikuandmed

Nimi:	Jelena Branovets
Sünniaeg:	09.06.1984
Sünnikoht:	Tallinn
Kodakondsus:	Eesti

Kontaktandmed

E-post:	jelena@sysbio.ioc.ee

Hariduskäik

2009–2022	Tallinna Tehnikaülikool, PhD
2006–2008	Tallinna Tehnikaülikool, MSc (geenitehnoloogia)
2003–2006	Tallinna Tehnikaülikool, BSc (geenitehnoloogia)
1991–2003	Tallinna Kesklinna Vene Gümnaasium

Keelteoskus

Vene keel	emakeel
Eesti keel	kõrgtase
Inglise keel	kõrgtase

Teenistuskäik

2009–…	Tallinna Tehnikaülikool, Küberneetika Instituut, insener
2008–2009	Tervise Arengu Instituut, teadur

Stipendiumid ja tunnustused

2016	Archimedes/Kristjan Jaagu välissõidu stipendium “Biophysical Society 60th Annual Meeting” konverentsil osalemiseks
2013	TTÜ Küberneetika Instituudi aasta parim noore teadlase teaduspublikatsioon

Kursused ja konverentsid

Veebruar 2016	Biophysical Society 60th Annual Meeting, Los Angeles, California, USA; posterettekanne “The influence of alternative energy transfer systems on respiration in creatine-deficient mouse cardiomyocytes”.
Veebruar 2016	Katseloomateaduse jätkukursus “Laboratory Animal Science II”, Eesti Maaülikool, AU.452
September 2015	44th European Muscle Conference 2015, Warsaw, Poland; posterettekanne “The influence of adenylate kinase and hexokinase on respiration in creatine-deficient GAMT -/- and AGAT -/- mouse cardiomyocytes”.
August 2015	Katseloomateaduse kursus “Laboratory Animal Science I”, Eesti Maaülikool, AU.441
Veebruar 2015	Biophysical Society 59th Annual Meeting, Baltimore, Maryland, USA; posterettekanne “The influence of adenylate kinase and hexokinase on respiration in creatine-deficient GAMT -/- mouse cardiomyocytes”.
Juuli 2013	37th International Congress of Physiological Sciences (IUPS 2013), Birmingham, UK; posterettekanne “Unaltered mitochondrial organization and compartmentation in creatine deficient GAMT-/- mouse cardiomyocytes”.

Veebruar 2013 Biophysical Society 57th Annual Meeting, Philadelphia, Pennsylvania, USA; posterettekanne “Unchanged mitochondrial organization and compartmentation in creatine deficient GAMT-/- mouse heart”.

Juhendatud lõputööd

Lucia Jaska, magistrikraad, 2021, (juh) Rikke Birkedal Nielsen; (kaasjuh) Jelena Branovets, Comparing respiration of isolated cardiomyocytes from young and old, guanidinoacetate N-methyltransferase (GAMT) knockout and wild type mice (Noortest ja vanadest guanidinoatsetaat-N-metüültransferaasi (GAMT) geenipuudulikkusega ja metsiktüüpi hiirtest eraldatud kardiomüotsüütide hingamise võrdlemine), Tallinna Tehnikaülikool, Küberneetika Instituut.

Publikatsioonid

Laasmaa, Martin; Branovets, Jelena*; Barsunova, Karina*; Karro, Niina; Lygate, Craig A.; Birkedal, Rikke; Vendelin, Marko (2021). Altered calcium handling in cardiomyocytes from arginine-glycine amidinotransferase-knockout mice is rescued by creatine. American Journal of Physiology-Heart and Circulatory Physiology, 3230 (2), H805−H825. DOI: 10.1152/ajpheart.00300.2020.

Vendelin, Marko; Laasmaa, Martin; Kalda, Mari; Branovets, Jelena; Karro, Niina; Barsunova, Karina; Birkedal, Rikke (2020). IOCBIO Kinetics: An open-source software solution for analysis of data traces. PLoS Computational Biology, 16 (12), e1008475. DOI: 10.1371/journal.pcbi.1008475.

Branovets, Jelena; Karro, Niina; Barsunova, Karina; Laasmaa, Martin; Lygate, Craig A.; Vendelin, Marko; Birkedal, Rikke (2020). Cardiac expression and location of hexokinase changes in a mouse model of pure creatine deficiency. American Journal of Physiology-Heart and Circulatory Physiology, 320 (2), H613−H629. DOI: 10.1152/ajpheart.00188.2020.

Branovets, Jelena; Sepp, Mervi; Kotlyarova, Svetlana; Jepihhina, Natalja; Sokolova, Niina; Aksentijevic, Dunja; Lygate, Craig A.; Neubauer, Stefan; Vendelin, Marko; Birkedal, Rikke (2013). Unchanged mitochondrial organization and compartmentation of high-energy phosphates in creatine-deficient GAMT-/- mouse hearts. American Journal of Physiology-Heart and Circulatory Physiology, 305 (4), H506−H520. DOI: 10.1152/ajpheart.00919.2012.

Smorodin, Eugeniy; Kurtenkov, Oleg; Sergeyev, Boris; Branovets, Jelena; Izotova, Jelena; Formanovsky, Andrey (2011). Specificity of serum anti-A(di) IgG antibodies from patients with gastrointestinal cancer. Journal of Immunoassay and Immunochemistry, 32, 170−190.

Kaer Kristel, Branovets Jelena, Hallikma Anni, Nigumann Pilvi and Speek Mart (2011). Intronic L1 retrotransposons and nested genes cause transcriptional interference by inducing intron retention, exonization and cryptic polyadenylation. PLoS ONE, 6(10): e26099. Epub 2011 Oct 13. DOI: 10.1371/journal.pone.0026099.

*Võrdne panus

ISSN 2585-6901 (PDF)
ISBN 978-9949-83-901-8 (PDF)